Determination and influence of the existence of partial discharges in a railway traction system using SiC-based components

Robin Acheen

THÈSE

En vue de l'obtention du

DOCTORAT DE L'UNIVERSITÉ DE TOULOUSE

Délivré par l'Université Toulouse 3 - Paul Sabatier

Présentée et soutenue par

Robin ACHEEN

Le 9 novembre 2020

Détermination et impact de l'existence de décharges partielles dans une chaîne de traction ferroviaire utilisant des composants à base de SiC

Ecole doctorale : **GEET - Génie Electrique Electronique et Télécommunications : du système au nanosystème**

Spécialité : **Génie Electrique**

Unité de recherche :
LAPLACE - Laboratoire PLAsma et Conversion d'Énergie - CNRS-UPS-INPT

Thèse dirigée par
Thierry LEBEY et Stéphane DUCHESNE

Jury

M. Andrea CAVALLINI, Rapporteur
M. Christopher GERADA, Rapporteur
Mme Sonia AIT AMAR - DJENNAD, Examinatrice
M. David MALEC, Examinateur
M. Thierry LEBEY, Directeur de thèse
M. Stéphane DUCHESNE, Co-directeur de thèse

Remerciements

Ce travail a été réalisé au sein de l'IRT Saint Exupéry, dans le cadre du projet HIGHVOLT du domaine Aéronef Plus Electrique, en partenariat avec le laboratoire Laplace et le LSEE, et en étroite collaboration avec l'entreprise ALSTOM. Avant même de rentrer dans le détail, je tiens à remercier toutes les personnes qui ont été impliquées, de près ou de loin, dans ce projet, et qui m'ont permis de mener à bien mon travail de thèse.

Je souhaiterais tout d'abord remercier Thierry Lebey et Stéphane Duchesne de m'avoir encadré pendant ces trois années (et quelques) de thèse. Chacun, selon son caractère et à sa manière, a su me guider et m'apporter des réponses lorsque j'en avais besoin. J'ai notamment beaucoup apprécié de travailler avec Thierry et de bénéficier de son savoir, mais aussi et surtout de sa vision et de son discernement. Il a su me motiver lorsque j'en avais besoin, composer avec ma personnalité, le tout avec beaucoup d'humour et « sans se prendre au sérieux » comme il aime à le dire. Quant à Stéphane, même si nos échanges ont étés plus brefs du fait de la distance, il m'a toujours réservé un accueil chaleureux (ce qui est appréciable à Béthune) lors de mes visites, et a su être complémentaire avec Thierry en m'apportant ici et là des conseils, connaissances ou autres analyses pour m'aider dans mon travail.

Je tiens à remercier sincèrement les membres du jury d'avoir pris le temps de lire mes travaux et pour leur présence à ma soutenance malgré les conditions difficiles.

Je voudrais également remercier Cédric Abadie de m'avoir encadré à l'IRT. En tant qu'encadrant « non-officiel », son nom apparaît moins que celui de mes directeurs de thèse, mais il est très clairement celui avec qui j'ai passé le plus de temps. Il m'a été d'une grande aide tout au long de mon travail de thèse, autant pour les aspects scientifiques que pour les aspects techniques et administratifs, et j'ai beaucoup apprécié de travailler avec lui.

De manière générale, je remercie également l'IRT de m'avoir accueilli et de m'avoir fait bénéficier d'un cadre privilégié, à mi-chemin entre les mondes académique et industriel. Je remercie toutes les personnes que j'ai pu y côtoyer, les anciens (Thibaut, Loïc, Laurent, Bouazza, Guillaume, Ludovic, Samuel…) comme les nouveaux (Mateusz, Cyril…). Merci à Gaëtan de m'avoir fait découvrir la lourdeur des blagues d'entreprise (« T'as pris ta demi-journée ? » « T'es tombé du lit ? »). Je tiens aussi à m'excuser solennellement auprès de toutes les personnes qui ont dû subir le bruit de mes manips en salle vieillissement. Enfin, j'espère qu'on aura tous l'occasion de boire un coup pour célébrer ma soutenance quand le contexte se sera amélioré !

Je tiens aussi à remercier le laboratoire Laplace, et plus particulièrement Marie-Laure, David et le groupe MDCE, de m'avoir aidé et fait profiter d'un environnement de travail agréable, même si je n'ai pas forcément été très présent. Dans une moindre mesure, je remercie également Sonia et le LSEE pour les quelques moments que j'ai pu y passer, qui ont été très agréables.

Je remercie, bien sûr, l'entreprise ALSTOM d'avoir contribué à ce projet, et de m'avoir ouvert ses portes pour effectuer une partie de mes travaux. En particulier, merci à Benali et Gérard puis Ronan de m'avoir suivi tout au long de cette thèse, et à Guillaume, Christophe et Thibault de m'avoir encadré, guidé et épaulé lors de mes essais sur le site de Tarbes.

Un grand merci à mes potes, et notamment mes amis co-thésards Jonathan, Théo et Matthieu, pour ces longues sessions de babyfoot, blind-test, mots fléchés, et bien sûr soirées qui m'ont permis de me changer les idées quand la motivation n'était pas au rendez-vous. Et bon courage pour la fin, vous êtes bientôt au bout !

Un grand merci également à ma famille, notamment mes parents qui m'ont permis d'en arriver là, et qui m'ont toujours soutenu même si ce que je faisais a toujours été un peu flou pour eux, mais aussi mon frère, et toute ma famille proche.

Enfin, je ne peux pas terminer sans remercier Paula de m'avoir supporté pendant toute la durée de cette thèse, et de me supporter de manière générale d'ailleurs, ce qui n'est pas si simple ! Merci de t'être adaptée, et pour ton soutien ! Dzięki skarbie !

Table of contents

Introduction

Electrical energy is used today for many transportation-related applications, notably in the railway, aeronautic, and automotive sectors. Rationalization of this energy is a major development axis in the current “More Electrical” context. The reliability of electrical systems, especially that of Electrical Insulation Systems (EIS), therefore involves data that is crucial for ensuring that electrical equipment operates accurately over its entire life cycle. Supply systems and subsystems continue to be subject to increasingly severe electrical stresses. Issues and operating environments may differ, but there is a single common goal: reliability must be ensured and aging must be anticipated and controlled to the greatest extent possible.

This is especially true given the fact that the spread of new power converters for Adjustable Speed Drive (ASD) applications have led to new stresses with significantly more harmful impact on machines. Similarly, the introduction of SiC-based components in the electromechanical chain presents numerous advantages, but also has consequences on the reliability of insulation systems in machines. These devices can create thousands of voltage impulses per second, with extremely fast rise times. Finally, impedance mismatches between inverters, cables, and motors may lead to wave reflection phenomena that cause significant overvoltages at the motor terminals. These phenomena ignite partial discharges (PD), which are responsible for specific aging mechanisms that progressively damage the electromechanical chain’s insulation systems, eventually leading to complete motor failure. To handle these different issues, a distinction was made between low voltage (Type I) and high voltage (Type II) machines. Type I machines are not likely to be subject to PDs, unlike Type II machines which are expected to operate in the presence of PDs.

Specifically, in the context of the railway sector, Type II machines with switching frequencies up to 5 kHz and dV/dt varying from 15 to 30 kV/µs must guarantee a system lifetime of around 40 years (or 200,000 hours). The question arises regarding the margin insulation systems in current equipment may have. It is thus necessary to determine whether phenomena, particularly partial discharges that did not previously exist or were not fully understood, will appear under normal operating conditions in machines with today’s transition towards SiC-based inverters, and more precisely in turn-to-turn, phase-to-ground, and phase-to-phase insulation systems.

The objective of this thesis is therefore to study the influence of the electrical stress imposed by inverters using SiC-based components on machine insulation and, more precisely, its impact on PD activity and aging over the longer term.

This thesis is the result of three years of work conducted within the “Aging” and “Partial Discharges” teams, and as part of the HIGHVOLT project, at the Saint Exupéry Institute of Research and Technology (IRT), Toulouse, France. Furthermore, our work here was developed under the care and supervision of the “Dielectrics Materials in Energy Conversion” team at the Laplace laboratory,

Toulouse, France, and the Electrotechnical Systems and Environment Laboratory (LSEE) in Béthune, France. Finally, this work was also carried out in close collaboration with ALSTOM and, more generally, with all of IRT's industrial partners.

This thesis is divided into four chapters. A brief description of each chapter is provided below.

Chapter I – State of the art

This first chapter describes the state of the art as evaluated in the early stages of this thesis work. Here, we present the general context as well as the major aspects of the topic, that is, the problem of static converters and electrical stress in machines, their influence in terms of partial discharges and, with a longer term perspective, their impact on insulation system aging. With aging mechanisms and reliability issues being of great interest in numerous areas of expertise, the state of the art is not in any way restricted to the railway sector, but rather covers electromechanical systems in general.

Chapter II – Electrical stress identification

The second chapter reports on a test campaign that performs thorough electrical stress mapping based on both geometric and electrical parameters to determine the electrical stress to which the machine is subject, and more precisely in turn-to-turn, phase-to-ground, and phase-to-phase insulation systems. The primary objective is to assess whether those constraints are significantly more stressful with SiC-based inverters with respect to conventional Si-based inverters. An analysis of the influence of various parameters on electrical stress along with partial discharge measurements are also provided.

Chapter III – Phenomenological study of PD activity and aging on Type I samples

This chapter pursues the findings of the previous chapter and presents an analysis of the impact of electrical stress on partial discharge features and aging. The different constituents of electrical stress are studied separately and a phenomenological approach that could explain their influence is presented. To help facilitate interpretation, the first step of the study is performed considering basic samples representative of Type I turn-to-turn insulation systems.

Chapter IV – Aging and underlying phenomena (Type II)

Finally, the fourth and final chapter establishes the link between the chapters II and III. It presents test results to reproduce the electrical constraints identified in the second chapter on more complex samples, representative of high voltage machine insulation systems in real environments. The purpose here is to both expand the results obtained for Type I machines to Type II machines, and to establish lifetime models and better understand the degradation of the insulation systems under stress.

Chapter I. State of the art

I.1 Background

I.1.1 General context

Reliability of insulation systems in electromechanical chains is a matter common to many domains, despite the various differences that can exist between them. Regardless of those differences, the consequences of low reliability are quite similar in each case and can vary from a simple insulation fault to the total breakdown of the insulation system, eventually leading to equipment failure. Issues and priorities may change, but the activities serve the same purpose: it is necessary to increase our knowledge about the phenomena responsible for aging, in order to ensure the reliability of electrical systems throughout their entire life cycle.

In the aeronautic industry, for example, the concept of "More Electrical Aircraft" was developed with a view to increase efficiency, reliability, maintainability, cost-effectiveness, and finally to rationalize the energy on board of aircraft by electrifying systems that today use hydraulic, pneumatic, or mechanical energy [1]. The higher power density of electrical equipment is intended to drastically reduce an aircraft's weight, as well as its fuel consumption and environmental footprint.

The emergence of this phenomenon leads to increasing demands for energy and therefore to a global increase of voltage levels, with the goal of generating and distributing more power without increasing cable weight or their section. These new voltage levels bring unknown phenomena to this industry that affect, among other things, electrical machines and, as a consequence, system reliability.

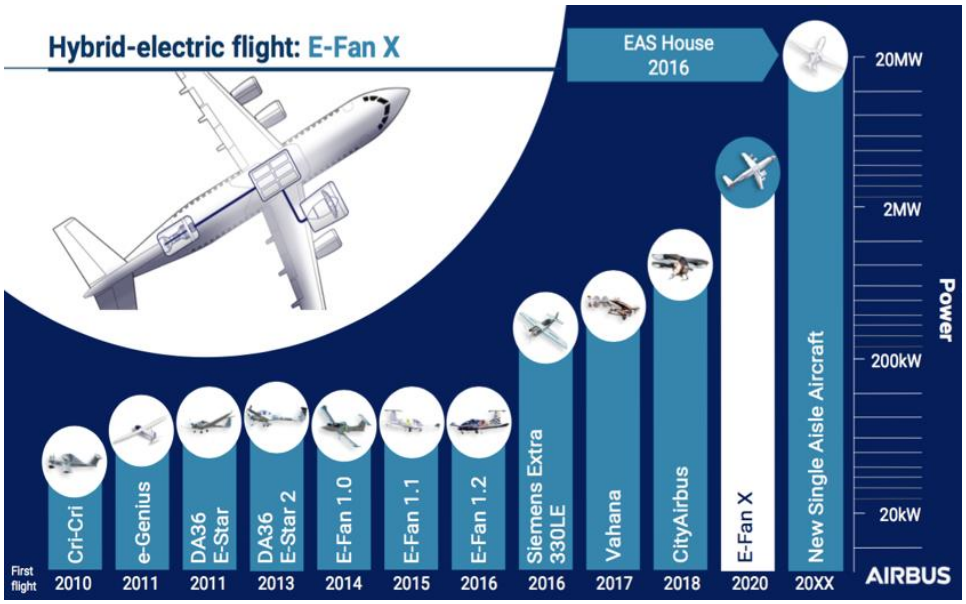

Figure I-1: *Electrical power evolution in aeronautics [2]*

At the same time, ecological concerns also play a major role in thinking about the vehicles of tomorrow. In recent years, the automotive industry has been pushed to find an alternative to replace internal combustion vehicles, which are responsible for emitting a large volume of greenhouse gases and fine particles. New solutions, such as hybrid and electrical vehicles, thus emerged to meet a growing and never-ending string of recommendations. However, while that type of vehicle can be competitive regarding urban traffic, their limited operating time and long battery recharging time, not to mention financial considerations, are non-negligible obstacles to their development. One research track consists of increasing the power density of motors while ensuring a lifetime long enough to enable the vehicle to be cost-effective. With vehicle lifetime being linked mainly to the insulation system lifetime, the automotive industry faces a problem similar to that of the aviation industry, despite different stakes and challenges: combined with the use of power components, higher voltage levels compromise reliability, and system aging must be studied and optimized in order to guarantee the required reliability.

The challenge of reliability, particularly through the aging and Partial Discharge (PD) phenomena, is thus a central common point in various areas of expertise, including automotive and aeronautics fields, as mentioned previously, but also railway. It turns out that rail transport, which is the primary context of the work presented here, is somewhat different from the other cases. More details regarding its specificities are presented below.

I.1.1 Specificities of rail transport

The railway sector is quite different from other fields. Notably, most railway traction systems in Europe are electrified and aging phenomena have even more impact because the level of stress imposed on equipment is much higher. Thus, with applied voltage regularly rising above the Partial Discharge Inception Voltage (PDIV), insulation systems are permanently subject to PDs and aging.

Table 1: *Electrical stress characteristics in rail transport compared to other fields*

Electrical constraints		
Aeronautics	Automotive	**Rail transport**
AC voltage: 97-134 V / 194-268 V DC voltage: 9-32 V / 220-320 V Frequency: 360-800 Hz Rise/fall time: 0.1 µs Voltage projection: > 1 to 3 kV	Batteries: 6-14 VDC HV batteries: 270-650 VDC AC voltage: around 400 V Frequency: 2-12 kHz Voltage projection: > 800 V	**AC voltage: up to 25 kV** **DC voltage: 750-3600 V** **Frequency: 100 Hz – 10 kHz** **Fundamental: up to 1 kHz** **dV/dt: 1-30 kV/µs** **Voltage projection: none**

Reliability is not a new area of focus. Numerous studies have already been performed on the topic. However, the introduction of new fast-switching components in static converters brings a new dimension to the problem of aging. Modern converters generate voltages with rise times between 50 ns and 2 µs. Furthermore, the voltage at motor terminals depends on multiple characteristics specific to inverter architecture, control, and interaction with other elements in the chain. All this makes the entire issue of reliability equally crucial in rail transport as it is in for automotive and aviation sectors, for example, but in separate context and for different reasons. In addition, in the today's context of global voltage increases mentioned previously, the specificities of rail transport can serve as a stepping stone and strong incentive to study the mechanisms involved in the aging of high voltage machines that will potentially be used to equip cars and airplanes of the future.

I.2 Partial discharge mechanisms

I.2.1 Partial discharge overview

A partial discharge (PD) is a fast and localized electrical discharge that only partially bridges the insulation material between a conductor's materials or electrodes. It does not lead to the immediate breakdown of the insulation system, but it contributes to degradation via its mechanical, thermal, and chemical effects when the electrical stress exceeds a critical value called partial discharge inception voltage (PDIV). PDs occur in residual air gaps within insulation systems. These cavities may be open or closed, but the physical phenomena are similar in both cases, as these cavities are often small in size and contain a gas, generally air [3][4].

Electrostatic laws explain that electrical fields are higher in gaseous cavities than in polymer, as polymer permittivity is greater than that of gas. The molecules inside a cavity are thus subject to a very intense electric field, which sets an initial electron, originating from cosmic radiation or already present for any other reason, into motion. This electron impacts the surrounding electrons belonging to electrically neutral molecules. When the field is high enough, electrons can be snatched from the molecules and, in turn, be set into motion by the electric field. Released electrons are likely to collide with other molecules and, above a certain threshold, cause an electronic avalanche. When those conditions are met, the gas inside the vacuole is ionized.

The Townsend mechanism bests represents the avalanche phenomenon, assuming a system with two parallel plane metallic electrodes, and considering a uniform electric field. Two coefficients are necessary to formalize the Townsend mechanism:

- The first Townsend coefficient, α, depicts the avalanche effect.
- The second Townsend coefficient, γ, depicts the secondary emission of electrons at the cathode.

The ionization process is characterized by the first Townsend coefficient, which represents the ratio of ionizing collisions per unit length. It is important to remember that only a fraction of the collisions

leads to ionization. The figure below illustrates the avalanche phenomenon: when an initial electron collides with a neutral molecule, the molecule will be ionized if the electron's kinetic energy is high enough. This ionization results in the release of a second electron and a charged particle (ion). In turn, the two electrons are accelerated and will ionize two other molecules, and so on.

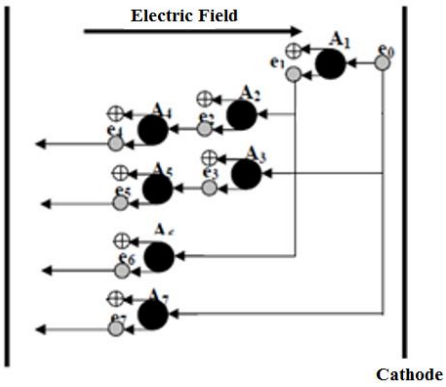

Figure I-2: *Diagram depicting the electron avalanche process*

The first Townsend coefficient can be expressed in a variety of ways, including the following:

$$\frac{\alpha}{P} = Ae^{\left(-\frac{B}{E/P}\right)} \quad (1)$$

Here, E is the electric field in $V.cm^{-1}$; P the pressure in torr; A and B, respectively in $(torr^{-1}.cm^{-1})$ and in $(V.torr^{-1}.cm^{-1})$, two constants depending on the gas. This equation expresses the ionization coefficient in a way that is only dependent on the electrical field/pressure ratio. This simplification is often used because pressure is a parameter that does not usually modify the other parameters in the problem and is an easily measurable macroscopic parameter.

The discharge thus created by the ionization process is called "non-sustaining discharge". It can become a self-sustaining discharge only if secondary effects complement the initial ionization. When all electrons are collected at the anode, the remaining positive ions between the electrodes move towards the cathode. If these ions have enough energy to pull some electrons from the cathode, a new avalanche develops. The second Townsend coefficient thus characterizes these secondary phenomena and represents the number of electrons snatched at the cathode by positive ions. The self-sustaining discharge condition for a distance d is therefore expressed as follows:

$$\gamma(e^{\alpha d} - 1) \geq 1 \quad (2)$$

If this condition is not met, the discharge stops because the number of electrons created by secondary emission does not compensate the electrons absorbed at the cathode. The secondary emission coefficient depends on the characteristics of the material at the cathode, the gas, and also the electric field. From equations (1) and (2), and by introducing the uniform field hypothesis, we can obtain the relationship between the voltage across the electrodes and the pressure-distance product:

$$V = \frac{BPd}{\ln\left(\frac{APd}{\ln\left(1+\frac{1}{\gamma}\right)}\right)} \quad (3)$$

Called Paschen's law [5], this equation expresses the minimum voltage from which a self-sustaining discharge can appear depending on the pressure-distance product. The graph of this equation is referred to as the Paschen curve, in which the horizontal axis represents the Pd product, and the vertical axis represents the discharge ignition voltage. The minimum Paschen value can be found by deriving this law with respect to Pd and setting the derivative to zero. If the voltage is lower than this value, for a given pressure-distance product, no discharge can occur. Depending on the values of parameters A, B and γ, this value is about 320 V in air at standard atmospheric pressure and at a distance of 7.5 µm. Figure I-3 shows the Paschen curves obtained for different gases.

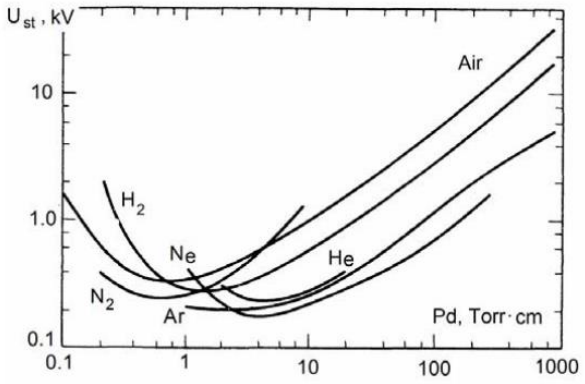

Figure I-3*: Paschen curves for different gases [6]*

I.2.2 Type and location of PDs

In order to address the problem of PD type and location, it is more convenient to distinguish two study perimeters: at the insulation scale, and at the machine scale. In a very general way, considering an electrical insulation system, there are four main types of partial discharge locations: internal, surface, corona, and treeing discharges [7]. (Figure I-4)

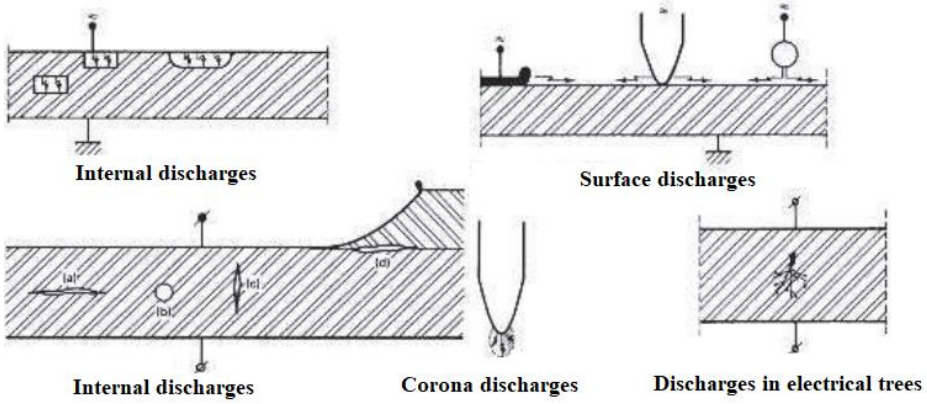

Figure I-4: *Partial discharge types and locations [4]*

Discharges occurring within short gaps or small diameter cavities, such as those occluded within insulating systems in power devices and cables, may be characterized by different forms of current or voltage pulses. The discharge pulses in such gaps can be classified into two categories: Townsend-type and streamer-like discharges. The former are characterized by a lower intensity and longer width, whereas the latter are relatively narrow pulses with more rapid rise times and much higher amplitudes.

In turn, three types of discharges may be distinguished among Townsend-type discharges. In a *spark-type discharge*, the breakdown proceeds along a relatively narrow channel bridging the gap. In contradistinction to the aforementioned spark- or pulse-type discharges, *pulseless or true glow discharges* occur over a widely diffused area that may encompass the entire electrode surface. They are a discharge in which expansion of the discharge channel takes place, leading to relatively low electron densities within the diffused discharge region. Finally, the *pseudoglow discharge* represents a transitory condition between a true glow discharge and a spark discharge in that it possesses features common to both spark and glow type discharges. Visually, they exhibit a diffused glow within the intervening gap space. The typical voltage waveforms across a helium gap associated to these different types of discharges are shown below.

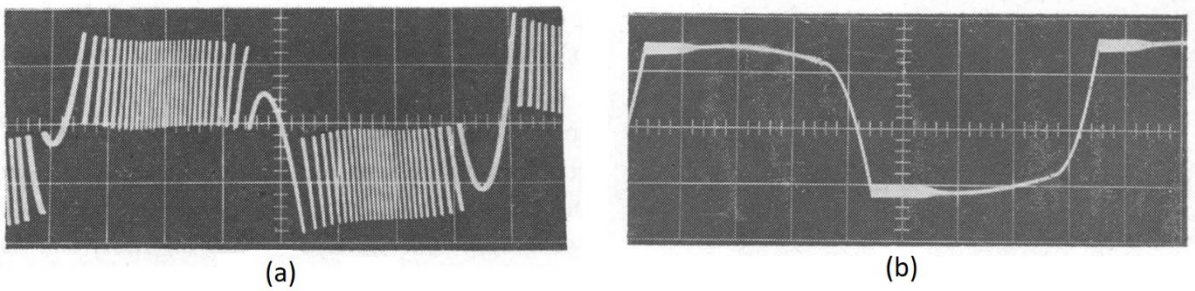

Figure I-5: *Typical voltage waveform across a helium gap: (a) under pulse discharge conditions (scale: 2 ms/div, 0.278 kV/div, gap length: 3 mm, pressure: 760 torr, applied voltage: 15 kV), and (b) with pseudoglow and true glow regions (scale: 2 ms/div, 0.139 kV/div, gap length: 0.6 mm, pressure: 760 torr, applied voltage: 5kV) [8]*

In turn, the different character of the discharges affects the response of conventional partial discharge pulse detectors, which is contingent upon both the pulse shape and its rise time. In addition, discharges that take on a pulseless glow or pseudoglow form may evade detection entirely by the pulse sensing circuit.

At the machine scale, when windings are subject to large voltage magnitudes, very high electrical stresses are created at the following locations:

- Between conductors of different phases
- Between one of the conductors and the ground
- Between adjacent turns

Depending on the voltage levels to which the machines are subject, insulation systems may not be designed to withstand PDs, or they may be brought by nature to operate with their presence. Moreover, insulation systems are not perfect and may present defects of their own, such as lack of impregnation. Misplacement and deterioration of insulation systems can also create defects. Finally, there may be areas where the electrical field, and thus electrical stress, is locally higher. These phenomena can lead all or part of the machine to be subject to PDs. Figure I-6 demonstrates two PD sites.

Figure I-6: *Manifestation of glow PDs in end-winding and probably between phases (left) and in the stator slot (right) [9]*

PDs constitute one of the main degradation mechanisms in insulation systems and therefore in electrical machines. Other factors of a different nature may exist, but they are always closely linked to PD phenomena. These other factors are detailed in Section I.5.2.

I.2.3 PD detection

Partial discharge measurement allows the detection of insulation defects in various electric power devices before an insulation failure occurs. It can also help improve the insulation performance reliability of devices, and support rational and economical design, lifetime prediction, and nondestructive inspection. Measurement is not only a way to ensure that the working environment is PD-free (Type I applications), but it is also a diagnosis tool studying and monitoring the degradation of insulation systems in machines or systems operating in the presence of PDs (Type II) [10][11]. Historically speaking, PD detection has evolved in each device and power cable category. Various detection methods exist, with the main ones as follows: [12][13]

- **Electrical detection** seeks to measure the pulse current generated by PDs. Based on the fact that an electron current flow is created at each partial discharge event, a current could be measured, with the total current depending on the number of charges transported by the partial discharge. Partial discharge currents tend to be short in duration, with rise times in the nanosecond realm. These current flows create voltage pulses across the impedance of the insulation system, which can then be measured by conventional electrical sensors.

- **Electromagnetic measurement** consists of measuring the high frequency electromagnetic waves generated by PDs and propagating away from the discharge location site in the gaseous medium. The discharge spectrum ranges from a few hundred kHz to several hundred MHz. With a suitable antenna, it is thus possible to detect PDs and obtain information regarding the magnitude of the discharge and its generation point.
- **Optical detection** is based on the fact that partial discharges also dissipate energy in the form of light. Measuring the light generated from the discharge with an adequate device, such as a photomultiplier, thus makes it possible to evaluate the discharge characteristics and provides another way of detecting and locating PDs.
- Finally, the mechanical vibration and sound generated by partial discharges can be converted and detected by means of **acoustic measurement methods.**

There is no universality in PD detection technology that is available to all kinds of power equipment. The choice of a detection method must take into account the nature of the detection (on-line/off-line), equipment structure, surrounding noise, similarities and differences among PD detection technologies and signal processing, as well as the desired criteria for equipment analysis. Furthermore, discharges that exhibit a glow or pseudo-glow character could fail to excite the response of conventional pulse-type discharge. In practical terms, this means that the detection device choice also depends on the discharge type. In that respect, electrical and electromagnetic devices are more suited for detecting spark-type discharges, whereas optical or acoustic detection methods are preferred in the case of glow or pseudoglow discharges.

PDs and their features are heavily influenced by voltage signal characteristics, which can cause modifications in terms of the electrical field and also affect detection. It is thus necessary to take those characteristics into account and define the extent to which the voltage shape used to supply the machine could be an aggravating factor. Investigations on voltage shapes induced by static converters will be covered in the following sections.

I.3 Electromechanical chain

I.3.1 Standard electromechanical chain structure

The electromechanical chain is the overall system for converting electrical energy into mechanical energy. In the rail transport context, the electromechanical chain is the traction chain. The chain structure comprises the same elements regardless of the application, namely a source, static converter, cable network, actuator, and load put into motion by the actuator.

The electromechanical chain aims to receive, convert, and distribute the electrical energy. The input voltage type and level vary depending on the grid. It is thus necessary to adapt voltage in order to supply the equipment.

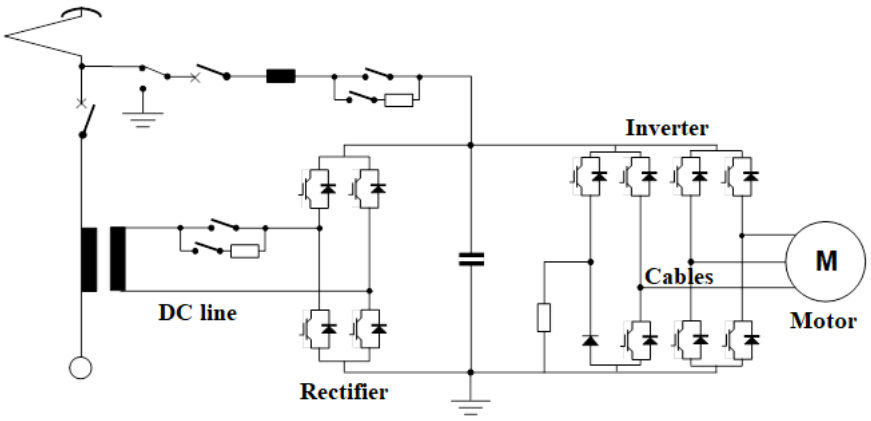

Figure I-7: *Schematic drawing of a railway traction system (load not represented)*

A converter (generally an inverter) converts the DC bus voltage from the grid into a voltage that can be used by the actuator. Converters use power electronic components such as Silicon-based IGBTs (Insulated Gate Bipolar Transistors), which have been the benchmark in terms of controlled switches for several decades. However, wide bandgap components such as SiC (Silicon Carbide) and GaN (Gallium Nitride)-based components are gradually replacing those technologies, mainly thanks to their fast rise and fall times which considerably reduce switching losses. Inverters are usually controlled using the Pulse Width Modulation (PWM) technique. The PWM operating principle will be reviewed in the next section.

Cables make the connection between the inverter output and the machine input in order to transport the electrical energy. Adverse effects related to cable length, nature, and disposition can occur and must be taken into account or suppressed to ensure proper machine operation.

The motor is the energy conversion element. There are several types of actuators depending on the application. In aeronautics or automotive applications, for example, permanent magnet synchronous machines, which ensure high power density, are preferred; whereas asynchronous motors might often be used in rail transport.

Finally, **filters** can be placed at the inverter input or output. Filters can be convenient for various functional reasons or to meet specific standards.

I.3.2 Type I/Type II machines: what is the difference?

Rather than differentiate machines by sector and by application, it is far more convenient to distinguish them according to their operating voltage. The IEC 60034-18-41 [14] and 60034-18-42 [15] standards address this problem by proposing classification into two categories: Type I and Type II machines, depending on whether they are intended to operate with (Type II) or without (Type I) PDs at

any point in the insulation system. Type I insulation systems are commonly used in low voltage rotating machines (< 700V) and are composed of random-wound coils. If any part of the insulation system is likely to undergo PDs during its life cycle, the system is defined as a Type II insulation system, and subsequently it must be comprised of PD-resistant materials. Machines with a nominal voltage higher than 700V generally use Type II insulation systems [16].

This classification thus enables us to treat low voltage and high voltage machines differently. Even if aging mechanisms are the same or very similar (which is not fully guaranteed), insulation systems are not supposed to present the same behavior in the presence of PDs. Furthermore, low voltage machines generally use random-wound coils, whereas high voltage machines use formed-wound coils. In random-wound coils, the conductor insulation is quite thin and often surrounded by air. It may also happen that the first and last turn of a coil are adjacent to each other, leading to an increased probability of PD inception, particularly between turns, if the voltage is high enough. The erosion caused by PDs may cause unnecessary damage to the insulation system; it is therefore crucial to ensure that no PDs can occur.

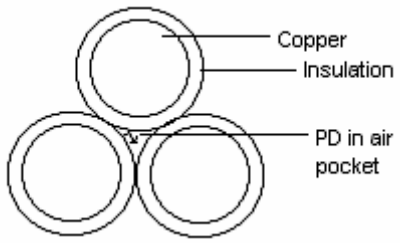

Figure I-8: *Illustration of partial discharge in air between several conductors under high stress [16]*

In the case of Type II machines, insulation systems are reinforced with materials that are highly resistant to erosion caused by PDs. They can therefore operate in the presence of PDs; aging is not eliminated, but it is slowed considerably.

The choice of insulating materials is an important issue when designing and constructing a machine. It is thus particularly important to characterize the mechanisms associated with PDs in order to select the most appropriate insulation system. Because of the wide variety of available insulating materials, it is appropriate to review the main types of insulation typically used in machines.

I.3.3 Insulation system state of the art

In the previous section, we presented the distinction between Type I and Type II insulation systems. It is important to point out that when the operating voltage of a machine is below 700V, it may include both Type I and Type II insulation systems. However, Type II insulation systems are required for machines with an RMS voltage value beyond 700V.

Electrical insulation systems are divided into several temperature classes which specify the insulation withstand, and which are defined according to tests described in the IEC 60085 standard. It

should be noted that other organizations such as NEMA define the same type of standards. These thermal indexes correspond to the maximal temperature for which a material can be used for at least 20,000 hours without reaching a pre-established end of life criteria. Table 2 presents the existing classes and the associated temperature ranges according to IEC 60085 and NEMA standards.

Table 2: *Definition of thermal classes according to IEC 60085 (1) and NEMA (2)*

Relative thermal endurance index (°C)	Thermal class (°C)	Designation
90 ≤ to < 105	90	Y (1)
105 ≤ to < 120	105	A (1)
120 ≤ to < 130	120	E (1)
130 ≤ to < 155	130	B (1)
155 ≤ to < 180	155	F (1)
180 ≤ to < 200	180	H (1)
200 ≤ to < 220	200	N (2)
220 ≤ to < 250	220	R (2)

The insulation systems typically used in both types of machines, as well as their descriptions depending on their location, are given below [6].

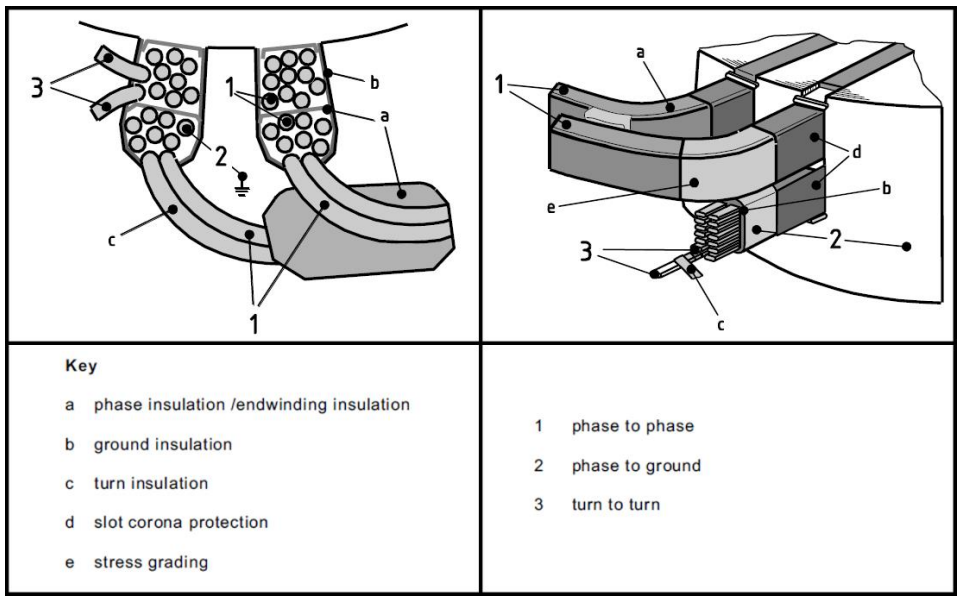

Figure I-9: *Random-wound (left) and formed-wound (right) design examples [15]*

I.3.3.1 Type I insulation systems

Figure I-10 shows the insulation systems commonly used in a three-phase random-wound low voltage machine (Type I). Conductors are usually insulated with a high temperature enamel, whereas phase-to-ground and phase-to-phase insulations are comprised of aramid paper (Nomex), Nomex-Mylar-Nomex, or any other class F or higher insulation materials.

Enameled wire, which is widely used to build the windings of Type I electrical machines, generally features two insulation layers. The first layer, which is in contact with copper, is a polymer of the polyester imide (PEI) family and ensures good adherence to copper. The external layer consists of a polyamide imide (PAI) material that provides good mechanical properties for the overall structure. This type of enameled wire has been used widely for many years and meets the numerous mechanical, thermal, and electrical requirements of most electrical motors. The overall thickness of the insulation system depends on wire diameter and varies between 30 and 60 µm.

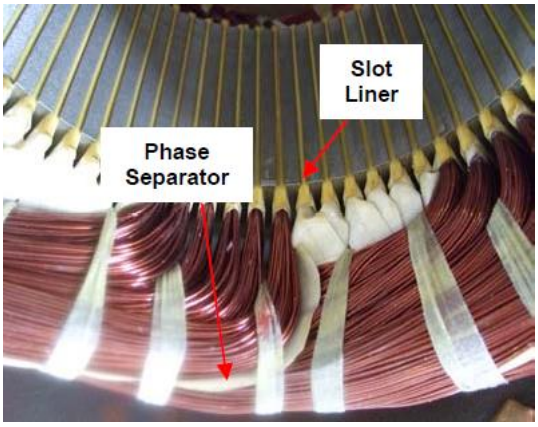

Figure I-10: *Insulation materials in the stator windings of a random-wound machine [16]*

The impregnation process can also provide complementary insulation. The initial purpose of such a process is to replace the potential air gaps in the insulation material by an impregnation liquid (generally resin or coating) that is cured afterwards in order to improve the structure's heat transfer, resistance, and mechanical strength.

I.3.3.2 Type II insulation systems

It is far more complex to manufacture a formed-wound stator winding and its insulation system. The different functions of the various insulation systems are detailed below.

Strand insulation aims to improve the machine's efficiency by reducing eddy current and skin effect losses. This insulation is typically a film coating applied on the magnet wire and/or as a Dacron glass served filament. In some applications, a polyimide tape such as Kapton can also be used.

Turn-to-turn insulation isolates the copper turns from each other. In modern motors, turn insulation is usually a Dacron and glass composite or mica paper. Sometimes, no dedicated turn insulation is used and strand insulation fulfills both functions.

Phase-to-ground and phase-to-phase insulations separate the copper conductors from the grounded stator core on one hand, and two different phases that can be present in a same slot on the other hand. Almost all motor stators use mica paper tape bonded together with epoxy as the ground wall insulation. These materials are almost always combined using the global vacuum pressure impregnation

(GVPI) process. There is usually no additional phase-to-phase insulation, as there are already two thicknesses of ground insulation present between phases.

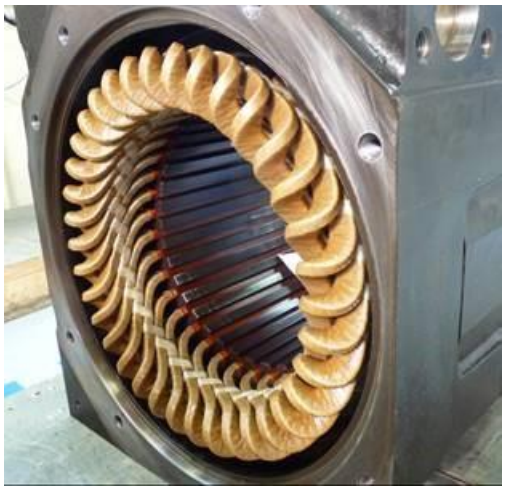

Figure I-11: *Insulation materials in the stator windings of a formed-wound machine*

Complementary insulation systems may exist for some applications. **A partly conductive paint or tape** sometimes covers the surface of the phase-to-ground insulation in both the stator slot area and a few centimeters beyond each end of the core. This coating prevents PDs that could occur in air gaps between the surface of the ground wall insulation and the sides of the stator slots. It is generally used only for a rated operation voltage of 3 kV or more. Finally, **a stress relief paint or tape** can also be used to overlap the slot conductive coating outside the slot, extending a few centimeters into the end winding. This coating linearizes electric stress along the surface of the coil at the end of the slot conductive coating, thus reducing the risk of PDs. The coating is often made of silicon carbide powder within tape. This additional insulation system is most often applied to motors rated for 6 kV or more.

I.3.3.3 Corona-resistant insulation systems

Dielectric materials used as insulators for electrical conductors may fail as a result of PDs occurring when the conductors and dielectrics are subject to voltages above the PDIV. PD-induced failure is particularly likely when the insulator material is a solid organic polymer. It has been shown that for some applications, such as railway, mica-based insulation systems are used as a solution to the problem, where the mica offers PD resistance. However, because of the poor physical properties inherent to mica, this solution is not ideal and cannot be transferred easily to other areas.

In this context, collaborative studies with the industry led to the development of polymers that are more resistant to the erosion caused by PDs. The term “corona-resistant” is used in literature [17]. These new materials are obtained by adding inorganic parts such as mica or glass to the insulation systems, as they are much harder than polymers and insensitive to the photon emission and ionic bombardment associated with PDs. Inorganic materials are added in powder form at the microscopic or nano scale

[18][19]. The quality of the insulation layers depends on the distribution of these micro or nanoparticles in the polymers. It is particularly challenging to obtain a uniform mixture before polymerization, especially when the inorganic powders are at the nano scale, notably because nanoparticles have high surface energy and naturally tend to form agglomerates or aggregates.

The resulting corona-resistant materials effectively prevent PD degradation of insulation leading to motor failure in normal use. Besides, the glass or mica composite occupies space in the core which otherwise could accommodate additional copper and thereby reduce the size of the motor.

I.4 About electrical stress in machines

I.4.1 Static converters and PWM-like signals

For several reasons, notably to minimize losses, it is necessary for the current flowing through the windings of an electrical machine to have a sinusoidal shape. Generally, this is possible only if the voltage signal also is sinusoidal. In the past, it was standard practice to use direct current machines for applications requiring variable speed control. Indeed, by varying voltage, it is possible to modify rotation speed accordingly. AC motors were only used for applications requiring fixed speed.

Today, generating sinusoidal signals for powering machines has become widespread and is now a reference for many reasons, including improved cost-efficiency and greater efficiency. Moreover, the harmonic content of such machines must be controlled in order to meet specified standards. Furthermore, a sinusoidal current shape makes it possible to rephase the voltage and current signals to reach a unity power factor if necessary.

In order to generate such sinusoidal signals, semiconductor components are used in association with the Pulse Width Modulation (PWM) strategy at very high switching frequencies. Speed variation is thus achieved via an inverter that generates high frequency voltage impulses with variable width at each phase in order to reconstruct a signal with varying fundamental frequency at the motor terminals, while rejecting harmonic content. The rise times associated with semiconductor components as they exist today are about a few hundreds of nanoseconds [20].

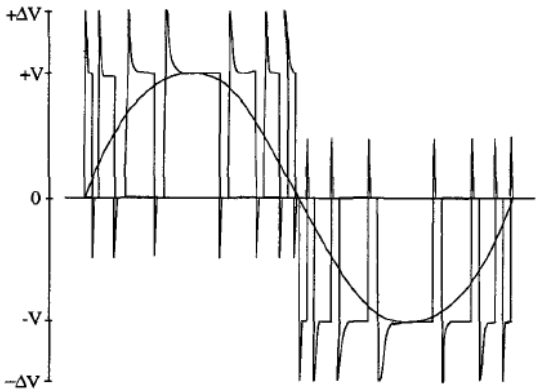

Figure I-12: *Example of a phase-to-phase voltage shape generated by a PWM inverter [9]*

Therefore, static converters controlled by PWM generate steep voltage slopes that create high frequency oscillatory behaviors in machine windings. It is thus necessary to characterize those undesirable phenomena, which result in previously nonexistent dysfunctions that may affect system reliability.

Pulse width modulation is a method for controlling the average power delivered by an electrical signal by effectively slicing it up into discrete parts. Consequently, an inverter using this control method is a voltage source whose magnitude, frequency, and "shape" are controllable. Due to its structure composed of two bidirectional switching cells, the voltage inverter is reversible on the condition that this is also the case for the DC source. For most applications, the idea is to generate a sinusoidal current waveform. The rate (or frequency) at which the power supply must switch, as well as the necessity to add or not add a filtering device, can vary greatly depending on the load and application. Several types of PWM control strategies exist [21]; the choice of a strategy is mainly dependent on the supply voltage, frequency, rotation speed of the motor, and above all, the user requirements regarding harmonic content suppression, torque ripple, loss management and, more broadly, desired performance.

The simplest way to generate a PWM signal is the intersective method, which requires only a saw tooth (or a triangular) waveform (easily generated using a simple oscillator) and a comparator. When the value of the reference signal is greater than the modulation waveform, the PWM signal is in the high state; otherwise it is in the low state. The triangular waveform determines switching frequency. Several techniques exist, depending on whether the triangular waveform is symmetrical, and whether the reference signal is sampled or not. Figure I-13 shows a three-phase sampled PWM with a symmetrical triangular waveform. Only two modulation functions and the resulting modulation are represented.

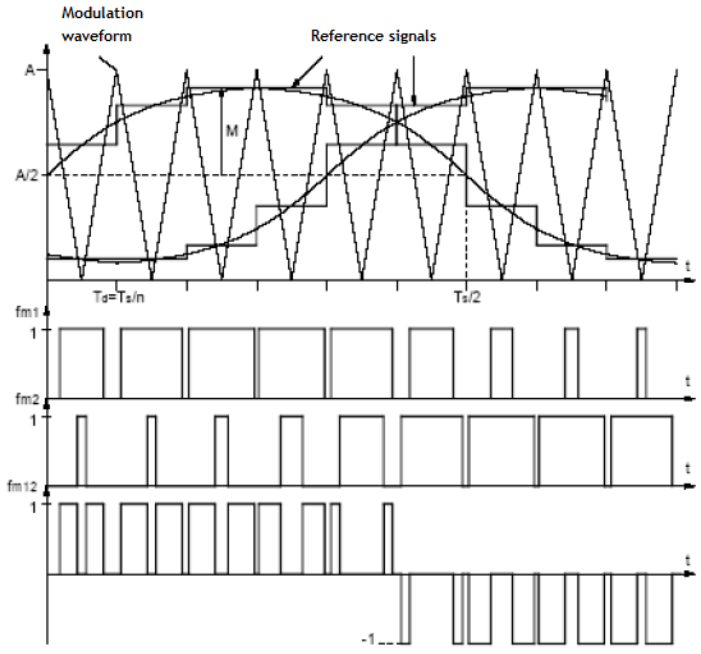

Figure I-13: *Example of intersective PWM for one phase of a 3-phase inverter [21]*

There are several subtypes of intersective PWMs, depending on whether they are synchronous or asynchronous, analog or digital or even depending on the symmetry of the triangular waveform; for the sake of brevity, those subcategories will not be detailed here [22] [23].

Along with these two main types of PWM control, several other types of methods exist and are used for controlling electrical machines. **SVM (Space Vector Modulation)** is one of the most efficient advanced methods of modulation, in particular for applications with variable frequency. Its use has gradually increased in recent years due to its robust performance. Numerous types of SVM exist, and the differences between them mainly lie in their quality and implementation requirements. The main interest of this kind of strategy is the reduction of total harmonic distortion (THD) associated with fast switching of the PWM. In **delta modulation**, the output signal is integrated and the result is compared to limits, which correspond to a reference signal offset by a constant. Every time the integral of the output signal reaches one of the limits, the PWM signal changes state. In **delta-sigma modulation**, the output signal is subtracted from a reference signal to form an error signal and the output changes state when the integral of the error exceeds the limits. **Direct torque control** is a method used to control AC motors. It is closely related with delta modulation. Motor torque and magnetic flux are estimated and then controlled to stay within their hysteresis bands by turning on a new combination of the device's semiconductor switches each time either of the signals tries to deviate outside the band. The **pre-calculated PWM method** consists of pre-calculating switching moments of power semiconductor modules to suppress specified harmonics in the inverter output voltage. Finally, a direct **full-wave command** can be used in some applications and under specific conditions, generally to take full advantage of available voltage while avoiding or minimizing inverter losses.

I.4.2 Impact of using PWM control

Numerous studies have been performed on electrical machines supplied by static converters [24] [25] [10]. In most cases, the studies tend to show a drastic rise of the failure rate coinciding with the presence of pulse signals with increasingly fast rise times and switching frequencies. The accelerated degradation of insulation systems, and as a result that of machines, is thus a direct consequence of the use of such signals generated by PWM commands. This section presents the main impact of PWM control on voltage stress and, in turn, on a machine’s insulation systems.

I.4.2.1 Rising edges and non-linear voltage distribution

Low voltage electrical machines, as highlighted above, often consist of random-wound coils whose turns can be raised to vastly different potentials during the transitional regime following the voltage rising edge. Given that the exact position of these turns in the slots is relatively random, there is a chance

for the first and last turn to be adjacent to each other. The probability to be in such an extremely unfavorable situation, with high potential differences between turns, is non-negligible.

Figure I-14 is the result of a statistical study [26] carried out on a slot containing 41 wires ordered in successive layers from the end of the slot. This extremely favorable case is very unlikely to occur. In order to calculate the probability of adjacency, a very large number of equiprobable selections of wire distribution in the slot are realized according to the Monte-Carlo method. The right-hand side of the figure shows the geometrical analysis of all the adjacencies for the purpose of determining the maximum turn number difference between two conductors at any point of the slot.

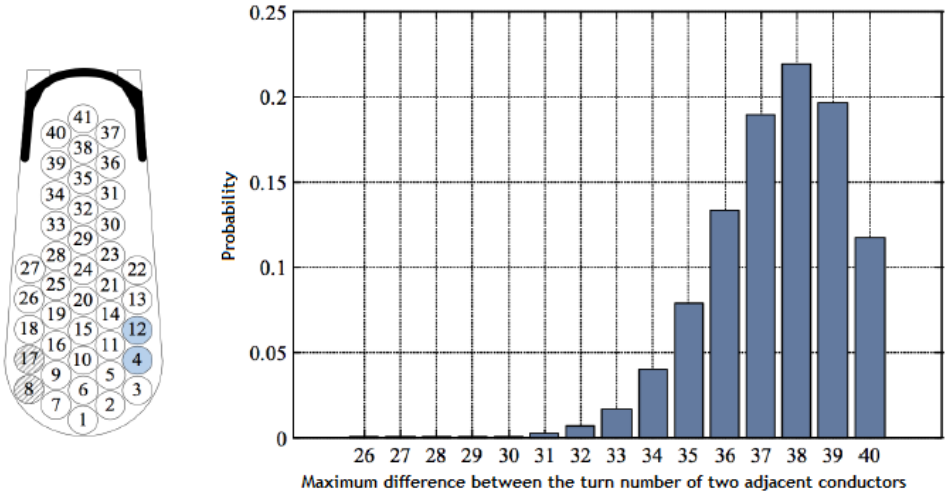

Figure I-14: *Cross-sectional view of the slot and adjacency likelihood vs turn number difference [27]*

The above graph shows that the probability of having the input conductor next to the output conductor is about 12%. It is thus necessary to ensure that the turn-to-turn insulation is able to bear the total voltage at the coil terminals.

In addition, when the machine undergoes very steep voltage slopes, the voltage distribution in the coils can no longer be considered as linear. Characterizing these high frequency effects is complex and must take into account all the parasitic effects related to these switching edges. A number of approaches can be adopted, such as the equivalent circuit method or the Multiconductor Transmission Line (MTL) theory; all these methods are based on rewriting Maxwell's equations to take parasitic elements into account [28]. The latter (capacitance, inductance, resistance, and conductance) are most often calculated using finite element computation and integrated into numerical models of the machine. In substance, it is shown that the rising edges are less steep as the voltage propagates in the coil. The slope is thus slowed and the oscillations following the maximum voltage tend to mitigate. Hence, the voltages in the windings are distributed and handled by complex transitory regimes, especially when the relative position of each turn is unknown.

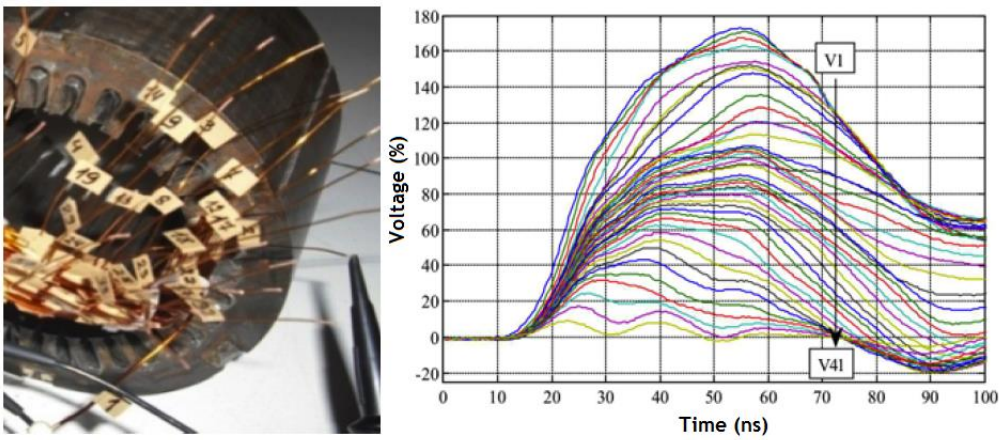

Figure I-15: *Voltage distribution in the 41 turns of a coil [26]*

I.4.2.2 Overvoltages

The fast voltage slopes transiting through the inverter, cables, and machine can also cause overvoltage phenomena. These overvoltages should not exist in the first place, and the insulation systems are not always designed to cope with those types of stress. The wave reflection phenomenon is the main mechanism that comes into play in creating these voltage surges. To illustrate the exact meaning, a drawing of an entire electromechanical chain, including the parasitic electrical elements of the circuit, is given below.

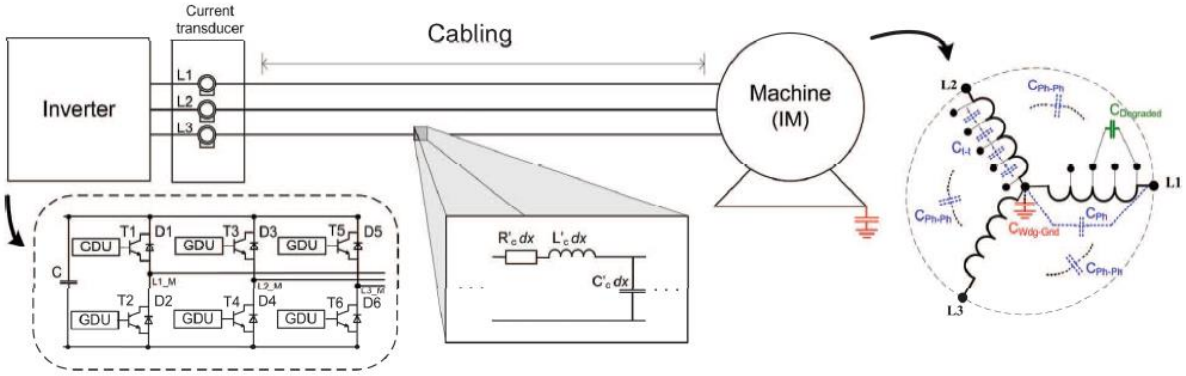

Figure I-16: *Complete electromechanical chain including parasitic elements [29]*

The three main elements of the system are represented above: inverter, cables, and machine. The inverter configuration is quite standard and comprised of three legs whose switching elements are controlled individually. The series of cables is represented by a resistance, inductance, and capacitance per unit length. Lastly, regarding the motor, in addition to the fundamental parameters – stator resistance and inductance – there are also parasitic parameters in the stator windings that are essentially capacitances between turns, between phases, and between phase and ground. These parameters characterize the high frequency behavior of the system and have an influence on overvoltages at the motor terminals [29].

While the phenomena are considered to be very fast, the equivalent impedance of the converter is very low compared to that of the cable, the latter itself being very low compared to that of the motor for high frequencies that are likely to cause resonance. This impedance mismatch between the three elements leads to reflection phenomena at both ends of the cable whose consequences depend mainly on cable geometry and length.

Based on the reflection coefficients, the incident wave propagates through the cables towards the machine and is reflected with the same magnitude and the same polarity. Similarly, the reflected wave is reflected again towards the machine, still with the same amplitude but an opposite sign. In the figure below, the voltage wave transits four times during one oscillation period ($T_{osc} = \frac{4l}{v}$ with l being the cable length, and v the wave propagation speed determined with the capacitance and inductance per unit length defined above).

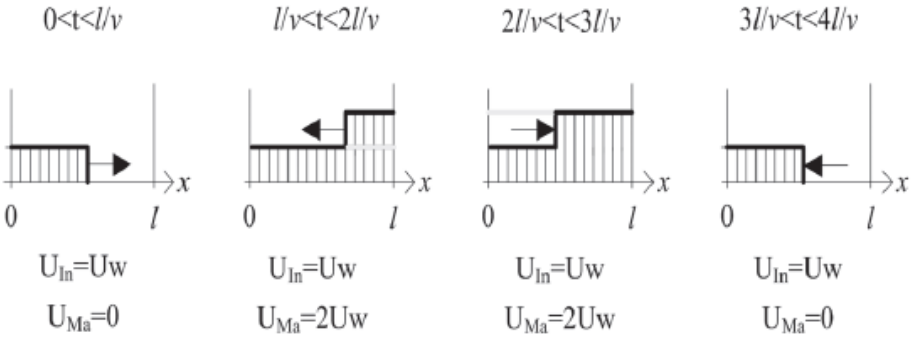

Figure I-17: *Wave propagation through a cable [29]*

Overvoltages resulting from these different wave reflection phenomena can be as high as the DC bus voltage at the inverter input. As a consequence, according to this theory, the total voltage at the motor terminals can reach up to twice the DC bus voltage. The magnitude of these overvoltages is highly dependent on cable length and voltage rise time. An example of voltage measured at coil terminals supplied by a fast-switching inverter is given below.

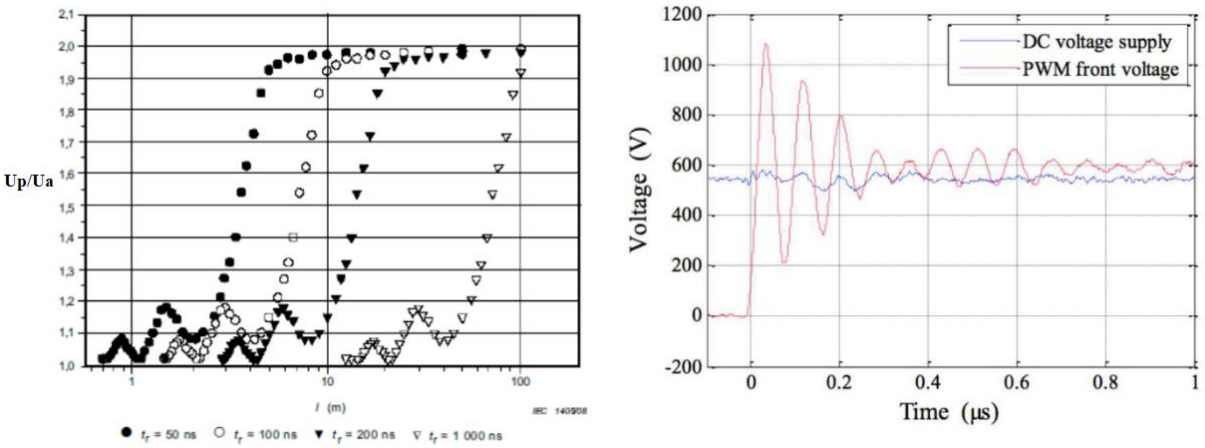

Figure I-18: *Overvoltage magnitude vs cable length depending on rise time (left) & voltage measured at the terminals of a coil supplied by a fast-switching inverter (right)[15][26]*

The main impact of this overvoltage increase in terms of amplitude, frequency, non-linearity, and rising edge, is an increase of PD activity [30][31]. A general review of the harmful effects linked to such phenomena and depending on voltage shape, among other things, is detailed in Paragraph I.5, which is exclusively dedicated to the aging of insulation systems.

I.4.2.3 PD measurement under PWM signals

PD detection is a particularly tricky problem when it must be performed in presence of very fast rise and fall times, such as those imposed by Si IGBT (Insulated Gate Bipolar Transistor) or SiC MOSFET (Metal Oxide Semiconductor Field Effect Transistor) switches. Under such operational conditions, it is crucial to select the most adequate detection tool to be able to detect PDs as effectively as possible.

The efficiency of most PD detection methods has been proven for DC or sinusoidal input voltages [32][33]. Concerning impulse voltage, however, the detection – particularly electrical detection – becomes far more complex due to switching noise. Indeed, the noise generated by power component switching tends to overlap with PD signals, which mainly occur at maximum voltage, *i.e.* during the rising and falling edges (Figure I-19).

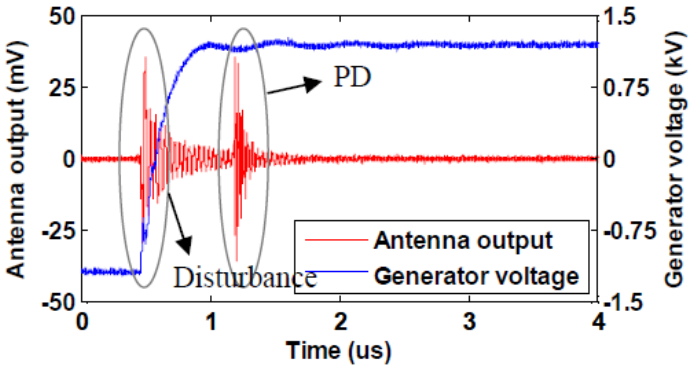

Figure I-19: *Overlap between PD signal and switching noise induced by an Si IGBT based inverter [34]*

Thus, the purpose of PD detection under PWM is to optimize the Signal to Noise Ratio (SNR), that is, to detect and differentiate PDs from the surrounding noise. The frequency spectrum of PDs extends into frequencies up to the GHz range, while switching noise is restricted to frequencies of only a few hundred MHz. Filtering therefore offers a viable solution for detecting PDs, provided that the cutoff frequency of the filter is adapted to the case being studied so that no PD information is lost.

As a complement to this method, other software or hardware denoising techniques, such as wavelet transform, provide excellent results and help identify PDs in the harsh conditions imposed by PWM signals [9].

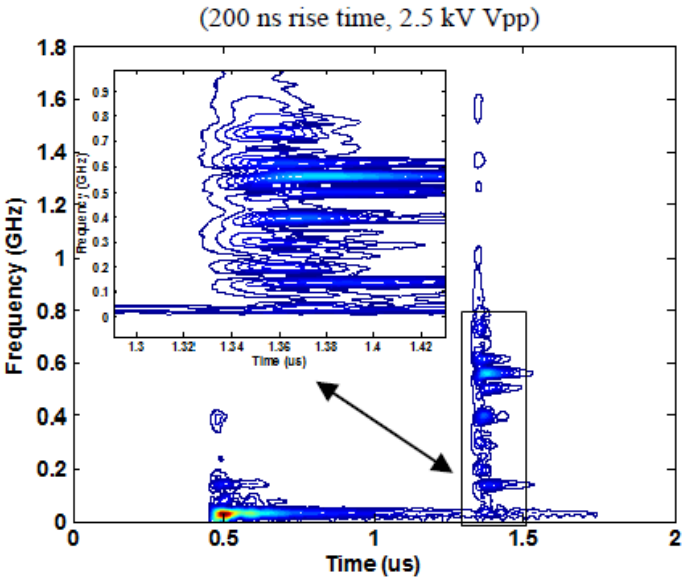

Figure I-20: *Frequency spectrum of the PD signal obtained with Fast Fourier Transform (FFT)[34]*

I.4.3 SiC introduction and consequences

High frequency and high voltage generators are increasingly being used in industry for various applications. The technical requirements originating from different industrial sectors, namely high power density as well as fast switching speeds for both low voltage and high voltage systems, are pushing designers to develop new solutions to satisfy these performance criteria.

Up to this point, silicon-based MOSFET transistors have been used in low power applications for switching frequencies up to 200 kHz. For high power applications, silicon-based IGBTs have been favored for a frequency operating range up to a few kHz. However, disruptive technologies emerging over recent years such as wide bandgap components, especially silicon carbide (SiC) components, appear to be the most promising alternatives to conventional silicon-based components for high frequency applications [35][36]. These technologies allow us to increase switching frequency with significant filter reduction and/or decreasing semiconductor losses, thus leading to increased reliability and reduced maintenance costs for converters. Figure I-21 shows a synthetic dV/dt and dI/dt comparison between 3.3 kV Si IGBT and SiC MOSFET technologies.

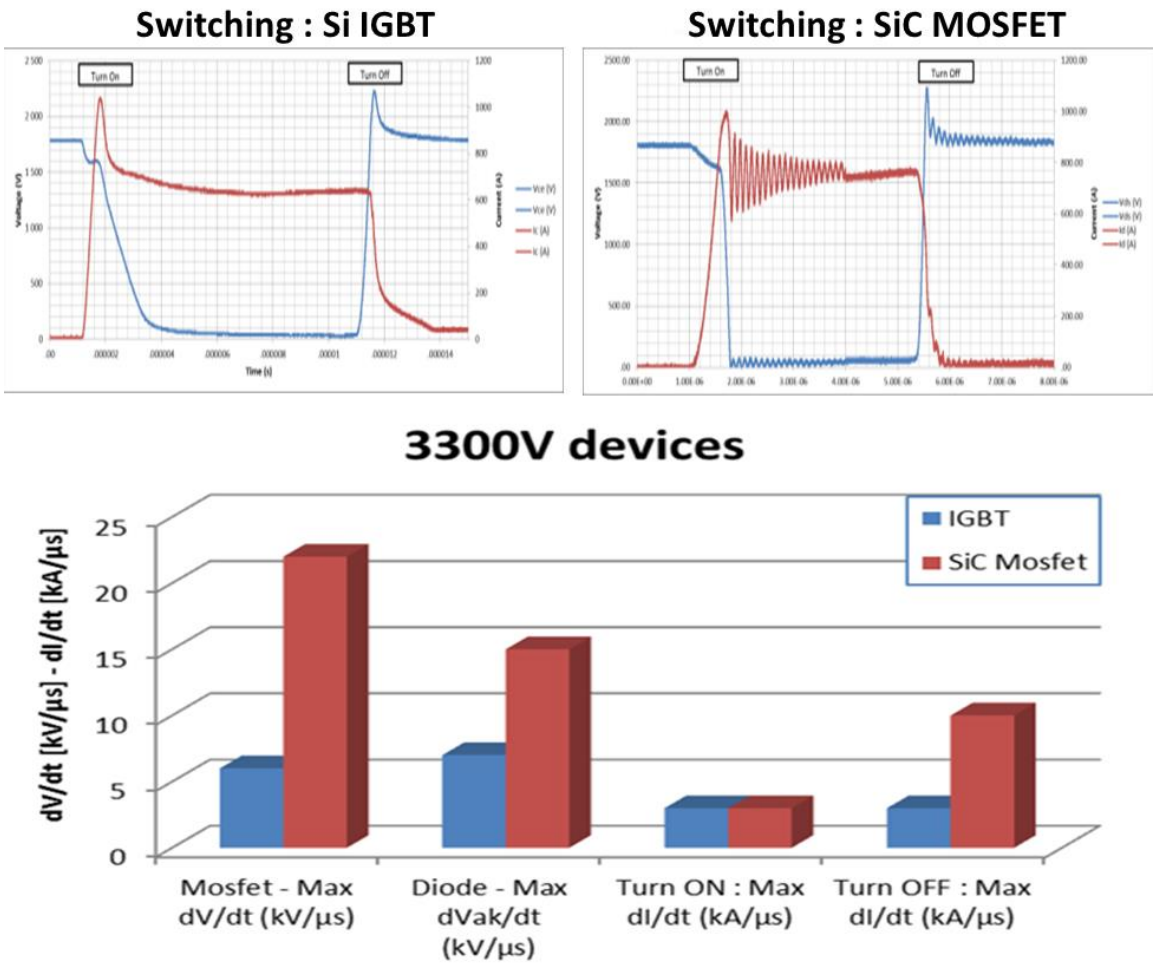

Figure I-21: *dV/dt and dI/dt comparison between 3.3 kV Si IGBT and SiC MOSFET technologies*

Despite the numerous benefits that this technology can bring, we showed earlier in this work that the existence of very fast rising edges combined with impedance mismatches between the inverter, cables, and machine may cause severe overvoltages that could be detrimental to efficient machine operation. Figure I-22 shows voltages at the inverter output and at the motor input of a low voltage random-wound machine (5.5 kW), supplied by both Si IGBT and SiC MOSFET based inverters.

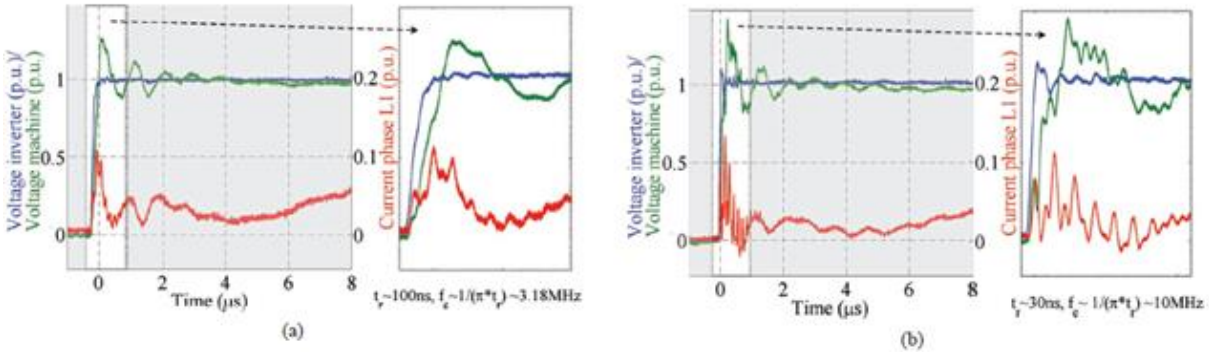

Figure I-22: *Voltages at the inverter output (blue), at the motor input (green), and associated phase current (red) with (a) Si IGBT inverter, (b) SiC MOSFET inverter [37]*

The overvoltage and oscillations after switching are clearly visible in both cases. Nevertheless, the measured overvoltage is about 30% of the DC bus voltage with the silicon-based inverter, while about 45% for the SiC-based inverter. The influence of SiC-based components is all the more serious when the voltage slope is steep. Introducing such components in static converters is thus likely to lead to new consequences (or to consequences that had previously existed to a lesser extent). This is why quantification and understanding are absolutely necessary to effectively anticipate the aging phenomena that will eventually emerge.

I.5 Consequences in terms of aging

I.5.1 Overview of aging

I.5.1.1 Definition

Reliability is a discipline that is directly related to the study of malfunctioning in Electrical Insulation Systems (EIS) and systems in general, contributing to knowledge, prediction, and control of failure. In a very general manner, the reliability of an EIS can be defined as its ability to fulfill its function without failure under determined conditions for a given period [38].

Mathematically, the reliability of an entity at time t is expressed by the function R(t), also called the survival function. It represents the probability of failure-free operation over the time interval [0, t]. Calling T the random variable representing lifetime, reliability can be written as follows:

$$R(t) = \text{Prob}\,(T \geq t) \tag{4}$$

From this definition of the survival function, and to better understand the life cycle of an insulation system or any other component, the failure rate can also be defined. It represents the conditional probability of an entity failing between the time points t and t+dt, given that it survived until time t. The evolution of this rate over time is a very particular “bathtub curve” that highlights the different degradation phases.

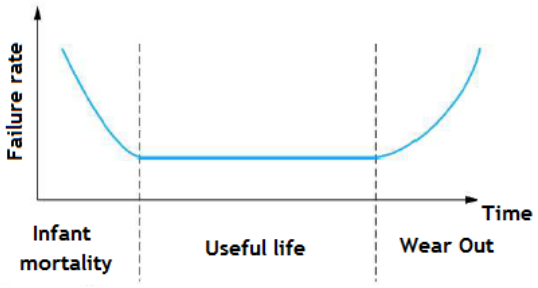

Figure I-23: *Failure rate over time*

According to this curve, the failure rate involves three stages. The “infant mortality” stage is characterized by a decreasing failure rate. It corresponds to design or manufacturing defects, or misused

or insufficiently validated components. The system is generally subject to a debugging process to mitigate these failures. The second stage corresponds to component's useful life, during which the failure rate is constant. Degradation mechanisms are time-independent during this period. Finally, the failure rate increases during the third and last stage. Failures occurring during this period are mainly due to the system/component wearing out and aging. On a broader level, failures caused by poor design, manufacturing, or installation are called intrinsic failures. Aging phenomena may be qualified as intrinsic failures. However, extrinsic failures are generally caused by misuse or improper operation due to maintenance, or as a consequence of another failure.

Aging mechanisms are numerous and diverse. They impact the insulation system primarily through the rupture of valency bonds between atoms constituting the macromolecules. EIS aging is a slow and irreversible phenomenon related to thermal, mechanical, electrical, and environmental constraints. The mechanisms involved are complex combinations of physicochemical interactions that eventually lead to a local breakdown of the insulation system.

In short, aging can be defined as an irreversible change of EIS properties when subject to stress. These constraints may be known, but their consequences and interactions are still not clearly understood. It is thus necessary to consider physical parameters in order to characterize and identify degradation. Theoretical models also exist and can be used to depict these aging mechanisms, with higher or lower levels of complexity.

I.5.1.2 Modeling

Statistical modeling is fundamental in the context of studying aging. Indeed, aging tests require a large number of samples to ensure satisfactory precision. It is thus important to use the appropriate aging models. This subsection presents an overview of the standard models generally used for each type of stress. It is worth pointing out that numerous parametric models exist, with different variants and complexity. However, the very basic models used to depict electrical and environmental aging are well defined and are thus the main focus in the following presentation.

- **Data distribution types**

In order to complement the notions previously presented, we must introduce several additional mathematical quantities. From the survival function presented in I.5.1.1, the probability density of failure at time t f(t) and the failure rate λ(t) can be defined as follows:

$$f(t) = \frac{dP_f(t)}{dt} = -\frac{dR(t)}{dt} \text{ where } P_f(t) = 1 - R(t) \quad (5)$$

$$\lambda(t) = \frac{f(t)}{R(t)} = -\frac{dR(t)}{dt}.\frac{1}{R(t)} \quad (6)$$

The MTTF (Mean Time To Failure) is also a good way of characterizing the reliability of an insulation system, and is defined as follows:

$$\mathrm{MTTF} = \mathrm{E(T)} = \int_0^{\infty} \mathrm{R(t)dt} \tag{7}$$

It is extremely important to determine the most suitable lifetime distribution in order achieve data processing that is as correct as possible, but also to identify all the variable of interest in terms of reliability. Among existing statistical distributions, some are particularly relevant for lifetime studies. These are described below.

Exponential law is the only law characterized exclusively by its constant failure rate. While it is one of the simplest laws for studying reliability, the fact that it depicts a "no memory" process with a constant failure rate makes it inappropriate for most cases. Exponential law applies to components that are not aged during a given time interval (the second stage of the previous bathtub curve) and undergo sudden failures, so there is no value in carrying out any preventive actions.

Table 3: *Exponential law features*

$f(t) = \lambda e^{-\lambda t}$	$R(t) = e^{-\lambda t}$
$\lambda(t) = \lambda$	$MTTF = 1/\lambda$

Log-normal law: A random positive variable T follows a log-normal law with parameters μ and σ² if its logarithm follows a normal law with mean μ and standard deviation σ². As a consequence, neither the reliability function nor the failure rate have an explicit expression, but they can be calculated numerically. All parameters of the law are defined as a function of Φ, the Gaussian distribution function. This law is frequently used in the context of reliability as it applies to positive random variables. Moreover, the shape parameter σ allows a large variety of representations.

Table 4: *Log-normal law features*

$f(t) = \frac{1}{t\sigma\sqrt{2\pi}} exp\left[-\frac{1}{2}\left(\frac{ln(t)-\mu}{\sigma}\right)^2\right]$	$R(t) = 1 - \Phi\left(\frac{ln(t)-\mu}{\sigma}\right)$
$\lambda(t) = \frac{\frac{1}{t\sigma\sqrt{2\pi}} exp\left[-\frac{1}{2}\left(\frac{ln(t)-\mu}{\sigma}\right)^2\right]}{1 - \Phi\left(\frac{ln(t)-\mu}{\sigma}\right)}$	$MTTF = exp\left(\mu + \frac{1}{2}\sigma^2\right)$

The Weibull law is characterized by two parameters: the scale parameter η and the shape parameter β, the latter determining failure rate variation: monotonically decreasing (0< β <1), monotonically increasing (β > 1), or constant (β=1, equivalent to an exponential law with λ=1/η). With

this flexibility, the Weibull law can be used to represent the three stages of a component's lifetime. It is thus widely used for studying reliability in various applications [39].

Table 5: *Weibull law features*

$f(t) = \frac{\beta}{\eta}\left(\frac{t}{\eta}\right)^{\beta-1} e^{-\left(\frac{t}{\eta}\right)^{\beta}}$	$R(t) = e^{-\left(\frac{t}{\eta}\right)^{\beta}}$
$\lambda(t) = \frac{\beta}{\eta}\left(\frac{t}{\eta}\right)^{\beta-1}$	$MTTF = \eta\,\Gamma\left(1+\frac{1}{\beta}\right)$ $\Gamma(n) = \int_0^{\infty} e^{-x}\,x^{n-1}dx$

Γ represents the gamma function, a commonly used extension of the factorial function to complex numbers. Several methodologies exist to verify the adequacy of a set of variables with respect to a distribution. To start, the distribution selection is generally made with the help of tools such as probability plots. Practically speaking, the value sets frequently follow the Weibull law. The parameters of the law must then be estimated. Once again, several methods exist, including maximum likelihood estimation, linear regression, and least squares regression. Finally, the set of values can be fitted to the chosen law. The data thus obtained are then used in lifetime models. In the context of electrical aging, the variables used in models are aging factors related to operational or environmental constraints. In literature, two main types of models can be associated with aging factors:

- **Physical models** are derived from physical or chemical theoretical laws depicting the aging process, generally unique, of an insulation system under stress.
- It is not necessarily simple to find a physical relationship between the insulation lifetime and the considered aging factor, in which case **empirical models** are preferred. Empirical models often result from experimentation. Identical components are tested under the same stress in order to deduce a general law describing the aging process.

The main degradation factors encountered in the aging of insulation systems and the associated models for lifetime prediction are presented below.

- **Models for lifetime prediction**

Electrical stress: The voltage applied to electrical equipment acts as an aging factor on the components of that equipment. In particular, an increase in voltage magnitude accelerates the degradation of the dielectric properties of materials, thus reducing their lifetime. Accelerated aging tests are based on a comparison of the lifetime between a sample to test and a reference sample whose lifetime has already been evaluated in operation. A commonly used lifetime model for electrical stress is shown

below, where n represents the voltage endurance coefficient, L the lifetime, U the applied peak voltage and, k a constant. The voltage endurance coefficient is the slope of the regression line.

$$L = kU^{-n} \tag{8}$$

The inverse power law is empirical. It supposes that the lifetime of a system varies inversely with the level of applied stress. This is a very standard model associated with electrical stress in the presence of PDs and applied to numerous components, including insulation systems.

Thermal stress: Temperature is a major aging factor in the context of electrical engineering. Generally speaking, the performance of a component degrades quickly at high temperatures. The thermal aging process can be described by the Arrhenius law, which expresses lifetime as an exponential function of the inverse of temperature. L represents the lifetime, T the temperature (in Kelvin), and A and b two constant parameters to estimate [38].

$$L = Ae^{\frac{b}{T}} \tag{9}$$

The Arrhenius law enables us to describe the speed variation of a chemical reaction as a function of temperature. As an empirical law, it has been verified experimentally for a large number of reactions. However, not all reactions follow this law.

The combined effect of thermal stress T and electrical stress E is often modelled by the generalized Eyring law [40]. It is also possible to take into account any non-thermal stress by adding (Bi + Ci/T) terms inside the exponential function.

$$L = \frac{A}{T^n} e^{\frac{b}{T} + \left(B + \frac{C}{T}\right)E} \tag{10}$$

Mechanical stress: Materials embedded in machines suffer constant mechanical stresses resulting from vibrations or mechanical shocks. Vibrations are characterized by repetitive constraints of low amplitude over a large number of cycles. In contrast, shocks are usually generated by larger accelerations of shorter duration. Those two types of stresses lead to the degradation of materials' physical properties, including deformation and breakdown. Just like electrical stress, the effect of mechanical stress can be modeled by an inverse power law (S being the value of the mechanical stress).

$$L = \frac{A}{S^n} \tag{11}$$

It must be noted that other simple empirical laws exist and can be used to estimate the lifetime of insulation materials. These laws are built mainly on tension-compression tests performed on steel and extrapolated to other materials. The Wöhler curve, which represents the experimental relation between stress amplitude and the number of cycles, is one of many examples of these other models.

Thermomechanical wear: The regular transition between extreme temperature levels can also be a factor in aging. A direct consequence of this cycling is the thermal expansion and contraction of the material, leading to a degradation of its properties. The number of temperature cycles before failure is related to the temperature difference as defined by the following empirical law [38]:

$$N = \frac{A}{\Delta T^n} \tag{12}$$

N is the number of cycles, ΔT the temperature difference, and A and n two parameters to be determined. The Coffin-Manson model also is a reference in terms of thermomechanical material wear with distinct dilatation coefficients. It is also used for studying low cycle fatigue [41].

$$N = \frac{1}{2}\left(\frac{\Delta\varepsilon_p}{2\varepsilon'}\right)^{\frac{1}{C}} \tag{13}$$

Here, N is the number of cycles, ε' the fatigue ductility coefficient, C the fatigue ductility exponent, and $\Delta\varepsilon_p$ the amplitude of plastic deformation.

Humidity: Moisture is another significant aging factor, as it is the main cause of oxidation and chemical degradation in insulation systems. In most cases, relative humidity, which represents the ratio of the partial pressure of water vapor to the equilibrium vapor pressure of water, is the relevant parameter to consider for quantifying the failure rate. An empirical model involving both temperature (Arrhenius law) and relative humidity (inverse power law) was introduced by Peck. In the equation below, L represents the lifetime, T the temperature (in Kelvin), RH the relative humidity, n a constant, and A and b two constant parameters to estimate.

$$L = \frac{A}{RH^n} e^{\frac{b}{T}} \tag{14}$$

All these lifetime models are non-linear functions of different aging factors. However, they are relatively simple to use, especially when using logarithmic transformation. Most of the models consider a constant level of stress, whereas real systems are often subject to variable stresses under operating conditions. Thermal cycling is, among others, one of the examples that makes it possible to better represent these stress variations.

I.5.1.3 Identification

The aging assessment of an insulation system, as well as the remaining lifetime estimation of a machine, are based on experiments and empirical laws determined through test campaigns. A quantity of observable data can be used to characterize aging evolution over time. In addition to lifetime evaluation, parameters that are intrinsic to the insulation system, as well as PD-related features, can be used for this purpose. This information makes it possible to show how changes in the dielectric

properties of materials take place, and above all how to relate those changes with applied stress and material aging.

- **Dielectric properties of materials**

Insulation resistance measurement during aging cycles is one of the main indicators of both the insulation condition and the speed of degradation. An insulation system has opposite characteristics to those of a conductor, namely it resists the flow of current when voltage is applied to system terminals. The better the insulation, the higher the insulation resistance, and the better its ability to maintain high resistance over time. As there is no such thing as "perfect insulation", a leakage current is always present and leads to a decrease in this resistance (see Figure I-24). Measurement at regular intervals is thus an effective way to assess insulation integrity.

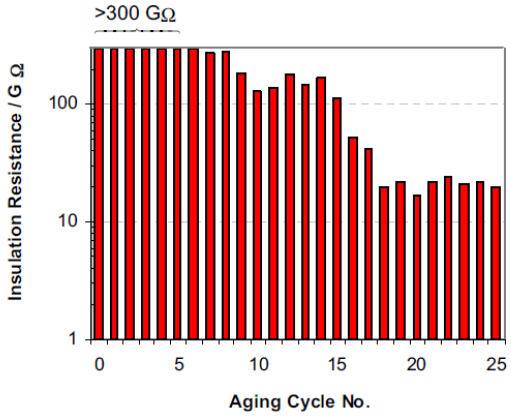

Figure I-24: *Insulation resistance measurement results after 1 minute [42]*

This measurement method is the simplest, but it is strongly affected by temperature and humidity. Other methods exist that allow normalizing measurements and taking into account the influence of the time of application, such as the Polarization Index (PI) or the Dielectric Absorption Ratio (DAR).

Dielectric permittivity is a physical property describing the response of a given dielectric to an electrical field. At the microscopic scale, permittivity is related to the electrical polarizability of molecules comprising the material. It is a tensor quantity that can become a scalar in an isotropic material. It is generally a complex number, with the imaginary part representing electric field absorption or emission phenomena. Dielectric loss quantifies a dielectric material's inherent dissipation of electromagnetic energy. It can be parameterized in terms of either the loss angle δ or the corresponding loss tangent tan δ. Both refer to the phasor in the complex plane whose real and imaginary parts are the resistive component of an electromagnetic field and its reactive counterpart. These losses can be taken into account by defining complex permittivity:

$$\varepsilon^* = \varepsilon' - i\varepsilon'' \tag{15}$$

Those losses are generally very low. In that case, the imaginary part is much lower than the real part. This then introduces the loss angle, which is the angle between the electrical field and the electric displacement vectors, expressed in percent and defined as:

$$\delta_e \approx \tan \delta_e = \frac{\varepsilon''}{\varepsilon'} \quad (16)$$

For brand new insulation, the dependency between loss angle and applied stress amplitude is very low. A variation of this factor can be observed after few cycles, which means it can be used as a way to characterize aging [43] [44].

Finally, **the capacitance** represents the real part of complex permittivity. As insulation systems are purely capacitive, they can be identified as capacitors and the measure of capacitance can be an additional marker for aging [42].

- **PD-related features**

Phase Resolved Partial Discharge (PRPD) pattern: Measurement and analysis of PDs are necessary tools for interpreting aging, especially for detecting defects that are usually difficult to locate with conventional dielectric methods. PD diagnosis can be performed both on-line and off-line, which makes it one of the best non-destructive methods [45] [46] [47].

Measuring PDs features over time, *i.e.* amplitude, number, and phase shift with respect to the voltage fundamental, provides information about the type, location, and severity of the discharges involved. One processing method in particular – the PRPD pattern – allows us to visually present and interpret results effectively. This method consists of a representation of the phase, amplitude, and number of PDs on a diagram (see Figure I-25). Phase and amplitude are represented respectively in abscissa and in ordinate, while the number is given by the color. The warmer the color, the greater the number of PDs. A comparison of this PRPD pattern at different aging stages and under different experimental conditions can provide information about the mechanisms involved.

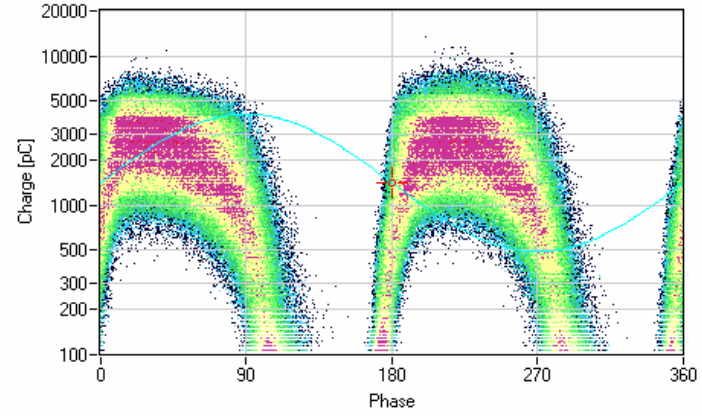

Figure I-25: *Example of PRPD pattern after 25 aging cycles [37]*

PDIV (Partial Discharge Inception Voltage) can also indirectly be considered as an aging marker. Indeed, PDIV varies depending on a number of parameters such as environment, temperature, and evolution of the EIS properties over time, and thus enables us to obtain a snapshot of the insulation system. PDIV is assumed to be independent of the frequency but strongly dependent on the condition of insulation. The more advanced the aging, the lower the insulation thickness, and the greater the PDIV. It is important to keep in mind that the partial discharge phenomenon is more a symptom of degradation than a default itself; PDIV and its evolution over time thus characterizes the aging associated with those symptoms.

Finally, measurement of **the discharge energy** is the last major aging indicator [48]. Partial discharges dissipate energy in different forms:

- Electromagnetic emissions (radio waves, light, heat)
- Acoustic emissions (into the audible and ultrasonic ranges)
- Gas emissions (including ozone and nitrogen oxides)

One of the most commonly used methods for measuring the energy associated with PDs is the Lissajous method, which consists of plotting the charges transferred through the gas against the applied voltage. The dissipated energy during one cycle can then be calculated from the Lissajous curve. P represents the electric power, and integration is calculated on one period of time.

$$E = \mathrm{P} * \mathrm{T} = \int \mathrm{V(t)dq} \tag{17}$$

The dissipated energy corresponds to the area under the Lissajous curve. This energy varies strongly with the aging time and conditions and can also give information about the aging process, or even allow comparing different operating points. This method has been proven for a sinusoidal voltage supply, but still needs to be improved for square wave voltages, primarily because of the difficulty in measuring the effective charge associated with PDs.

There is a long list of diagnosis and aging evaluation methods, as well as aging indicators. For the sake of brevity here, only the most commonly used ones, both during operation or by interrupting the aging, were presented [49] [50].

The direct consequence of the continued presence of degradation phenomena over time is EIS aging. The manifestations of this aging are numerous. They depend on the applied stresses and are expressed in different ways, through the variation of different parameters. In order to best identify aging mechanisms, from cause to effect, the next subsection describes aging as it takes places in electrical machines and, more specifically, discusses the influence of the main electrical and environmental constraints on PD features and aging, as well as their interactions. As a second step, the following subsection points out on one hand the interest and necessity of reproducing this aging on samples, and on the other hand, the procedures and strategies for conducting these accelerated aging tests.

I.5.2 Influence of electrical stress on PD features and aging

Electrical aging mechanisms vary according to whether the system operates with or without PDs. Voltage stress therefore becomes a strongly non-linear factor in lifetime prediction. In the context of this study, we only consider aging mechanisms in presence of PDs. In this context, there is a large number of voltage stress characteristics that can all contribute to the aging process [46] [51]. The effects of these different parameters are detailed below.

Voltage magnitude has a significant impact on the aging rate. Generally, the greater the voltage magnitude, the faster the aging. It was pointed out earlier that an inverse power law or an exponential law could be effective ways to model the relationship between voltage magnitude and lifetime. When samples representing local portions of insulation systems are considered, and under sinusoidal stress, the voltage magnitude is considered as one of the two main aging factors, along with frequency. In contrast, when considering samples closely resembling real systems (such as windings) and supplied by square-wave voltages, there is mixed evidence on the effects of additional characteristics such as the rising edge. In any case, overvoltages related to the use of PWM signals and fast-switching converters have a major influence on aging. Figure I-26 shows lifetimes as a function of frequency, obtained for three types of EIS [19]: one classic polyimide insulation system and two other systems that are reinforced with nanoparticles (B_aSO_4 and S_iO_2).

TABLE VI
RESULTS OF AGEING TESTS

Material	V_{pp} [V]	Average T_{bd} [s]
PEI	5000	1878
	3600	6660
	2200	35132
PEI+NB	5000	2440
	3500	5877
	2000	54896
PEI+NS	5000	14638
	4500	41570
	3800	394694

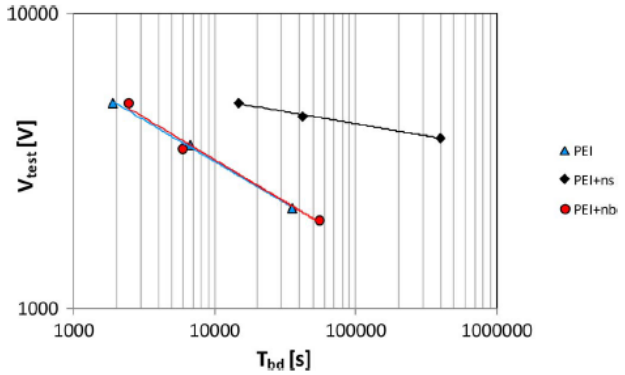

Figure I-26: *Voltage vs. lifetime for different types of EIS [19]*

These curves illustrate the voltage dependence over lifetime. Performance varies with wire diameter, thickness, type of insulation, and other characteristics such as the presence of nanoparticles, corona resistance, etc. Several degradation mechanisms can be distinguished with respect to PDs. Initially, PD activity varies with the supply voltage. In addition, new cavities and defaults are formed throughout the course of the aging process, further increasing PD activity. Finally, increasing voltage magnitude may lead to higher PD energy, and additional PDs could be incepted in cavities which were not subject to partial discharges at a lower voltage. Generally speaking, the greater the voltage amplitude, the greater the PD intensity and activity, and thus the faster the aging [25].

Frequency also plays an important role in the aging process. An increase in frequency significantly reduces the lifetime of an EIS. In the case of a sinusoidal signal, lifetime is generally inversely proportional to frequency [52]. The repetition rate of the impulse voltage can also have an effect on the number of pulses before breakdown [51]. In other words, in the case of impulse voltage, the fundamental or switching frequency can have a nonlinear effect on lifetime. Local heating can cause adverse effects on PD activity, such as a modification of dielectric permittivity and/or an increase of internal pressure in cavities [53]. Space charges can impact the PD activity as well. These effects can modify the PDIV, leading to a longer or shorter lifetime. Finally, the oscillatory nature of the impulsion can affect the deterioration rate. As a general rule, lifetime in the case of a square-wave signal tends to decrease with increasing frequency, as with a sinusoidal signal, but with a different and not necessarily fixed rate.

The polarity of the voltage signal also has an influence on PD activity and aging. Unipolar impulses generally have less impact on the insulation system than bipolar impulses of the same magnitude. Likewise, for devices under test having non-uniform electric fields, voltage polarity can affect aging. Figure I-27 sums up the combined effects of frequency and polarity on aging.

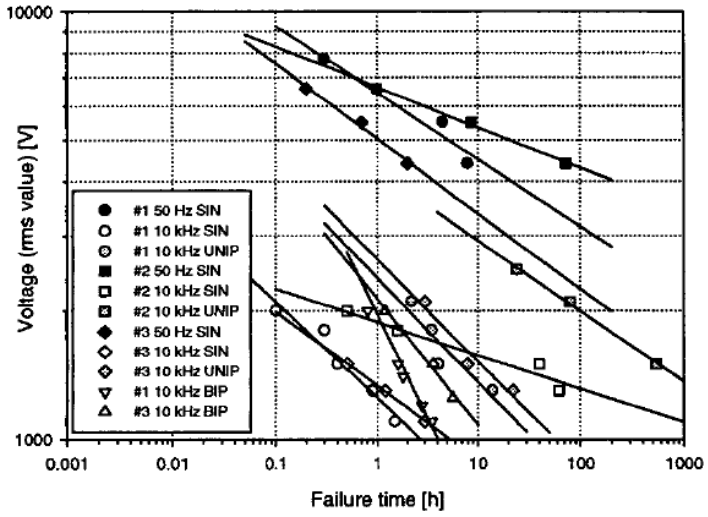

Figure I-27: *Influence of polarity and frequency on the lifetime of several insulating materials (#1 standard polyimide-amide enamel; #2 and #3 corona resistant enamels) [20]*

The rise time of impulse voltage can have an effect on the aging rate [30]. Opinions vary regarding the details of this influence [16][25][34]. Voltage and frequency are considered as the primary aging factors, but some authors consider that if PDs are the cause of degradation, short rise times could lead to a shorter lifetime. Assumptions made are that the energy associated with PDs is higher in the case of shorter rising edges, or that in some systems with multiturn windings, the shorter the rise time, the larger the voltage proportion between adjacent turns. Furthermore, charge accumulation could be time dependent and affect electric field distribution. In short, the influence of the rising edge is real, but understanding of the phenomena involved is still relatively unclear and imprecise.

The accumulation of **space charges** can affect insulation degradation significantly. The charge stored within the insulation and at its surface can induce distortions in the electrical field respectively inside the insulation and in the space between two adjacent conductors. These charge accumulations are strongly dependent on frequency and voltage shape (unipolar/bipolar). In addition, the features of these accumulations, namely the quantity and stability of the created charges over time, can be correlated with insulation features such as charge trap density and depth. The following figure illustrates the behavior of the electrical field with and without these space charges in a twisted pair of enameled wires. By symmetry, only one side is represented (air-enamel interface). Figure I-28B clearly shows that the space charge accumulation inside the enamel and at the interface may strongly modify electrical field magnitude and thus PD onset conditions [54].

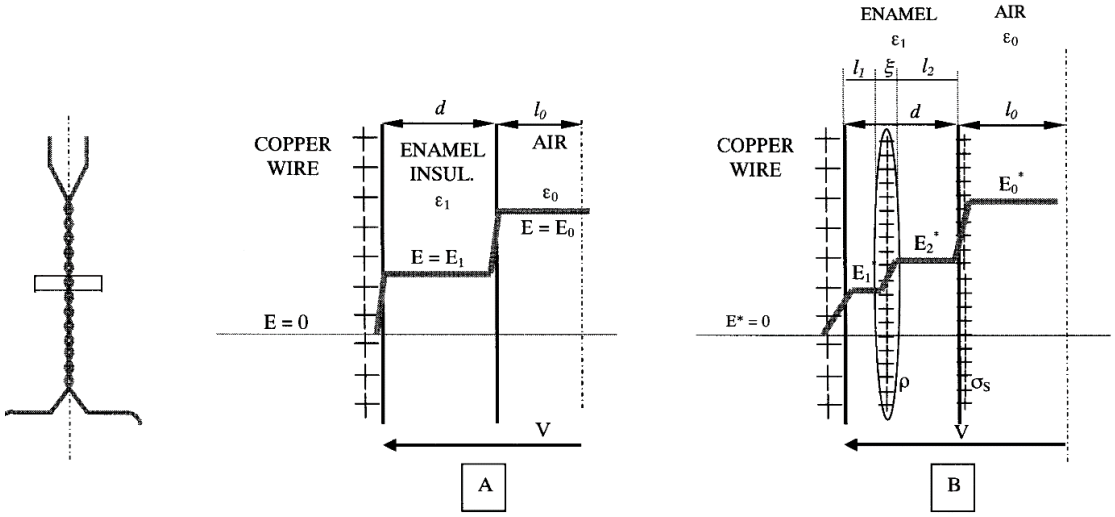

Figure I-28: *Electrical field behavior in the insulation system: A-In absence of space charges B- In presence of space charges [54]*

E_0 and E_1 represent the electric fields in air and in the enamel. E_0^*, E_1^*, and E_2^* respectively represent the new electric fields induced by space charges. ε_0 and ε_1 are the permittivity of air and enamel, d and l_0 their width, and V the applied voltage. Finally, σ and ρ respectively are the charge per unit area and per unit volume, and l_1, l_2, and ξ are the new dimensions including the accumulated space charges.

Finally, other factors such as duty cycle, pulse duration, and the ratio between applied voltage and PDIV, have a clear influence on the electrical aging of insulation systems [11][32][46][51][55]. As an example, unipolar impulses are less severe for insulation than bipolar impulses of same magnitude. Overall, variations in these factors have a negative impact on aging. Numerous studies have been made on the subject. At the core of our study, these issues are addressed in a more extensively in Chapter III.

I.5.3 Environmental influence on PD features and aging

I.5.3.1 Thermal aging

The increase of ohmic, magnetic, and dielectric losses inside machines can lead to insulation heating. This phenomenon is linked to PDs to the extent that insulation heating causes a modification of its characteristic parameters (permittivity, geometry, conductivity, PDIV) and, in turn, greatly modifies field distribution and the insulation's resilience to PDs.

Thermal stress consists largely of thermal agitation within the material and irreversible chemical reactions. During normal machine operation, heating is mainly a result of Joule, eddy current, and mechanical losses. Temperature, when constant, acts as a catalyst rather than actually degrading the material itself. The degradation rate can be increased if dielectric losses are increased, in turn leading to local enhancement of temperature in an area with high electrical stress. A temperature increase can also lead to an increase in permittivity, causing higher electrical stress in adjacent cavities, lower PDIV, and thus enhanced PD activity. Furthermore, it can have an influence on the gas pressure in closed cavities, and on charge trapping and de-trapping times. In addition to the thermal energy gained by electrons, higher temperature can lead to a reduction in relative air density, which is inversely proportional to the mean free path. As a consequence, electrons must travel a longer distance between two collisions and store more energy. This produces PDs that are more energetic and certainly more damaging for insulation systems (Figure I-29).

When thermal cycles are imposed, degradation is referred to as thermomechanical aging [56]. This aging type is primarily due to differences in the thermal dilatation coefficients between constituents and the insulation system. These differences can create constraints which, in turn, may generate or expand pre-existing delamination, and/or increase PD activity, amplitude, and repetition rate. These constraints are enhanced by thermal cycling, as the temperature of materials does not vary at the same speed in that case. In short, temperature acts as an indirect factor in aging by impacting many other parameters and phenomena.

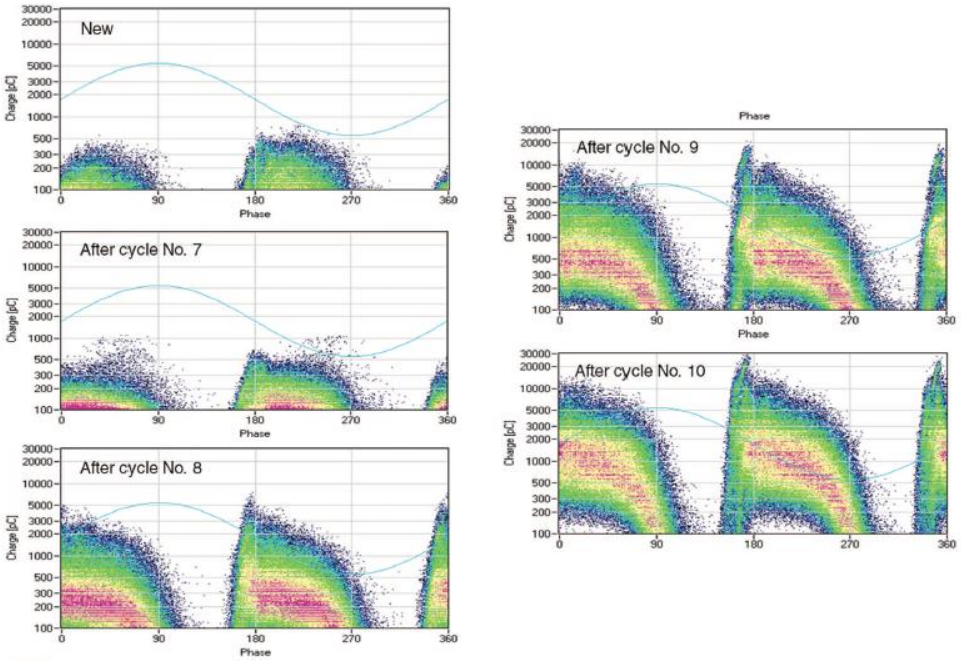

Figure I-29: *Changes in discharge mechanisms during thermal cycles (10 kV, stator bars) [42]*

I.5.3.2 Pressure

As with temperature, pressure above all has an impact on PDIV and PDEV [1]. For closed cavities, PDIV diminishes when temperature rises; the opposite trend is observed with pressure. Table 6 below shows a series of measurements performed on twisted pairs at various pressure levels.

Table 6: *PDIV and PDEV variations with pressure [9]*

1013 mbar		700 mbar		400 mbar		100 mbar	
PDIV (V)	PDEV (V)	PDIV (V)	PDEV (V)	PDIV (V)	PDEV (V)	PDIV (V)	PDEV (V)
675	660	440	433	400	365	304	285
675	665	439	436	390	365	314	277
675	655	443	435	385	365	310	287
675	660	453	435	380	360	310	278
675	660	453	435	380	365	312	280

Experimental results from tests performed in many studies show that PDs are more likely to be incepted in a low pressure environment and, most importantly, at low voltage. Moreover, insulation lifetime is proportional to discharge energy. Finally, it is also worth noting that pressure effects are often combined with thermal and humidity effects [15].

I.5.3.3 Humidity

The humidity of an EIS and its surroundings can modify the dielectric strength of air, as well as the electrical stress distribution or electric charge conduction on the insulation surface, thus leading to modified surface PD activity and degradation [48][57]. It appears that a critical value of relative humidity exists, for which lifetime decreases regardless of the evolution in relative humidity. It also seems that this value varies when the applied voltage decreases. In addition, surface damage increases with relative humidity. These phenomena can be explained by the interaction between relative humidity, surface and material properties. When relative humidity is below the critical value, PD activity seems to be located on a narrowed surface. Conversely, when relative humidity is above the critical value, the effect on surface characteristics prevails: surface conductivity rises due to the formation of by-products linked to the discharges, thus leading to the creation of a semi conductive layer on the damaged surface. Lifetime is reduced in both cases, although the underlying mechanisms are different. Other phenomena, such as condensation and electronegativity changes in gases with humidity, must also be taken into account as they can affect PD features, including PDIV.

I.5.3.4 Mechanical aging

Mechanical stresses, both static and dynamic, can increase electrical aging significantly, in particular by creating or widening insulation defaults. There are three main sources of mechanical stress in a rotating machine. The first is due to the centrifugal force exerted by the rotor, which tends to compress and distort insulation. The second is related to stator vibrations, which also exert a force on the windings or on the turns at the slot base, eventually leading to abrasion of the insulation paper and resin. Finally, the last source of stress occurs during the transitory phases of the motor, particularly upon startup. These phases induce transient currents that are much higher than the current in the machine. As a result, the mechanical force induced by the magnetic field (proportional to the square of the current) increases strongly. Generally speaking, mechanical stresses are often associated with other stresses, either simultaneously or during multi-stress cycles. They can then create insulation breakdowns, creep, or delamination, to name but a few.

I.5.3.5 Other phenomena

Other phenomena such as environmental constraints and mechanical fatigue due to voltage impulses generated by converters do not necessarily cause system aging but, combined with other stresses, can contribute to the degradation of the insulation systems. Here, “environmental” refers both to the usual environmental constraints such as pressure, humidity, and temperature, as well as the environment in the literal sense: oil from bearings, humidity and condensation, dust and debris, chemical

products. All these changes may lead to an increase in the material's conductivity, dielectric losses, and power factor, as well as a decrease in insulation resistance, further weakening the insulation lifetime.

I.5.4 Multi-stress aging

Although there are different combinations of stress factors depending on the field of study, the main constraints presented above generally act simultaneously, therefore emphasizing the degradation and aging processes. Furthermore, their features and intensity influence each other. The models considered thus far are accurate but tend to be based on strong assumptions in order to reduce complexity and the number of variables. At the same time, they tend to drift away from actual operating conditions.

In this context, it may be worthwhile to consider multi-stress models, instead of the standard models that only take into account one variable at a time, to study the effects of several constraints and their interactions. The latter are divided into two categories [58]:

- The interaction between two stresses is referred to as **direct** when the result is substantially different from the aging factors considered separately. Chemical degradations related to thermal stress such as oxidation and hydrolysis are a good example of this kind of interaction.
- **Indirect interactions** take place when the aging caused by one factor has an influence on the aging of another factor, even if those two factors are not applied at the same time. For example, if the cavities resulting from applying a mechanical or thermal stress are permanent, the enhanced electric field inside those cavities will eventually lead to increased PD activity. Figure I-30 highlights these two types of interactions.

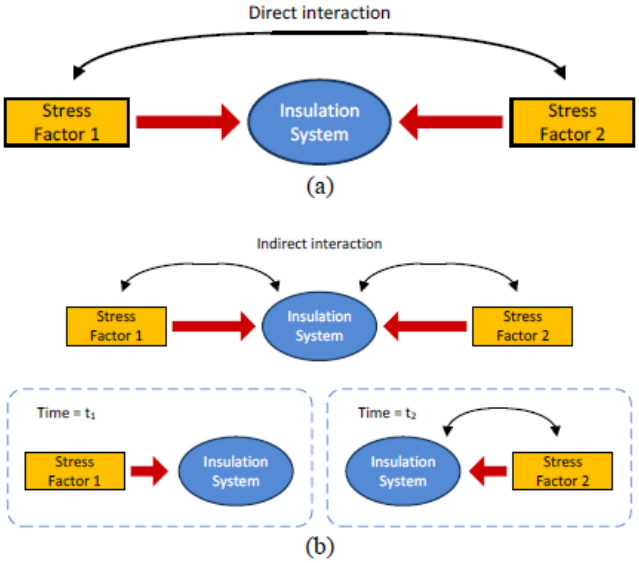

Figure I-30: *(a) Direct interaction and (b) indirect interaction between two aging factors [58]*

One of the cons of the multi-stress method is that it can be difficult to determine which constraint specifically affected aging. However, it allows highlight combined aging mechanisms that are likely to occur under real operating conditions.

In terms of experiments, it is quite costly and challenging to consider multi-stress models involving all the parameters related to the aging process. Statistical methods considering only a restricted number of variables thus exist to model lifetimes and answer the following important questions:

- What are the most influential factors?
- Are there any interactions between those factors?
- Is it possible to linearize the process as a function of those factors, and is the obtained model predictive?
- How can we minimize the number of experiments to make while ensuring the maximum amount of information?
- Is there any bias in measurement results?

Design Of Experiments (DoE) is one of many methods that make it possible to answer these questions, and it can be applied for various processes [59]. DoE consists of an ordered series of tests aiming to determine – with the lowest possible number of tests and the maximum level of precision – the influence of various parameters for optimizing cost and/or performance.

To date, most aging models and experiments consider variables separately. Modeling the lifetime of insulation systems when considering several stresses simultaneously is therefore a further step towards understanding the influence of a whole set of parameters and their interactions on any given phenomenon. Some studies take this problem very seriously and already propose multi-stress models [58][60][61]. With respect to multi-stress aging in the form of cycles, these models also make it possible to study the influence of combined stresses, but rather in terms of indirect interactions. The latter are generally preferred in the industry.

I.6 Conclusion

The issues of partial discharges and aging mechanisms of insulation systems used in rotating machines were addressed throughout this chapter. A state of the art of the degradation mechanisms and the systems on which they appear was presented. The influence of electrical stress and control strategy on aging was reviewed in detail and, finally, the aging phenomenon itself was defined and illustrated.

Insulation system aging is a common issue in a number of areas, in particular with the expanding use of electrical energy. Despite different challenges and structures, the phenomena involved are similar: mainly PDs and their consequences on insulation systems. These systems may be designed to react differently to these discharges, but in any case, PD presence is an issue that affects the reliability of the entire electromechanical chain.

This is particularly true due to the fact the converters used to supply these machines have a specific design that leads to the generation of very harmful stresses at the motor terminals. Moreover, the transition from conventional silicon-based components to new wide bandgap components only makes matters worse.

The aging of insulation systems is the direct consequence of these severe new constraints. Modeling, identification, and reproduction of this aging are thus key aspects for understanding degradation mechanisms, and potentially preventing and predicting the effects of aging.

Analysis of partial discharge influence in an electromechanical chain using fast switching inverters can be divided into three steps:

- Identification of the electrical stresses as seen by the machine
- Influence of these constraints on PD activity
- Consequences of these PDs in terms of aging

The first of these steps is discussed in the next chapter. The state of the art presented above is intended to provide a general overview of aging issues regardless of the type of machine considered. From this point forward, our work focuses more specifically on the railway context (Type II machines). Nonetheless, the parallel with low voltage machines will remain a recurrent thread of this study.

Chapter II. Electrical stress identification

II.1 Purpose of the study

An important step in studying the reliability of insulation systems is the characterization of electrical stresses. More particularly, clear insight regarding the distribution of electrical stresses to which the machine is subject is a first step towards the systematic determination of the conditions of occurrence for partial discharges, as well as their consequences on insulation system lifetime.

Numerous studies have been made on the subject of low voltage machines [62][63][64][65][66]. However, studies concerning high voltage machines are more rare or outdated. It is thus necessary to have insight into electrical constraint mapping in the motor – more specifically on the turn-to-turn, phase-to-ground, and phase-to-phase insulation systems – in order to be able to reproduce those constraints on samples but also to understand the aging process as a whole from PD ignition to breakdown.

With that in mind, the following part of this work seeks to perform thorough electrical stress mapping depending on both geometric and electrical parameters. The final objective is to establish a comparison between the electrical stresses generated by Si IGBT-based and SiC MOSFET-based inverters. A series of measurements of turn-to-turn, phase-to-ground, and phase-to-phase stresses was performed with different configurations and in accordance with a detailed test plan previously established based on preliminary tests.

The experimental setup overall, as well as the results of the test campaign and analysis are presented below. In addition, partial discharge measurements are performed to complement these results and achieve insight into not only the severity of the stresses but also their impact in terms of PDs.

II.2 Experimental setup

The electrical stresses at motor terminals depend on multiple parameters, both geometric and electric. In particular, inverters using SiC-based components enable the generation of dV/dt much higher than the usual levels provided by Si-based inverters. Furthermore, these stresses differ vastly depending on the insulation system and are altered throughout their propagation in winding. In order to perform thorough electrical stress mapping, it is important to control many parameters and to have access to multiple locations in the motor. To carry out this task, we built an experimental test bench. The objective is to characterize the influence of those parameters on equipment insulation, and consequently to understand the extent to which PD activity is affected, by identifying voltage distribution in the winding (voltage increase between turns, phase-to-ground…) of a type II machine.

II.2.1 Description of the power chain

A voltage source supplies the chain with a DC bus. This voltage is then filtered and converted using an inverter driven by a control device. This converted voltage goes through cables and finally supplies an asynchronous formed wound motor equipped to provide access to particular points in the motor. A general bench description and a series of photos of the electromechanical chain are given in Figure II-1.

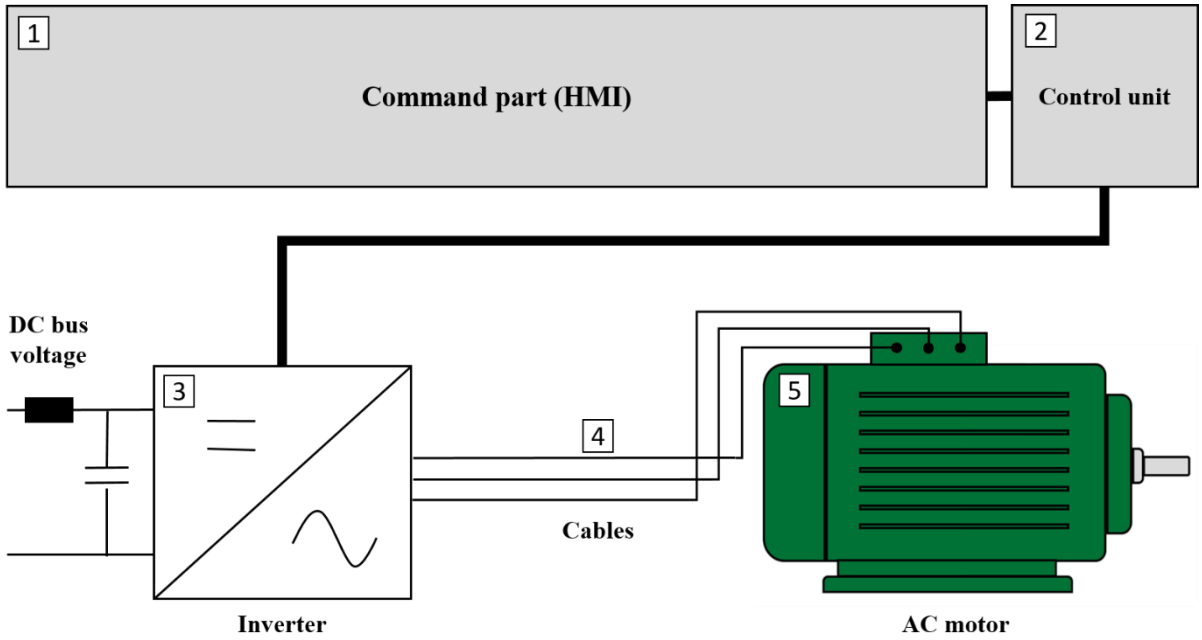

(a)

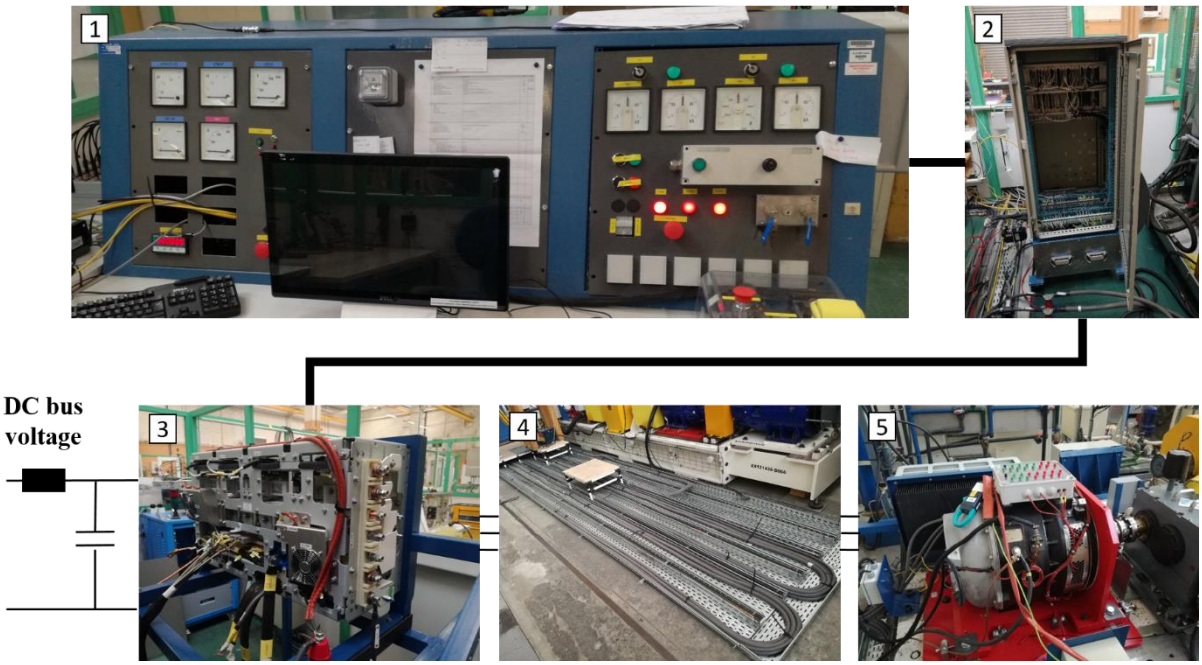

(b)

Figure II-1: *General description (a) and photos (b) of the experimental test bench configured for characterizing voltage constraints on insulation*

More specifically, a controller allows for the transmission of information to the inverters and thus the adjustment of parameters such as DC bus voltage, torque, and rotation speed of the motor. Sensors are placed all along the electromechanical chain to gather information regarding system operation. Therefore, information flows bidirectionally between the controller and inverter. Several inverters are used in this study. The two main inverters, which are designated in this document as inverters A and B, have a similar structure but different power modules, enabling the comparison of Si IGBT and SiC MOSFET technologies. A third inverter (referred to as inverter C) also uses SiC MOSFET technology, but with higher performance in terms of switching speed. Finally, two additional inverters (respectively inverters D and E) were studied to a lesser extent and only allow comparison at a larger scale for some parameters. It must be noted that inverters A and B are expected to operate at a higher DC bus voltage than inverters C, D, and E. Table 7 provides a brief summary of performance with the values of the maximum voltage slope (in kV/µs) for each inverter. These values were obtained based on voltage measurements performed at each inverter output. For all inverters, simplified designations are provided and will be used later for the sake of clarity.

Table 7: *Maximum rising edge at the inverter output for all technologies*

Inverter name	Technology	Maximum rising edge (kV/µs)
A	Si IGBT	4.43
B	SiC MOSFET	8.17
C	SiC MOSFET	23.26
D	Si IGBT	1.29
E	SiC MOSFET	8.07

Two types of input voltages are considered in this study. The inverters can be controlled by means of a double pulse as voltage input by operating two of the inverter legs simultaneously, while the last leg is either disconnected or set to an off state. It is also possible to use PWM signals that were specially designed to ensure that the switched current range is as large as possible. (Figure II-2). The first type of input voltage is much simpler to set up and makes it possible to overcome operating constraints (the machine is not running) to focus on electrical stress only. For the second type, the interest is to reproduce the machine's operating environment. It must be noted that most tests were performed using PWM signals, as the purpose of the study is to identify electrical stresses inside the machine under operating conditions. With respect to the earthing (grounding) system, the motor as well as the -HV source (Figure II-2) on the inverter side are grounded locally. Normatively speaking, the considered earthing system is a TT network.

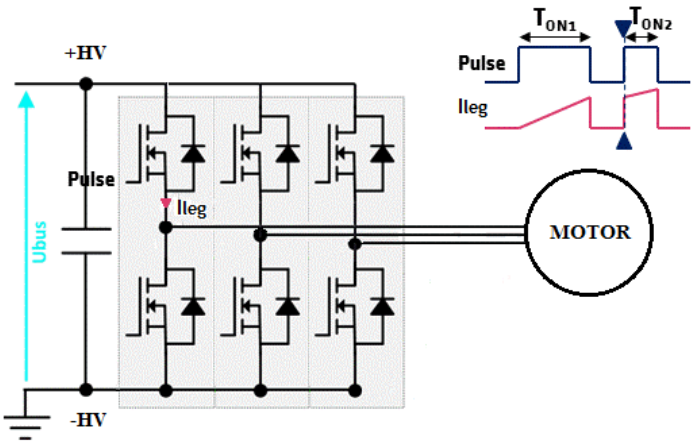

Figure II-2: *Circuit diagram and illustration of the considered double pulse*

The cable length between inverter and motor can also be changed. Overall, the parameters that can be varied with this setup are:

- Cable characteristics (length 1 - 40m, disposition, ground plane)
- Rotation speed (0 - 2000 rpm)
- DC bus voltage (0 - U_{nom})
- Switched current (0 ±1000 A)
- Technology of the semiconductor device (Si IGBT/SiC MOSFET)
- Type of input voltage (PWM/double pulse)

From this point forward, cable length will be referred to as L_{cable}, rotation speed as Ω, and DC bus voltage as U_{bus}. The latter is always expressed as a function of the nominal DC bus voltage U_{nom}. The switched current, which represents the machine's phase current, as well as the type of input voltage, do not have a particular designation and are specified in each case. Finally, the technology used for the semiconductor device is identified using the inverter names defined above.

II.2.2 Instrumentation

The motor used for the study is a three-phase high voltage (formed wound) asynchronous motor composed of four parallel branches per phase and four coils per branch, for a total of 16 coils per phase. A coil is formed by nine turns, giving a total of 36 turns in series per phase and per branch. The coil span factor of the considered motor is 10/12. This motor is equipped to provide access to specific points of the winding.

The first phase and the first coil of the second phase are instrumented. Concerning phase 1, measurement points are located at the terminals of each coil on two branches (identified as U1 to UN and U'1 to U'N), and at each turn of two coils belonging to two different branches (identified as Us1 to

UsN and Us'1 to Us'N). Furthermore, two additional measurement points are located at the terminals of one of the second phase coils. The result is a total of 30 measurement points to which the power supply terminals (identified as U0, V0 and W0) are added.

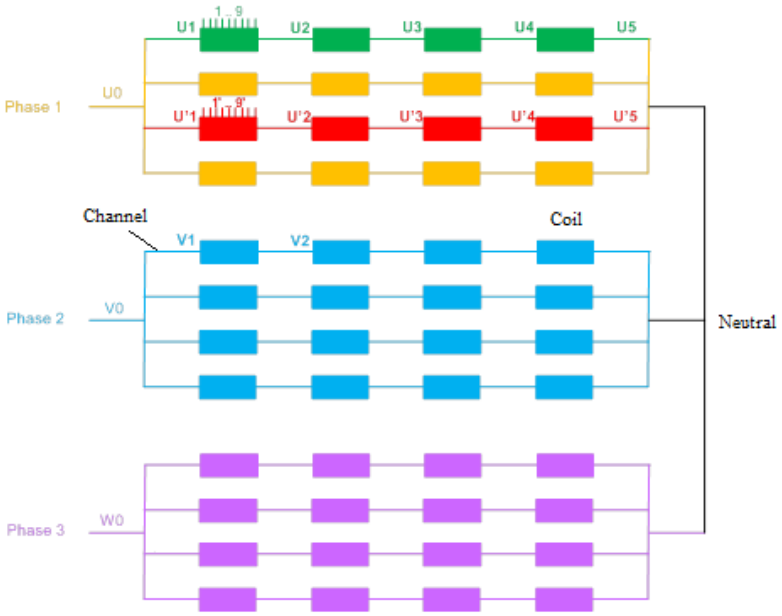

Figure II-3: *Diagram of the electrical instrumentation*

II.2.3 Measurements and acquisition

Four types of oscilloscopes were intermittently available for acquisition, with bandwidths varying from 500 MHz to 2 GHz, and sampling frequencies ranging from 5 to 20 GS/s. Depending on availability and based on need, two oscilloscopes among the four (not necessarily the same from one case to another) were used jointly to record waveforms both at the inverter output and at the motor input. However, despite the synchronization between the two oscilloscopes (which were set to trigger on the same signal, *i.e.* one of the phase-to-ground voltages), it was not possible to record the waveforms of both oscilloscopes at exactly the same time due to the delay induced by the distance between the inverter and the motor part of the bench. Figure II-4 represents the sketch of the installation, including the oscilloscopes and synchronization strategy.

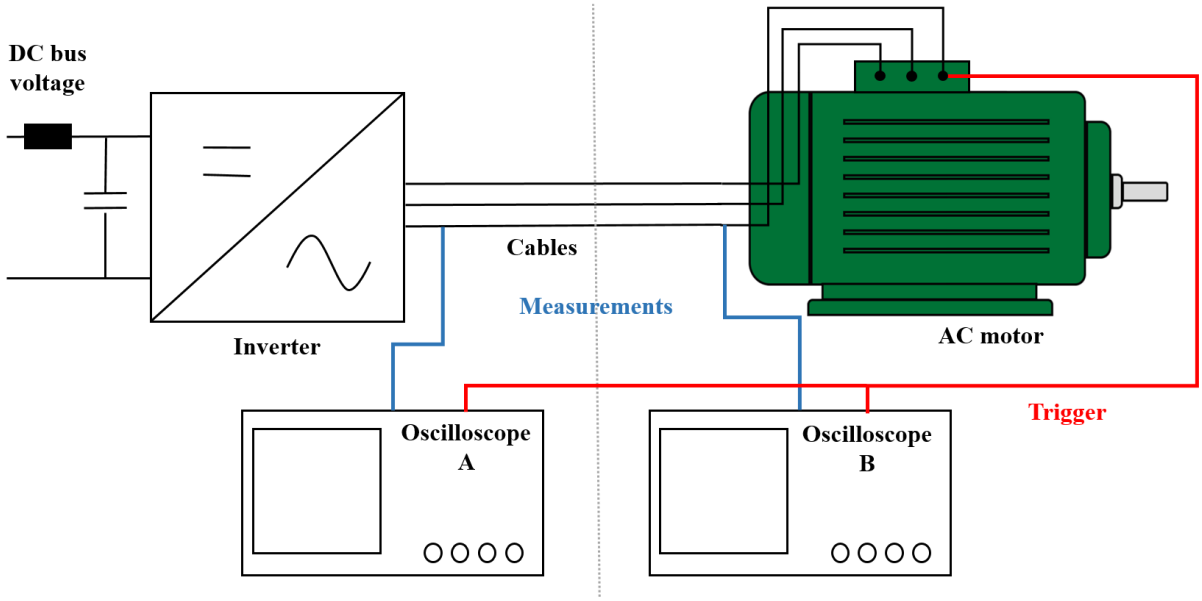

Figure II-4: *Sketch of the installation, including measurements and acquisition devices*

Regarding the sensors, a comparison of various probes was made in order to ensure measurement accuracy. As a result of that comparison, we chose to use passive probes (LeCroy, 6 kV, 400 MHz). Given the number of oscilloscope channels available, differential probes were also used in some cases to complement the passive probes. The phase current measurement was achieved with a Rogowski coil sensor (PEM CWT15R) placed on one or more phase cables. Finally, the PD sensor used for this study is presented in detail in section II.6.

II.2.4 Test plan

We carried out a preliminary study prior to this work to verify proper system operation and to identify the points where constraints are the most severe. The highest phase-to-ground stress was found to be located at the input of the first coil of channel 1. The voltage between phases was measured between phases 1 and 2, and phase current was measured on phase 1. Finally, turn-to-turn measurements were performed on coil U_1 and only the largest of all turn-to-turn stresses were considered.

An analysis of the influence of various parameters, such as switched current and rotation speed, also led to a reduction of the test plan, without overlooking any relevant results. Details of this analysis are presented in Section II.4.

From the 30 measurement points described in Section II.2.2, it was then possible to perform adequate turn-to-turn, phase-to-ground, and phase-to-phase voltage measurements. A vast number of measurements were performed on all inverters. For sake of brevity here, only the most relevant measurements are presented. In each paragraph, the considered inverters may be subject to change. Nevertheless, the choice of the most adequate inverters is explained, while maintaining the comparison between Si and SiC based inverter performance as the main objective.

II.3 Electrical constraints in the machine

Although the voltage shapes and amplitudes suffered by each type of insulation are not always controlled in low voltage machines, the higher-risk areas are quite well known, as well as the consequences arising from these stresses [62] [67]. However, the situation might be quite different with Type II machines. In Type I motors, the weakest point of insulation (and for PDs) is usually turn-to-turn insulation. Partial discharges appear because of the combined effects of random winding with a large number of turns, propagation phenomena, and rising edges [10]. In Type II motors, the winding is formed and comprised of few turns. One may wonder how stressful the constraints are in this particular case. In the following section, an overview of the stresses at the motor terminals aims to answer this question.

II.3.1 Turn-to-turn voltage

Unlike Type I machines, which most often use random wound coils, and in which it is possible for the first and last coil to be next to each other, high voltage machines present formed wound coils [68]. These coils are constituted of flat wires stacked on top of each other (Figure II-5). Measurements must therefore be performed only between adjacent turns.

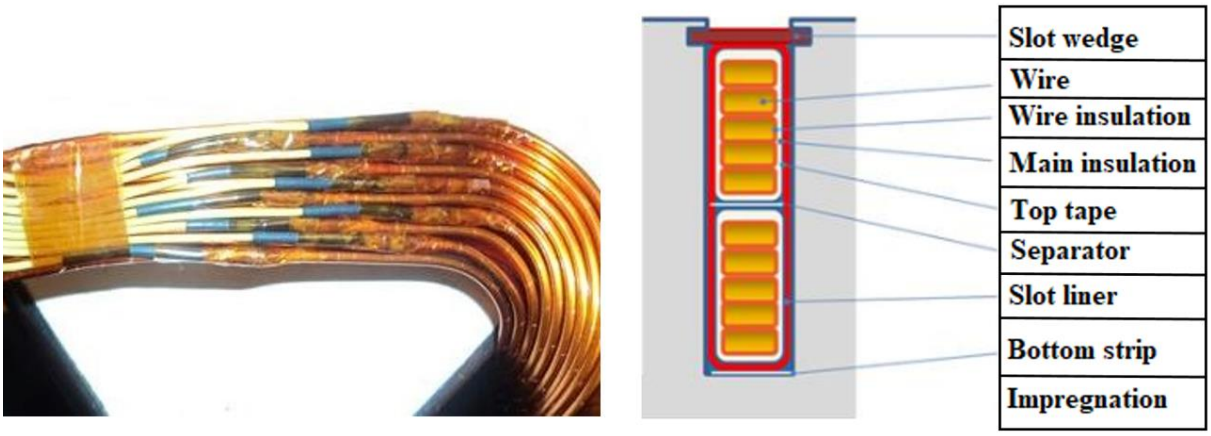

Figure II-5: *Detail of turn arrangement and disposition in the slot*

Turn-to-turn voltage measurements are given in Figure II-6. Inverters A and B were chosen for comparison between converters using equivalent power modules and configuration, but with different semiconductor technologies. Inverter A also displays the voltage and current waveforms over a longer period of time, thus enabling us to study stress variation with switched current.

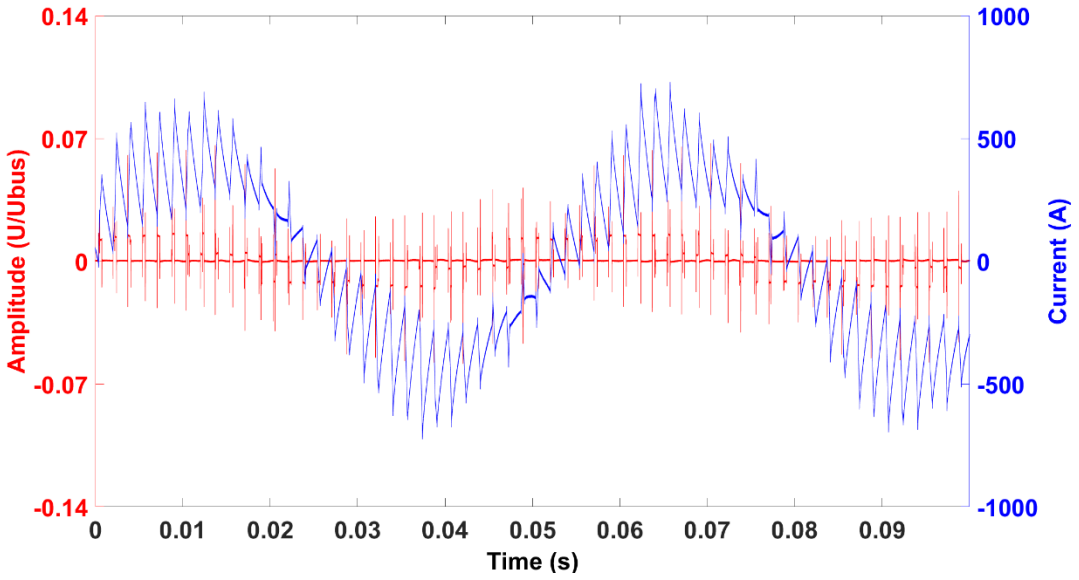

(a)

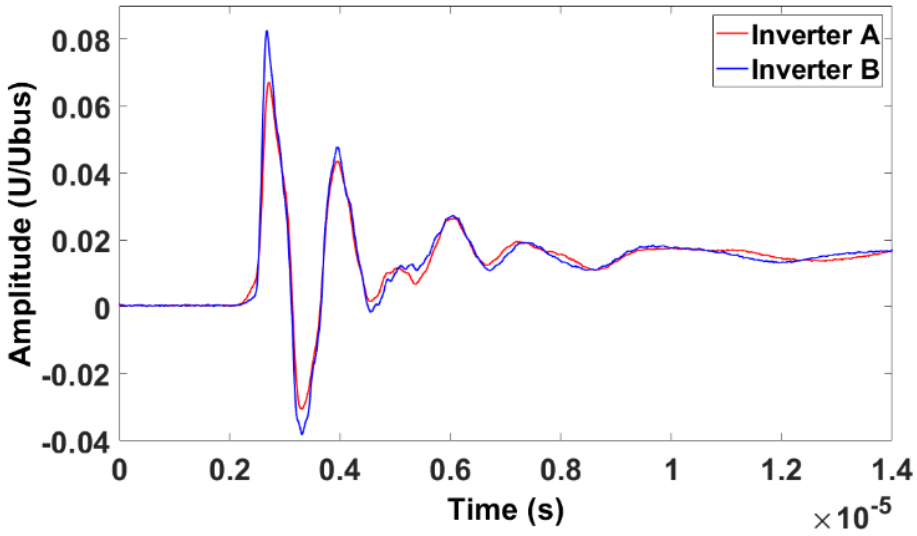

(b)

Figure II-6: *(a) Turn-to-turn voltage (red) and switched current (blue) for inverter A (U_{bus} = 0,5xU_{nom}, L_{cable}= 40m, Ω = 500 rpm), (b) maximum turn-to-turn voltage: inverter A (red) and B (blue)*

The voltages shown in Figure II-6 (b) are the maximal turn-to-turn stresses encountered with each inverter in one time period. These voltages were superimposed to highlight the difference between Si IGBT and SiC MOSFET, but do not necessarily occur at the same temporal position in both cases. Experiments showed that the voltage distribution between turns is very homogeneous and its magnitude remains very low. A variation with the introduction of SiC can be observed: the rising edges are slowed more significantly from one turn to another than with Si IGBT inverters, generating higher turn-to-turn voltage amplitudes.

Experiments were also carried out with a double pulse signal. To achieve this, only two of the inverter legs were supplied, while the last leg remained without connection, for a nominal DC bus voltage value (nearly twice that of the previous case), a switched current of 100 A, and an 11 m cable

length. The maximum stress between turns was observed to be around 5.2% of the DC bus with IGBT, and around 8.3% of the DC bus with SiC. Thus, even if the absolute turn-to-turn constraint doubles when the DC bus voltage doubles, the maximum relative stress value remains mostly unchanged.

A variation of the turn-to-turn stresses with the switched current can also be observed. Maximum voltage occurs when the absolute value of the switched current is also at its maximum. Rotation speed, which influences the switched current directly, also influences the turn-to-turn voltage. The impact of such parameters are discussed in detail in Section II.4.

Finally, a test in a critical case was carried out with a shorter cable length (around 1 m), at nominal voltage, and with the fastest inverter (inverter C). The maximum stress value is expected to be obtained when using a very short cable. Indeed, in such a case, the rising edges are very fast and the spread between two turns is most pronounced. The outcome was a maximum stress value of 20% of the DC bus.

As is generally the case in Type II machines, the turn-to-turn insulation consists of a polyimide film coating reinforced with Teflon-FEP. Experiments and simulations performed on samples representative of this insulation showed that the average value of the PDIV and breakdown voltage are respectively around 1.5 and 10 kVpk (see Section IV.2.2.1). Considering that the voltages shown in Figure II-6 are less than one hundred volts and that the turn-to-turn voltages do not exceed a few hundred volts in general, there is little chance of any PD occurrence. These voltage levels certainly remain too low to trigger partial discharges and are even below the minimum Paschen value, which represents the critical value below which PDs could not even be incepted in air. Even with SiC components, the structure of the winding homogenizes voltage distribution and does not allow PD inception between turns.

II.3.2 Phase-to-ground voltage

Turn-to-turn insulation is not the only area where PDs can be incepted in the machine. Machine structure itself can also lead to very high stresses between phases as well as between phase and ground. As a consequence, phase-to-phase and phase-to-ground insulation systems, although designed to undergo such constraints during normal operation, are exposed to risk, particularly in terms of PDs.

We therefore performed PWM tests to highlight the influence of various parameters on phase-to-ground voltage stress, in particular on rising edges and overvoltages. Inverter C was used to highlight voltage propagation through the winding, as shown in Figure II-7, which represents the turn-to-ground voltages for the first, third, and fourth turns (a), as well as a zoom on the rising edge (b).

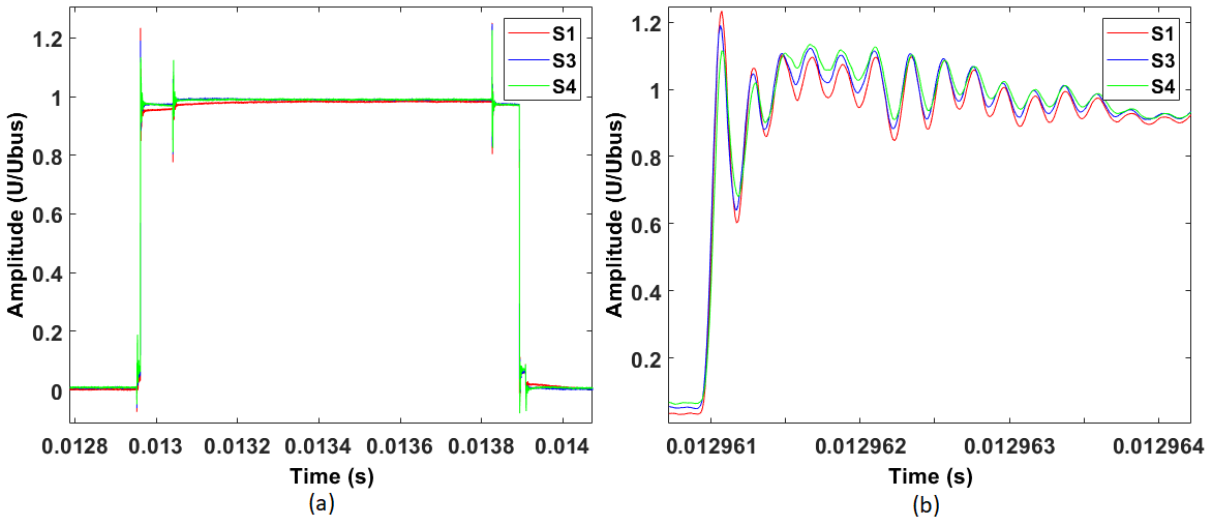

Figure II-7: *Turn-to ground measurements on the first three turns of the first coil (channel 1 of first phase): (a) zoom on two consecutives switches, (b) zoom on the rising edge*

Voltage distribution is not homogeneous. The steep voltage edges generate surges within the inverter, cabling, and machine winding system due to reflection and oscillations. These overvoltages, as well as rise and fall times, decrease as voltage moves through the winding. Furthermore, it should be noted that this propagation phenomenon is even more visible when considering coil-to-ground voltages (see below). In turn, voltage differences between coils can be significant. Depending on winding geometry, two coil ends may be very close to each other; consequently, the insulation systems between coils undergo very stressful constraints.

DC portions of the voltage can also be observed before and immediately after switching. To illustrate this point, the coil-to-ground voltages, *i.e.* the voltages between the input of each coil and the ground, are given below for two types of inverters.

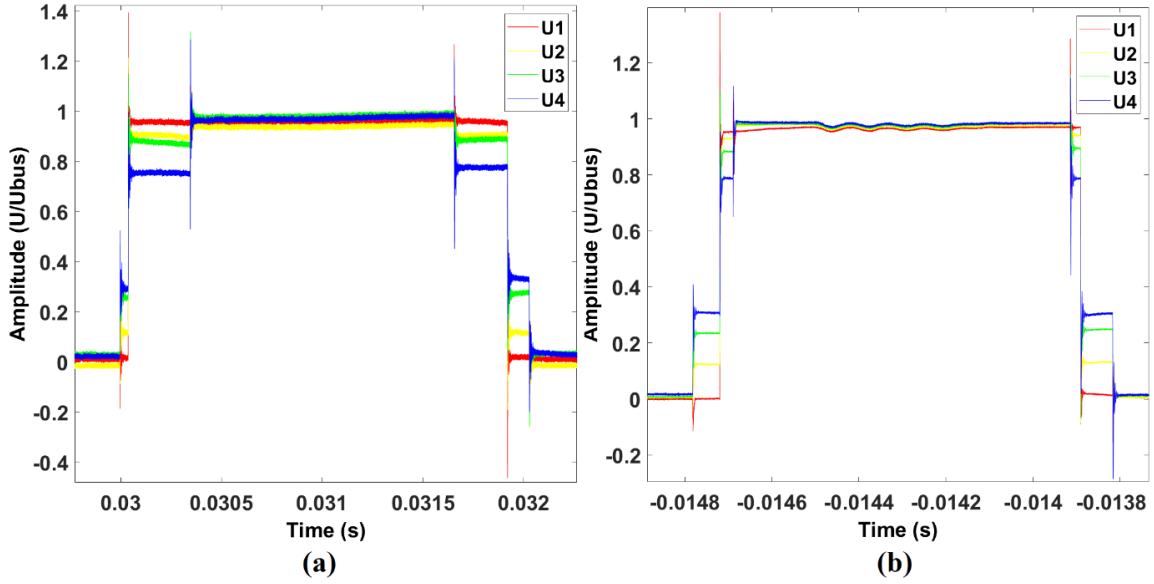

Figure II-8: *Voltage distribution for the different coils of channel 1 (a) inverter B, U_{bus} = 0.5xU_{nom}, L_{cable}=11m, Ω = 500 rpm, (b) inverter C, U_{bus} = U_{nom}, L_{cable}=1m, Ω = 500 rpm*

For phase-to-ground voltages, the overvoltage decrease from coil 1 to 4 can be explained by the delay between the voltage pulses at each coil input and dV/dt attenuation, both related to the propagation phenomena. In contrast, the unusual shape of the voltage mentioned earlier, which is more marked in the case of coil-to-ground voltages, is instead linked to machine structure and the nature of the PWM signal. The algorithm for PWM control associated with this type of inverter is Space Vector Modulation (SVM). An example of the theoretical phase-to-ground voltages that can be obtained with such control is given in Figure II-9.

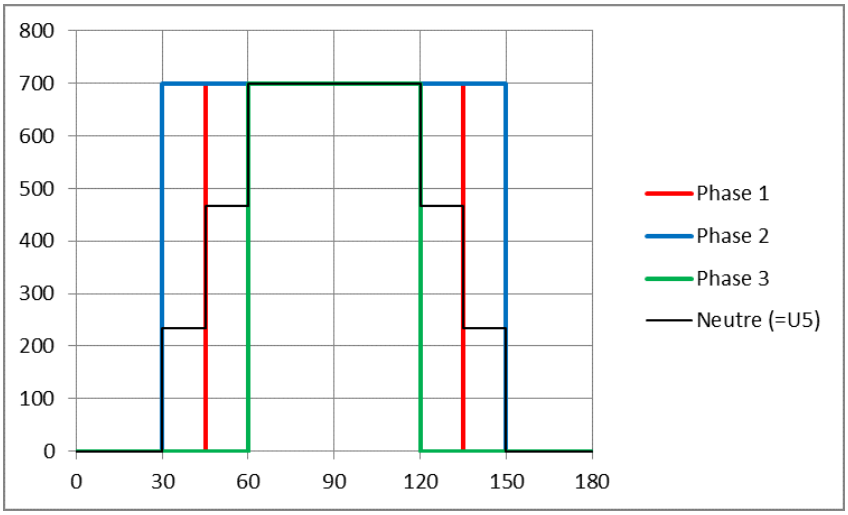

Figure II-9: *Example of phase-to-ground and neutral-ground voltages obtained with SVM*

Both red curves in Figure II-8 and Figure II-9 correspond to the voltage at the input of phase 1 before propagating in the coils. The black curve in Figure II-9 shows the neutral-ground voltage, which corresponds to voltage U5 (*i.e.* the voltage at the output of phase 1 after propagation) and is determined from these phase-to-ground voltages. (Figure II-10)

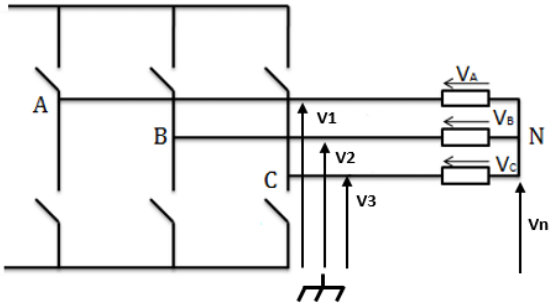

Figure II-10: *Simplified diagram of the inverter and machine*

$$V_A + V_B + V_C = 0 = V_1 + V_2 + V_3 - 3V_N \rightarrow V_N = \frac{V_1 + V_2 + V_3}{3} \qquad (18)$$

The coil-to-ground voltages between those two points, such as the ones depicted in yellow, green and blue in Figure II-8, can be deduced from these voltages by taking into account the additional voltages

across the coils throughout the channel. The general shape of the coil-to-ground voltages is due to the shape of the neutral-ground voltage, which itself is determined by the different phase-to-ground voltages. The presence of coils all along the channel also modifies the magnitude of the observed DC portions from one coil-to-ground voltage to another. The presence and amplitude of these DC portions of voltage therefore depend both on the voltages at the other phase's terminals and on the voltage across the coils throughout the channel. In short, the structure of the machine, as well as the command strategy, help explain the presence of these plateaus during switching. Furthermore, the observed increase in amplitude of these local constant voltages heading away from the first coil happens to be non-linear. As the geometry of the coils is supposed to be the same, this increase should be linear. In practice, however, that is probably not the case, and additional effects such as capacitive coupling between phases may exist.

The phase-to-ground voltages for inverters A and B are shown in Figure II-11 for further analysis concerning the stress comparison between inverters using Si IGBT and SiC MOSFET technologies. This also allows us to establish qualitative and quantitative electrical stress variations based on a concrete example.

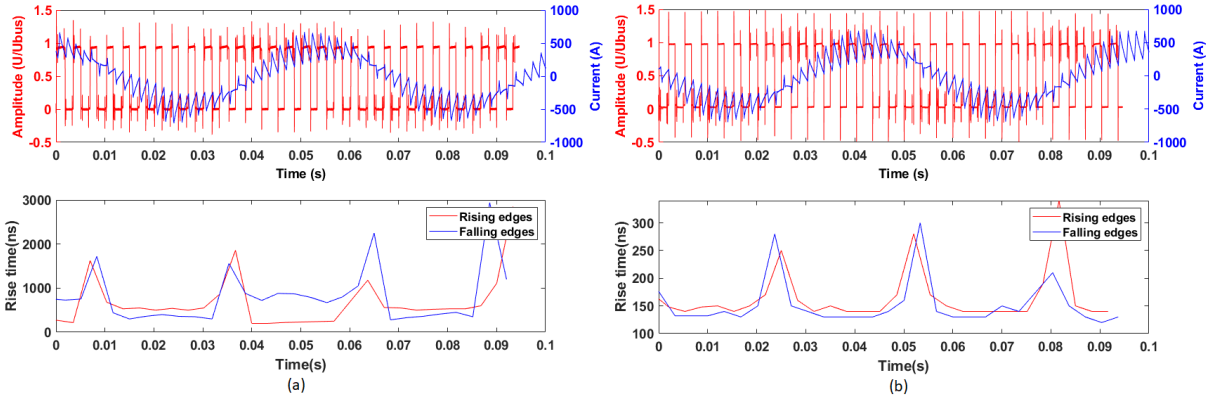

Figure II-11: *Phase-to-ground voltage and switched current vs. time (top) and rise time vs. time (bottom) (U_{bus} = 0,5xU_{nom}, L_{cable}= 40m, Ω = 500 rpm) (a) inverter A, (b) inverter B*

The rising edges at the inverter output are strongly influenced by the switched current, as well as overvoltages. The slope, in general with all inverters, increases with the absolute value of the current. The overvoltages also vary with the switched current in a less trivial manner. This is discussed in more detail in section II.4.1.1. The trend is the same for inverters C, D, and E. Having the fastest rise time, inverter C has the highest relative overvoltage (up to 97% of the DC bus), but also the largest voltage slope (up to 11.37 kV/µs at the motor terminals).

Rise time is strongly dependent on the time position and thus on switched current. The largest rise times correspond to the time when the current passes through zero. Curve shapes for rise time vs. time position are consistent with results found in the literature on this subject [12]. Rise times for the Si-based inverter range between 250 and 3000 ns, and between 100 and 300 ns for the SiC-based inverter, roughly ten times faster than Si technology.

Consequences of these fast switching components in terms of electrical stress are given in Table 8. All parameters, except those in the first column, are measured at the motor terminals and correspond to the extreme values for one period of time (p-to-g = phase-to-ground, p-to-p = phase-to-phase, t-to-t = turn-to-turn).

Table 8: *Comparison of electrical constraints generated by Si IGBT and SiC MOSFET inverters*

Inverter	dV/dt inverter (kV/µs)	Rise time (ns)	dV/dt motor (kV/µs)	P-to-g overvoltage (%Ubus)	P-to-g average overvoltage (%Ubus)	P-to-p overvoltage (%Ubus)	T-to-t voltage (%Ubus)
A	4.43	190	4.68	34.6	21.4	67.6	6.98
B	7.78	120	7.05	57.8	51.1	85.9	7.73
Variation	+3.35	-70	+2.37	+23.2	+ 30.3	+18.3	+ 0.75

The SiC-based inverter is clearly much faster than the Si-based inverter. In turn, the levels of stress are much higher with the SiC-based inverter, both between phases and between phase and ground. The increase is less marked regarding turn-to-turn voltage. The trend is the same for other configurations. Therefore, there is a good chance for partial discharges to be ignited when fed by such inverters.

II.3.3 Phase-to-phase voltage

Measurements of phase-to-phase voltage were performed with the same A and B inverters that served as a basis for comparison. The results are shown in Figure II-12.

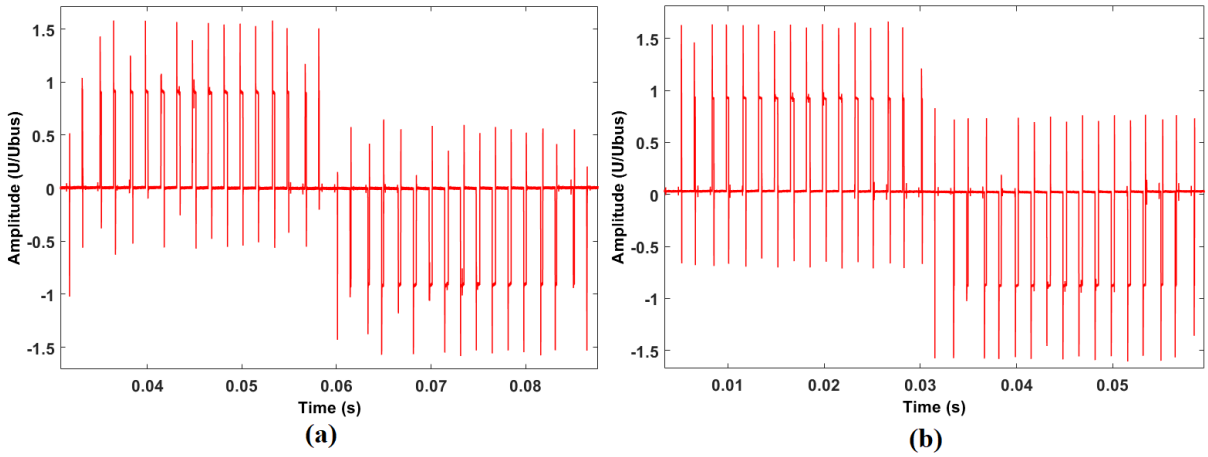

Figure II-12: *Phase-to phase voltage at the motor terminals (U_{bus} = 0,5xU_{nom}, L_{cable}= 40m, Ω = 500 rpm) - (a) inverter A, (b) inverter B*

It can be seen that overvoltages are higher than with phase-to-ground voltage (see Table 8). The voltage slopes are more or less in the same range when compared to the turn-to-ground tests (respectively up to 4.43 and 7.78 kV/µs for Si IGBT and SiC MOSFET). With phase-to-ground voltage, the maximum phase-to-phase relative voltage is reached with inverter C (up to 2.07xU_{bus}). The phase-

to-phase stresses are the largest; the overvoltages are huge in magnitude, and are amplified with the transition to SiC components and increase of DC bus voltage, not to mention the influence of cable length and torque (and current, indirectly). As a result, phase-to-phase insulation may also be subject to partial discharges.

These first investigations of the machine reveal that the weakest point of the machine is not the turn-to-turn insulation, as is the case for low voltage machines, but rather the phase-to-ground and phase-to-phase insulation systems. Even if they are supposed to be designed for these larger stresses, additional factors such as cable length and the use of SiC-based components can increase constraints significantly [69]. Consequently, these EIS must be considered carefully and constitute the focus of the following analysis.

II.4 Influence of different parameters

This section is devoted to analyzing results, with close attention to the influence of the different parameters in terms of electrical stresses. Those parameters are both electrical (rise time, switched current…) and geometrical (cable length and disposition). The goal is to understand the extent to which constraints are affected and to identify the relevant factors involved.

II.4.1 Electrical parameters

The experimental setup established for this study enabled us to vary numerous parameters related to machine operation. Some of those parameters were studied with particular consideration. They are identified as “electrical parameters”, as they are closely related to input electrical stress. Those parameters are the switched current, rotation speed (and indirectly torque), and DC bus voltage magnitude. Their influence on dV/dt and overvoltages at the motor terminals are presented below. An analysis of the influence of geometrical parameters, and in particular of cable characteristics, is provided hereafter.

II.4.1.1 Switched current

Switched current is one of the parameters with the highest influence on electrical stresses, whether between turns, phases, or to the ground. It notably impacts dV/dt at the inverter output. It was possible to modify this switched current by varying either the engine torque (for comparison reasons, the torque is defined as a value between 0 and 100%) or rotation speed. This work serves the dual purpose of relating switched current and stress, as well as ensuring that torque variation only implies a current variation and does not otherwise impact the stress itself.

Switched current ranges from 100 to 400A for inverter C, and from 300 to 500A for inverters D and E. Inverters A and B had switched current up to 1000A. The differences of switched current are mainly due to the fact that different PWM signals are used for the control. A preliminary study focusing

on torque was performed in order to demonstrate whether electrical stress, especially the rising edges and overvoltages, depends on current only, or also on torque. More precisely, for a given configuration, voltage and current waveforms were recorded on one period of time for different torque values, and the dV/dt and overvoltage values were then measured on the basis of these waveforms and plotted as a function of switched current. A distinction was made between the dV/dt and overvoltages associated with the rising edges (from the zero value to U_{nom}) and the falling edges (from U_{nom} to the zero value). The results are given in Figure II-13.

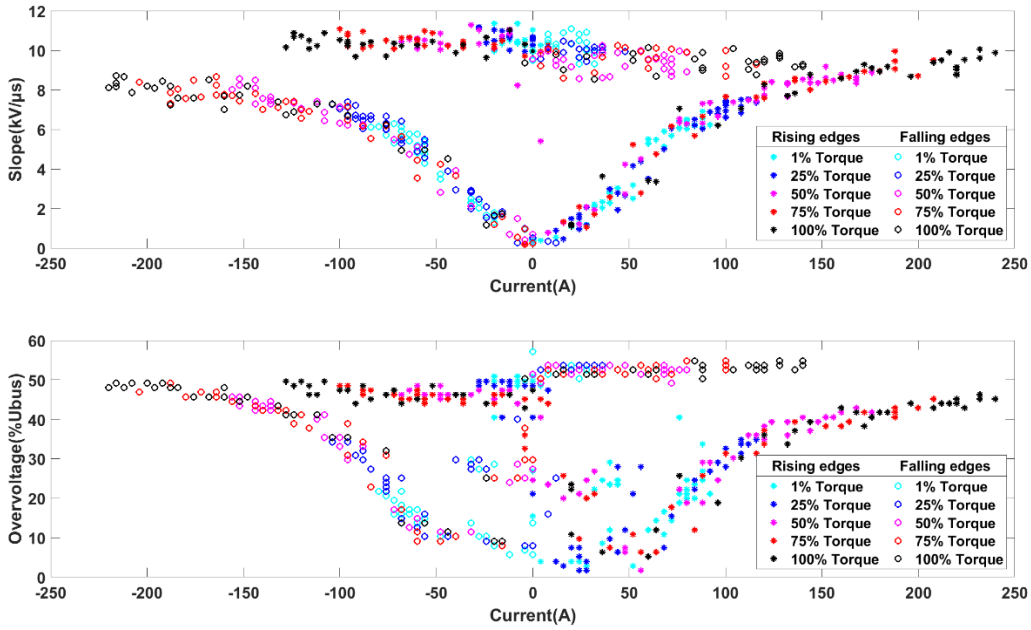

Figure II-13: *Phase-to-ground dV/dt and overvoltages vs. current for different torque values (inverter C, $U_{bus} = U_{nom}$, $L_{cable} = 1m$, $\Omega = 500$ rpm)*

Several conclusions can be drawn from this study. Figure II-13 illustrates the fact that the greater the torque, the larger the absolute value of the current. An increase in torque thus makes it possible to cover a broader range of switched current, and as a result to study the influence of switched current on electrical stress on a broader scale. It can also be seen that, even if the more stressful constraints are reached for high torque values, there is continuity in dV/dt and overvoltages vs current curves when varying torque. In other words, the torque itself does not seem to impact rise times and overvoltages. The voltage rise time and spike are the same for a given current, regardless of torque value. Therefore, the torque value was set to 100%, which corresponds to the largest possible switched current.

Regarding the variation of constraints with switched current, Figure II-14 shows the phase-to-ground voltage for a given configuration with inverter B, as well as the corresponding slope and overvoltage versus current curves. This inverter was chosen because it is the one that generates the most stressful constraints, combining both fast rising edges and high DC bus voltage.

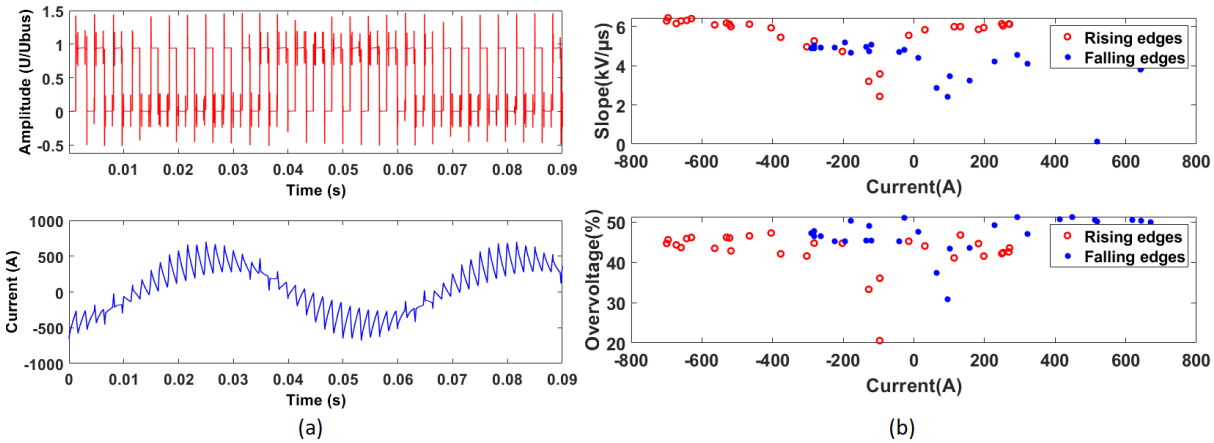

Figure II-14: *(a) Phase-to-ground voltage (up) and current (down), (b) overvoltages and rising edges vs. switched current (inverter B, U_{bus} = 0,5xU_{nom}, L_{cable}= 28m, Ω = 500 rpm)*

Voltage plots are zoomed on one period, which explains why the number of switching operations does not match the number of points on the curve (b). A variation of the rise time with current can be observed. dV/dt is at a minimum when the switched current is close to 0. It is also clear that the highest rise times correspond to the time when the current passes through zero. dV/dt then increases when the absolute value of the current increases, and eventually stabilizes at its highest value (up to 7 kV/µs in this case).

There is a slight difference regarding overvoltages: positive overvoltages increase more when the current decreases in its negative half, and conversely. The trend is more or less evident depending on the inverter. The variation ranges between 20% and more than 50% of the DC bus for this inverter. In addition, the transition between minimum and maximum values corresponds to the current's polarity change.

Finally, asymmetry can be observed around the zero current value, both for slopes and overvoltages. This asymmetry may be due to the fact that, depending on current polarity, different components are switching. On one side of the vertical axis passing through zero, slopes and overvoltages increase with the current (here, on the left side) while, on the other side, they seem to increase much more quickly to reach a constant threshold (here, on the right side). It is more pronounced with some inverters than others (as shown in Figure II-13 with inverter C). It is worth pointing out that behavior is similar with phase-to-phase voltage. Regarding turn-to-turn voltage, dV/dt values are not an important consideration, but the peak voltage experiment shows the same variations.

II.4.1.2 Rotation speed

Rotation speed also has a significant influence on switched current, and thus on constraints. Indeed, the PWM signal is directly dependent on speed, resulting in a change of current magnitude. Table 9 summarizes the type of PWM signals used for each case.

Table 9: *Description of PWM signals (SV: Space Vector, FW: Full Wave, PC: Pre-Calculated)*

Speed \ Inverter	A, B	C	D, E
200 rpm	SV	SV	SV
500 rpm	SV	SV	SV
1000 rpm	FW/PC	SV	PC
1500 rpm	FW/PC	FW/PC	FW/PC
2000 rpm	FW/PC	FW/PC	FW/PC

It is worth noting that the PWM signal choice also depends on engine torque (for FW/PC cases). Thus, the impact of rotation speed depends both on the type of inverter and on torque.

Switching frequency is also heavily dependent on the PWM signal and thus on rotation speed. The PWM signal choice, which defines, the current and switching frequency values, among other things, is made with a desire to optimize machine performance within the limits imposed by specific criteria (torque, switching losses, temperature, maximum current, modulation index), which are themselves affected by rotation speed. The transition between the different types of PWMs differs according to the inverters, and conditions the maximum switching frequency value in each case. The switching frequency ranges roughly between 100 and 600 Hz for inverters A and B, between 100 and 800 Hz for inverters D and E, and finally between 800 and 1800 Hz for inverter C. Those values are not very high for several reasons, especially when using SiC-based components. First, the maximum value of the switching frequency is conditioned by pulse length, which cannot go below a threshold value for safety reasons. Furthermore, in this particular case, loss management is given preference over an increase in performance. In more concrete terms, the idea here is to observe the benefits of introducing SiC based components in terms of losses for a given conception, without improving performance. Finally, and still in this same direction, the SiC-based inverters were not pushed to their limits to ensure a viable comparison between Si-based and SiC-based inverters. The maximum switching frequency is thus limited by the Si IGBT power modules. Overall, the variation of switching frequency with rotation speed is far from trivial, highly non-linear and, more importantly, imposed. The influence of this parameter was therefore not studied. However, to ensure a fair comparison, the same PWM signals were used for inverters having the same configuration but with different component technologies.

One might wonder, as in the case of engine torque, whether rotation speed only has an indirect influence on electrical stress by conditioning the PWM signal choice and, as a consequence, the switched current waveform, or if it also has any direct impact on electrical constraints. To answer this question, a preliminary test similar to that performed in II.4.1.1 was performed to check whether the voltage rise time and spike are the same (Figure II-15) for a given current regardless of speed.

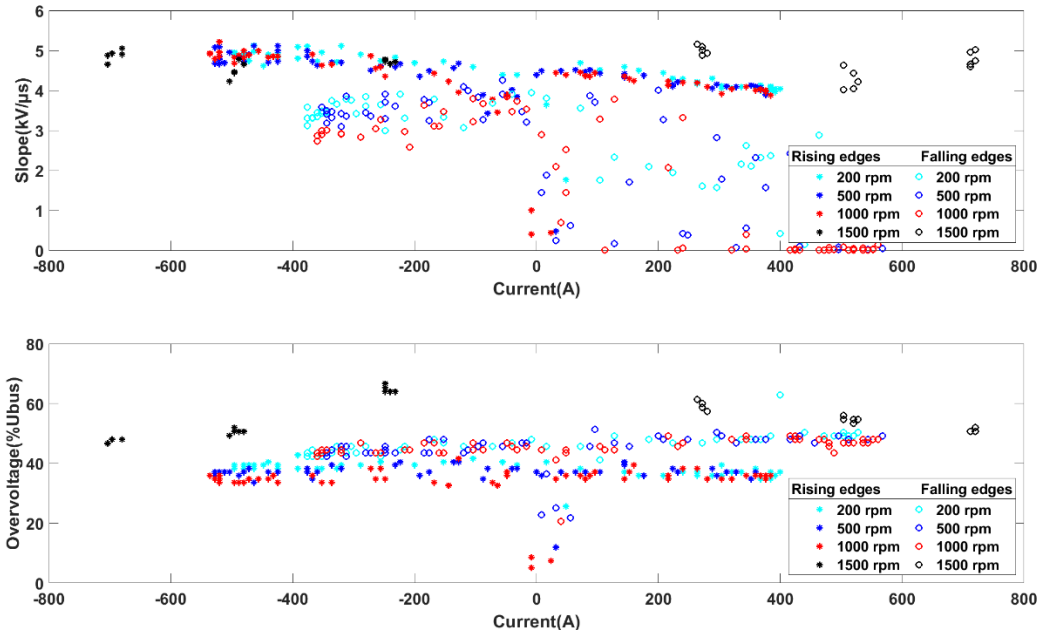

Figure II-15: *Phase-to-ground dV/dt and overvoltages vs. current for different rotation speed values (inverter E, $U_{bus} = U_{nom}$, L_{cable}= 40m, Ω = 200-1500 rpm)*

As in the case for torque, the larger the rotation speed, the larger the current. At high speed, the switching frequency is much lower than at low speed. As a consequence, the current is so distorted (as shown in Figure II-16) that voltage rising edges occur for negative current values only, and vice versa for voltage falling edges. Despite some very long fall times values in the positive part of the current, it turns out that a continuity of the slopes and overvoltages vs current curves is observed when varying rotation speed, as with torque variation, for the 200, 500, and 1000 rpm cases. However, it seems that rise times and overvoltages in particular are larger for a given current in the 1500 rpm case. The trend is the same with other inverters. We also noticed that the faster the motor rotates, the larger the current, but the lower the switching occurrences. To summarize: the 1500 rpm case covers a wider current range, while the 200, 500, and sometimes 1000 rpm cases are very similar, as the PWM signal remains unchanged. On the basis of this information, and considering that only two different types of PWM are used in most cases (as shown in Table 9), we therefore decided to perform most of the experiments for two rotation speed values (500 and 1500 rpm), in order to cover both the low speed case with a large number of switching occurrences and thus a large number of data points, and the high speed (and high current) case to obtain the critical values for slopes and overvoltages.

Figure II-16 shows the phase-to-ground voltage and the slope and overvoltage versus current curves for the same configuration as that in Figure II-14, but with a rotation speed of 1500 rpm. As mentioned earlier, the switching frequency here decreases drastically compared to Figure II-14 (for a given time interval, the number of rising and falling edges is significantly lower), in contrast to the peak value of the switched current, which is higher than in the 500 rpm case. The current waveform is quite degraded as a result of the low switching frequency. It should be pointed out that the PWM signals were

designed specifically to attain very high current values but may not be representative of operating conditions.

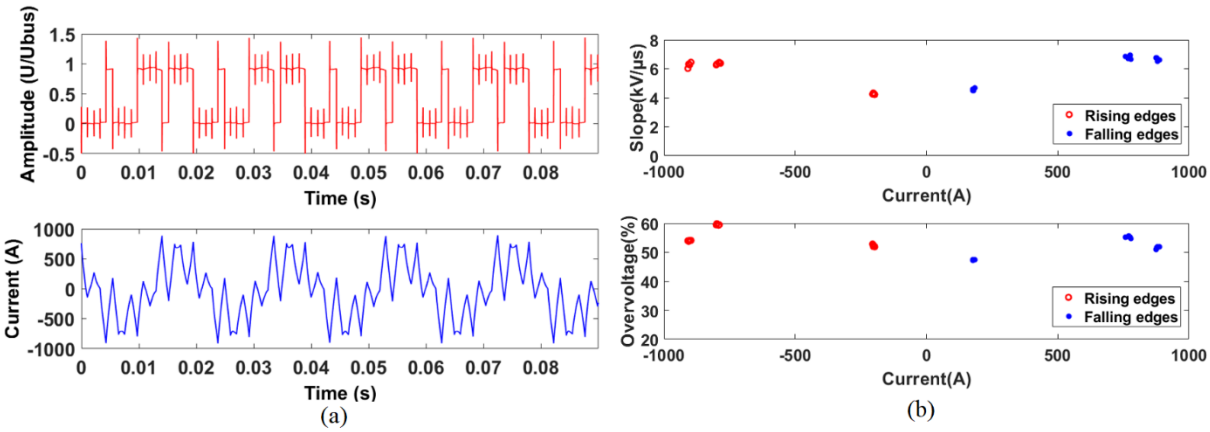

Figure II-16: *(a) Phase-to-ground voltage (up) and current (down), (b) overvoltages and rise edges vs. switched current (inverter B, U_{bus} = 0,5xU_{nom}, L_{cable}= 28m, Ω = 1500 rpm)*

In concrete terms, the behavior here is the same as in the 500 rpm case, namely showing an increase of dV/dt and overvoltages with the switched current. The main differences are the higher current and the change in the number of occurrences, both related to the PWM signal change, which lead to more stressful constraints. Finally, a test was carried out with inverter C, which has the special feature of having two very close PWM signals at both speeds. It turns out that the obtained values are essentially the same. It can therefore be assumed that only the switched current has an impact on electrical stresses and that the other parameters only modify them indirectly.

II.4.1.3 Supply voltage

Our study on the impact of supply voltage hinge around two main aspects: the influence of the DC bus voltage value, and a comparison between stress at the motor terminals under PWM and double pulse signals. The influence of DC bus voltage is not extremely easy to highlight, as most of the tests under PWM were performed at constant voltage, among other reasons. However, despite these restrictions, it was possible to establish a trend in terms of overvoltage amplitude in relation to DC bus voltage, when supplying the motor with a double pulse signal.

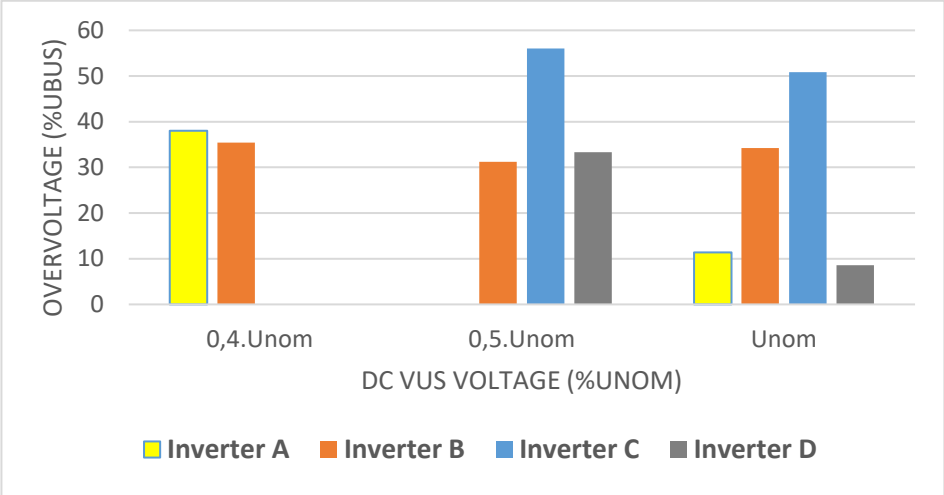

Figure II-17: *Overvoltage vs DC bus voltage amplitude for four types of inverters*

Overvoltages generally decrease when the supply voltage increases and approaches its nominal value. These results must be qualified, as only the double pulse signal case was studied, and given the small number of voltages that were considered. However, one factor could account for this trend. The overvoltages at the motor terminals are due mainly to propagation phenomena along the cables. In the case of an impedance-matched line, there is no reflected wave coming from the load. Indeed, the wave progressing through the transmission line towards the load is not subject to an impedance variation. In contrast, when the load is not adapted in impedance, the reflected wave must be taken into account. One of the parameters with the most impact in such a phenomenon is the voltage wave rise time. If the reflected wave has time to return to the source (back and forth) before the incident wave reaches its maximum value, then the overvoltage is reduced. This is the case when the electric wave rise time is more than twice the propagation time of the wave. As rise time generally increases with DC bus voltage, it means that the lowest voltages (*i.e.* those with the shortest rise times) help the emergence of higher overvoltages, and vice versa. Nevertheless, it should be noted that despite this overvoltage decrease when increasing DC bus voltage, in terms of reliability, PDs are more likely to occur at high voltage as the voltage stress is naturally closer to the PDIV. Conversely, at low voltage, voltage surges may be of larger amplitude, but the overall voltage remains below this threshold; therefore, the machine is less subject to PDs.

The main difference between a PWM signal and double pulse signal – apart from the input voltage itself – is that in the first case, the machine is working; whereas in the second case, the signal simply passes through the entire chain but the machine does not rotate. Only the DC bus voltage, cable length, and current can be set. A comparison between overvoltages and rise times in both cases was thus made to highlight the influence of operating conditions. Particular points were chosen in the PWM signal to be as close as possible to the current set for the double pulse signal (100 A).

Table 10: *Comparison between double pulse and PWM for two operating points (Inverter D)*

Configuration	DC bus voltage (V)	Cable length	Torque (%)	Speed (rpm)	Current (A)	Rise time (ns)	dV/dt motor (kV/µs)	Max overvoltage (%Ubus)
Double pulse	**Unom**	**11**	**/**	**/**	**100**	**274**	**2.15**	**8.6**
PWM	Unom	11	33	200	96	280	2.31	8.6
PWM	Unom	11	33	200	120	280	2.32	8.6
PWM	Unom	11	33	1000	96	310	2.19	5.1
PWM	Unom	11	33	1000	88	290	2.26	4
PWM	Unom	11	100	500	88	270	2.35	5.1
PWM	Unom	11	100	500	104	280	2.29	5.1
Double pulse	**Unom**	**40**	**/**	**/**	**100**	**270**	**2.32**	**32.5**
PWM	Unom	40	100	500	112	300	2.01	24.6
PWM	Unom	40	100	500	80	550	1.05	25.7

Qualitatively, the results are similar between double pulse and PWM signal, within a few percentage points. Only part of the results is presented here, but it seems that the influence of torque and rotation speed on dV/dt and overvoltages for a given current is lower, as discussed in sections II.4.1.1 and II.4.1.2. This tends to show that there is no major difference if the machine rotates or not, and regardless of the input voltage. However, it is difficult to reach any firm conclusions concerning the influence of operating conditions on electrical stress at the motor terminals. Phenomena that come into play are very different depending on whether the machine rotates and all inverter legs are used, or if the motor is simply supplied by a double pulse signal. The time under stress is also a factor that must be taken into account. Regarding PDs, constraints related to the machine operation aside, the main difference in terms of input voltage between double pulse and PWM signals resides in the fact that only two pulses propagate through the winding in the first case, and are thus likely to incept PDs; while in the second case, it is a continuous process favoring the emergence of memory effects associated with charge deposited by previous PD events.

II.4.2 Cable characteristics

II.4.2.1 Cable length

We have shown that several parameters, particularly switched current, influence the voltage signal at the inverter output and subsequently at the motor terminals. However, these parameters only increase or decrease existing overvoltages. Those overvoltages are due mainly to two causes: cable length and impedance mismatches. Indeed, propagation mechanisms occur in the cables between the inverter and the motor, leading to wave reflection phenomena and thus to overvoltages at the motor terminals [29]. Broadly speaking, voltage impulses behave like waves during their propagation through the cable and can be reflected according to the frequencies and impedances of the inverter and the motor. When there are impedance mismatches between the transmission line and the actuator, one can define a reflection coefficient depending on the different impedances; total voltage can be expressed by means of this

coefficient and a time lag linked to propagation, while taking into account all incident and reflected waves. Rise time, which determines the quantity of reflections that can occur, plays a significant role on the magnitude of overvoltages. The impedances for each inverter may also be different. This helps explain the differences between the different inverters.

Figure II-18 shows the average dV/dt and overvoltages (on one current period) at the motor terminals depending on the cable length, considering phase-to-ground and phase-to-phase voltages for each inverter. The DC bus voltage was set to its nominal value for inverters C, D, and E, and at 56% of its nominal value for inverters A and B. It is clear that the slopes decrease with cable length. For most of the inverters, tests were only performed for two cable lengths, thus limiting interpretation. For the particular case of inverter C, a test was carried out with a very short cable length (one meter). This allows us to see that dV/dt decreases significantly between 1 and 10 meters (from around 20 kV/µs to 9 kV/µs), which might lead one to think that variation is strongest in this range.

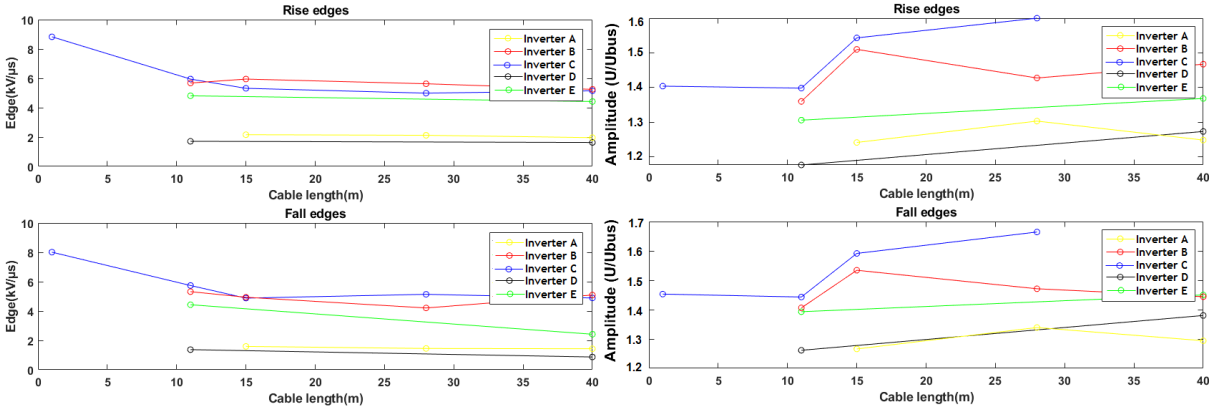

(a)

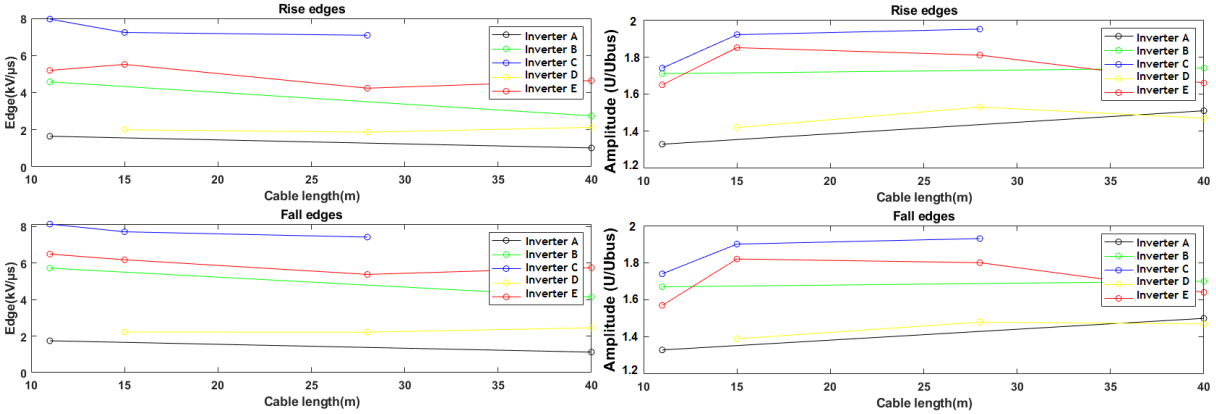

(b)

Figure II-18: *Slope (left) and peak voltage (right) vs. cable length (rising edges on top, falling edges on the bottom), Ω = 500 rpm (a) phase-to-ground voltages, (b) phase-to-phase voltages*

The low level of flexibility in terms of cable length variation does not allow for the recognition of the cable length-overvoltage charts provided by standards for different rise time values [15]. To be more

specific, if referring to this standard, the calculation of the rise times associated with dV/dt values shows that in the case of inverter C, the considered cable length variation range highlights a substantial variation in overvoltages (especially considering phase-to-ground voltages), whereas for the other inverters, it falls within a part of the curve where there is not yet any real increase. A greater cable length variation might have produced a clearer picture for the slowest inverters. In any case, this result in itself justifies the relevance of the study: new problems that did not exist before are raised by the introduction of fast-switching components in power electronics.

Nevertheless, it can be observed that the longer the cable, the larger the overvoltage, especially with the fastest inverter. For the four remaining inverters, the increase turned out to be more moderate. One can expect a behavior similar to the curve given by the standard, namely an overvoltage variation depending on rise time, even if the length values delimiting the different areas of the curve must be different and linked to the geometrical features of the cable as well as to the impedance of the motor. The trend is the same concerning phase-to-phase voltages, with higher values (average peak voltage up to 2xU_{bus} for inverter C).

II.4.2.2 Connectors

The cables used for this study were designed in such a way that it was possible to cut them at various lengths and then reconnect them in order to have a fair range of cable lengths. It was thus possible to compare tests performed with and without connectors. Consistent with work done to-date, the goal is to highlight the influence of introducing these connectors. Figure II-19 allows us to compare slopes and overvoltages depending on switched current, in both cases, and considering inverter B. Up to three connectors were introduced on the cable, for a maximum of four different cable segments.

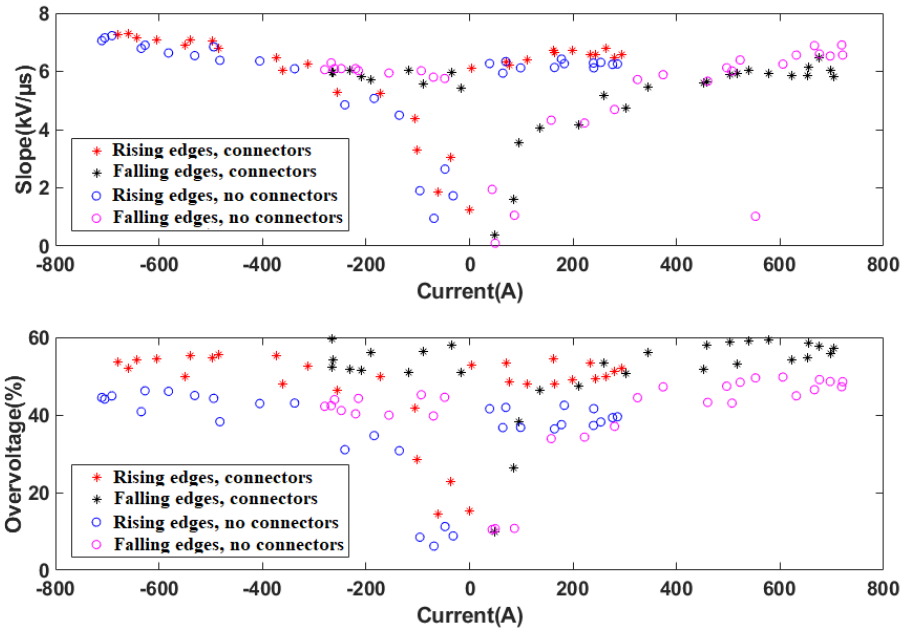

Figure II-19: *Slope (top) and overvoltage (bottom) vs. switched current with/without connectors (Inverter B, U_{bus} = 0,5xU_{nom}, L_{cable}= 11m, Ω = 500 rpm)*

Rising and falling edges are not affected by the introduction of such connectors, but a 10% increase in overvoltages can be observed. It must be emphasized that there is little difference between the voltage and current shapes in both cases. The impact is also greater for short cable lengths. Concerning turn-to-turn voltage, an average difference of a few volts between both cases was observed. Generally, the impact of introducing connectors is lower (for turn-to-turn voltage, it could even be a measurement error inherent to the instrument), except with short cable lengths for which overvoltages are affected. Introducing connectors must certainly affect system impedance, which could explain the observed changes. However, it is difficult to provide a detailed analysis of the phenomenon as it is very dependent on connector type, quantity, and location.

II.4.2.3 Disposition/ground plane

Cables, which were initially resting on a ground plane, were likewise elevated in order to analyze the impact of the distance between cables and the ground plane. Results for inverter E are given in Figure II-20. As for the previous case, rising and falling edges are affected in a very limited manner. In contrast, regarding overvoltages, differences between elevated and non-elevated cables (around 10%) can be observed.

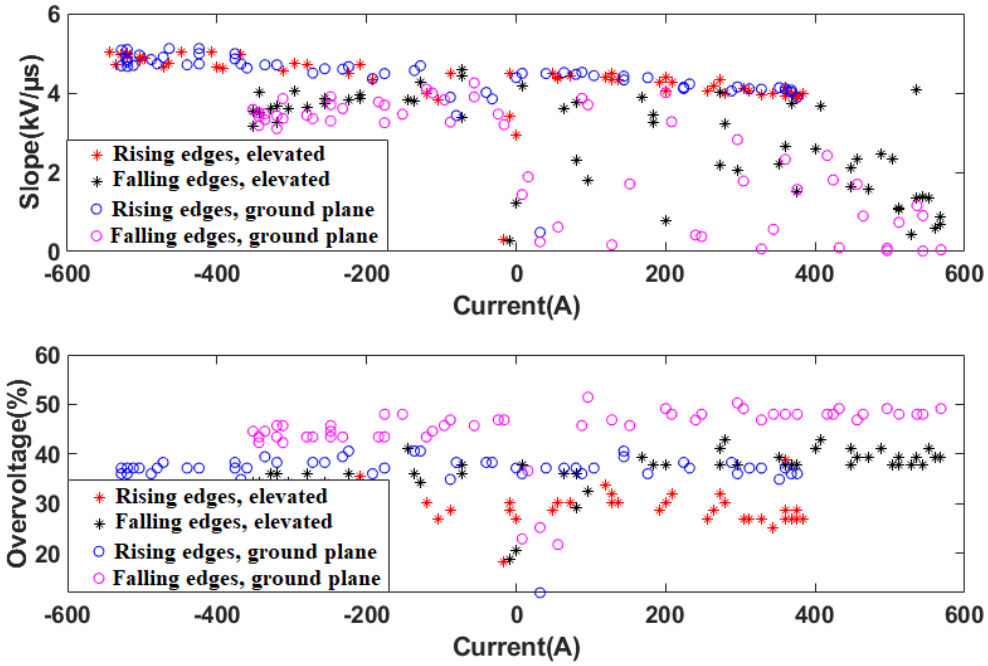

Figure II-20: *Slope (top) and overvoltage (bottom) vs. switched current with/without elevation (inverter E, $U_{bus} = U_{nom}$, $L_{cable} = 40m$, $\Omega = 500$ rpm)*

Common mode capacitance increases when cables are close to the ground plane. Subsequently, cable impedance decreases. Impedance mismatch is therefore increased, which means that the reflection coefficient increases too. Being directly proportional to this coefficient, overvoltage also increases. Conversely, when cables are elevated and moved away from the ground plane, common mode

capacitance decreases, the impedance mismatch is decreased, along with the reflection coefficient and finally the overvoltage.

Additional tests were performed to highlight the influence of three-phase cable arrangements. Three arrangements are encountered in the context of using our machine (Figure II-21): bundling cables, bulk cables, and flat-formation cables.

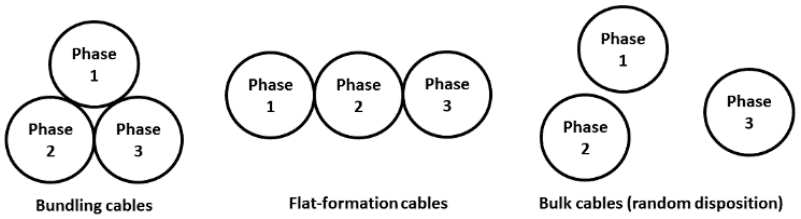

Figure II-21: *Possible arrangements of the three-phase cables*

It turns out that no significant differences were observed due to cable arrangement, mainly because the three dispositions are relatively similar. Further testing with more degrees of freedom would be needed to reach a firm conclusion. One can expect modifications in such a case: parasitic capacitances between cable and ground plane, as well as other per unit length parameters, would change and induce impedance modifications, thus leading to an impact on the shape and amplitude of the voltage stress at the motor terminals

II.4.3 Brief overview of Si IGBT vs SiC MOSFET technologies

The purpose of this final section is to point out the influence of introducing SiC-based components. Several figures are presented here. Figure II-22 shows the evolution of phase-to-ground and phase-to-phase overvoltages depending on dV/dt for each inverter and for a given cable length; histograms in Figure II-23 provide a clearer illustration of the different phenomena, especially regarding the statistical aspect.

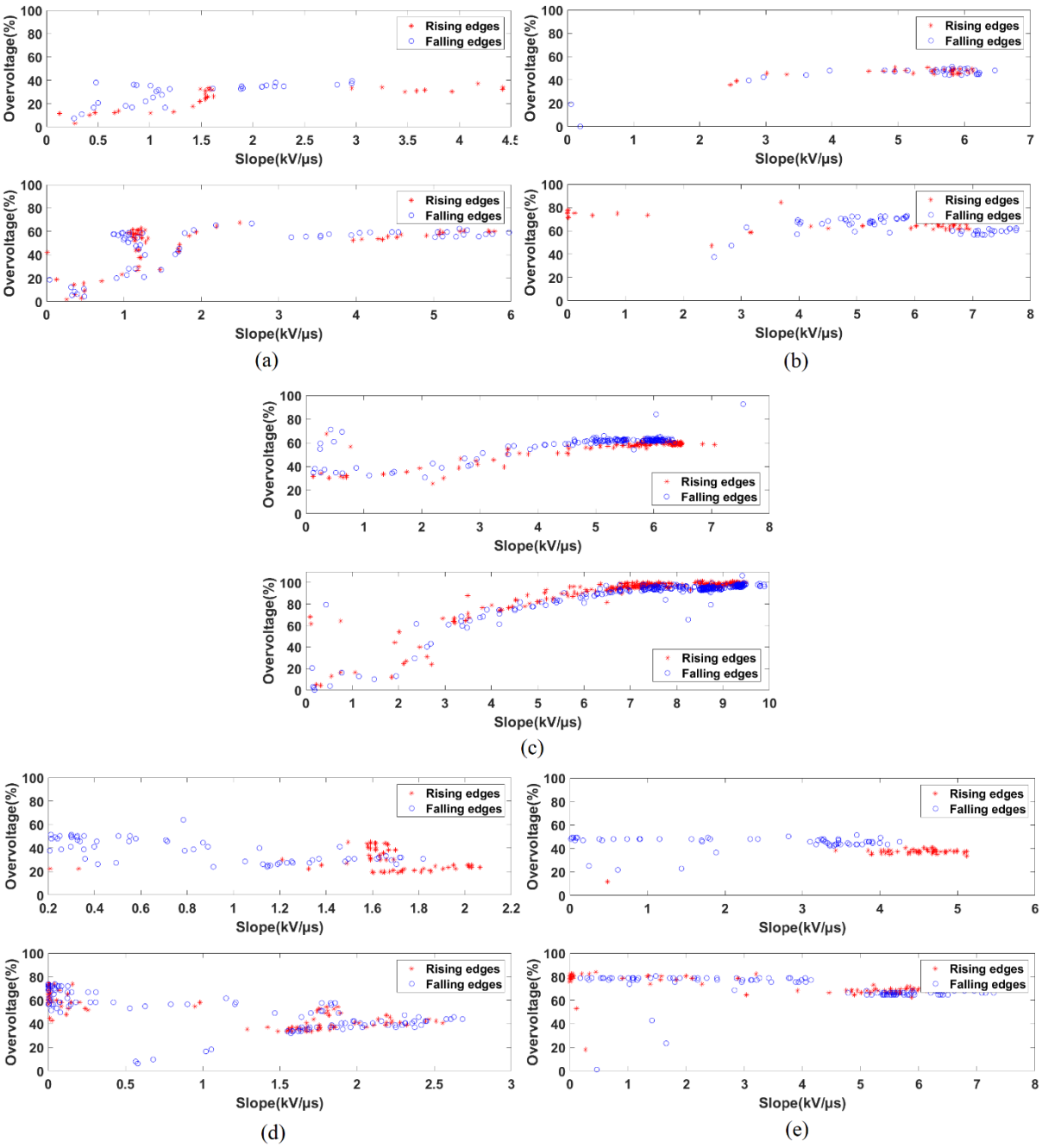

Figure II-22: *Overvoltages vs dV/dt: phase-to-ground voltage (top) and phase-to-phase voltage (bottom): (a) inverter A; (b) inverter B (U_{bus} = U_{nom}, L_{cable}= 40m, Ω = 500 rpm); (c) inverter C (Ubus = U_{nom}, L_{cable}= 15m, Ω = 500 rpm); (d) inverter D; (e) inverter E (Ubus = 0.5xU_{nom}, L_{cable}= 40m, Ω = 500 rpm)*

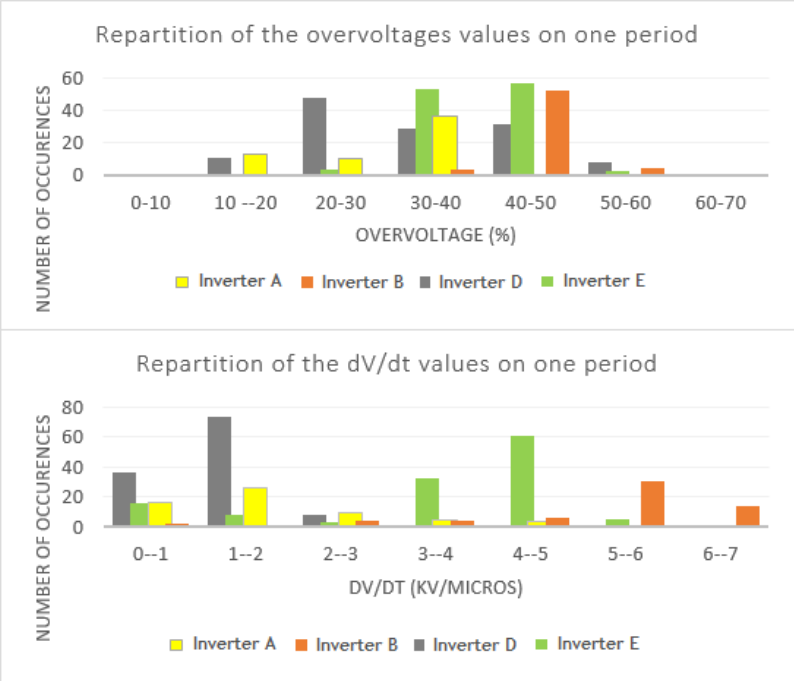

Figure II-23: *Histograms representing the repartition of dV/dt and overvoltage values on one period (Inverters A, B, D and E, $U_{bus} = U_{nom}/0.5xU_{nom}$, L_{cable}= 40m, Ω = 500 rpm)*

Figure II-22 shows that, in all cases, overvoltage increases when dV/dt increases until a threshold is reached. The behavior is the same for phase-to-ground and phase-to-phase voltages. Switching from Si IGBT to SiC MOSFET technology, the electrical stress increases from 20% to 30% of the DC bus voltage; this increase factor remains the same regardless of cable length. One can also see that most points on the curves are concentrated in a very dense area, and values that do not exhibit the same trend are a minority. The histograms in Figure II-23 are provided as an illustration of these aspects related to distribution. The majority of the dV/dt values range from 1 to 2 kV/µs for Si IGBT technologies, whereas they range from 4 to 6 kV/µs for SiC-based inverters. In terms of overvoltages, the values range from 20% to 40% with Si technologies and from 40% to 50% with SiC technologies. Despite a similar trend, a global increase of dV/dt and overvoltage amplitudes with the introduction of SiC based components can be observed, reflected on the histograms by a shift of the maximum levels to the right. This type of figure shows the entire PWM signal, as it takes into account the distribution of occurrences as well as average dV/dt and overvoltage values. It helps overcome problems such as non-representative voltage spikes that are mainly due to resonances or noise induced by switching.

The discrepancies between stresses induced by Si IGBT and SiC MOSFET based inverters were assessed specifically based on a concrete example and summarized previously in Table 8. Stress variations for the other comparative cases studied in this work are summarized in the following table.

Table 11: *Summary of electrical stress variations between Si (A,C) and SiC-based (B,D,E) inverters*

Configuration	Variation (SiC MOSFET vs Si IGBT)					
	Min rise time (ns)	Max dV/dt motor (kV/µs)	Max p-to-g overvoltage (%Ubus)	Average p-to-g overvoltage (%Ubus)	Max p-to-p overvoltage (%Ubus)	Max t-to-t voltage (%Ubus)
Inverters C & D, Ubus = Unom, Lcable= 11m, Ω = 500 rpm	-160	+3.49	-2.29	+13	+22	+9.49
Inverters C & D, Ubus = Unom, Lcable= 40m, Ω = 500 rpm	-180	+3.06	-4.57	+9.57	+19	+5.2
Inverters A & B, Ubus = 0.5xUnom, Lcable= 11m, Ω = 1500 rpm	-402	+6.14	+27.6	+23.5	/	+5.41
Inverters A & B, Ubus = 0.5xUnom, Lcable= 40m, Ω = 500 rpm	-80	+2.04	+13.7	+22	+7	+1.47
Inverters A & B, Ubus = 0.5xUnom, Lcable= 40m, Ω = 1500 rpm	-340	+4.88	+0.69	+0.5	-7	+3.78
Inverters A & B, Ubus = 0.5xUnom, Lcable= 28m, Ω = 1500 rpm	-330	+5.30	+5.37	+10.2	+7	+3.57
Inverters A & B, Ubus = 0.5xUnom, Lcable= 11m, Ω = 500 rpm	-50	+1.86	+1.24	+12.5	+8	+0.77

These results tend to confirm our observations quantitatively so far: SiC-based inverters generate electrical constraints up to 30% more stressful than classical inverters using IGBT technology.

II.5 General summary of maximum stresses at motor terminals

Table 12: *Summary of maximum stresses in the motor (double pulse signal)*

Inverter	dV/dt inverter (kV/µs)	dV/dt motor (kV/µs)	P-to-g overvoltage (%Ubus)	T-to-t voltage (%Ubus)	Rise time (ns)
Inverter A ($U_{bus} = U_{nom}$)	3.29	2.87	11.39	5.13	200
Inverter B ($U_{bus} = U_{nom}$)	/	10.38	51.11	8.62	160
Inverter C ($U_{bus} = U_{nom}$)	14.5	12.08	50.86	17.66	46
Inverter D ($U_{bus} = U_{nom}$)	2.16	2.32	32.57	5.71	187
Inverter E ($U_{bus} = 0.5xU_{nom}$)	4.35	2.05	41.33	/	120

Table 13: *Summary of maximum stresses in the motor (PWM signal)*

Inverter	dV/dt inverter (kV/µs)	dV/dt motor (kV/µs)	P-to-g overvoltage (%Ubus)	P-to-p overvoltage (%Ubus)	T-to-t voltage (%Ubus)	Rise time (ns)
Inverter A ($U_{bus} = 0.5xU_{nom}$	4.43	4.94	47.1	75.9	7.14	180
Inverter B ($U_{bus} = 0.5xU_{nom}$	8.56	7.78	57.8	88.2	8.86	100
Inverter C ($U_{bus} = U_{nom}$)	23.26	11.37	96.86	107.29	45.71	60
Inverter D ($U_{bus} = U_{nom}$)	/	2.92	66.86	78.28	7.03	205
Inverter E ($U_{bus} = U_{nom}$)	/	6.41	42.86	78.28	15.6	100

II.6 Partial discharge investigations

Complementary to previous results regarding electrical stress mapping in the machine, PD measurements were performed on the power chain in order to correlate measured voltage distribution and PD activity, and to confirm the trend pointed out in the previous tests. Detection was performed with the most stressful inverters, both in terms of voltage magnitude and rising edges, *i.e.* inverters A, B, and C. The precise configurations of the inverters with the variation ranges for each parameter were as follows:

- **Inverter A**: $U_{bus} = 0.5xU_{nom}$, L_{cable}= 40m, Ω = 500-1500 rpm
- **Inverter B**: $U_{bus} = 0.5xU_{nom}$, L_{cable}= 11-40m, Ω = 500-1500 rpm
- **Inverter C**: $U_{bus} = U_{nom}$, L_{cable}= 11-40m, Ω = 500-1500 rpm

The non-intrusive sensor used to detect partial discharges takes advantage of a capacitive effect between the sensor fitting and the cable core, and has already been used in numerous studies [9] [10] [70]. The sensor is based on a Jack-SMA connector, connected to a coaxial cable (Figure II-24). With this connector, it is possible to create a sensor that is robust, inexpensive, and standardized. However, due to its geometry, achieving good contact and adequate holding on the power cable can be challenging, particularly due to vibrations during on-line tests. For this reason, special 3D-printed clips were developed to ensure good contact regardless of the cable gauge. Sensor sensitivity can be increased simply by improving the coupling capacitance value. This is achieved by increasing the contact surface by putting copper tape on the surface of the power cable to control the interacting area and thus the value of the induced capacity. Sensor sensitivity is directly proportional to capacitance: increasing capacitance value by a factor of two doubles sensitivity. In order to achieve capacitive coupling, it is necessary for the cables to not be shielded. All tests were therefore carried out without shielding.

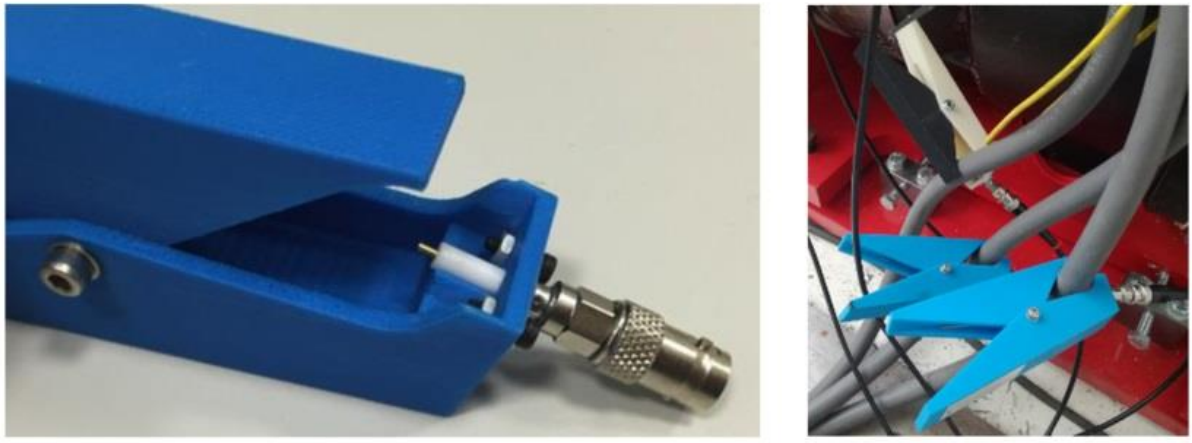

Figure II-24: *Zoom on the connector (left) and sensors directly placed on the cables (right)*

When performing measurement using a non-intrusive sensor, it is customary to connect a high-pass analog filter to remove noise from inverter drive switches or power amplifier. The typical cutoff frequency range from 200 MHz to 500 MHz was used in the following experiments. Three sensors were used to detect PDs in each phase. A schematic diagram of the overall experimental setup is given below.

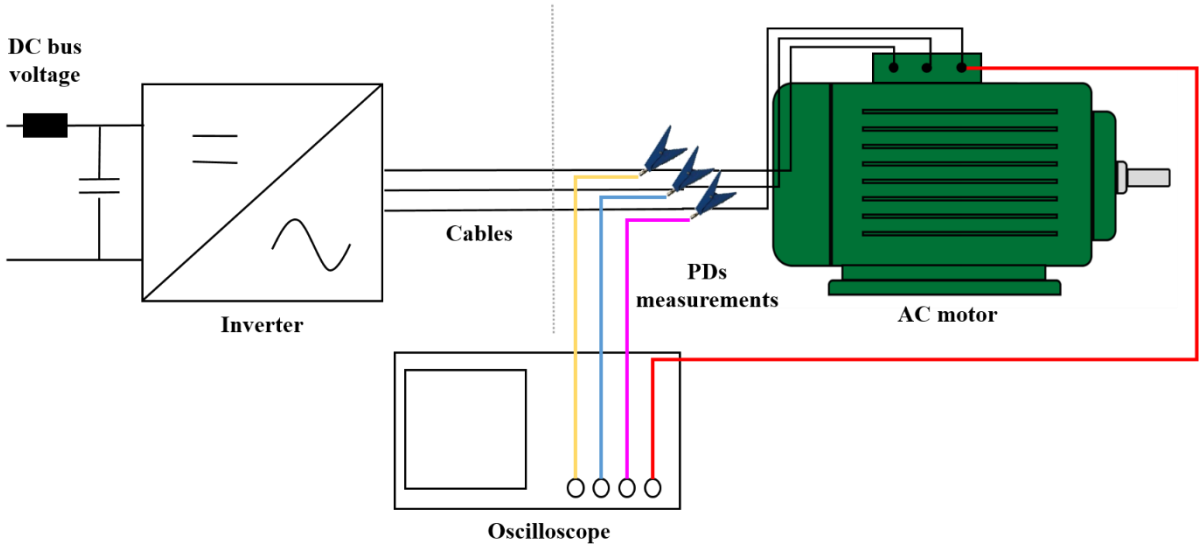

Figure II-25: *Description of the experimental setup including PDs detection*

Preliminary tests were performed to determine whether PDs were only located in the motor, or if they also occurred at the inverter level. To do this, the three sensors were placed on the cables as close as possible to the inverter. It turns out that no PD activity was detected. We were therefore in a position to conclude that PDs were only located in the motor. Subsequent tests therefore focused on measuring PDs in the motor.

II.6.1 Configuration no. 1: Inverter C

PDs were first investigated on inverter C, which presents the fastest rise time among all the inverters considered here. Three sensors were placed on the cables close to the motor to perform PD detection. One of the phase-to-ground voltages was also measured to correlate PD measurements with the voltage signal. High pass filters with a cutoff frequency of 400 MHz were used. There were no characteristic signals coinciding with all edges, indicating that the filter was adequate for removing noise-induced switching. Examples of PD measurements are shown below.

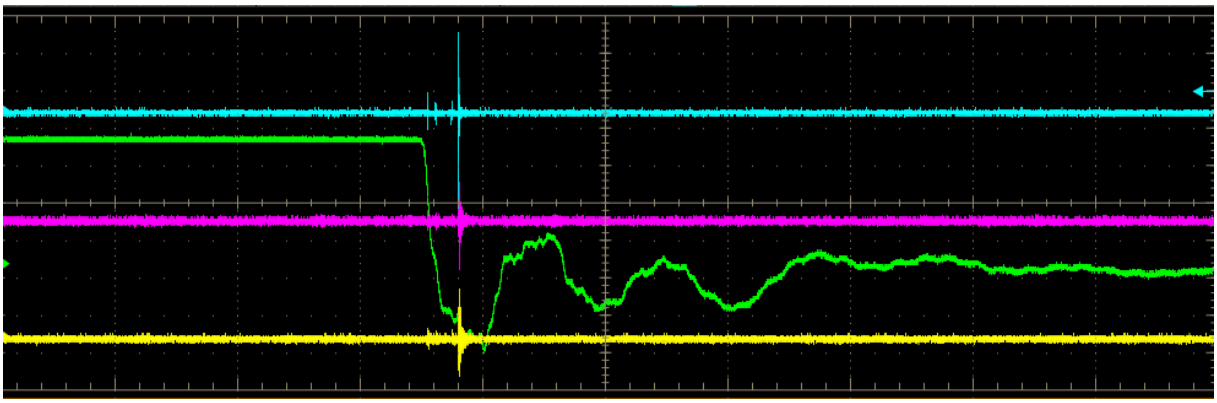

Figure II-26*: PD (blue, purple and yellow for each phase) & phase-to-ground voltage (green) measurements on a falling edge*

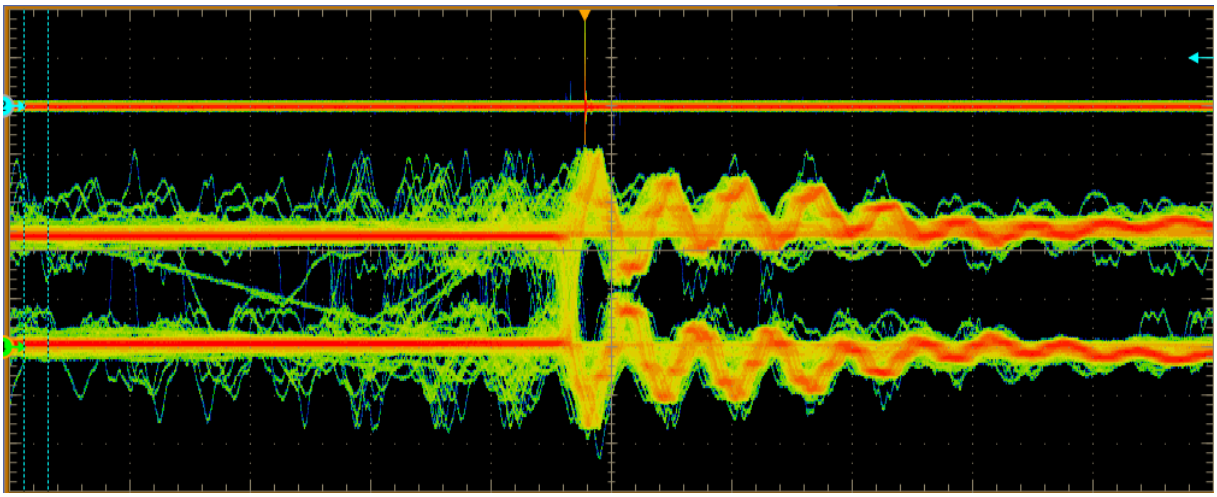

Figure II-27*: Fast acquisition of PD signal (top) and phase-to-ground voltage (bottom)*

Observed signals have low recurrence and coincide with peak voltages. Those are typical characteristics indicating the presence of discharges. Figure II-27, which consists of a fast acquisition of PD pulses over a given time interval, shows that the same number of PDs were observed on rising and falling edges. With the voltage level on a falling edge when the discharge occurs theoretically being too low to incept PDs between phase and ground (less than 300 V), one may conclude that discharges are probably located in the phase-to-phase insulation. It should also be noted that rotation speed has an impact on partial discharge activity, with respect to cable length. Regarding the repetition rate of PDs, it is difficult reach a firm conclusion given the variations from one test to another, and also considering that the sensor being used only detects the presence or absence of PDs. It does not quantify them. However, it can be stated that, as a result of low DC bus voltage (compared to inverter A and B), the voltage stress only rarely exceeds the PDIV. As a consequence, PD activity is quite low with this type of inverter.

II.6.2 Configuration no. 2: Inverter B

Two oscilloscopes were used simultaneously for this test, thus allowing us to record PDs and phase-to-ground voltages on all three phases. As a reminder, for this inverter as well as for inverter A, the DC bus voltage is higher in comparison to inverters C, D, and E, thus leading to higher electrical stresses at the motor terminals without even considering overvoltages. In low-voltage motors or in the case of the previous inverter, *i.e.* working at voltage levels generally lower than the PDIV, only overvoltages may lead to PD ignition. This is why discharges appear during the voltage edge and why denoising is such an important issue. It therefore seems particularly interesting to study the distribution over time of PDs with inverter B, which combines a high voltage rating and fast rise time.

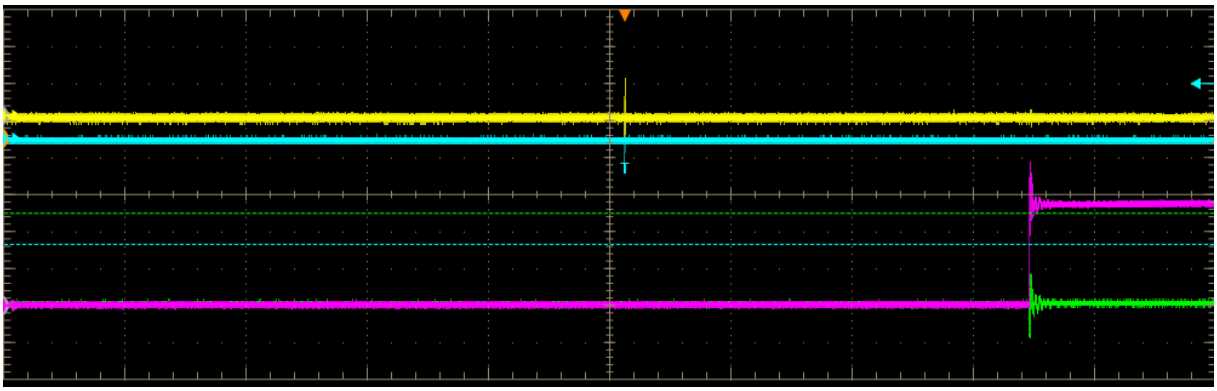

Figure II-28*: PD (blue and yellow) & corresponding phase-to-ground voltage (purple and green) measurements (plateau part of the voltage)*

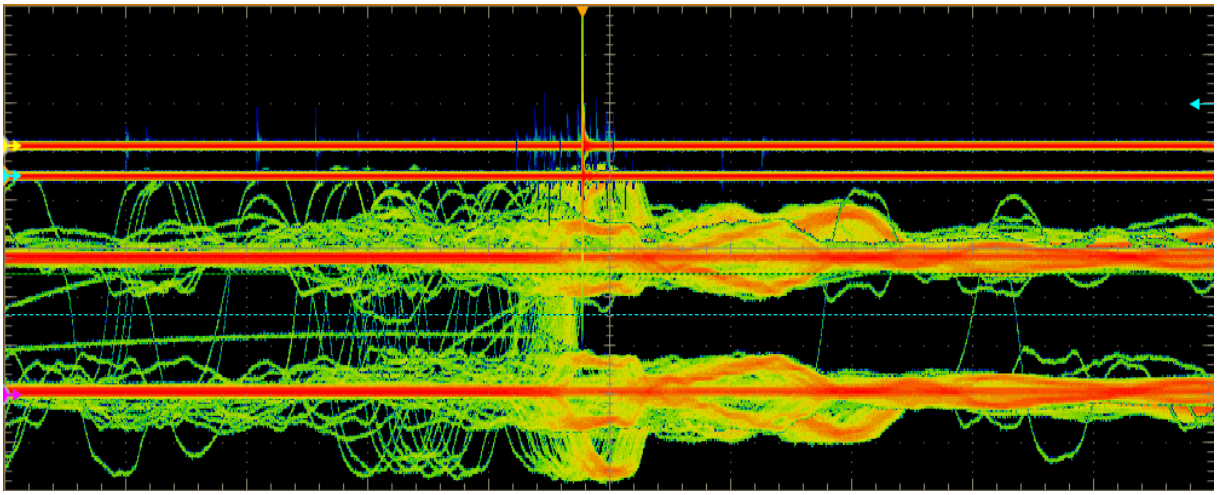

Figure II-29*: Fast acquisition of PD signals (top) and phase-to-ground voltages (bottom)*

Figure II-28 and Figure II-29 clearly illustrate that PDs not only appear during the voltage front, but also during the plateau part of the voltage. Such behavior corresponds to the PDs pattern observed and reported in literature. In the case of motors operating at higher voltages, the appearance of PDs has been studied more extensively [54] [71]. Detection during the continuous part (plateau) of the voltage is much simpler because there is less need to filter the signals. Thus, due to the fact that the voltage is higher in this case, PDs seem to be located between phases and also probably between phase and ground. In terms of changes according to rotation speed and cable length, the trend is the same as that with inverter C. Finally, PD activity is higher than in the case of inverter C, again for the same reasons, and further increases when increasing the DC bus voltage (this is clearly visible with fast acquisition, as a given number of PD occurrences is reached faster in a same time interval).

Another interesting result of this study concerns the ability of detecting PDs despite the use of filters with a high cutoff frequency. It has been observed, in other studies, that the amplitude of the frequency components of PDs, appearing under PWM for 3 kV/µs edges, is very low beyond 300 MHz [72]. In the case of an SiC inverter, despite of the use of filters with a cutoff frequency up to 500 MHz, PD signals were detected, which shows that the PD frequency spectrum spreads over a higher frequency

range in this case than for 3 kV/µs edges. dV/dt thus appears to have an influence on the PD frequency spectrum.

II.6.3 Configuration no. 3: Inverter A

Finally, a test was carried out with inverter A to assess the differences between Si-based and SiC-based inverters. A PD waveform example is given below. Basically, with the amplitude of the constraints being lower with Si IGBT technology, partial discharge activity decreases as well. There are fewer PD occurrences, with lower magnitudes and only visible on one phase. However, as the voltage level is as high as in the case of the previous inverter, PDs are still located both on the rising and falling edges and on the plateau part of the voltage. For the other aspects, conclusions here are the same as for the previous configurations.

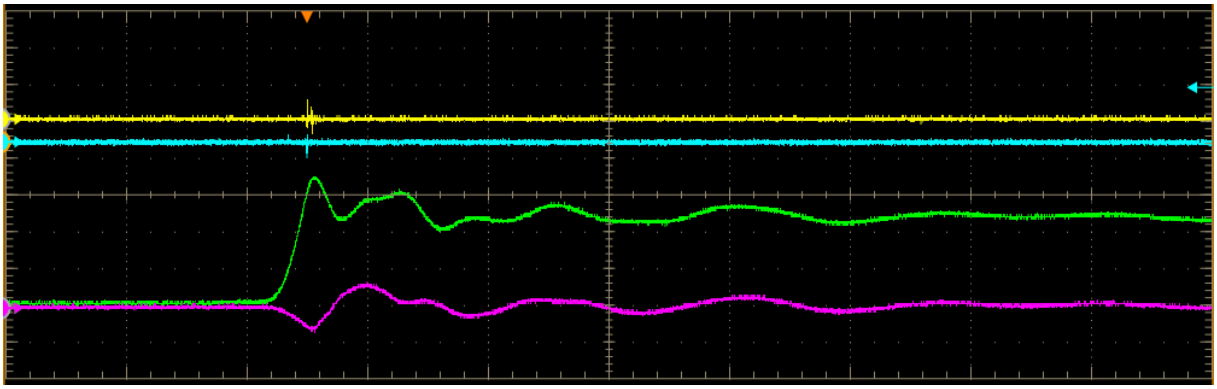

Figure II-30*: PD (blue and yellow) & corresponding phase-to-ground voltage (purple and green) measurements on a rising edge*

II.6.4 Key points to remember

- PD detection with PWM is possible despite the switching noise induced by SiC-based converters.
- In that case, PDs occur only in the motor and not at the inverter level.
- PDs between phases are observed with the inverter having the lowest DC bus voltage; regarding inverters A and B, as the voltage is higher, PDs are also incepted between phase and ground. Furthermore, the PD repetition rate (and activity in general) increases when voltage magnitude increases
- Rotation speed has a non-monotonic influence on PD activity through the change of PWM command associated with this speed change. At high speed, the current associated with the change of PWM command is higher, leading to critical values for slopes and overvoltages, and most certainly to PD events with a larger magnitude. However, at the same time, at low speed,

the current is lower but there is a large number of switching occurrences, and thus possibly an increased number of PDs. It is thus difficult to rule on the precise impact of the rotation speed on PD activity.

- Cable length has little influence on PDs, or at least influence that is difficult to quantify; in most of cases, the voltage slope shows little change when the cable length is modified, and the voltage increase is not large enough to induce significant modifications in PD activity.
- At high voltage, PDs are not only observed on the rising edges but also on the plateau part of the voltage.
- dV/dt has an influence on the PD frequency spectrum.
- The transition to SiC-based components increases PD activity.

II.7 Conclusion

This chapter identified the electrical stresses in a machine supplied by Si-based and SiC-based inverters. By using a custom-made experimental bench, we were able to study the influence of various parameters related to the power chain and, on the basis of those results, to obtain insight regarding the turn-to-turn, phase-to-ground, and phase-to-phase voltages in the machine. Furthermore, PD measurements were performed as a complement to this electrical stress mapping to highlight the direct impact of these more stressful constraints on machine reliability, and high voltage machines in general.

In Type I random-wound motors, partial discharges appear because of the combined effects of random winding with a large number of turns, propagation phenomena, and rising edges. In Type II motors, winding is formed and composed of few turns. We have seen that the turn-to-turn voltage values are low in this type of motor. Given these voltages, power electronics and thus rising edge propagation can have little influence on the ignition of partial discharges between turns. Nevertheless, the use of fast-switching SiC-based inverters causes an increase of overvoltages for phase-to-ground and phase-to-phase voltages. Therefore, these insulation systems constitute the weakest point of the system in terms of reliability. These overvoltages are mainly induced due to propagation phenomena between the inverter and the motor, but they also depend on numerous internal and external parameters, such as switched current, rotation speed, and cable length. These more stressful constraints eventually lead to an increase in partial discharge activity between phases or between phase and ground. For this reason, such electrical stress mapping under operating conditions is one of the key building blocks for achieving better understanding [73], reproduction [74], detection [11], and monitoring [37] of the phenomenon.

The next step in this work is now to establish a correlation between electrical stress and partial discharge activity. A first step was taken with PD measurements performed on the machine, but that only enables us to obtain a broad vision of PD activity inside the machine. Now that the electrical stresses inside the machine are well known, a detailed study on the influence of every component of these voltage stresses in terms of PDs and aging must be performed. This will be examined in the following part of our work, notably by performing PD measurements and running accelerated aging on representative samples from simple Type I samples to more complex Type II insulation systems.

Chapter III. Phenomenological study of PD activity and aging on Type I samples

III.1 Presentation

III.1.1 Accelerated aging tests: aim and procedures

III.1.1.1 How and why to perform aging tests on EIS?

Aging has emerged as an important issue involving physical phenomena related to insulation material properties, power supply type, environmental conditions, and machine type. Regardless of the application, performing aging tests under stress is a necessary step for understanding the mechanisms involved and to be able to prevent and/or predict the induced changes.

For Type I machines, the purpose of this type of testing is mainly to determine the PDIV based on multiple parameters. Studying aging over time under environmental constraints can also be a relevant focal area. Type I insulation systems are supposed to operate without PDs over their entire life cycle. It is therefore important to ensure that no PDs can occur at the specified operating voltage – from the very first moment of operation and throughout the entire life cycle of the machine. The nature of tests is significantly different in the case of Type II insulation systems, which are supposed to operate in presence of PDs. These tests typically involve the aging of different types of insulation systems in order to estimate their respective lifetimes and eventually to be able to model, predict, and extrapolate them to real systems at their nominal operating points. Whatever the type of the insulation systems, aging tests are often destructive.

Aging tests can be divided into two types: qualitative and quantitative tests. Qualitative aging tests are performed at the design and production stages. Their goal is to identify the main failure modes and mechanisms in order to improve machine reliability. These tests are quite severe and go far beyond nominal constraints, with the objective of identifying potential weaknesses in the design or manufacturing processes. Various types of qualitative tests exist in industry, such as: *Highly Accelerated Life Testing (HALT), Highly Accelerated Stress Screening (HASS), Environmental Stress Screening (ESS), etc*. [75] [76]. If the device under stress fails to survive a given test, the default is then identified and eliminated at the design stage. Due to their severity, these tests are not intended to predict the behavior of a component or insulation system under nominal conditions.

In contrast, quantitative tests are performed to determine the main characteristics of a system in terms of reliability, that is, to predict average lifetime, establish lifetime models, estimate statistical distribution, and more. Devices under test also are subject to harsher constraints than their nominal conditions, but in a manner intended to be more representative of those conditions and aging mechanisms so that results can be extrapolated accordingly.

III.1.1.2 Acceleration of aging

Aging mechanisms modify material characteristics and decrease their insulation properties. It has been shown that different factors can operate separately, but also, and in most cases, in combination. It is therefore difficult to shift from a predictive microscopic model to a macroscopic model. Accelerated tests thus are the most suitable means of characterizing aging. An accelerated test refers to a test in which the applied environmental or electrical constraints are stronger than those experienced under nominal conditions [22]. For a given reliability level, test duration is therefore shorter with accelerated tests.

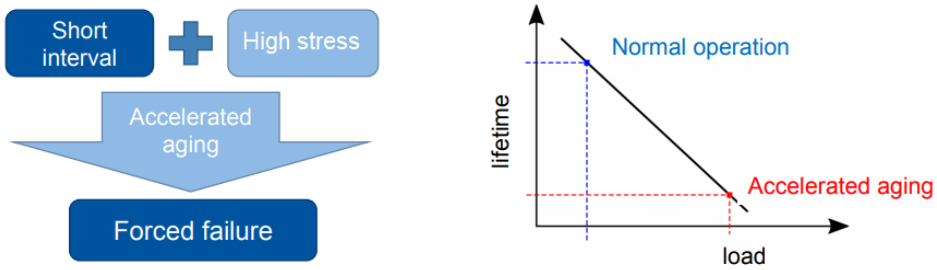

Figure III-1: *Illustration of the principle of accelerated aging*

Accelerated aging can be implemented by increasing electrical stresses (voltage level, frequency, magnitude, duty cycle, slew rate…), environmental stresses (humidity, pressure, temperature, mechanical stress), or any other level of constraint. The acceleration factor must not be too high in order to ensure a single aging mechanism, and to not create additional phenomena that would not otherwise exist in nominal operation. The higher and the closer the levels of stress, the greater the lifetime model uncertainty. On the other hand, choosing levels of stress that are too low or too close to operating conditions could lead to long-lasting tests with a very low number of failures. The approach is therefore to find a trade-off between test duration and model precision to estimate insulation systems lifetimes accurately in a realistic environment.

III.1.1.3 Translation from real systems to samples

Aging tests cannot be achieved systematically with real equipment, for obvious reasons of time duration and cost. Instead, samples that are representative of the machine's insulation systems must be used.

For Type I applications, **twisted pairs of enameled wires** or **crossed conductors** can be used to perform aging between turns [15]. For Type II applications, pairs of insulated conductors held together with the terminals splayed apart, and processed according to production standards, can be used to represent a turn-to-turn insulation system. The insulated conductors should be in contact along the length of the straight portion to simulate contact between turns in a coil. To maintain this contact, it may be

necessary to process samples using pressing operations and/or Vacuum Pressure Impregnation (VPI), as appropriate for the design and materials.

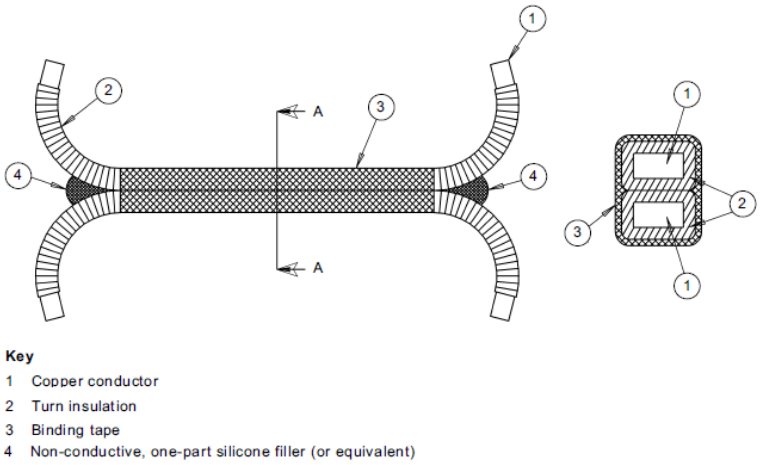

Figure III-2: *Example of construction of a turn/turn test sample for rectangular conductors [15]*

Coils built to production standards and fitted into representative slots are tested to qualify the phase-to-phase and phase-to-ground insulations to be used in the stator. In this case, the test objects should be created according to the full manufacturing specification for a production machine, but perhaps with reduced slot length to minimize capacitive load (as shown in Figure III-3). This type of specimen is studied and described in more detail in Section IV.3.

Figure III-3: *Example of a phase-to-phase / phase-to-ground test sample*

III.1.1.4 Aging procedures according to standards

The evaluation of an insulation system's ability to resist degradation under electrical stress is regulated by standards established by the International Electrotechnical Commission (IEC). Although some parameters such as test voltage and frequency, or sample type, may vary depending on the application, some general rules must be followed when performing accelerated aging tests [14][15][77].

Aging tests can be performed for a single test voltage, in comparison with a reference insulation system that has been previously tested, in order to determine the design that improves endurance. An EIS can also be tested under variable environmental and/or electrical stresses to identify the effects of

those various factors. Finally, endurance tests can be carried out to evaluate the relationship between applied voltage and lifetime for each insulation system. It is customary to only vary one constraint at a time to segregate and interpret results effectively. The results of these tests depend on multiple parameters which must be clearly identified and controlled, in addition to the insulation's intrinsic characteristics.

The Device Under Test (DUT) must be suitable for the application scope. A larger number of samples must be considered if high statistical precision is needed to detect small differences. It is preferable to use at least five samples per stress level to obtain the minimum requirement in terms of precision. Test results must then be processed statistically using one of the distributions presented in Section I.5.1.2. On the basis of shape and scale parameter estimation, the MTTF (Mean Time To Failure), number of pulses before breakdown, and percentage of failures can be determined. Confidence intervals for parameters and percentages can also be calculated. 90% probability is recommended.

PDIV and PDEV must be determined prior to testing. For impulse voltage, it is common practice to rather consider RPDIV and RPDEV (Repetitive Partial Discharge Inception/ Extinction Voltage), that is, the minimum peak-to-peak voltage at which more than five PD pulses occur on ten voltage impulses of the same polarity (note: this is a mean value for the specified test time and a test arrangement where the voltage applied to the test object is gradually increased from a value at which no partial discharges can be detected). The operating conditions and at least three levels of voltages above this threshold must be chosen to perform tests, with a difference of at least 10% between two consecutive levels. Finally, the degradation mechanism must be the same across the full range of voltages and similar to those encountered under operating conditions.

For the sake of brevity here, the above recommendations are included in the specifications advocated by the different standards. For more information, please refer to the IEC 60034-18-41[14], IEC 60034-18-42 [15], IEC 60851-5 [78], and IEC 62068 [77] standards, to name but a few.

III.1.2 Purpose of this study

The first step of this study overall was dedicated to identifying the electrical stress inside a machine supplied by Si IGBT and SiC MOSFET based inverters, in order to have clear insight regarding the risk for Type II machines depending on various parameters. Building on this preliminary work, the aim of the following parts is now to understand the influence of relevant constraints on partial discharge activity and, in the longer term, on the aging of the machine's insulation systems. To move forward, a three-stage approach was adopted based on samples ranging from the simplest Type I sample to more sophisticated systems closer to a real Type II machine.

The first stage consists of performing a study based on a phenomenological approach. This stage is carried out using classic and standardized Type I twisted pairs. These samples were chosen for several reasons: they are easy to manufacture in a reliable and repeatable manner; their very basic configuration is well suited for understanding the phenomena involved; and finally, they also make it possible to reduce test duration thanks to their relatively reasonable lifetime. The constituent elements of electrical stress were identified (Figure III-4), and tests and measurements were performed to study the influence of these various parameters on aging and PD activity.

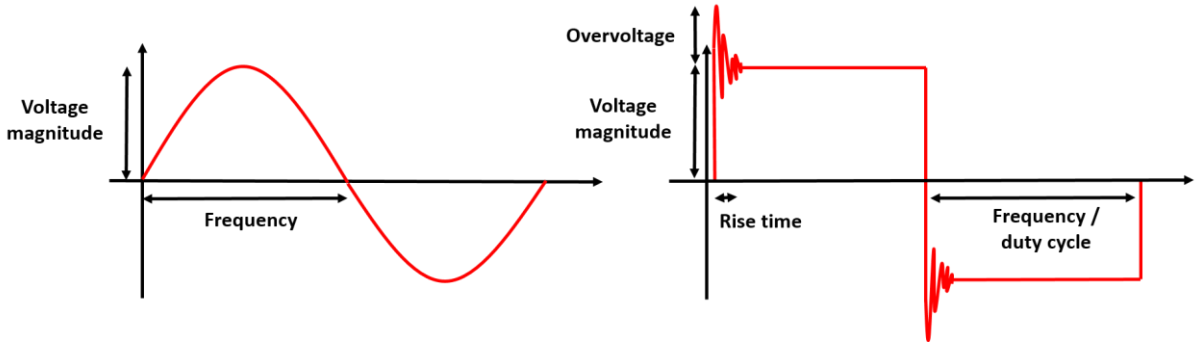

Figure III-4: *Identification of the constituent elements of electrical stress*

The second stage aims to transpose the previously obtained results to equivalent Type II samples. Similar tests were performed on a smaller scale to confirm or refute the trends observed in the previous case, in an intermediate configuration midway between a basic sample and a real system. Finally, the third and last stage consists of studying samples much closer to a real system, representative of phase-to-ground and phase-to-phase insulation systems. The samples studied thus far are representative of the turn-to-turn insulation system. However, it has been shown that the weakest points of the insulation system in Type II machines, as opposed to low voltage machines, are phase-to-phase and between phase and ground rather than between adjacent turns. As a result, a specific test bench was designed to study the aging of Type II “motorettes” under electrical stress and in the presence of PDs. A summary of all these results is presented below, providing a complete perspective regarding the influence of the existence of PDs on both Type I and Type II insulation systems.

As explained earlier, the purpose of this test campaign is to highlight the influence of electrical stress components on samples representative of Type I turn-to-turn insulation systems, more specifically in terms of partial discharges and aging. Initially, tests were limited to a comparison between the aging of samples supplied by sinusoidal and square-wave stresses. The signal amplitude and frequency were the same, with a duty cycle of 50% in order to study the influence of the voltage slope only. However, in the light of our preliminary results, the scope of the study was expanded to a global analysis of the influence of electrical stress on PDs and aging. The experimental setup and PD measurement protocol is presented in detail, along with preliminary results and the influence of each of the electrical stress constituents on PDs and aging. For the sake of brevity, only the most relevant graphs and results are

presented here. A final summary presents the various results and suggests ideas for discussion about the influence of electrical stress on partial discharge activity.

III.2 Experimental setup and test plan

III.2.1 Samples

The samples used in this study are twisted pairs constituted of two 1 mm thick copper wires. The number of turns and strength to apply were determined according to the EIC 60 851-5 [78] standard. Five samples per configuration are used for statistical reasons. Sample twisted pair wires are shown in Figure III-5.

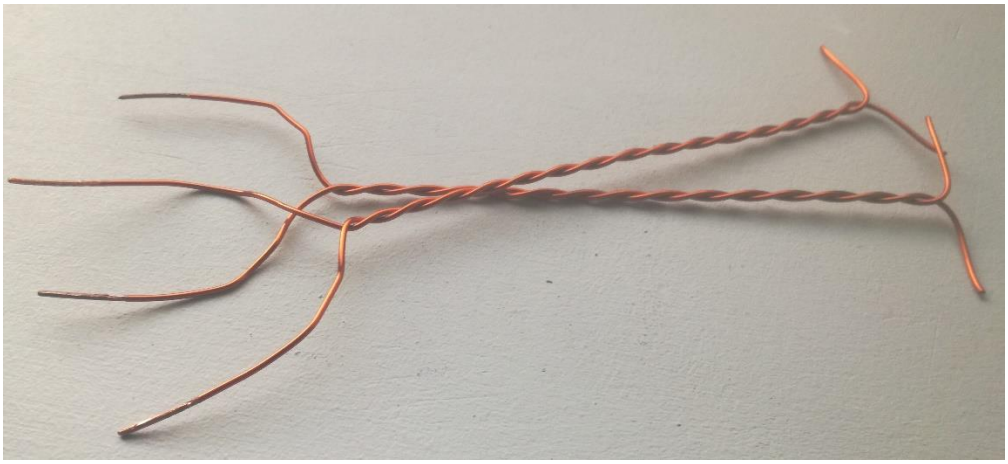

Figure III-5: *Standardized twisted pairs used for the study*

III.2.2 Stress generation

Two types of power sources are used for generating voltage stress. Adjustable in both frequency and amplitude, sinusoidal stress is created using an arbitrary waveform generator and a voltage amplifier (Small and large signal bandwidths: DC to respectively greater than 30 and 2.5 kHz). A high voltage probe (Tektronix P6015A 1000x) connected to an oscilloscope (Tektronix MSO 5204, 2 GHz, 5 Gs/s) is used to measure voltage. Lifetime is calculated on a computer connected to the oscilloscope and by using the amplifier's current limitation. When the current is too high, voltage collapses. The computer detects when voltage is below a specific threshold and can thus calculate sample lifetime. Square-wave experiments are carried out on an existing test bench that was modified to satisfy our requirements [59]. A pulse generator provides bipolar voltage, which is adjustable in amplitude, frequency, and duty cycle. Up to five samples can be aged simultaneously. An electronic device calculates lifetimes and pilots the experiments. As for the sinusoidal case, voltage is controlled with a high voltage probe and lifetime is estimated using the voltage supply's current limitation. An automatic system detects when breakdown occurs, and then isolates the concerned sample to finally re-apply the voltage on the remaining samples.

When a breakdown occurs on a sample, the rise time is not exactly kept constant on the other samples, but the change in rise time value resulting from a change of the capacitance of the load is considered low enough not to affect the results. Due to the cable length between the source and samples, the pulses generated by the square-wave voltage supply present overvoltages that are not acceptable in the context of this study. Indeed, the objective here is to independently vary all the constituents of electrical stress and study their influence on PDs and lifetime. In order to ensure that the effect of overvoltage does not confuse the impact assessment of other parameters, RC filters made of a combination of a 500 pF capacitance and 50, 100, and 200 ohm resistances were used on one hand to suppress these overvoltages when necessary, and on the other hand, to vary the dV/dt and rise time values in addition to the variation of magnitude, frequency, and duty cycle. Overall, four parameters (rise time, duty cycle, voltage magnitude, frequency) can be determined with this setup, and one (overvoltage magnitude) can either be imposed or not.

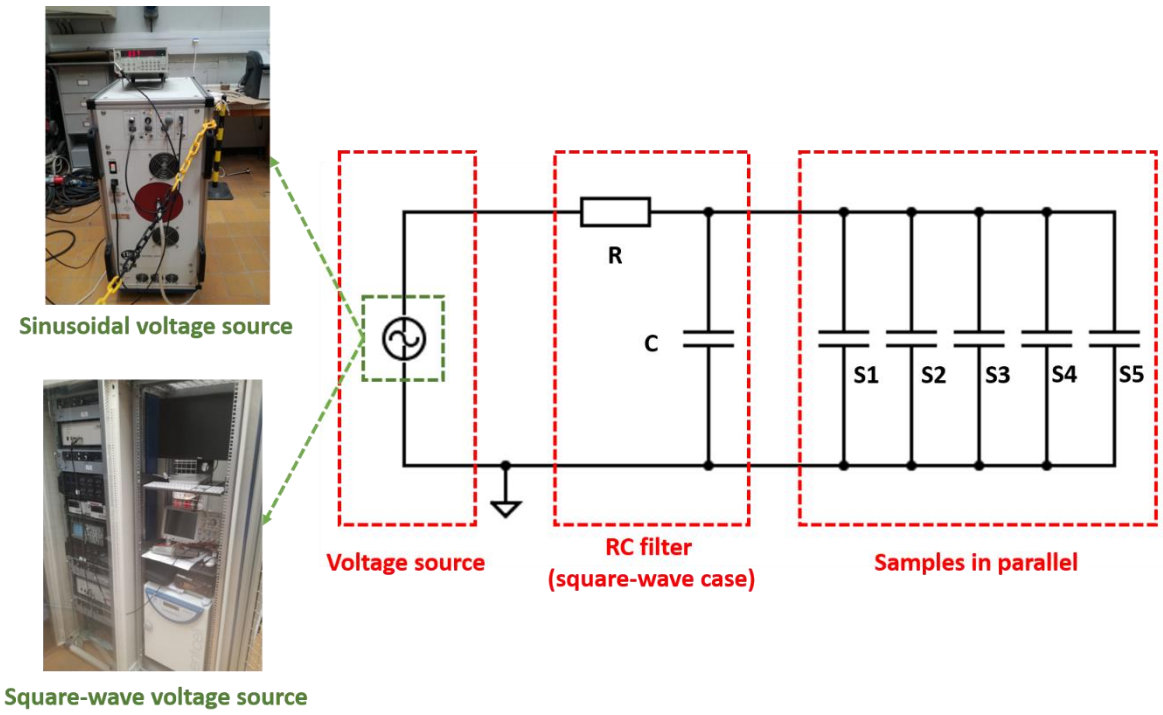

Figure III-6*: Experimental setup for sample aging under sinusoidal and square-wave voltages*

A few adjustments were made during the process to ensure that observed data was correct and usable. In addition, we introduced voltage amplitude monitoring to ensure that voltage was constant throughout the experiment. An example of both sinusoidal and square-wave signal waveforms are shown in Figure III-7.

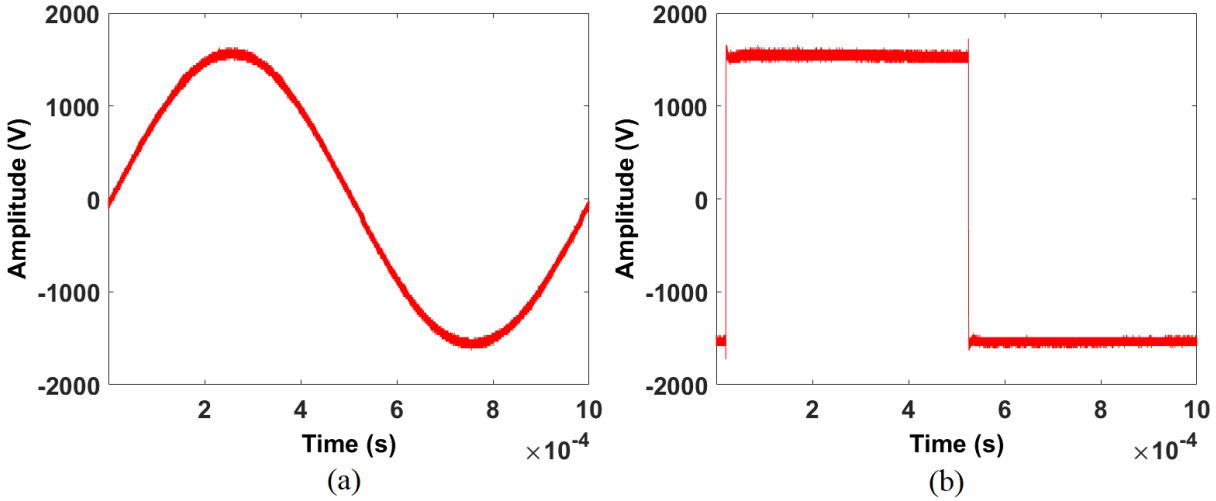

Figure III-7: *Example of waveforms of the applied signals; (a) sinusoidal, f=1 kHz, U=1.6xPDIV, (b) square-wave, f=1 kHz, U=1.6xPDIV, t_m=315 ns, α=50%*

III.2.3 Test plan

The stress levels to use were determined on the basis of PDIV measurements on five different samples. Inception voltage was determined using an AC signal (50 Hz). Indeed, experiments showed that frequency and voltage shape in the range under study have little or no influence on the determination of PDIV [14][52][79][80]. Voltage was increased progressively (voltage rise time: 100 V/s) until the inception of partial discharges. The operation was repeated four times to keep the average PDIV of the last three tests. In addition, breakdown tests were performed to determine the upper value for choosing voltage magnitude. Voltage rise time was set to 1 kV/s. The results are given below.

Table 14: *Reference PDIVs and breakdown voltages of different twisted pairs*

Sample number	PDIV (Vpk)	Breakdown voltage (kVpk)
1	970	12.92
2	980	14.53
3	920	13.03
4	990	13.70
5	960	13.77
Average	**964**	**13.59**

Based on these measurements, a variation range was defined for voltage amplitude and in a general manner for all the parameters. The voltage amplitude ranged from 20% above the PDIV (1157 Vpk) to 75% above the PDIV (1687 Vpk) to ensure that the samples would be subject to PDs over their entire lifetime while remaining quite far from the breakdown voltage. The frequency could vary between 1 and 10 kHz, and, by using filters, the rise time could range from 315 ns to 250 µs (sinusoidal case) without any overvoltage. Finally, it was possible to vary the duty cycle between 20% and 80%. Those

variation ranges enabled us to cover the broadest possible spectrum within the limits of the different sources. Furthermore, they are fairly representative of the levels of stress induced by Si IGBT and, to a lesser extent, SiC MOSFET based inverters at the motor terminals. The table below summarizes the considered test plan as well as the variation ranges of the different electrical stress characteristics.

Table 15: *Summary of the variation ranges for each parameter – test plan*

Parameter	Variation range
Magnitude (%PDIV / Vpk)	120 /1157 – 140 / 1350 – 150 / 1446 – 160 / 1540 – 175 / 1687
Frequency (kHz)	1 – 5 – 7.5 – 10
Rise time (ns)	315 – 380 – 500 – 700 – 250 000 (sinus)
Average dV/dt (kV/µs)	0.0058 (sinus) – 2.05 – 2.90 – 3.74 - 4.60
Duty cycle (%)	20 – 30 – 50 – 70 – 80
Overvoltage	Presence – absence

III.3 PD monitoring protocol

As a complement to the aging tests and resulting lifetime data, PD measurements were made in order to relate the two and obtain a clear view regarding PD activity in any of the configurations listed above. The same sensor as that used in Section II.6 was placed on the system's ground cable system and used for detection. To reduce switching noise induced by the square-wave source, a high-pass filter with a cutoff frequency of 500 MHz was used. It was not possible to remove noise entirely, but thanks to the filter, the noisy part of the signal was small enough that it could be distinguished from PD events, which mainly occur during rising and falling edges. Nevertheless, we noticed during preliminary tests that partial discharges also occur during the steady part of the voltage and that, in some cases, they could evade detection when the signal was filtered. It was therefore decided to perform double detection (with and without filtering) to ensure that all PD data was collected. Finally, it is important to note that, contrary to what was done previously, PD measurements were performed on one single sample at a time to ensure that retrieved data corresponds to the PD activity of that sample only and to ensure the consistency of the study. A schematic diagram of the PD detection setup is shown in Figure III-8.

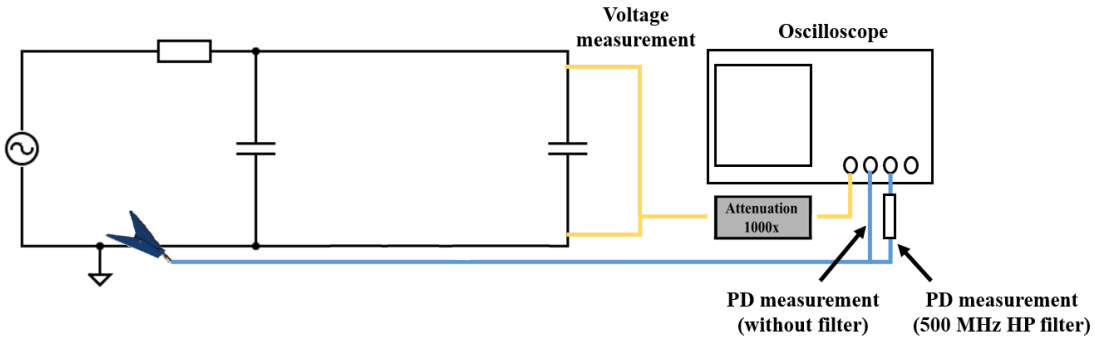

Figure III-8: *Partial discharges detection setup*

Regarding data acquisition, we had to find a trade-off between duration of the signal to retrieve, sample rate, and data size. Indeed, a sample rate that is too high can lead to an excessive volume of data. At the same time, resolution decreases if the duration of the signal to retrieve is too high for a given sample rate, which is problematic especially because PD events can be as short as a few tens of nanoseconds. In addition, performing real-time PD acquisition is by no means an easy task, even with a high-performance oscilloscope. In the light of these considerations, we decided to perform 20 consecutive acquisitions over one period of time, at the early, mid, and last stage of aging (Figure III-9), with a time lapse between the successive acquisitions equivalent to the acquisition and saving time of the oscilloscope (a few seconds at most). This method allows retrieving a fair amount of data at different stages of the life cycle while keeping volume reasonable. Moreover, the total acquisition time remains quite low compared to sample lifetime.

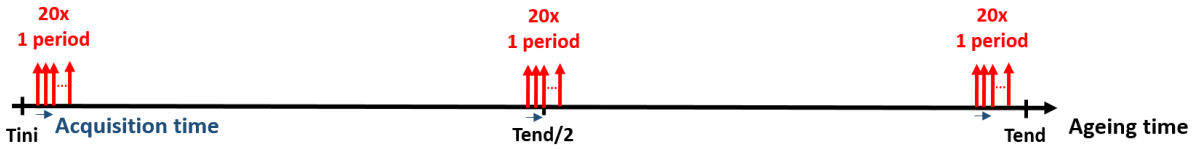

Figure III-9*: Schematic representation of the acquisition process*

After retrieval, data is stored on a computer and post-processed using a numerical computing method. In the sinusoidal case, a PD recognition program simply detects the PD events and calculates their main characteristics. Regarding the square-wave case, the filtered and non-filtered signals are processed in order to obtain voltage signal and PD characteristics both during the rising and falling edges and the steady part of the voltage, based on the PD events that were distinguished from switching noise beforehand (Figure III-10). Finally, once the 20 acquisitions are processed, additional and cumulative PRPD patterns are also determined. An example of measured signal before and after processing, as well as a detailed flowchart of the post-processing routine, are given below.

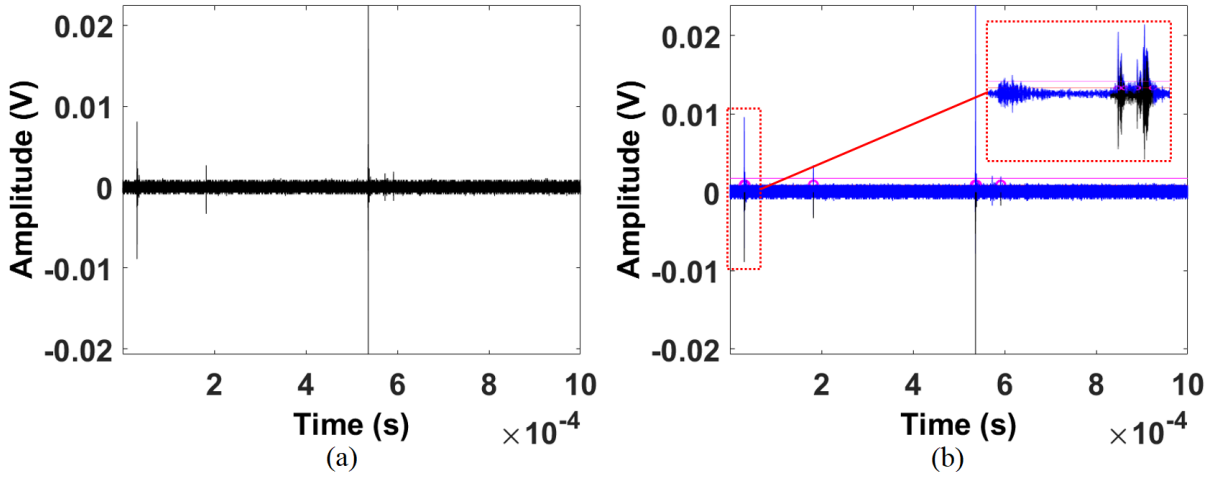

Figure III-10: *Example of PD signal (with 500 MHz filtering) (a) Before processing, (b) after processing with a zoom on PDs occurring during the rising edge*

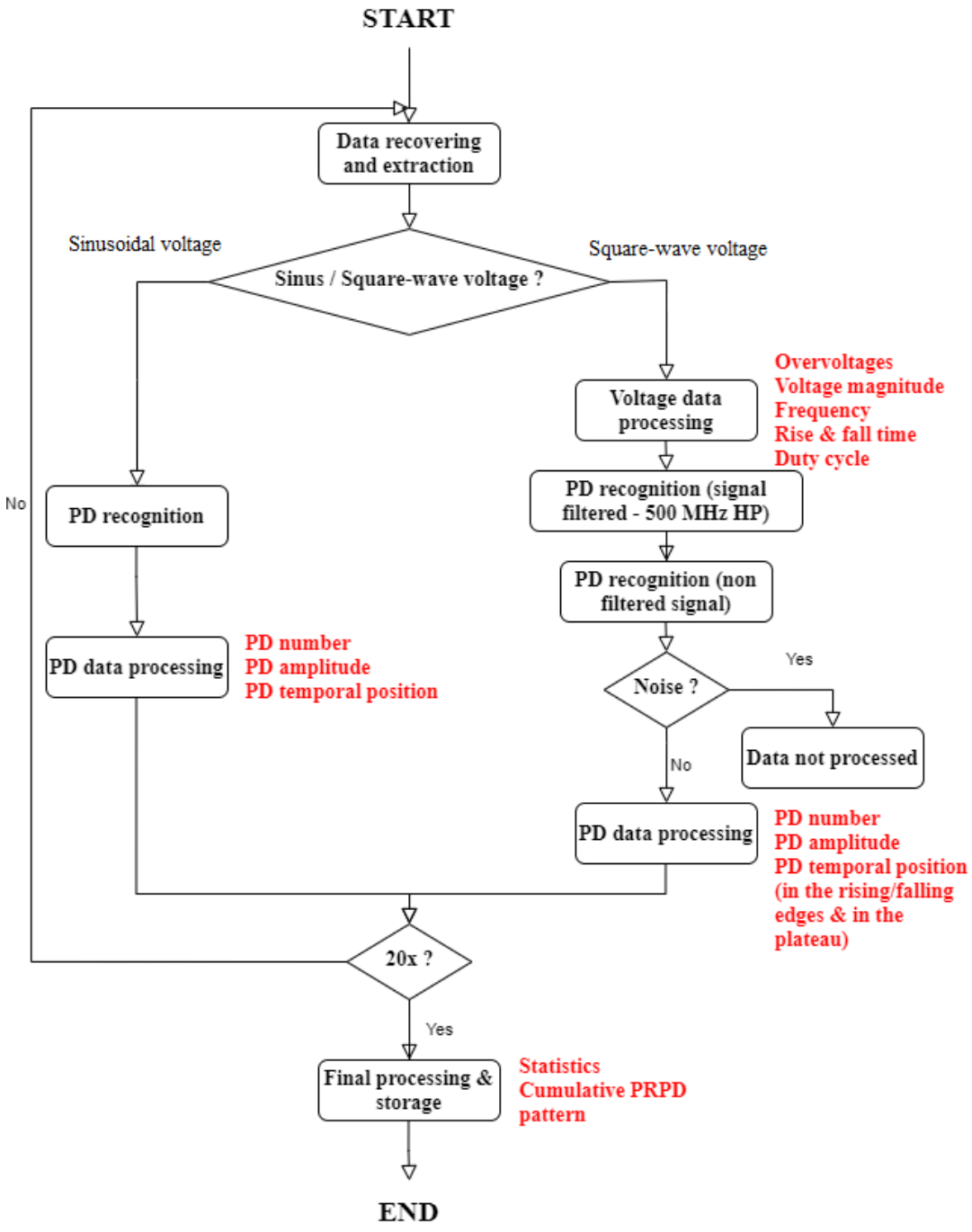

Figure III-11*: Flowchart of the PD post-processing method*

III.4 Preliminary results

III.4.1 Weibull statistics

Among all the modeling approaches presented in Section I.5.1.2, the Weibull distribution was chosen for processing data relevant to aging. The Weibull distribution is one of the most widely used lifetime distributions in reliability engineering. It is a versatile distribution that can take on the characteristics of other types of distributions based on the value of the shape parameter. A two-parameter

Weibull distribution was considered in the context of this study. The principle is as follows: based on aging data, the associated median rank plotting positions (*i.e.* unreliability values) are calculated. Weibull distribution parameters are then estimated using different methods. Conventional methods for Weibull parameter estimation are the Maximum Likelihood Estimation (MLE), method of least squares, and linear regression method. The representative curves of the Weibull distribution, which correspond to the functions in Table 5, are shown below as a reminder.

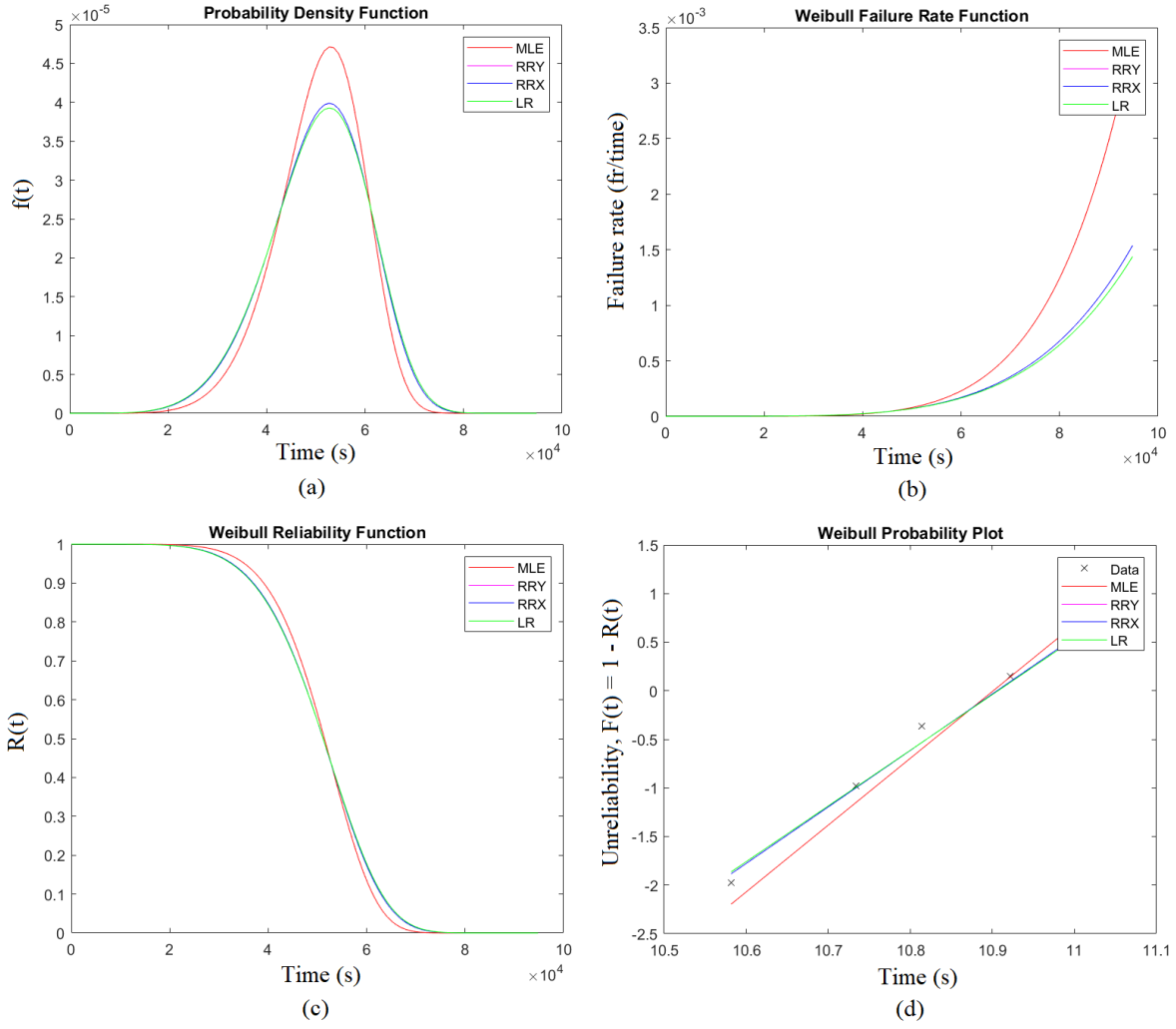

Figure III-12: *(a) Probability density function, (b) failure rate function, (c) reliability function, and (d) Weibull probability plot with parameters estimated by four different methods (MLE, rank regression on Y - RRY, rank regression on X - RRX, linear regression - LR)*

From this set of parameters, additional parameters such as the 10th and 90th percentiles, Weibull mean and variance, standard deviation, correlation coefficient, and coefficient of determination can also be obtained to assess the characteristics of aging and curve fitting accuracy. Among these parameters, the shape parameter β in particular is more than a little interesting when it comes to interpreting aging. A value of $\beta > 1$ indicates that the failure rate increases with time. This happens if there is an "aging" process, or if there are parts that are more likely to fail over time. Moreover, it is customary to say that

a variation of the beta parameter value from case to case is indicative of a change in the aging mechanism. In this context, and before going more into technical details, a general study on beta distribution was performed, considering the entire test series of tests. The graphs below show beta distribution for all the tests on one hand, and for specific categories of tests on the other hand (for example, for the sinusoidal case or the 1 kHz case only).

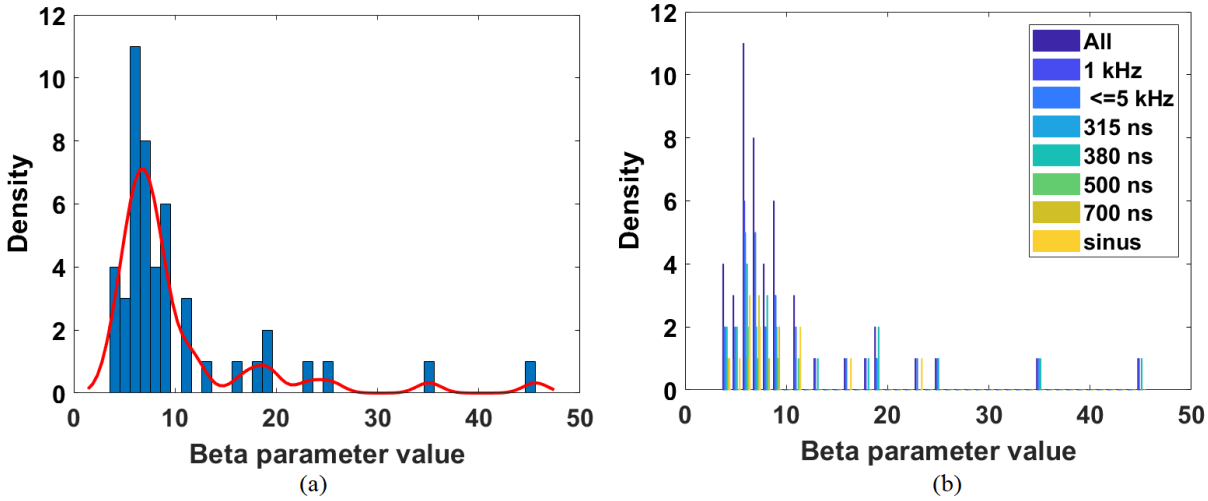

Figure III-13: *(a) Density plot of the β parameter and kernel-smoothing distribution fit for the entire series of tests, (b) density plot for specific categories of tests*

All β values are higher than 1, which is not surprising given that the studied mechanism is for electrical aging in presence of PDs. It can also be observed that most β values are clustered, roughly ranging from 4 to 12. Regarding the "abnormal" β values outside that range, the correlation between the β value and the determination /correlation coefficient in each case ensures that these high values are not related to the test itself. In view of the sporadic character of these extreme values, and considering the fact that they do not correspond to a specific configuration, they are instead attributed to a very low dispersion between the values of a given series than to a difference in the aging mechanisms. To follow up on the values inside the range, it is apparent that no clear trend emerges for a given configuration. For example, the range of β variation is roughly the same whether the 315 ns, sinusoidal, or 1 kHz cases are considered. The large variability of beta could also be explained by other factors such as a different enamel thickness from batch to batch, or even a difference of humidity between the tests. Finally, variation of the β parameter within the range defined above has lower impact on Weibull characteristics functions. A simple interpretation of the β parameter therefore does not provide insight into the aging mechanisms related to the electrical stress constituents. The global mechanism, *i.e.* partial discharge, is the same for all configurations and a thorough PD analysis is necessary to take the analysis one step further.

III.4.2 PD location (transient vs. steady state voltage)

It is common knowledge in literature that ideally, when a default in an insulation system is subject to a sinusoidal stress equal to its PDIV, discharges are generally found to occur at each half cycle of the applied voltage wave. The number of discharges occurring over each half-cycle is determined mainly by the integer amount that the applied voltage peak exceeds the insulation PDIV. Thus, discharges are observed to occur at definite discharge epochs on the voltage wave and also to follow a certain sequence. The illustration of this phenomenon is shown in Figure III-14. E_a=E_b represents PDIV, while θ_n represents the phase at which the n^{th} PD occurs.

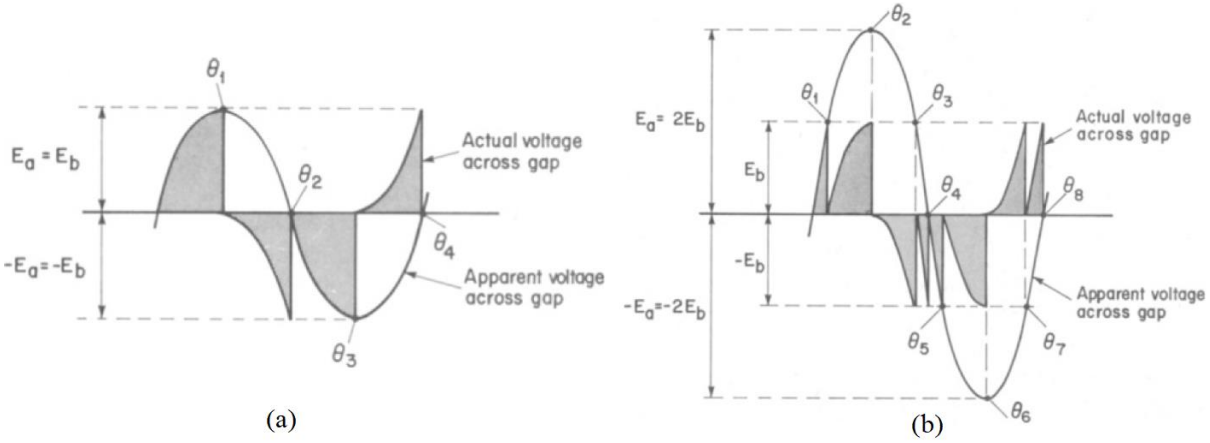

Figure III-14*: Voltage waveforms across an idealized cavity with equal breakdown voltages and zero residual voltages in the two polarities (a) at PDIV, (b) at 2xPDIV [3]*

The situation is the same when considering impulse voltage, except for one aspect: square-wave voltage, unlike sinusoidal voltage, is composed of a transient part (rising and falling edges) and a steady-state part. PDs are known to occur during the transient parts of the voltage, *i.e.* during the rising and falling edges. In fact, this is precisely what makes the detection and separation of PDs from noise difficult. However, it was observed in II.6 that PDs also seem to occur at high voltage during the steady part of the voltage. The PD measurements obtained on Type I twisted pairs of enameled wires echo these first results. Figure III-15 shows a signal containing PD events both during the transient and steady part of the voltage. The source of these PDs occurring during the steady part of the voltage is yet to be determined. They may, however, be comparable to discharges occurring under DC voltage stress [3]. Indeed, considering that the insulation system can be regarded as a capacitive system, the steady-state voltage distribution across the default is determined by capacitances rather than remaining purely constant. This could eventually lead to the inception of discharges not only during the rising and falling edges, but also during the steady part of the voltage. Further study is needed to better understand the mechanisms involved.

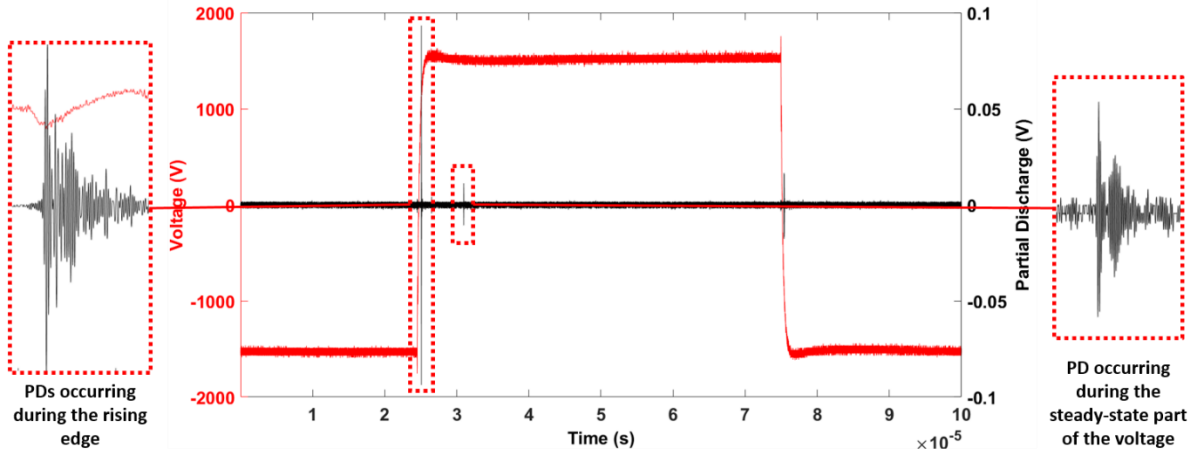

Figure III-15: *PD events occurring during both the transient and steady parts of the voltage*

Nonetheless, due the presence of these particular PD events, changes in the initial setup had to be made, as we noted that they sometimes evade detection when the PD signal is filtered. In addition, Fast Fourier Transform (FFT) analysis was performed on both types of PDs to understand the frequency spectrum in both cases. It turned out that the steady-state discharges still visible on the PD signal after filtering have a very similar frequency spectrum to that of classic discharges, with a frequency content up to the GHz level. Inversely, steady-state discharges that evade detection after filtering have a frequency content that does not exceed a few hundred MHz, which explains why they are only detectable without filtering. Given these results, a distinction has been made throughout this work between these two types of discharges and analysis was conducted with consideration for these phenomena.

III.5 Influence of the various voltage constituents on PDs and aging

Throughout this chapter, lifetimes are defined as Weibull means (Mean Time Between Failures, MTBF) over five different samples. Concerning PDs in general, the number of PDs (total, during edges, and during steady-state) is expressed as average of the number of PDs obtained for each of the 20 periods of time. The cumulative number of PDs of the 20 periods is considered for certain specified cases, such as the drawing of the PRPD pattern. Lastly, PD amplitude is expressed either as the average of the magnitude of each PD for all cycles, or as the average of maximum PD magnitude obtained for each of the 20 periods of time.

III.5.1 Voltage magnitude

As pointed out in I.5.2, voltage magnitude has a significant impact on the aging rate. Among all the studied parameters, voltage magnitude is the one that has the greatest impact on insulation system lifetime. The electrical stress magnitude can be divided into two elements: steady state voltage and overvoltage magnitude. Those two elements each have effects on aging and must be considered separately.

Overvoltages are the outcome of the wave reflection phenomena induced by fast voltage slopes transiting from the inverter through cables to the machine. These fast rising and falling edges therefore have a double impact on EIS aging: direct impact related to the voltage slope, and indirect impact through the overvoltages that they may induce. To further illustrate this point, tests were performed at 1 kHz, 1.5xPDIV, with a rise time of 380 ns and for a duty cycle of 50%, with and without overvoltage. The results are given in Figure III-16.

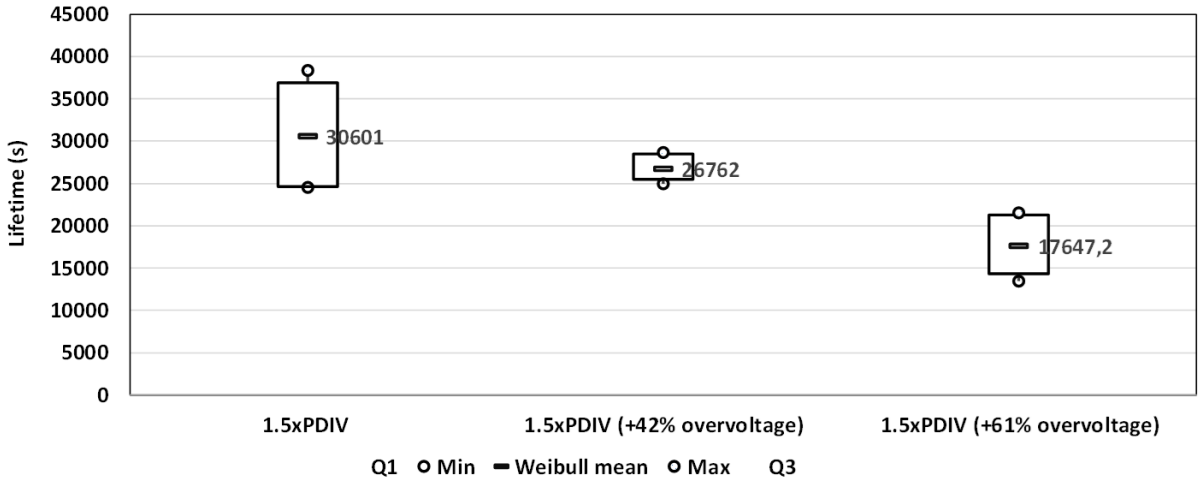

Figure III-16: *Influence of overvoltage on lifetime (f=1 kHz, U=1.5xPDIV, t_m=380 ns, α=50%)*

The presence of overvoltage has a non-negligible influence on aging. The lifetime of a twisted pair of enameled wires decreases from more than eight hours to about five hours for the largest overvoltage value (0.61xPDIV – 578 V). It should be noted that, as the overvoltages are generated and then suppressed by RC filters, the rise time value also varies between configurations. Thus, the lifetime decrease is the consequence of both the effect of the overvoltage itself and the effect of the short rise time (around 20 ns without the filter). The effect of the voltage slope on its own is addressed in III.5.2. Still, according to the sequence presented in III.4.2, the presence of overvoltages allows the inception of more PD events of greater magnitude, thus leading to reduced lifetime. Moreover, additional PDs are incepted in areas that were not subject to partial discharges at a lower voltage.

An additional test was performed in order to weigh the impact of discharges occurring during the edges and the steady state of the voltage. In the previous configurations, steady-state voltage was set to 1.5xPDIV with no overvoltage (Figure III-17-2), and then with an overvoltage of respectively 42% and 61% of the PDIV (Figure III-17-3). As steady-state voltage remained unchanged, the observed decrease in lifetime was most likely due to a modification of PD activity associated only with the additional overvoltage. A final test with overvoltage set to 1.5xPDIV and steady-state voltage below the PDIV (Figure III-17-1) was thus performed to isolate the influence of the discharge incepted during the steady part of the voltage. As with the preceding tests, the rise time was modified between the three configurations. It turned out that the lifetime was much higher for the last configuration (the test had to

be stopped after 100 hours) compared to the previous cases. Based on the assumption that PDs only occur during the edges, the fact that the steady-state voltage is below the PDIV should have no impact on lifetime, and a faster rise time should eventually lead to a decrease in lifetime for case (1) compared to case (2). The fact that this is not what happened not only confirms the presence of PDs on the steady part of the voltage, but it also suggests that their impact on aging is clearly non-negligible.

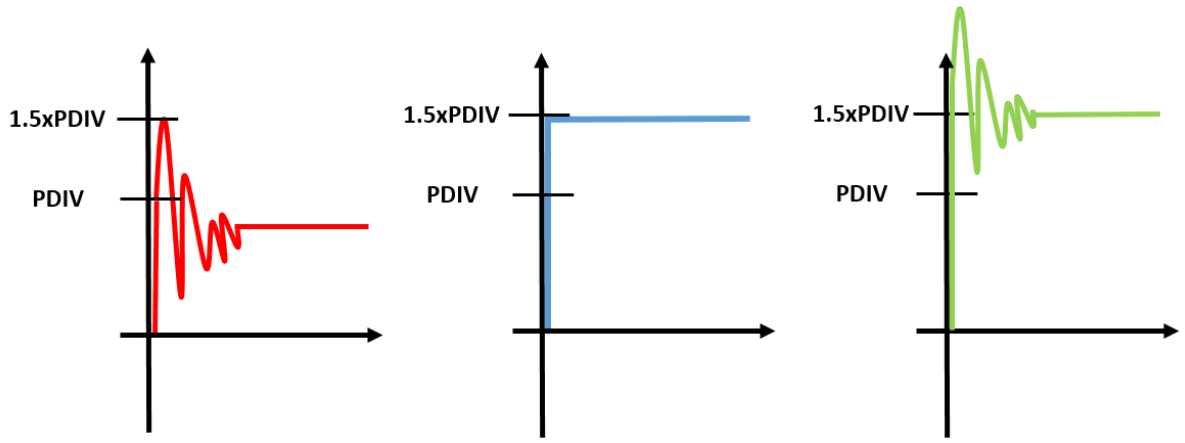

Figure III-17: *Voltage waveforms associated with the different test configurations*

The impact of steady state voltage magnitude was studied by suppressing the overvoltages using RC filters (configuration 2). Lifetime vs. voltage curves were plotted at 1 and 5 kHz, and considering square-wave (rise time 380 ns) and sinusoidal voltage stresses. The results are given below (Figure III-18).

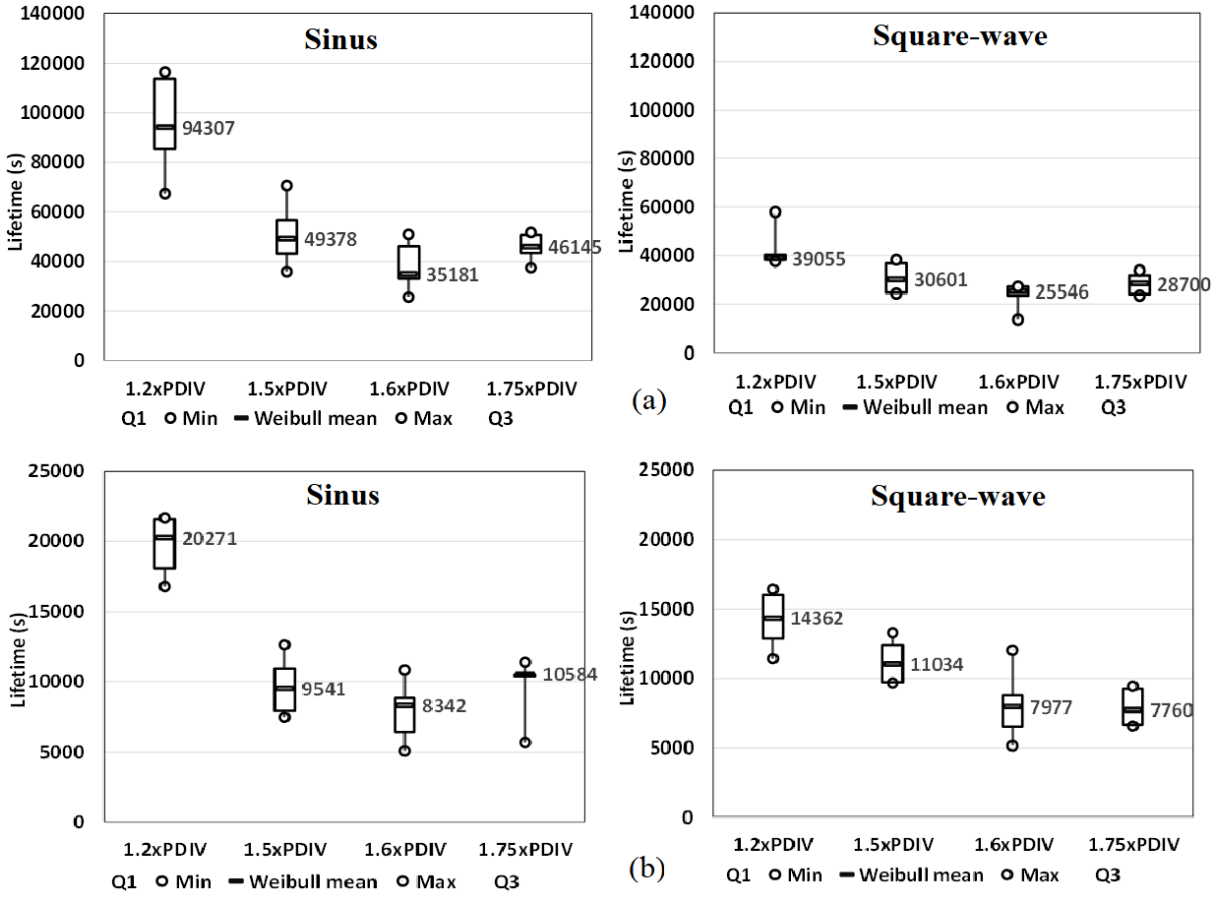

Figure III-18: *Lifetime vs voltage curves - sinusoidal & square-wave voltage (tm=380 ns, α=50%) (a) 1 kHz, (b) 5 kHz*

As might be expected, lifetime decreases with applied voltage. An increase in voltage magnitude accelerates insulating material degradation, thus leading to a reduced lifetime. Despite a minor inconsistency that is sometimes visible at 1.75xPDIV, the curve essentially follows an inverse power law. In addition to these lifetime curves, PD measurements were performed according to the protocol defined in Section III.3 in order to examine PD activity during aging. From the processed data derived from these measurements, boxplots were built representing the number of PDs per cycle as well as their average magnitude as a function of voltage magnitude, in both cases, and for a frequency of 1 kHz. The boxplots are provided in Figure III-19. As noted in the foreword of Section III.5, the number of PDs is defined as the average of the number of PDs for each of the 20 periods, while the average magnitude is defined as the average of the magnitude of each PD for all cycles. On each box, the central mark indicates the median, and the bottom and top edges of the box indicate the 25th and 75th percentiles, respectively. The whiskers extend to the most extreme data points not considered outliers, and the outliers are plotted individually using the '+' symbol.

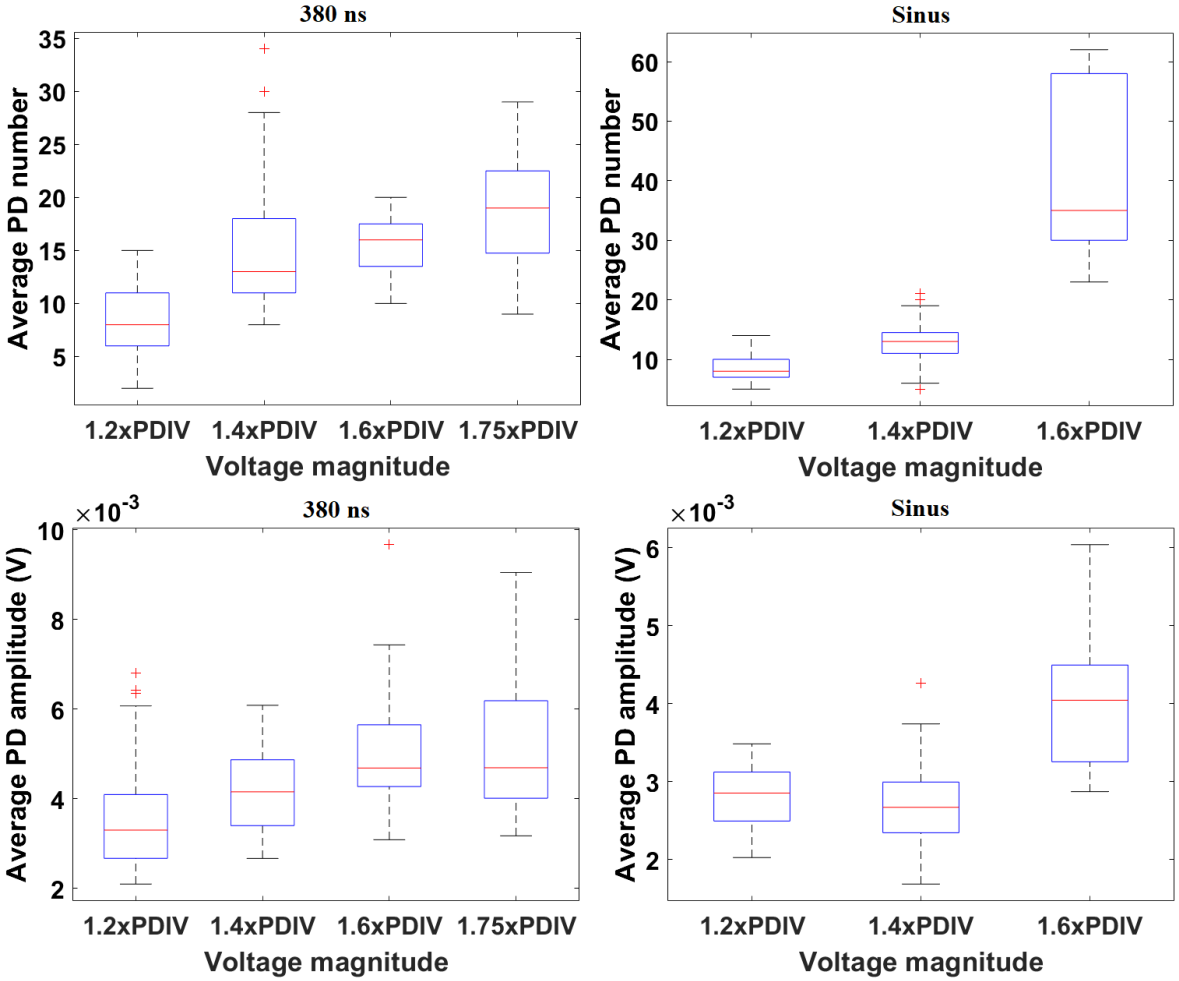

Figure III-19: *Average number of PDs (top) and average PD amplitude (bottom) on one period of time (f=1 kHz, tm=380 ns / sinus, α=50%)*

As expected, the average number and amplitude of PDs per cycle increase with steady-state voltage magnitude. The maximum PD amplitude per cycle demonstrates the same behavior. It is worth noting that the number of PDs occurring during the voltage edges increases regularly with voltage magnitude. At the same time, the number of steady-state partial discharges also increases, but to a lesser extent. Finally, these aging tests performed under both sinusoidal and square-wave voltages highlight the fact that a difference exists between the two, despite the same voltage magnitude and frequency. The influence of rise time on aging and PD characteristics, which is a very topical matter, is discussed in the next section.

III.5.2 Rise time

Numerous studies have been conducted on the influence of fast rise times and high dV/dt on PD activity and aging [81][51][55][82][83]. Conclusions are more or less the same regarding the influence of rise time, but rather varied concerning the source of the problem, especially as the square-wave

voltage environment raises some major issues, such as proper PD detection and calculation of the energy associated with PDs. We propose to address that issue in this section.

Endurance tests were performed for different rise time values and for two voltage values (1.5xPDIV & 1.6xPDIV), in order to assess the effect of rise time on aging. The results are given below.

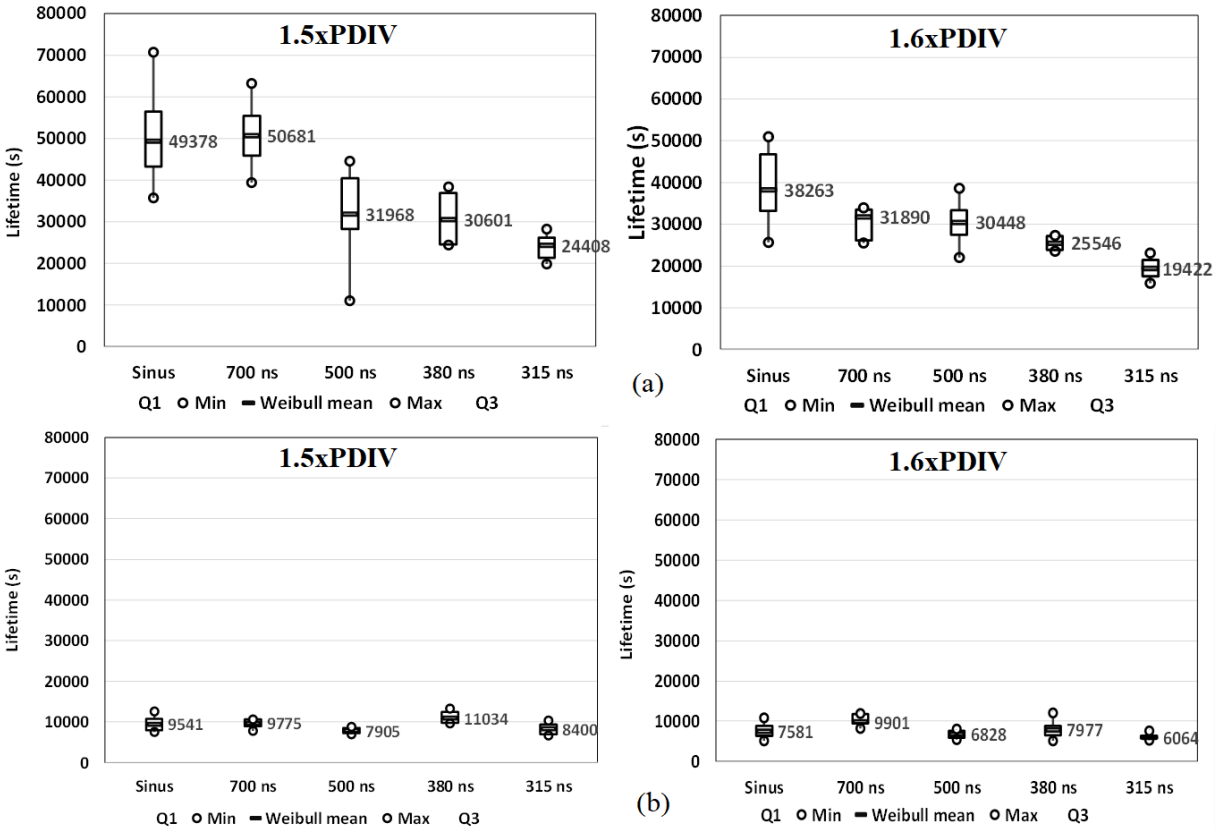

Figure III-20: *Endurance plots for various rise time and voltage values (a) f=1 kHz, (b) f=5 kHz*

On the basis of these results, it is appropriate to state that lifetime decreases with rise time. However, this behavior seems to be dependent on the frequency. At low frequency (1 kHz), the impact of rise time on aging is quite pronounced; whereas at higher frequencies (≥ 5 kHz), the effect of rise time seems to be gradually mitigated. In other terms, there seems to be a flattening effect at higher frequencies. However, it is clear that the monotonicity of the curves at 5 kHz differs from that of the 1 kHz case. Moreover, the trend is the same for the tests carried out at 7.5 and 10 kHz frequencies. The next section is devoted to studying this rise time-frequency behavior and the effect of frequency more generally.

Several hypotheses have been put forward in literature to explain this phenomenon. The most common explanation involves the energy related to PDs, which could supposedly be higher in the case of square-wave voltages with fast rise times. In order to reach a conclusion on this point, PD measurements were performed for different rise times. PD characteristics were extracted, in particular the number of PDs and amplitude per cycle. The results are given below.

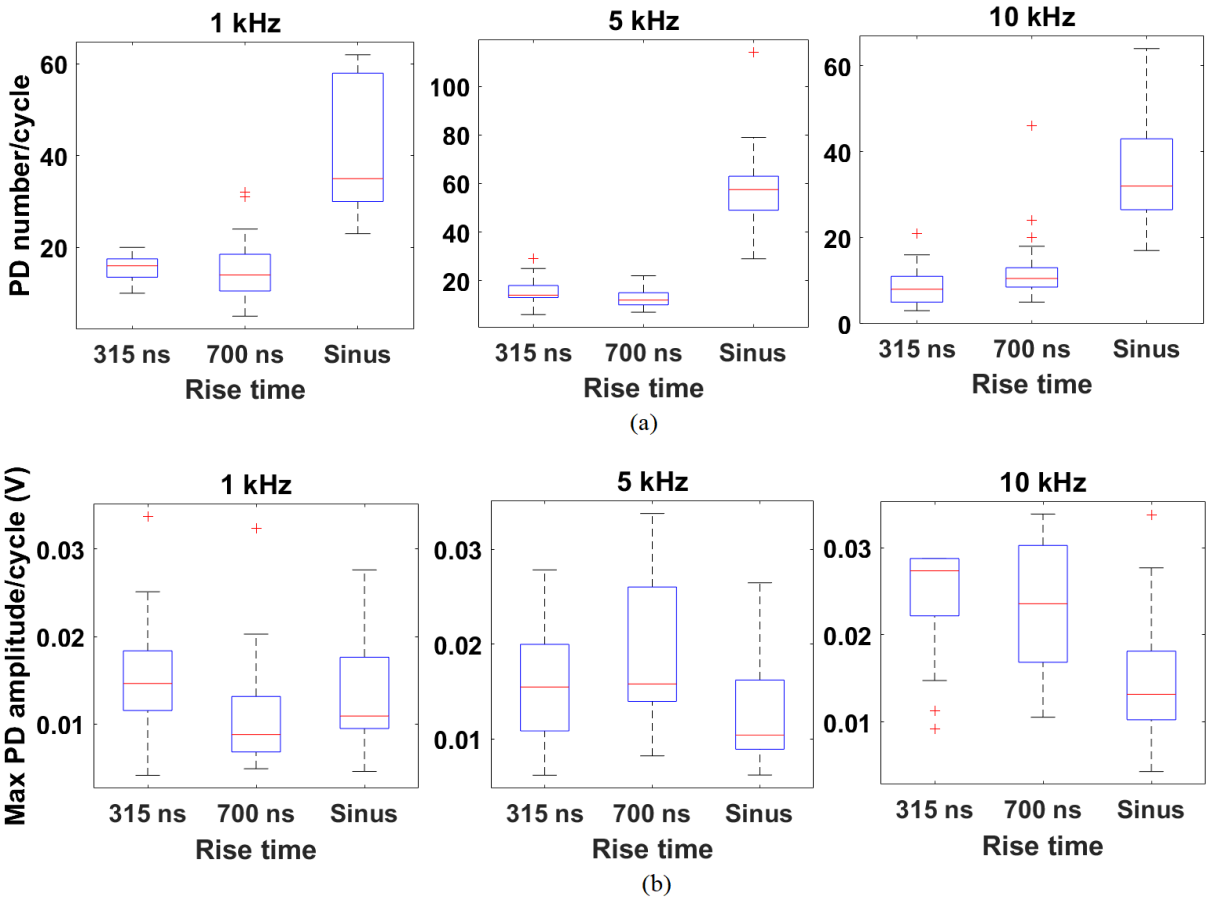

Figure III-21: *(a) Average number of PDs and (b) maximum PD amplitude per cycle as a function of rise time (U=1.6xPDIV, f=1-5-10 kHz, α=50%)*

The above curves show that while the average number of PDs increases with rise time, the maximum PD amplitude generally seems to decrease. The average PD amplitude experiments show the same behavior. It is not surprising to see that the number of PDs is higher for the slowest rise times: the longer transient phases associated with these slower rise times allow the inception of more PD events between the PDIV and peak voltage value. At the same time, several hypotheses have been put forward in literature to explain the variation of amplitude with rise time, such as a modification of the local electric field, modification of the PD frequency spectrum, nature of the discharge, or the delay time between the time the voltage exceeds the PDIV and the inception of the discharge, to name a few. Regarding PD amplitude and number, it is worth noting that because PD processing was based on waveforms obtained on an oscilloscope, and white noise is dependent on oscilloscope range, it was necessary to perform both low caliber acquisition (to distinguish low amplitude PD events from white noise, and obtain information about the PD number) and high caliber acquisition (to avoid saturation on the PD signal, and obtain information about PD amplitude), as shown in Figure III-22. Both signals were then processed, and the results were combined to obtain precise information about PD characteristics. However, the maximum and average PD amplitudes might be undervalued for the square-wave cases (where the PD signal could reach saturation).

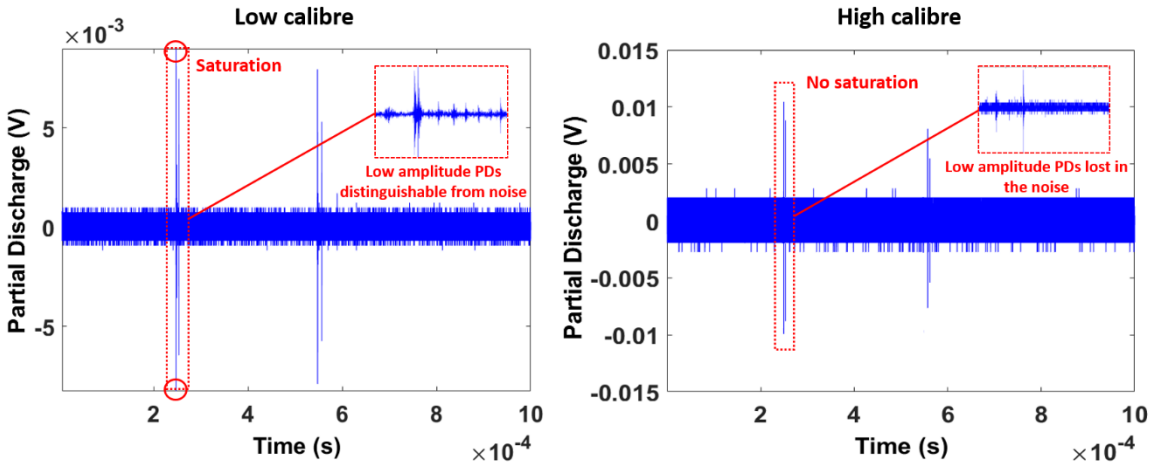

Figure III-22: *Illustration of the differences induced by range choice on the oscilloscope*

Getting back to the topic at hand, PD amplitude is effectively higher when it comes to square-wave stresses. However, the number of PDs is, at the same time, substantially lower than in the sinusoidal case. Thus, the highest PD amplitude under square-wave stresses may not be sufficient to justify the lifetime discrepancies. Measuring PD energy would certainly make it possible to establish a clearer theory on the matter. To go further in understanding the cause-and-effect relationship between PD activity and aging discrepancies as a function of rise time, the average number of PDs during the transient and steady parts of the voltage were determined and are shown below. The 1 kHz case was chosen to bypass the influence of high frequency.

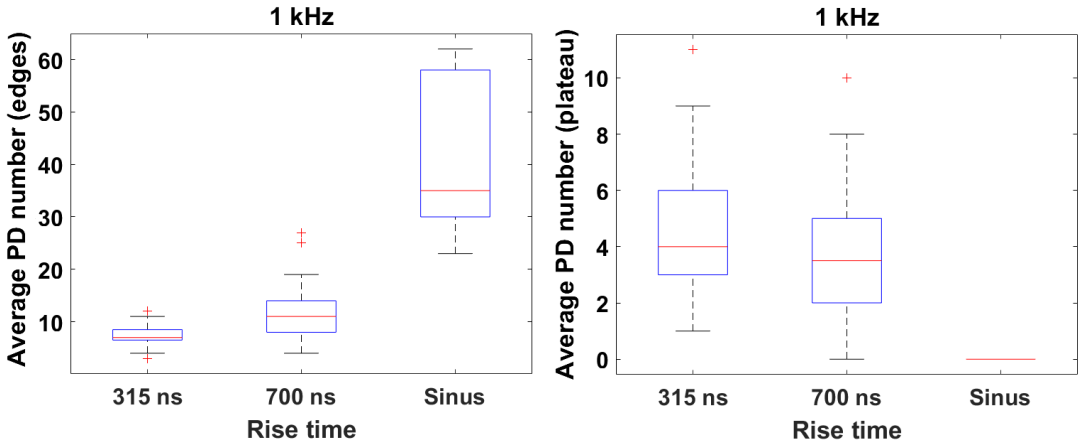

Figure III-23: *Average number of PDs during the transient (left) and steady (right) parts of the voltage (U=1.6xPDIV, f=1 kHz, α=50%)*

In the case of a sinusoidal stress, the average number of PDs during the steady part of the voltage happens to be zero, as the sinusoidal wave is considered to be composed of two transient parts without any steady-state. With square-wave voltage, the average number of PDs during the transient parts of the voltage increases with rise time. By contrast, the steady-state partial discharge number decreases with rise time until it reaches zero for the sinusoidal case. In the light of these results, one can hypothesize that steady-state PDs could be the factor accounting for lifetime discrepancies as a function of rise time.

Assuming that the energy associated with PDs remains unchanged during the transient parts of the voltage, as the average PD amplitude varies inversely with the average PD number, the presence of these steady-state partial discharges for the fastest rise time may lead to a decrease in lifetime. This is a very strong assumption, but the results regarding frequency tend to point in that direction. Another explanation could come from the fact that multiple discharge points are present with different individual PDIVs. Thus, the longer the rise time, the larger the inception delay for high-PDIV defects, the larger the PD at different points during the rise time, and the lower the number in the flat part.

III.5.3 Frequency

As for the influence of rise time and voltage magnitude, numerous studies have been carried out regarding the influence of frequency on the aging of insulation systems, whether they are recent or long established [51][84][85][86][81]. The outcomes in terms of PD characteristics are mixed, as for the previous case. In the case of a sinusoidal signal, in general, lifetime is inversely proportional to frequency. Multiplying the frequency by two means dividing the lifetime by two. PD activity is simply multiplied by two. However, when it comes to impulse voltages, this relationship is no longer necessarily true. It was demonstrated above that frequency, in addition to having a direct impact on lifetime, also has a flattening effect on lifetime vs rise time plots. To support these preliminary results, Figure III-24 shows the lifetime as a function of frequency, under sinusoidal and square-wave (t_m=380 ns) stresses.

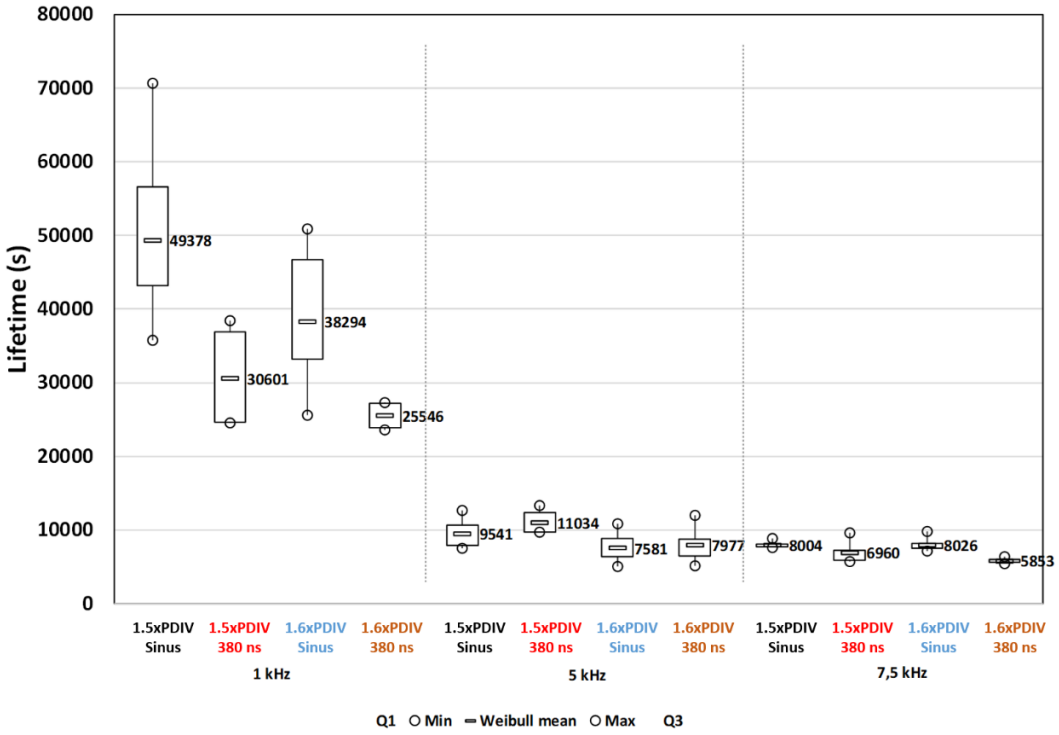

Figure III-24: *Lifetime vs frequency curves (U=1.5-1.6xPDIV, f=1-5-7.5 kHz, t_m=380 ns – sinus, α=50%)*

The difference between lifetimes under square-wave and sinusoidal stresses is quite pronounced at low frequency. However, when the frequency exceeds 5 kHz, the influence of rise time seems to be

mitigated. Table 16 shows the ratio between lifetime at 1 kHz and lifetime at 5 kHz as a function of voltage and rise time.

Table 16: *Ratios between the 1 kHz and 5 kHz lifetimes for different configurations*

Voltage / Rise time	1.2xPDIV	1.5xPDIV	1.6xPDIV	1.75xPDIV
Sinus	4.65	5.17	4.59	4.36
700 ns	4.69	5.18	3.22	4.98
380 ns	2.71	2.77	3.20	3.70

In the case of aging under sinusoidal stress, the ratio between lifetimes at 1 kHz and 5 kHz is very close to 5, regardless of the voltage level. Indeed, the failure mechanism is governed entirely by partial discharge activity during the transient parts of the voltage, and it may be assumed that the PDs themselves are of the same type from one frequency to another. However, the faster the rise time, the more the ratio diverges from this reference value. This implies that, for the fastest rise times, frequency has a nonlinear effect on aging. This nonlinear effect could be attributed to an additional degradation phenomenon. As for the previous case, the average number of PDs per cycle during both the transient and steady parts of the voltage were retrieved and plotted to have a clearer view of PD behavior as a function of frequency. Results are given below.

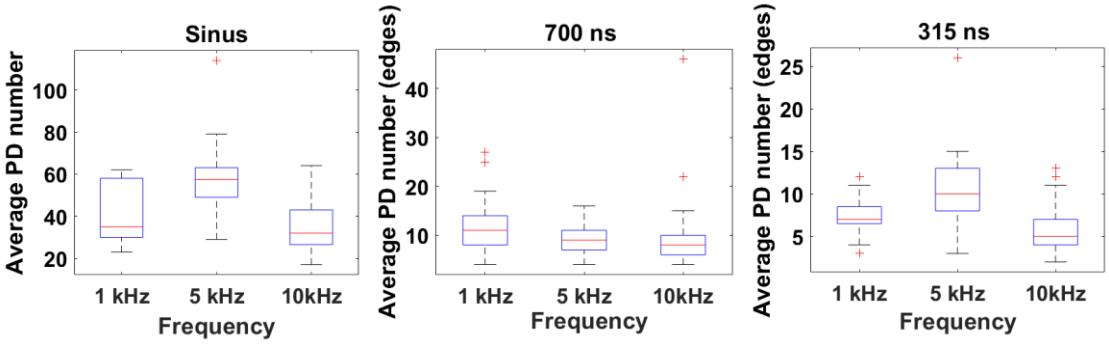

(a)

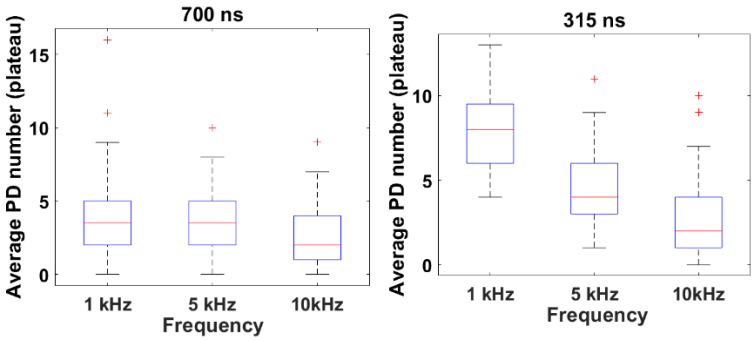

(b)

Figure III-25: *(a) Average number of PDs (edges) and (b) average number of PDs (steady-state) vs frequency (U=1.6xPDIV), t_m=315 ns – 700 ns – sinus, α=50%)*

It can be observed that there is no particular trend in terms of the average number of PDs during edges vs frequency. The number of discharges occurring during the transient part of the voltage is globally maintained as frequency increases, albeit with some fluctuations at 5 kHz. However, the average number of steady-state PDs tends to decrease with frequency and, for the 315 ns case, the ratio between the number of steady-state PDs at 1 and 5 kHz appears to correspond to the ratio between lifetimes for the same frequencies. Regarding the maximum and average PD amplitude, a non-monotonic behavior with frequency is observed. These results build on the work presented in the previous sections. It seems that PDs occurring during the steady part of the voltage could be the source of the discrepancies observed when increasing frequency or rise time. When frequency varies, the voltage rise time undergoes very little change. As a consequence, PD activity during the transient part of the voltage, and in particular the number and amplitude of PDs, remain within the same order of magnitude. By contrast, a variation in frequency leads to a modification of the voltage pulse duration. De facto, steady-state PD activity is modified and the number of these discharges decreases. A similar mechanism might occur when modifying rise time; for the fastest rise times, the number of these steady-state discharges is higher than for the lowest rise times. The slower the rising and falling edges, the fewer the steady-state discharges, and the closer the behavior is to the sinusoidal case. That would help explain the observed differences between aging under sinusoidal and square-wave stresses, as well as the flattening effect that was observed for higher frequencies (≥5 kHz).

In order to add weight to these results, a final electrical stress component was studied: duty cycle, in particular its influence on both PD activity and aging. These issues are the subject of the following section.

III.5.4 Duty cycle

Tests similar to those carried out in the previous paragraphs were performed, this time to highlight the influence of the duty cycle on PDs and aging. The following figure shows the results of endurance tests performed with various duty cycle values for a rise time of 380 ns and two different frequencies.

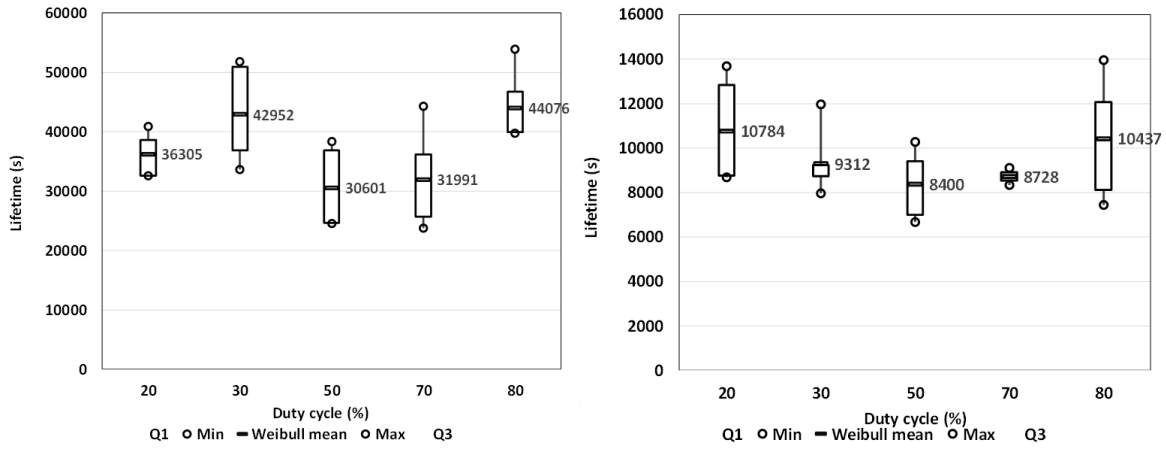

Figure III-26: *Lifetime vs duty cycle curves (left) U=1.5xPDIV, t_m=380 ns, f=1 kHz (right) U=1.5xPDIV, t_m=380 ns, f=5 kHz*

These figures indicate that lifetime is minimal when the duty cycle is set to 50%, that is, when the pulse duration is the same on the positive and negative halves of the voltage. Inversely, lifetime increases when the duty cycle value moves away from this value. As in previous cases, in order to correlate lifetime data with partial discharge activity, the average number of PDs during the edges and the steady parts of the voltage, as well as the average PD amplitude per cycle, were plotted as a function of duty cycle. These values are given below. In addition, the average number of PDs per cycle, the cumulative number of PDs over 20 cycles, and PD distribution between positive and negative halves of the voltage are also provided to provide an overall picture of PD activity as a function of duty cycle.

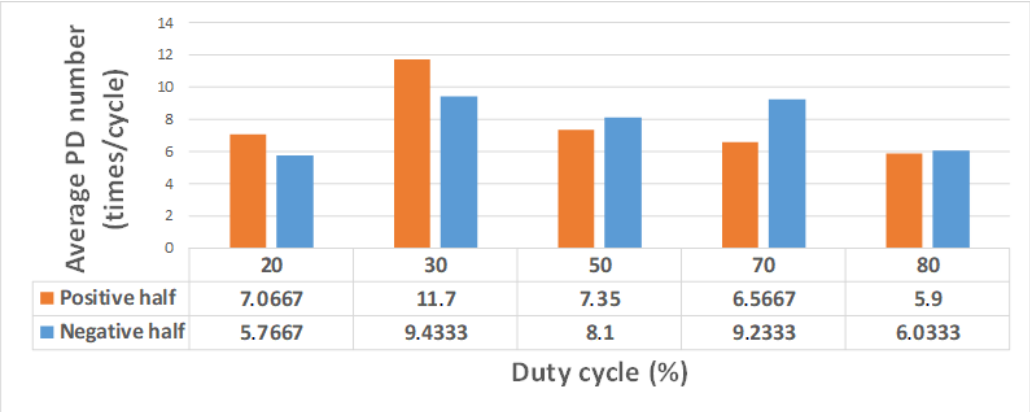

Figure III-27: *PD distribution between positive and negative halves of the voltage as a function of duty cycle (U=1.5xPDIV, tm=380 ns, f=1 kHz)*

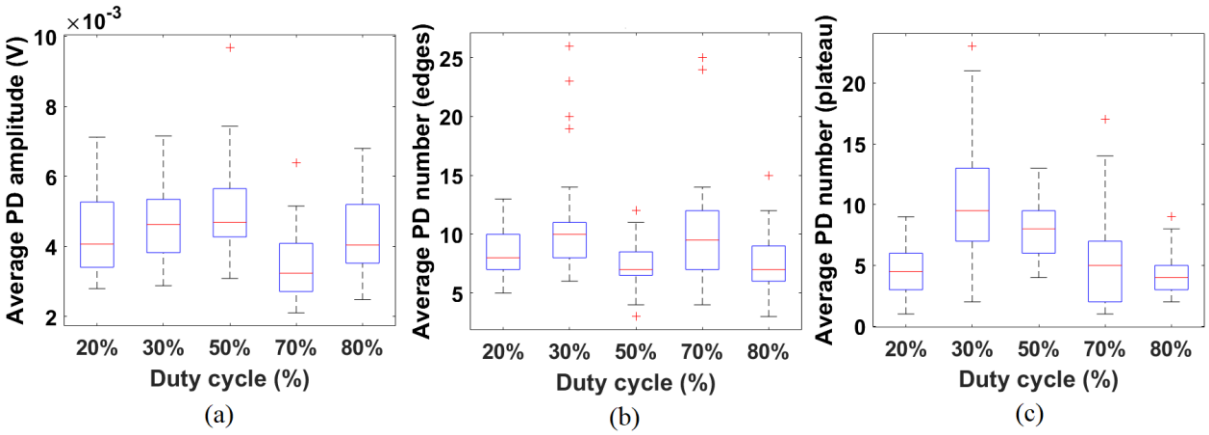

Figure III-28: *(a) Average PD amplitude, (b) average number of PDs during edges, and (c) average number of PDs during the steady part of the voltage (U=1.5xPDIV, tm=380 ns, f=1 kHz)*

Table 17: *Average number of PDs per cycle and cumulative number of PDs as a function of duty cycle (U=1.5xPDIV, tm=380 ns, f=1 kHz)*

Duty cycle	20%	30%	50%	70%	80%
Cumulative number of PDs (20 cycles)	257	422	309	316	239
Average number of PDs per cycle	13	21	15	15	12

Table 17 shows that the number of PDs varies significantly with duty cycle. The average number of PDs per cycle is lower when the duty cycle moves away from the 50% level, that is, when the asymmetry between the positive and negative parts of the voltage is most pronounced. It is even more obvious considering the cumulative number of PDs over 20 cycles. At the same time, it can be seen in Figure III-27 that PD distribution between positive and negative halves of the voltage is also affected. It is worth noting that, for the tests realized with a duty cycle value of 50%, the difference throughout the study between the average number of PDs in the positive and the negative parts of the voltage rarely exceeded 1. Nonetheless, when the duty cycle moves away from this central value, differences of about two or three PDs per cycle can be observed between the two parts of the voltage. This may seem inconsequential, but it could have significant impact over the entire system lifetime. Finally, Figure III-28 shows that duty cycle fluctuations do not appear to affect the average PD amplitude or the average number of PDs during the rising and falling edges. This is not particularly surprising, as the edge characteristics, in particular the dV/dt and rise time, remain unchanged between configurations. By contrast, the average number of steady-state PDs experiences variations when varying the duty cycle. This number is at its maximum for a duty cycle value of between 30% and 50%. These results follow in the footsteps of what was said before: lifetime discrepancies related to changes in frequency, voltage magnitude, rise time, or duty cycle values could be directly related to the presence or absence of PDs during the steady part of the voltage, rather than tied to the traditional PDs that can be found during the edges. In the light of this assumption, aging and PD activity issues were addressed separately for each constituent of the electrical stress. To conclude on this subject, a general analysis is presented below to address all points discussed and summarize the results of this chapter.

III.6 General analysis & conclusion

This work primarily allowed us to determine the influence of the different electrical stress constituents on aging. Then, as a second step, the obtained lifetime data was correlated with associated PD activity. Generally speaking, the impact of electrical stress on PDs and aging is consistent with information found in literature. However, new phenomena were also observed and an innovative approach was taken in efforts to analyze the mechanisms responsible.

Studying the influence of voltage and overvoltage magnitude showed that, although the presence of overvoltages increases the number and amplitude of PDs, and thus PD activity in general to a significant extent, the steady-state voltage magnitude and in particular its level compared to the PDIV may have an even greater impact on the lifetime of Type I samples due to the possible presence of partial discharges during the steady part of the voltage. To further illustrate the impact of voltage magnitude, Figure III-29 shows the cumulative PRPD patterns obtained for different voltage values and corresponding to different rise time values. The color code reflects the PD density depending on the

phase: the warmer the color, the more PD events there are. In addition, a summary of the average number of PDs during the edges and steady part of the voltage is given in Table 18.

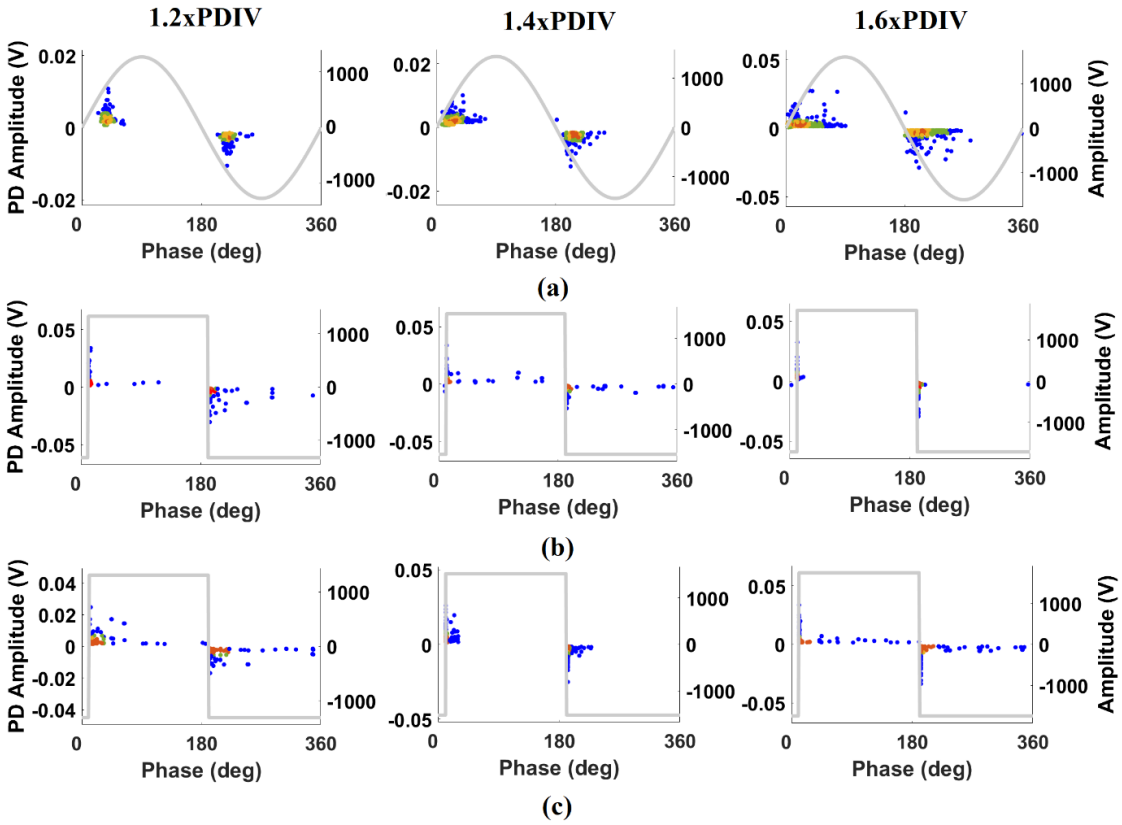

Figure III-29: *PRPD patterns depending on voltage magnitude (f=1 kHz, α=50%) (a) sinusoidal stress, (b) square-wave stress, tm=700 ns, (c) square-wave stress, tm=315 ns*

Table 18: *Summary of the average number of PDs (during edges and plateau) for each voltage/rise time configuration*

Voltage / Rise time	1.2xPDIV		1.4xPDIV		1.6xPDIV	
	Edges	Plateau	Edges	Plateau	Edges	Plateau
Sinus	8.27		12.75		41.15	
700 ns	8.79	6.17	11.27	6.07	11.35	3.87
315 ns	2.57	6	8.43	6.93	7.4	8.05

Studying frequency and rise time showed that while the fastest rise times have a negative impact on aging for the lowest frequency (1 kHz), this effect tends to disappear at higher frequencies (≥5 kHz). Moreover, drawing on the outcomes of PD measurements, it was stated that the steady-state PDs which had previously been pointed out may be responsible for both the influence of rise time on aging and the mitigation of this effect for high frequencies. In addition to results provided in Sections III.5.2 and III.5.3, cumulative PRPD patterns are given in Figure III-30 for different rise time and frequency values. It is worth noting that while in some cases it may seem that the number of PDs during the steady part of the voltage increases with frequency, that is not the case in reality. Indeed, it is related to the fact that pulse duration is modified as the frequency varies and that, as a consequence, the so-called steady-state

PDs are more densely clustered near the transient area at low frequency. To emphasize this point, an additional PRPD pattern, as well as a zoom on the area near the transient part, is given in Figure III-31. As in the previous case, a table summarizing the number of PDs in each case is also provided.

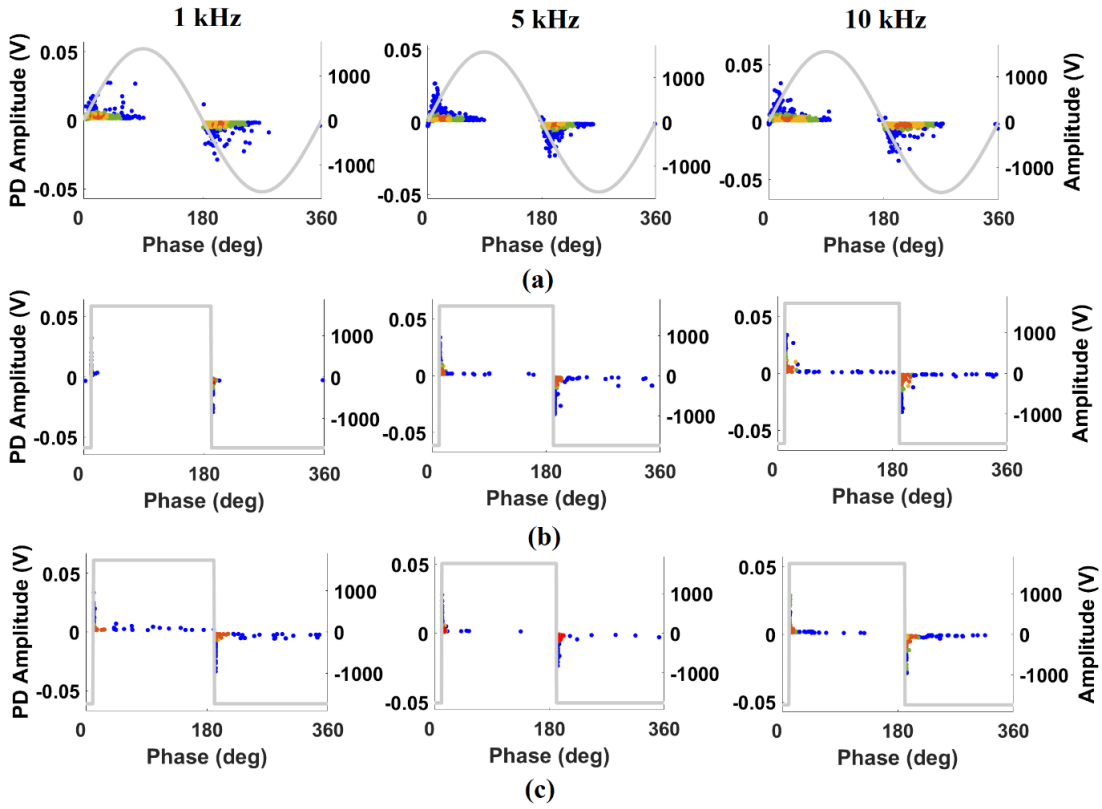

Figure III-30: *PRPD patterns depending on frequency and rise time (U=1.6xPDIV, α=50%) (a) sinusoidal stress, (b) square-wave stress, tm=700 ns (c) square-wave stress, tm=315 ns*

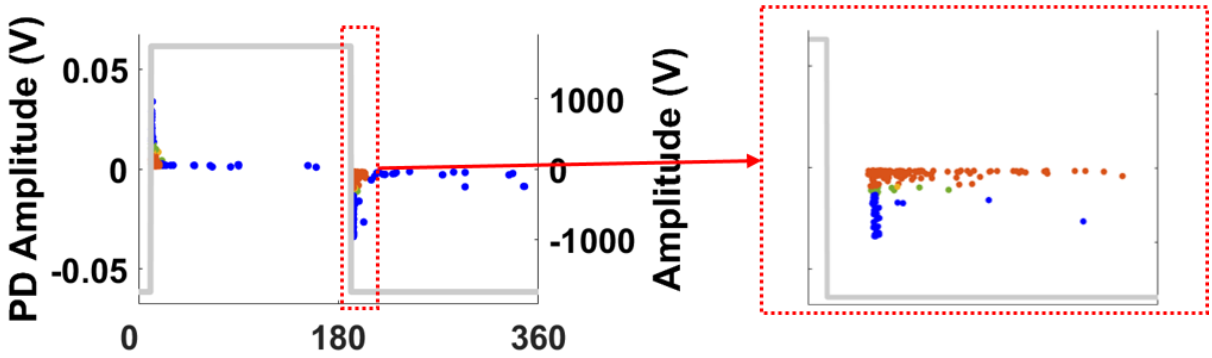

Figure III-31: *PRPD pattern and zoom on the area just after the falling edge (U=1.6xPDIV, tm=700ns, f=5 kHz, α=50%)*

Table 19: *Summary of the average number of PDs (during edges and plateau) for each rise time/frequency configuration*

Rise time \ Frequency	1 kHz		5 kHz		10 kHz	
	Edges	Plateau	Edges	Plateau	Edges	Plateau
Sinus	41.15		57.47		34.75	
700 ns	11.35	3.87	9.05	3.78	9.35	2.65
315 ns	7.4	8.05	10.5	4.85	5.75	2.70

Finally, a study on the influence of the duty cycle was carried out and enabled us to consider a configuration where only the pulse duration varies. It was confirmed that the presence or absence of these steady-state PDs has an influence on aging and that pulse duration has an influence on PD distribution between the positive and the negative halves of the voltage. As in the previous cases, PRPD patterns for different duty cycle values and a summary of PD distribution for each case are given below, complementing previous results.

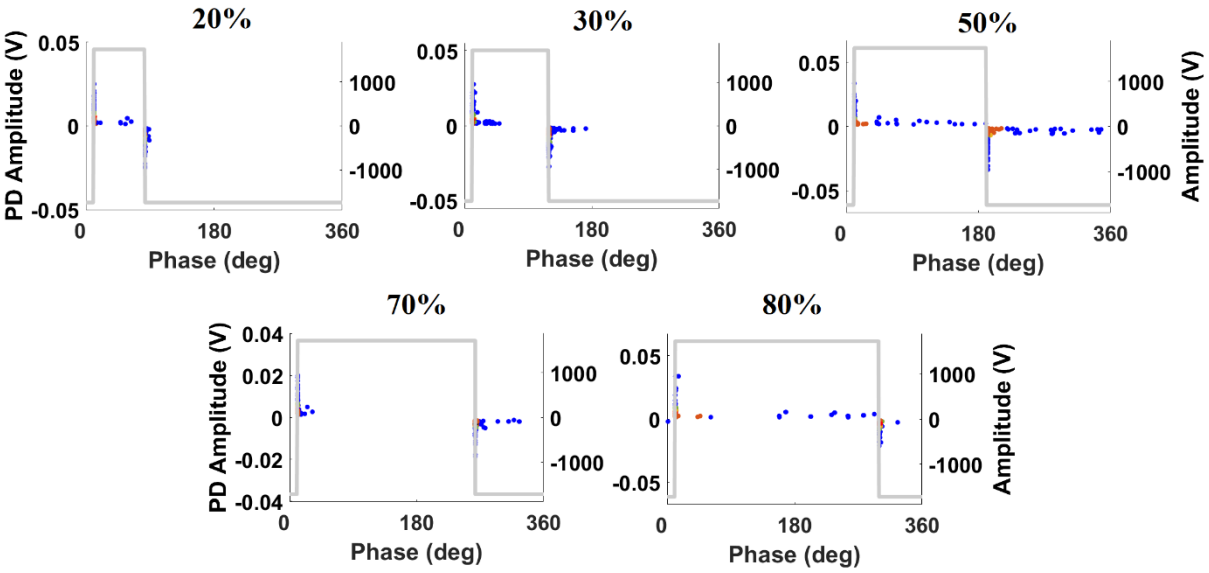

Figure III-32: *PRPD patterns depending on duty cycle (U=1.6xPDIV, t_m=315 ns, f=1 kHz)*

Table 20: *Summary of the average number of PDs (during edges and plateau) as a function of duty cycle (U=1.6xPDIV, t_m=315 ns, f=1 kHz)*

Duty cycle \ PD number	Edges	Plateau
20%	8.33	4.5
30%	10.97	10.17
50%	7.40	8.05
70%	10.2	5.6
80%	7.53	4.40

To summarize in more general terms, this chapter offered an opportunity to shed light on the influence of electrical stress components on PD activity and aging. Several conclusions can be drawn

from the tests and measurements that were carried out. First, from a practical point of view, the various results show that it may be relevant to perform electrical aging under sinusoidal stress. With the exception of the tests performed with varying duty cycle that do not apply to the sinusoidal case, it can be seen that the trends regarding aging are very similar under sinusoidal and square-wave stresses, whatever the applied constraints. Furthermore, the differences that may exist between the two stresses tend to be mitigated at high frequency. It is thus conceivable to perform aging tests on Type II samples in an industrial context under sinusoidal voltage, on the condition that these conclusions can be transposed to Type II insulation systems.

From a scientific and evidential point of view, it is difficult to draw any clear-cut conclusions concerning the relationship between lifetime and PD activity. There seems to be a correlation between degradation and partial discharge activity, especially with separate consideration for the discharges occurring during the edges and the steady part of the voltage. But the link between the two seems to be relatively more complex than a direct relationship between their number and/or energy. This work is only the first step towards fully understanding the mechanisms involved when varying electrical stress. Other factors, such as the type of PD [85][87], current, or simply the energy associated with the discharges could help explain or contribute to understanding the discrepancies induced by the variation of electrical stress constituents.

Now that electrical stress has been identified over a range of operating conditions, and the influence of this stress on PDs and aging has been assessed on very basic samples, the last step of this work consists of making the link between the two. In other words, the results obtained for samples representative of Type I turn-to-turn insulation systems must now be transposed to equivalent Type II samples, and the electrical stress identified in Chapter II must be reproduced to study the aging of Type II samples closer to the real system. These latter subjects are the focus of the last chapter in this work.

Chapter IV. Investigations into aging and underlying phenomena in Type II machines

IV.1 Brief introduction

After a brief examination of the state of the art, research reported in previous sections enabled us to identify the electrical stress in a Type II machine as a function of various electrical and geometrical parameters, and to assess the influence of this electrical stress on aging and partial discharge activity considering very basic samples representative of Type I turn-to-turn insulation systems. However, it is necessary to go further to address both the causes and effects of the existence of PDs in a Type II electromechanical chain using SiC-based components. With this goal in mind, the purpose of this last chapter is now to assess the influence of electrical stress on samples that are representative of the actual system itself to bridge the gap between phenomenological study and stress identification and, at the same time, between Type I and Type II.

This chapter is divided into two parts: the first part is devoted to the translation from Type I turn-to-turn insulation systems to Type II equivalent insulation systems that are actually used in high voltage machines. The second part focuses on extending of the study of PD activity and aging to Type II phase-to-phase and phase-to-ground insulation systems. As it was explained in Chapter II, these insulation systems are indeed more likely to be subject to partial discharges. This chapter is the last building block of the full study, offering complete consistency of information related to the study of PDs and aging in an electromechanical chain in the presence of constraints related to SiC, in the context of Type II machines.

IV.2 Transition from Type I to Type II conductor pairs

IV.2.1 Purpose of the study

In the previous chapter, a study on the influence of the different electrical stress constituents on PDs and aging was performed on twisted pairs of enameled wires, representative of Type I turn-to-turn insulation systems. The purpose of this section is now to determine whether or not the conclusions emerging from that study can be transposed to Type II insulation systems, which are more complex because they are composed of different types of organic and inorganic insulating materials. A reduced test plan, compared to that of Chapter III, was therefore set up to check whether the main trends are the same.

The details of the experimental setup, test plan, as well as the main results of this study are given below following the same structure as that used in Chapter III.

IV.2.2 Experimental setup & test plan

IV.2.2.1 Investigation on sample characteristics

As specified in Section II.3.1, Type II high voltage machines generally present formed wound coils constituted of flat wires stacked on top of each other. In general, the turn-to-turn insulation of such machines consists of a polyimide film coating, sometimes reinforced with Teflon-FEP, as is the case here. The samples used for this study are therefore representative of this type of insulation system. They comprise pairs of insulated conductors that are held together, with the terminals splayed apart and processed according to production standards. The insulated conductors are in contact along the length of the straight portion to simulate the contact between turns in a coil. The contact between those conductors is maintained by a wrapping that provides the pressing function [15]. Pictures of the samples are provided below.

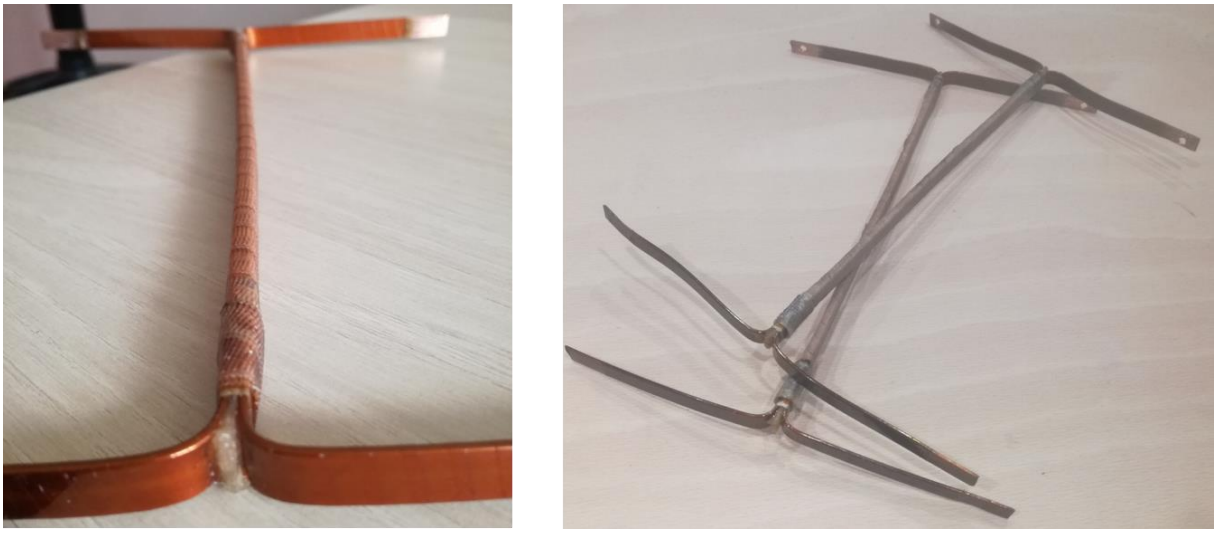

Figure IV-1: *Type II pairs of insulated conductors*

Two types of insulated conductor pairs were considered in the study. The first type, which is referred to as “Type O”, is representative of the materials that are actually used for the turn-to-turn insulation of machines. The second type, which is referred to as “Type A”, is an improved version (in terms of electrical insulation) of the “Type O” sample. The insulating materials remain unchanged between the two. The only difference resides in the thickness of the covering material, *i.e.* the polyimide film coating.

Investigations into the electrical characteristics of the samples were carried out in order to assess their tolerance towards PDs and also to determine the levels of stress to apply during aging. PDIV measurements and breakdown tests were thus performed following the same procedure as that applied in III.2.3. The results are given in Table 21 for both types of pairs of conductors. In parallel, simulations were carried out to estimate this same PDIV and compare the value to experimental results, as well as

to obtain a view of the electric field lines and potential distribution in the area of the two conductors. A simulation tool developed by IRT Saint Exupéry called AIRLIFT – pArtial dIscharge Risk evaLuatIon soFTware - was used to run these simulations. To summarize, this simulation tool uses a 2D model based on the current state of discharge physics in homogenous fields (Townsend's theory) derived for inhomogeneous fields to model partial discharge inception voltage in a numerical way. The results are also given below.

Table 21*: PDIVs for both types of samples (Type O and Type A)*

Sample number	Type O		Type A	
	PDIV (kVpk)	Breakdown voltage (kVpk)	PDIV (kVpk)	Breakdown voltage (kVpk)
1	1.44	8.68	2.029	13.22
2	1.353	10.21	2.305	14.32
3	1.62	9.78	2.41	15.34
4	1.528	10.18	2.411	15.26
5	1.442	10.18	2.101	14.83
Average	**1.4766**	**9.806**	**2.2512**	**14.594**
Simulation	**1.410**		**2.590**	

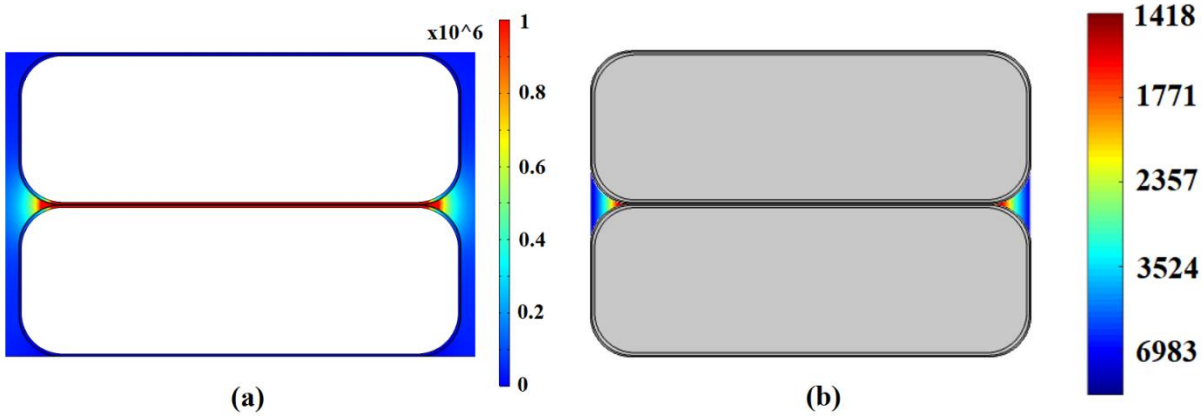

Figure IV-2: *(a) Electric field distribution (V/m) and (b) PDIV distribution (V) in the area of a Type O sample*

The PDIV values obtained experimentally and numerically are quite similar to each other. This is especially true in the case of Type O samples, for which the proposed simulation method is highly representative of reality and able to identify the most likely area for PD inception. Regarding Type A samples, the gap between experimental and numerical values is slightly larger. This gap, as well as the PDIV difference between the two types of samples, can be explained by the difference between the percentage overlap of the tape in both cases. In the cases of Type O samples, the percentage overlap of the tape is such that the total insulation thickness is a multiple of tape thickness throughout the length of the conductors. As the geometry is independent of the length, it is thus convenient to use a 2D model to estimate PDIV values. By contrast, the percentage overlap is higher for Type A samples, such that the insulation thickness is not the same throughout the length of the conductors (Figure IV-3 illustrates

this point). As a consequence, there are areas where insulation thickness is the same as for Type O samples, and areas where the insulation is thicker. This explains why the PDIV is higher for Type A samples, as well as why the gap between experimental and numerical values is larger in the latter case: the 2D model does not take full account of the thickness inhomogeneity throughout the length. Simulation was thus carried out considering an average value for insulation thickness.

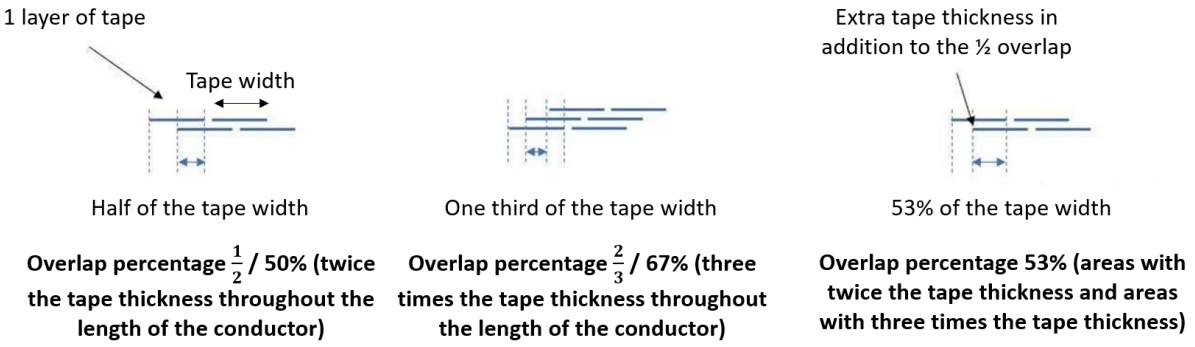

Figure IV-3: *Illustration of the different types of overlap used for Type II machine insulation*

Based on these results, preliminary conclusions can be drawn regarding the existence of partial discharges in turn-to-turn insulation systems. Given the average PDIV values (respectively 1477 and 2251 Vpeak for Type O and Type A conductor pairs), and considering the results of the stress identification performed in Chapter II, it is confirmed that there is little chance of PD inception occurring in the insulation between turns. It is still important to note that, compared with a real machine, the PDIV of back-to-back specimens can be higher as the impregnation is nearly perfect (the straight part is not put in a metallic enclosure). The maximum turn-to-turn voltage was found to be a few hundred volts for the fastest inverters, so the insulation system structure prevents the appearance of any PD events. This holds all the more true as the insulation of the considered samples is representative of machines that are supposed to operate with the lowest DC bus voltage in the range. For the highest DC bus voltages, it may be assumed that the insulation is all the more reinforced, whereas the maximum turn-to-turn stresses may not necessarily be much more stressful than in the case of the lowest DC bus voltages. To be more specific regarding this last point, and referring back to the results given in Section II.5, it can be seen that the worst case in terms of maximum relative turn-to-turn stresses is encountered for inverters C and E (respectively 45.71% and 15.6% of the DC bus voltage, and a few hundred volts in absolute terms). Those inverters are both supposed to operate at the lowest DC bus voltage. For the highest DC bus voltages, however, the worst case is encountered with inverter B (8.86% of the DC bus voltage). An extrapolation of this result for the nominal voltage value leads to a maximal absolute turn-to-turn value that also does not exceed a few hundred volts, despite the voltage increase. Therefore, given the fact that the maximal absolute turn-to-turn values are quite similar in both cases, there are potentially far fewer chances to incept PDs between turns in a machine operating for the highest DC bus voltages and thus equipped with a reinforced electrical insulation system.

As a consequence of the fact that the turn-to-turn insulation does not represent the weakest point in the machine, that aspect was not the main focus of the study. The number of tests and, in turn, the test plan were reduced drastically, and the purpose of the following part is mainly to assess whether the results obtained in the previous chapter can be transposed to Type II insulation systems.

Due to the nature of the samples representative of Type II turn-to-turn insulation systems, which are somewhat different from the basic Type I twisted pairs of enameled wires that were studied previously, the experimental setups used for this part of the study are different from those presented in Section III.2. Experiments were carried out at two different locations, with the tests under sinusoidal stress at one site, and the tests under square-wave stress at the other.

IV.2.2.2 Aging under sinusoidal stress

Endurance tests under sinusoidal stress were performed using the same voltage supply to be used for aging the motorettes representative of Type II phase-to-ground and phase-to-phase voltages. This voltage source was specially designed for aging very capacitive samples based on their characteristics and the results obtained during the previous study. This scaling is the subject of particular attention in Section IV.3.2. However, at this point, it can be stated that this voltage source can deliver a sinusoidal voltage up to 10 kV peak, with a frequency ranging from 1 to 10 kHz. This voltage supply is comprised of six independent amplifiers, each coupled with a main transformer. This makes it possible to supply six channels independently. A schematic layout of the voltage source is given below.

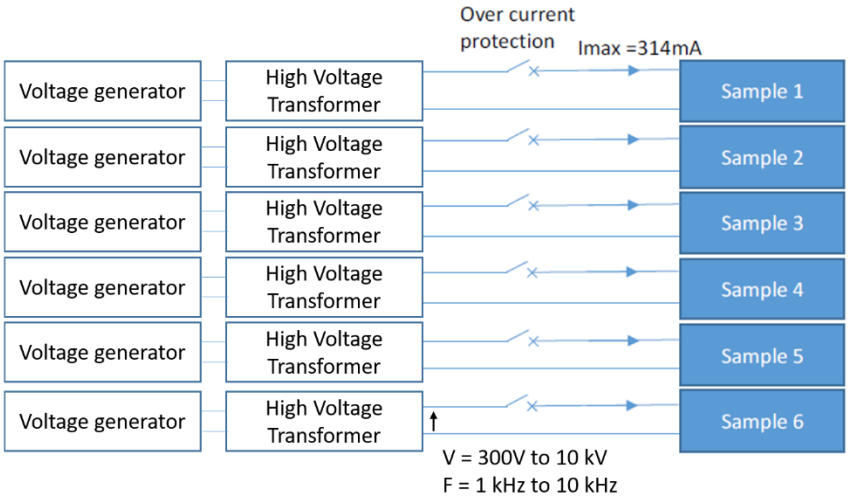

Figure IV-4: *Schematic layout of the experimental bench used for aging under sinusoidal stress*

As with the experimental setup in Chapter III, lifetime is estimated on each channel independently using the current limitation of the voltage supply. Voltage is controlled both using a high voltage probe (Testec TT-SI 9010) and via a measurement taken directly on the voltage source. Finally, PD measurements are also achieved according to the same model as that in Chapter III, except that the 20 acquisitions are repeated every hour instead of only during three different aging stages. Finally, the data

previously retrieved from the oscilloscope (Rohde & Schwarz RTE 1104, 1 GHz, 5 Gs/s) is processed using the same methodology as in Section III.3 for the sinusoidal case.

IV.2.2.3 Aging under square-wave stress

The experimental setup is quite different from the sinusoidal case regarding aging under square-wave voltage. The alternating voltage is generated by associating an autotransformer (230V/50Hz – 3 KVA) and a step-up transformer (230 V-4.5 kV). A voltage regulator upstream of these transformers enables us to limit the mains voltage variation to about 2%. At the transformer output, a single-phase rectifier with three 3300 µF filtering capacitances in series converts the alternating voltage into DC voltage. This voltage then supplies an inverter made of IGBT modules (3.3 kV – 450A). The cable length between the inverter and the sample is about 20 centimeters. Two additional 1 µF capacitances are used to filter the voltage and limit overvoltages to respectively 10% during rising edges and 15% to 20% on falling edges. Despite introducing the filter, the rising edge reaches the value of 400 ns for a dV/dt of 5 kV/µs. The duty cycle value is set to 50% and cannot be modified. Its influence, unlike other parameters, is not studied here for Type II insulation systems. Finally, it was only possible to age one sample at a time. As in the sinusoidal case, pictures and a schematic layout of the experimental setup are given below.

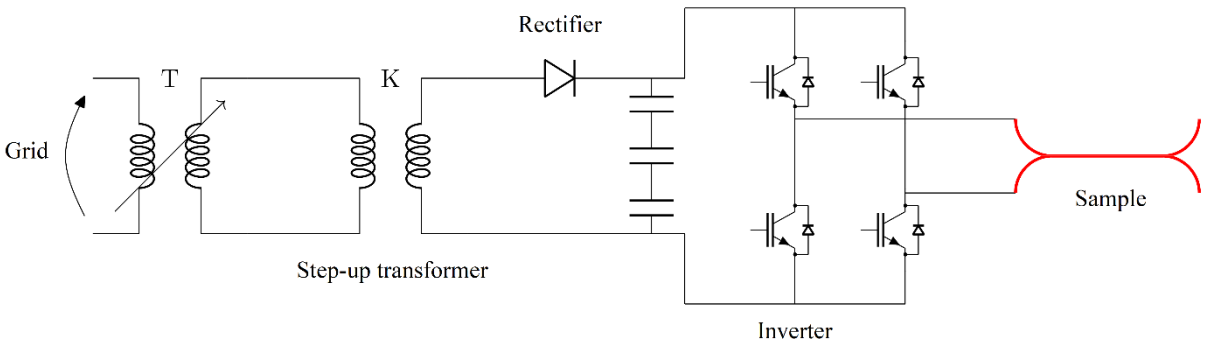

Figure IV-5: *Schematic layout of the experimental bench used for aging under square-wave stress*

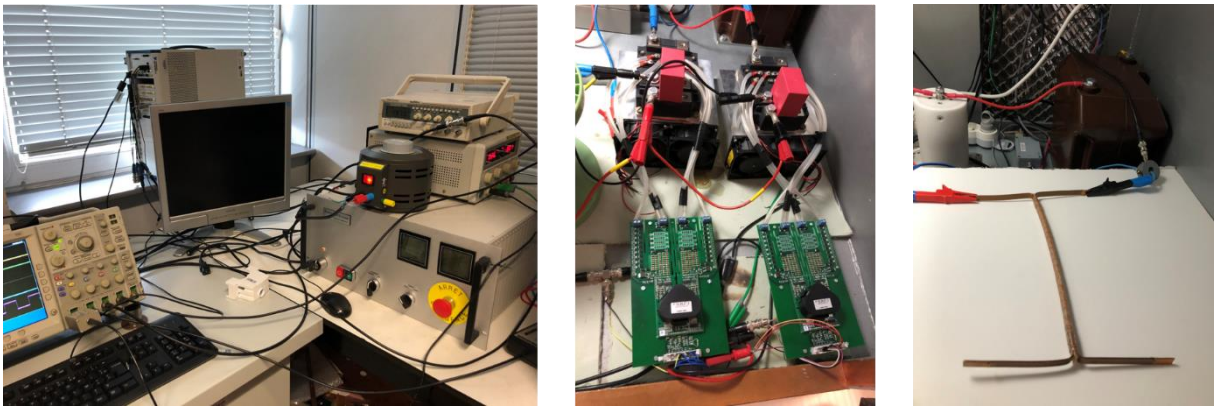

Figure IV-6: *Pictures of the experimental bench used for aging under square-wave stress*

Breakdown was detected by means of a fuse located on the primary side of the transformer, enabling us to estimate sample lifetime. The DC bus voltage and the voltage at the sample terminals were controlled using two voltage probes (Tektronix P6015A). Finally, it was not possible to perform PD measurements on this experimental setup due to limitations in terms of sensors and filtering. As such, it was not possible to fully replicate the Type I study conducted earlier in Chapter III.

Based on the sample characteristics, and within the limits imposed by the different experimental setups, it was possible to define a test plan to compare the aging mechanisms involved between Type I and Type II. The details of this test plan are provided below.

IV.2.2.4 Test plan

As previous tests have shown, turn-to-turn insulation systems are very unlikely to be subject to partial discharges. Nevertheless, studying the endurance of such insulation systems under sinusoidal and square-wave stresses can offer valuable insight into the resilience of those materials to PDs. Tests were thus performed considering the worst-case scenario, that is, in the presence of PDs over the entire lifetime. Only Type O samples representative of the insulation systems present in actual machines were studied. On the basis of the PDIV and breakdown voltage measurements presented above, and within the limits imposed by the different experimental setups, a test plan was elaborated to study the effect of frequency, rise time, and voltage on aging, as was done for Type I earlier. As already mentioned, the duty cycle could not be studied because it was not possible to modify its value. The range for voltage amplitude was from 20% above the PDIV (1819 Vpk) to 75% above the PDIV (2653 Vpk). The frequency could vary between 1 and 10 kHz. The voltage shape was either sinusoidal or pulse-like with a rise time of 400 ns. Finally, the duty cycle was set to 50%. The table below summarizes the variation range for each considered parameter.

Table 22: *Summary of the variation ranges for each parameter – test plan*

Parameter	Variation range
Magnitude (%PDIV / Vpk)	120 /1819 – 160 / 2426 – 175 / 2653
Frequency (kHz)	1 – 5 – 7.5 – 10
Rise time (ns)	400 – 250 000 (sinus)
Average dV/dt (kV/µs)	0.011 (sinus) – 5.55
Duty cycle (%)	50
Overvoltage	10% (rising edges) – 15-20% (falling edges)

IV.2.3 Aging and PD activity: Type I vs Type II

Experiments with Type I samples showed that the main electrical stress constituents have various effects on PD activity and aging. An increase in voltage (amplitude or overvoltage) or amplitude leads to a shorter lifetime, while the shortest rise times have a tendency to increase lifetime. Regarding duty

cycle, the critical value in terms of lifetime is 50%, when the duration of the positive and negative halves of the voltage are the same. A rise time-frequency effect was also noticed: the higher the frequency, the more mitigated the effect of rise time on lifetime. A similar analysis was conducted with Type II samples on a much smaller scale to see whether this tendency is confirmed. Figure IV-7 shows the lifetime vs frequency curves, both under sinusoidal and square-wave stresses, considering the Type O pairs of conductors presented above (up to six samples were aged for each aging point).

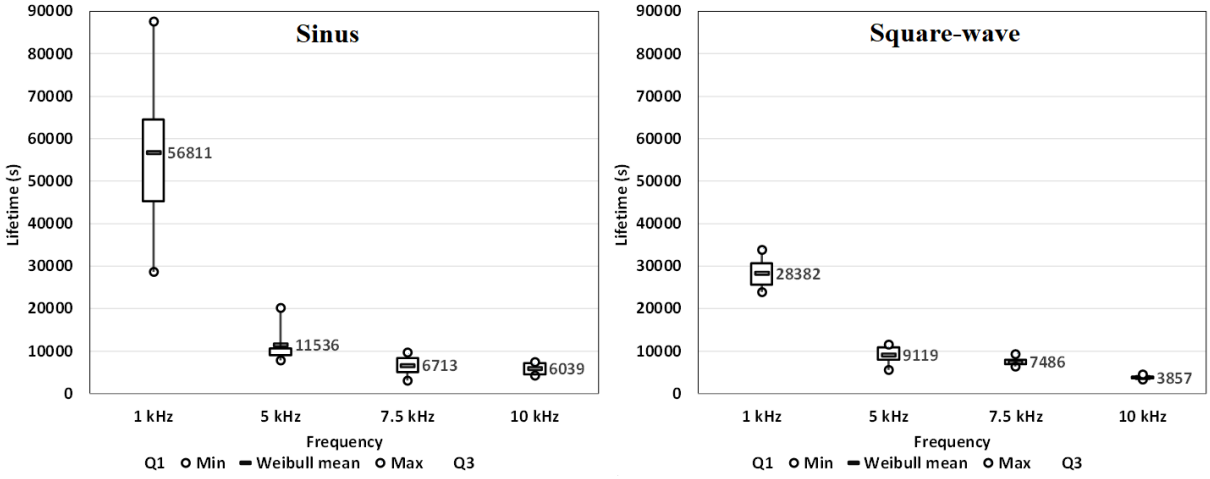

Figure IV-7: *Lifetime vs frequency curves under sinusoidal and square-wave stresses (U=1.6xPDIV, f=1-5-7.5-10 kHz, t_m=400 ns – sinus, α=50%)*

Results tend to confirm observations made in the previous chapter. The tendencies in terms of aging are essentially the same as those observed with Type I samples. It can be seen that the effect of rise time on lifetime is substantial at low frequency, while it seems to be mitigated at higher frequencies. This is especially true given the fact that, in contrast to the square-wave that was used in the previous chapter, this waveform presents overvoltages during the rising and falling edges, although relatively low. As a consequence, lifetimes under square-wave stress could be even longer considering a pure square-wave shape. The effect of frequency is summarized in Table 23, which shows the values of the ratio between the lifetimes for different frequencies and for both sinusoidal and square-wave stresses.

Table 23: *Ratios between lifetimes at different frequencies and for different configurations*

Ratio / Rise time	1 kHz / 5 kHz	1 kHz / 7.5 kHz	1 kHz / 10 kHz
Sinus	4.92	8.46	9.4
Square-wave	2.83	3.94	7.18

Under sinusoidal stress, there is a linear relationship between lifetime and frequency. As with the case of Type I, it can be supposed that only the PDs occurring during edges have an impact on aging, and that there is a proportional relationship between number of PDs and frequency. However, concerning pulse-like voltage, a non-linear frequency effect can be observed. Unfortunately, no PD

measurements can support this assessment, as it was not possible to perform PD detection under square-wave voltage. Regarding the influence of amplitude under sinusoidal stress, similar behavior to that found for Type I was observed, that is, a decrease in lifetime with amplitude related to an increase in number and amplitude of PDs. In short, these results tend to confirm the trends observed with Type I samples, at least in terms of aging. PD measurement would have ensured that the behavior of partial discharges was similar as well, but the absence of detection under square-wave voltage stress and difficulties related to measurement under sinusoidal stress impeded efforts to obtain more meaningful results.

These last results, in particular mitigation of the effect of rise time with frequency, are interesting from a phenomenological perspective. They may also have more concrete consequences in terms of aging acceleration and reproduction. Indeed, the results would mean that rise time has a lesser influence on aging at high frequency and that, as a result, lifetimes under sinusoidal and square-wave stresses are the same. Sinusoidal voltages could therefore be used instead of square-wave voltages to aging insulation systems. The sinusoidal voltage source introduced in IV.2.2.2, and which is detailed further in IV.3.2, was dimensioned based on this assumption.

Chapter II and Section IV.2 respectively showed and confirmed that turn-to-turn insulation has few chances to be subject to PDs over the course of its lifetime. It is now time take a look at what is actually happening at the machine's weakest point, *i.e.* the phase-to-phase and phase-to-ground insulation systems. The following section, which is the last section of this work, explores the aging of advanced Type II samples representative of those insulation systems.

IV.3 Extension to Type II motorettes

IV.3.1 Purpose of the study

The previous section enabled us to make the transition from Type I to Type II turn-to-turn samples. The purpose of this section is now to extend the analysis that was performed on twisted pairs of enameled wires (Type I, turn-to-turn insulation) and pairs of conductors (Type I, turn-to-turn insulation) to samples closer to the real system and representing the machine's weakest point (Type II, phase-to-ground and phase-to-ground insulations). The characteristics of the new samples, the experimental setup, as well as a global analysis regarding their lifetime and endurance to PDs is presented. Finally, we provide a discussion on aging and degradation results and their extension to real environments.

IV.3.2 Experimental setup and test plan

IV.3.2.1 Investigations on sample characteristics

The samples used to study mainwall insulation were built to production standards and fitted into representative slots. The test objects fully respect manufacturing specifications for a production machine, but are of reduced slot length to minimize capacitive load. Unlike the previously studied samples, these new samples are motorettes representative of phase-to-ground and phase-to-phase insulation systems. A motorette itself literally consists of part of a machine. In this case, it is composed of six pairs of insulated conductors placed in their respective slots, for a total of 12 conductors, and enshrined in a metal structure. In real machines, entire coils composed of several turns are placed in the slots. However, in this case, considering that the turn-to-turn insulation system was not identified as a risk area, the turns were brazed together, leaving only two conductors per slot, with each conductor representing one phase. The insulation systems between phases, and between phase and ground, are representative of those that can be found in real machines. Finally, no stress grading systems were used. Pictures of the samples are given below.

Figure IV-8: *Motorettes to study phase-to-phase and phase-to-ground insulation systems*

Two types of motorettes were studied. The first type, identified as “Type R” (which stands for “reference”), is representative of the insulation system that can actually be found in machines, in particular the machine studied in Chapter II. The second type, identified as “Type N” (for “new”), is an alternative version of the Type R motorette composed of a reduced insulation system. In both cases, the entire insulation system between conductors, and between phases and ground, is consistent with that described in I.3.3.2. Conductors are insulated using mica and paper tape. An additional layer made of Nomex enables us to separate the conductors from the slot. At the top of the slot, Nomex and Kapton are calendered and bonded together with a silicon adhesive. Another layer of Nomex reinforces the insulation between the two conductors. Finally, the entire system is impregnated with a silicon resin using the VPI process. The only difference between the two types of motorettes (in terms of phase-to-ground and phase-to-phase insulation) resides in the fact that Type N motorettes are designed with a reduced amount of mica. It should also be noted that the turn-to-turn insulation in Type R motorettes

corresponds to the insulation of the Type O conductor pairs described in IV.2.2.1. Likewise, the turn-to-turn insulation of Type N motorettes corresponds to that of the Type A conductor pairs. However, as mentioned earlier, the turns were brazed together as the turn-to-turn insulation was identified as a low risk area. That type of insulation was therefore not studied here.

As with the case of conductor pairs, investigations into the electrical characteristics of the samples were carried out in order to assess the conductor pairs' tolerance towards PDs, determine the levels of stress to apply during aging, and also to dimension the voltage supply used to perform aging. Capacitances and PDIV measurements were taken to address these points. Capacitances were measured using an LCR meter. The PDIV measurement protocol is the same as that described in Section III.2.3 and Section IV.2.2.1. Regard the latter, as in the previous section, simulations were also carried out in parallel to assess the electric field and PDIV distribution depending on sample geometry. The results are given below for both types of motorettes.

Table 24*: PDIV, capacitances, and tan δ measurements between phase and ground (Type R - Type N)*

Measurement point	Type R			Type N		
	PDIV (Vpk)	Capacitance (pF)	Tan δ	PDIV (Vpk)	Capacitance (pF)	Tan δ
1/ground	3336	146.62	0.01381	2207	186.5	0.00585
3/ground	3138	152.95	0.01084	2188	202.72	0.00710
5/ground	3151	159.25	0.00962	2223	194.35	0.00685
7/ground	3189	160.65	0.01050	2061	185.9	0.00654
9/ground	3327	153.13	0.01109	2009	188.5	0.00627
11/ground	2972	149.51	0.01436	1991	187.06	0.00866
Average	**3185**	**154.74**	**0.011703**	**2113**	**190.84**	**0.00687**
Simulation	**3050**			**2210**		

Table 25*: PDIV, capacitances, and tan δ measurements between phases (Type R - Type N)*

Measurement point	Type R			Type N		
	PDIV (Vpk)	Capacitance (pF)	Tan δ	PDIV (Vpk)	Capacitance (pF)	Tan δ
1/2	5165	91.55	0.00670	3404	138.65	0.01219
3/4	5164	95.63	0.00741	2778	139.57	0.01130
5/6	5211	97.47	0.00845	3586	139.89	0.01160
7/8	4789	100.59	0.00697	2892	124.98	0.01412
9/10	5301	95	0.00810	3268	140.67	0.01152
11/12	4657	94.28	0.00678	2550	138.25	0.13818
Average	**5048**	**95.75**	**0.0074**	**3080**	**137**	**0.01199**
Simulation	**5430**			**3240**		

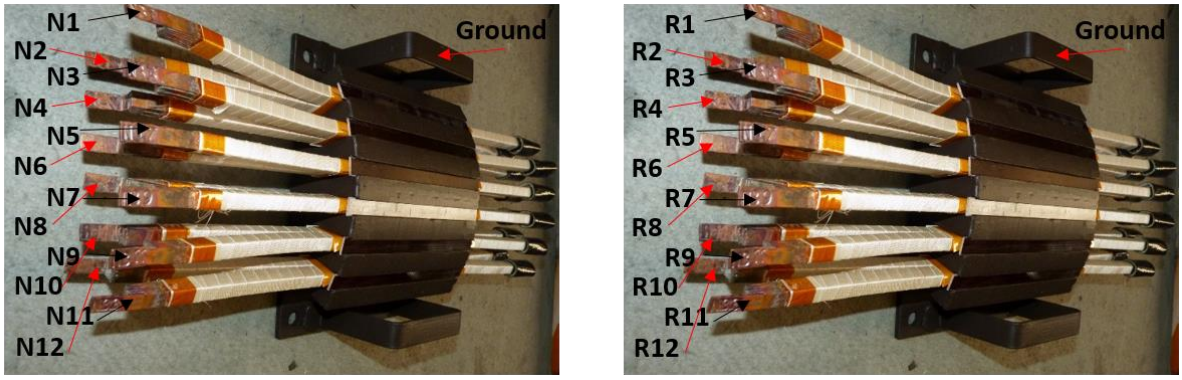

Figure IV-9: *Description of measurement points for Type R and Type N motorettes*

As a consequence of the high-performance insulation system, the obtained PDIV values are quite high, especially between phases. Furthermore, there is a major difference between the PDIV values for Type N and Type R motorettes. This comes as no surprise, as the layer of mica tape – the difference between the two configurations – is a non-organic material serving as the primary barrier against PDs.

The results obtained by numerical simulation are highly satisfying, given the complexity of the samples and, in particular, of the insulation systems. A variance of less than ten percent is observed, compared to the average value obtained with conventional PDIV measurement. This suggests that the numerical model used to calculate PDIV distribution represents the real system accurately. At the same time, using this simulation tool and building the model made it possible to highlight the influence of various geometric parameters on PDIV distribution, such as insulation type and thickness, of course, but also less intuitive parameters such as conductor dimensions (bend radius, length, width) and the percentage of tape overlap.

Despite the fact that the samples are manufactured industrially, there is a non-negligible dispersion of PDIV values, particularly between phases. When considering twisted pairs of enameled wires, it is not unusual to have dispersion, which may be attributed to human error. However, the results obtained for both conductor pairs and motorettes tend to show that this dispersion also exists when the samples are carefully and industrially produced, and that the dispersion is difficult to manage. Capacitances and tan δ measurements, which were performed in the first place to justify this dispersion, are not sufficient to explain it, as there are no significant differences and, more importantly, no correlation between the trends in terms of PDIV, capacitances, and loss angle.

Given these results, it seems that the risks of PD inception are quite low, even for phase-to-ground and phase-to-phase insulation systems, and considering the maximum stresses than can be encountered in such areas. However, unlike the case of turn-to-turn insulation where the risk is nearly non-existent, the phase-to-phase and phase-to-ground voltages are not far from – and may reach – the PDIV for the highest DC bus voltage values. Moreover, the value of this PDIV is certainly not the same under real operation. The first reason is that, here, PDIV is simply measured off-line and on a representative sample. The second reason is geometry-related, such as the sheer geometrical difference between the

sample and an actual machine, or the fact that there are likely to be more defaults in a real machine. This helps explain the presence of PDs during the measurement campaign presented in II.6.

In contrast to the previous section, the purpose of this part is more to perform endurance tests on the insulation systems to assess their lifetime rather than to discuss the influence of electrical stress on PDs and aging. However, these results were taken into consideration for dimensioning the experimental setup necessary to perform aging on Type II phase-to-ground and phase-to-phase samples. A detailed description of this setup is presented in the next section.

IV.3.2.2 Choice of voltage shape for aging

The measurements performed in the previous section showed that the considered samples are highly capacitive (up to about 200 pF; in comparison, twisted pairs of enameled wires have capacitances of about a dozen pF). Therefore, one of the major challenges in this work was to dimension an experimental setup able to age highly capacitive samples for voltage up to several kilovolts and frequency up to several kilohertz. Choices therefore had to be made, in particular regarding the voltage shape to apply to the samples. It was shown in Chapter II that the actual voltage stress undergone by the insulation systems has a very complex shape, with overvoltages and dV/dt values varying with current, but also with variable pulse durations and duty cycle. In addition, the voltage waveform is not unipolar or bipolar only, but composed of unipolar pulse trains with a single polarity reversal per period in the case of phase-to-phase voltages (see Figure IV-10). In short, the complexity of the voltage shape makes it very difficult to reproduce on samples.

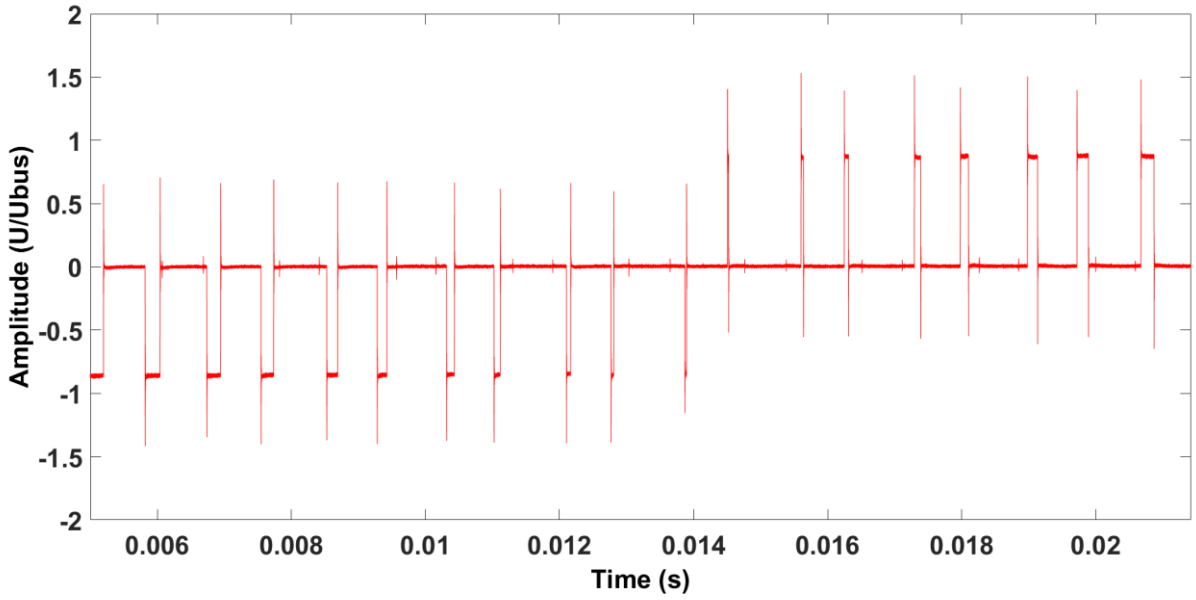

Figure IV-10: *Illustration of the voltage shape between phases (U_{bus} = U_{nom}, L_{cable}= 40m, Ω = 500 rpm, Inverter D)*

To address this issue, we decided to consider the worst case that could potentially be encountered by the insulation system. To achieve such a configuration, the best solution would be to consider a pure

bipolar square-wave voltage with an amplitude equal to the maximum measured overvoltage value, at a frequency equal to, or a multiple of, the switching frequency and a duty cycle of 50%. Aging performed under such stress could not be directly extrapolated to a real environment, but would both ensure that the lifetime of the real system is strictly superior to that obtained with accelerated aging, as it represents the worst case possible, and also to use lifetime curves to compare the endurance of samples under stresses induced by both Si-based and SiC-based inverters. The extrapolation of results in itself is discussed in more detail in Section IV.4. However, in order to dimension a test bench and use it to perform aging tests within a reasonable amount of time, and in the light of the results of Chapter III and Section IV.2, which highlighted the fact that the influence of rise time on aging tends to be mitigated for the highest frequencies, it was decided to consider sinusoidal voltage instead of the square-wave voltage described above, given that the tests would be performed at high frequency for acceleration reasons. On the basis of the previous assumption, which is a strong assumption, this approach has the dual advantage of not impacting lifetime in any manner and reducing the complexity of the system to be designed.

IV.3.2.3 Technical description of the bench

A first overview of the voltage source used for aging Type II motorettes was given in Section IV.2.2.2. The figures below show the detailed schematic layout of one of the six channels in the setup, and a picture and rack drawing with the mains connection data.

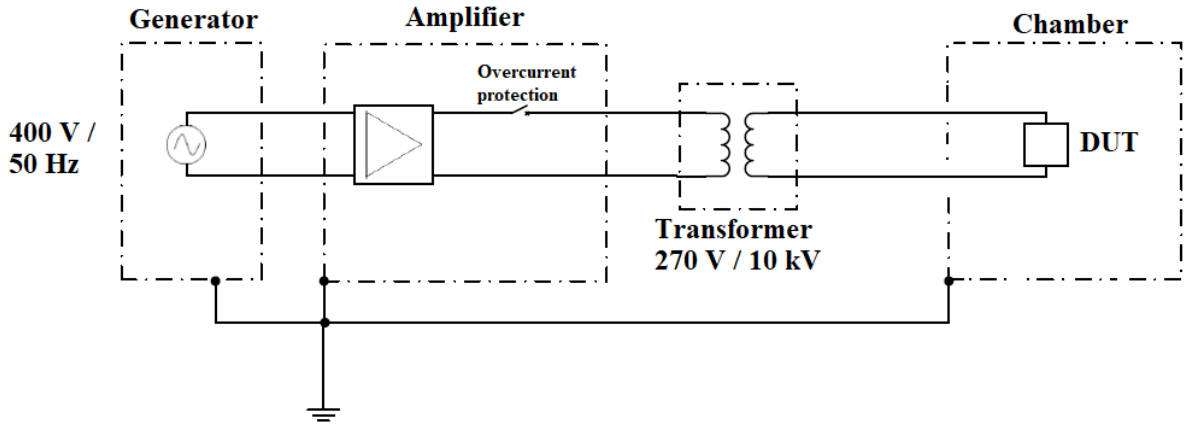

Figure IV-11: *Schematic layout of one of the six channels comprising the experimental setup*

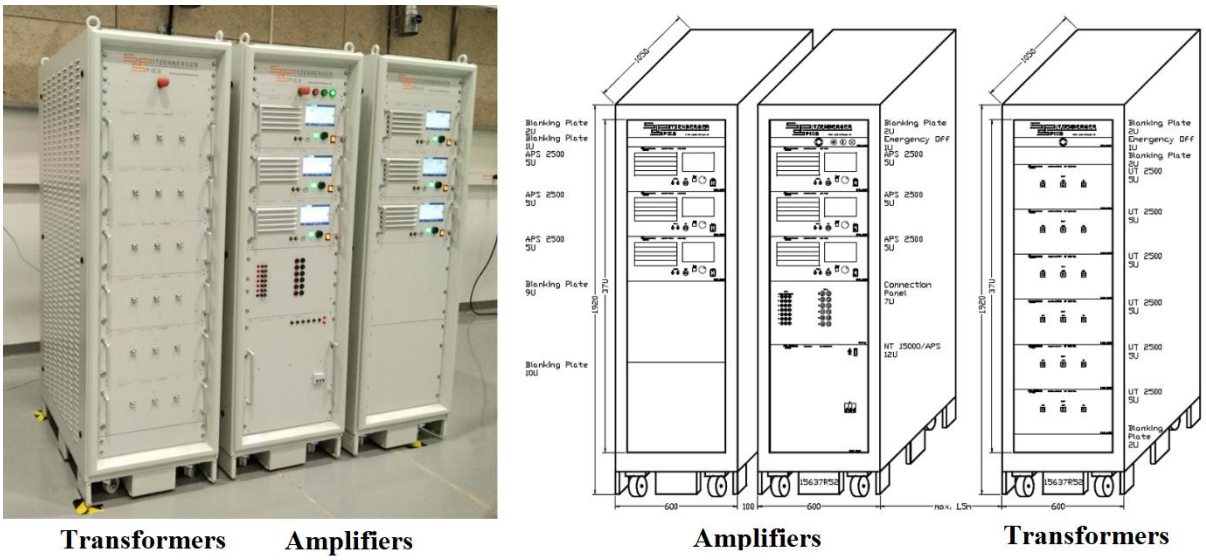

Figure IV-12: *Picture and rack drawing of the voltage source*

The overall voltage source comprises six independent channels, each of them composed of a generator, an amplifier, and a high frequency transformer (*Figure IV-11*). This enables the system to power six samples individually in order to perform accelerated aging and define lifetime models and behavior laws. The output signal is sinusoidal and the electrical parameters (voltage and frequency) are adjustable. Voltage can be varied from around 300 V to 10 kVpeak, while the frequency has a variation range from 1 to 10 kHz. At lower voltage, it is possible to go beyond these frequency limits (600 Hz – 30 kHz). The limitation current is adjustable on each amplifier; when this current value is reached, the voltage is switched off and lifetime is estimated using this limitation. Maximum operating current was determined on the basis of sample capacitances and is 6x314mA at peak performance (10 kV, 10 kHz). Each of the six channels of the voltage source is connected to one of the six conductors constituting the upper or lower part of the device under test. The fact that each of these samples is supplied individually makes it possible to sidestep the issues related to interconnection and breakdown between samples. Details for measurements, connections, and the test plan are provided in the next section.

IV.3.2.4 Test plan

An initial test plan was set up to extend the study carried out on the samples representative of Type I and Type II turn-to-turn insulation systems, and to determine behavior laws for both types of motorettes over a wide range of voltages and frequencies. However, due to the limited amount of available samples, the existence of interdependence between the upper and lower conductor lifetimes of a given motorette, and considering that the lifetime of such samples can be very long (machines for railway traction are designed to have a lifetime of about 40 years under operating conditions), the test plan was adapted downwards. Moreover, also due to time constraints, higher voltages were considered for Type R motorettes with respect to Type N motorettes. The primary objective of the following tests is to obtain insight regarding samples lifetime as a function of voltage, at high frequency, in order to compare the

performance of both types of motorettes and also to determine behavior laws that might be extrapolated under certain conditions to real operation. In addition, PD measurements enable us to correlate aging and partial discharge activity. The considered test plan is summarized below.

Table 26: *Test plan for aging Type II phase-to-ground insulation systems*

Parameter	Variation range (motorette N)	Variation range (motorette R)
Frequency (kHz)	10	10
Rise time (ns)	Sinus	Sinus
Magnitude (%PDIV / Vpk)	150 /3045 – 160 / 3248 – 175 / 3552 – 200 / 4060	175 / 5574 – 200 / 6370 – 225 / 7166

IV.3.3 Measurement protocol

Voltage in the experimental setup described in the previous section is controlled both via a high voltage probe and measurement performed directly at the voltage source. As mentioned earlier, the six channels of the voltage source are connected to the motorette. To perform aging of the phase-to-ground insulation systems for each channel, the high voltage side is connected to each of the six conductors of the upper or lower part of the motorette, while the neutral side of all transformers is connected to the metal part. Regarding aging of the phase-to-phase insulation systems, the high voltage side must be connected to each of the six conductors of the upper part of the motorette and the neutral side must be connected to each of the six conductors of the lower part of the motorette, or vice versa. Due to the reduced number of available samples and considering that the most sensitive area in terms of PDs is located between phase and ground, only phase-to-ground insulation aging was performed. A schematic diagram of the overall setup for phase-to-ground insulation aging is shown in *Figure IV-13*.

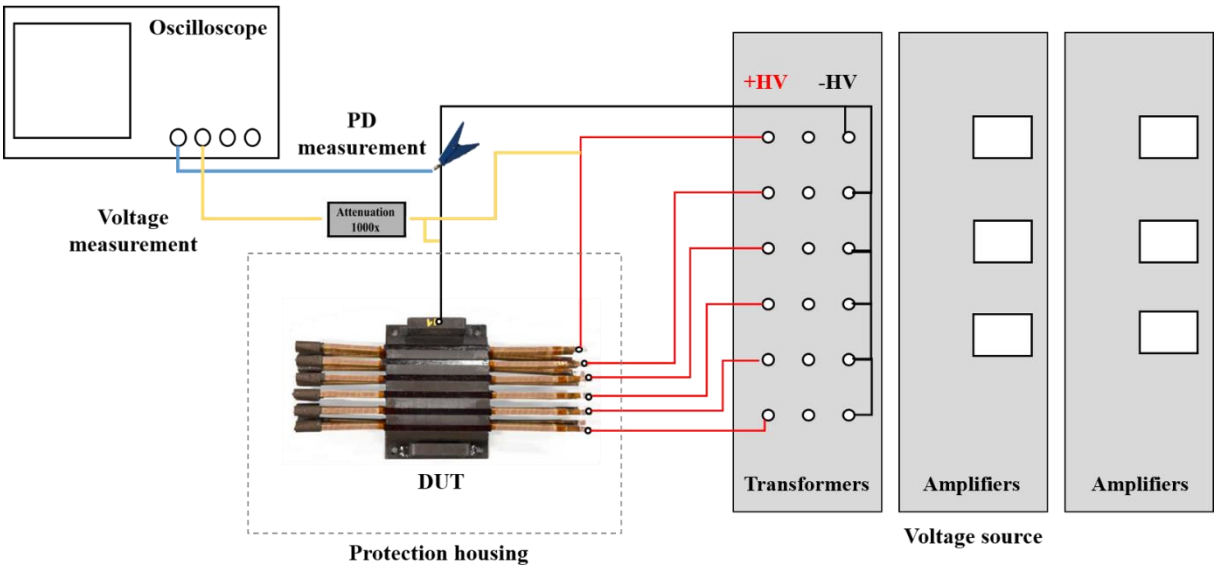

Figure IV-13: *Schematic diagram of the overall setup for phase-to-ground insulation aging*

PD measurements were taken using the same model as that in the previous section, with 20 consecutive acquisitions repeated every hour, and on a sample that was aged separately, to ensure that the PD measurements were related to that one sample only and not to the cumulative PD activity of the five samples aged simultaneously. This data was then processed using the same methodology as in Section III.3 for the sinusoidal case.

IV.3.4 Preliminary results

For reasons related to test duration, the specified tests could not all be carried out, as they required more time than was available to complete them. However, on the basis of the test plan defined above, a few tests could be completed to study the electrical aging of Type II phase-to-ground insulation systems. It was thus possible to gain some insight regarding lifetime and PD activity with the motorettes defined in the previous section, as well as additional valuable results regarding degradation of Type II insulation systems in general. Results are presented below.

IV.3.4.1 Aging and PD measurement: Type N motorettes

In the first instance, preliminary tests were performed on both types of motorettes to roughly identify those that were the least resilient to PDs. As might be expected, the phase-to-ground insulation of the Type N motorettes proved to be those with the shortest lifetime. Thereafter, aging tests were performed according to the reduced test plan defined in the previous section. The boxplots representing the evolution of lifetime vs. aging, as well as a log-log representation and extrapolation to the PDIV value, are given below. In addition, the empirical law associated with the lifetime curve is also provided. Coefficients K and n were determined by linearization of the inverse power law. The inverse power law appears as a straight line when plotted on a log-log scale. Obtaining K and n is then as simple as finding the slope and intercept in the associated equation.

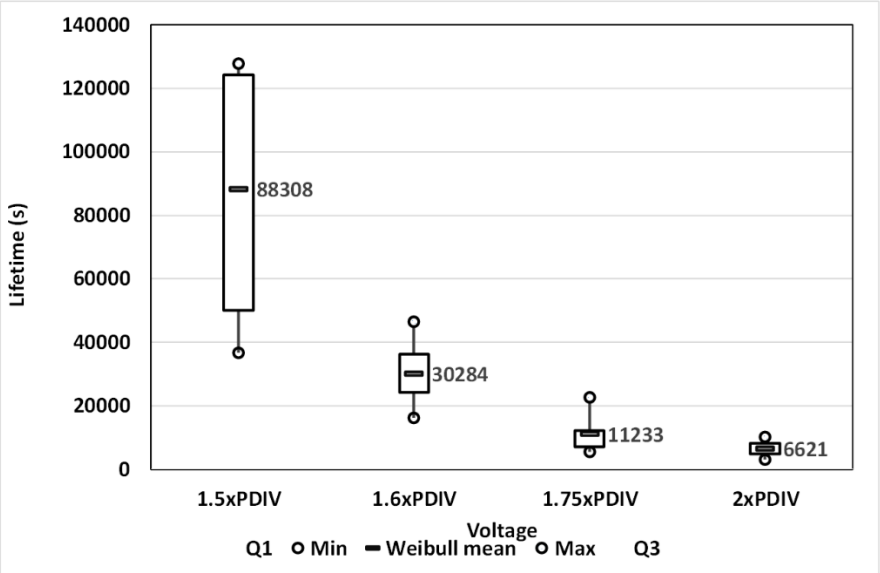

Figure IV-14*: Boxplots representing the evolution of lifetime as a function of voltage*

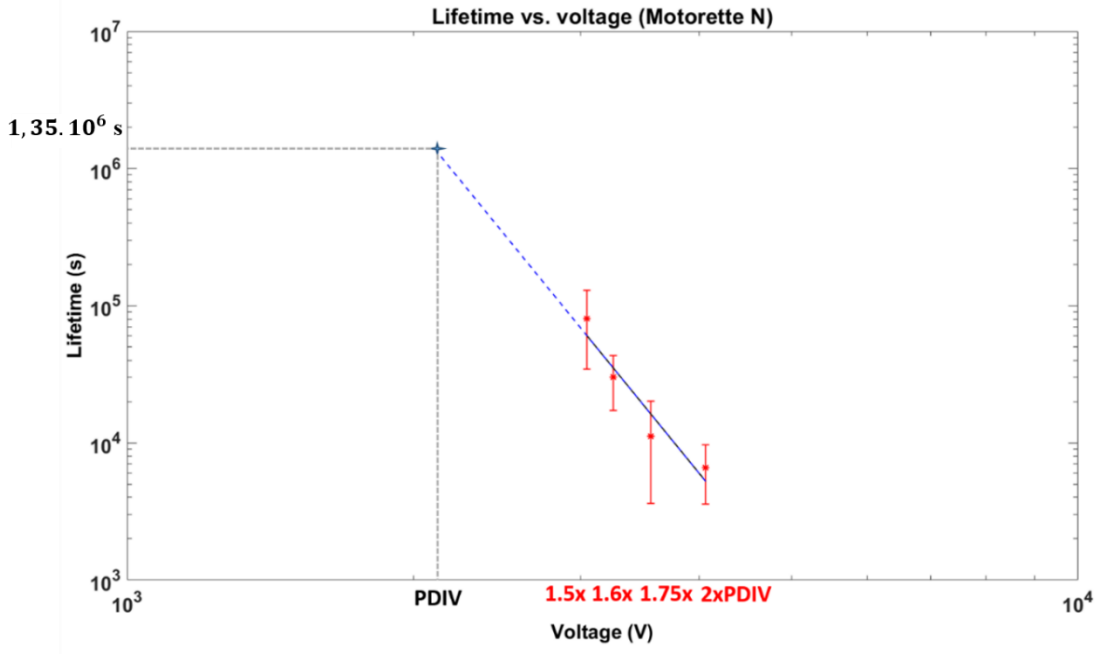

Figure IV-15: *Lifetime vs voltage plot, fitting and extrapolation for PDIV value*

$$L(U) = KU^{-n} = 10^{35.29}U^{-8.75} \quad (19)$$

Figure IV-14 highlights the dispersion existing in terms of lifetime between the different conductors of a motorette. It was reported in Section IV.3.2.1 that there can be significant dispersion between the PDIV from one conductor (and the ground) to another. This is confirmed with lifetimes that can vary as much as 100 percent for a given configuration, despite the fact that these samples are manufactured industrially.

It can be observed that the lifetimes corresponding to Type N phase-to-ground insulation systems appear at first to be relatively low. This is not surprising considering that the mica tape, which primarily serves as a barrier against PDs, is not present in these types of samples. The inverse power law presented in Section I.5.1.2 was used to model lifetime as a function of voltage. Linearization of this law enables us to obtain a direct relationship between the lifetime logarithm and the voltage logarithm, in the form of a first-degree polynomial. Polynomial curve fitting then makes it possible to identify the parameters of the polynomial, and finally to extrapolate the law for values outside the tested variation range. The extrapolation in Figure IV-15 shows that if aging mechanisms are considered to be the same whether or not voltage is far from the PDIV, a Type N phase-to-ground insulation system subject to a voltage equal to the PDIV would have an estimated lifetime of $1.35x10^6$ seconds, or approximately 16 days. As the relationship between lifetime and frequency are linear under sinusoidal stress, it can be estimated that for the highest frequency of machine use, which is of about 2 kHz, insulation lifetime would be about 80 days. Such a duration is quite low with respect to the application, particularly because this value is obtained for sinusoidal voltage, given the fact that there is a gap between lifetimes under sinusoidal and

square wave voltage at low frequency. Extrapolation of results under sinusoidal stress to a real environment is emphasized in Section IV.4.

PD was measured in parallel to aging tests to obtain insight regarding PD activity throughout the course of aging. Cumulative PRPD patterns at the beginning of aging, as well as a table summarizing the main PD features as a function of voltage, are given below.

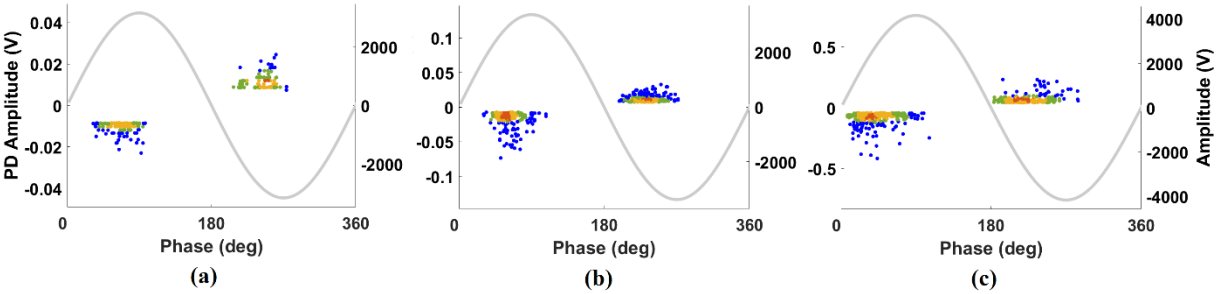

Figure IV-16: *Cumulated PRPD patterns for different voltages (20 acquisitions, beginning of aging) (a) 1.5xPDIV, (b) 1.6xPDIV, (c) 2xPDIV*

Table 27: *PD features as a function of voltage magnitude*

Voltage	Total number of PDs	Average number of PDs (positive half)	Average number of PDs (negative half)	Average number of PDs	Average PD magnitude (V)	Max PD magnitude (V)
1.5xPDIV	240	5.79	6.84	12.63	0.0111	0.0173
1.6xPDIV	615	17.84	14.53	32.37	0.0134	0.0414
2xPDIV	593	12.37	18.84	31.21	0.0813	0.2167

Data related to PD activity is consistent with what typically occurs. PD activity increases with voltage as the number and amplitude (average and maximum) of PDs increases as well. It also seems that the number of PDs no longer varies significantly after a certain voltage magnitude value, unlike their amplitude, which increases strongly. Finally, the variation of the number of PDs over time is also in line with what is typically found. The number of PDs is at its maximum at the very beginning of aging, then decreases until stabilization is reached, and finally increases gradually and then sharply when close to breakdown.

IV.3.4.2 Aging and PD measurement: Type R motorettes

In a second phase, tests were performed to assess the endurance of phase-to-ground insulation in Type R motorettes, which, as mentioned earlier, are representative of the insulation systems actually found in today's machines. These tests were performed following the reduced test plan defined in the previous section, with the objective of comparing results for the two types of motorettes. However, due

to the fact that the tests took longer to complete than initially anticipated, only partial results were obtained. The results are given below.

Table 28: *Lifetime values as a function of voltage (Type R, raw data)*

Lifetime \ Voltage	1.75xPDIV	2xPDIV	2.25xPDIV
1/ground	2857.90 h+ (ongoing)	345.52 h	81.17 h
2/ground	2939.20 h+ (ongoing)	270.80 h	26.11 h
3/ground	1081.50 h	278.72 h	72.76 h
4/ground	2939.20 h+ (ongoing)	338.37 h	122.03 h
5/ground	2939.20 h+ (ongoing)	450.90 h	23.03 h
Average	1081h 30min 08s (45 days as of this writing)	335h 53min 20s (14 days)	63h 26min 30s (3 days)

The influence of mica tape (which is the only difference between Type N and Type R insulation systems) in terms of aging is striking: lifetimes are extremely long and it is difficult to even obtain enough points to adequately model lifetime. Despite the challenge, a starting model was made on the basis of available results in order to have an estimation of the insulation lifetime that would be obtained at the PDIV value, for sake of comparison with Type N samples. As for Type N motorettes, the lifetime curve for Type R motorettes, as well as the associated empirical law, are given below.

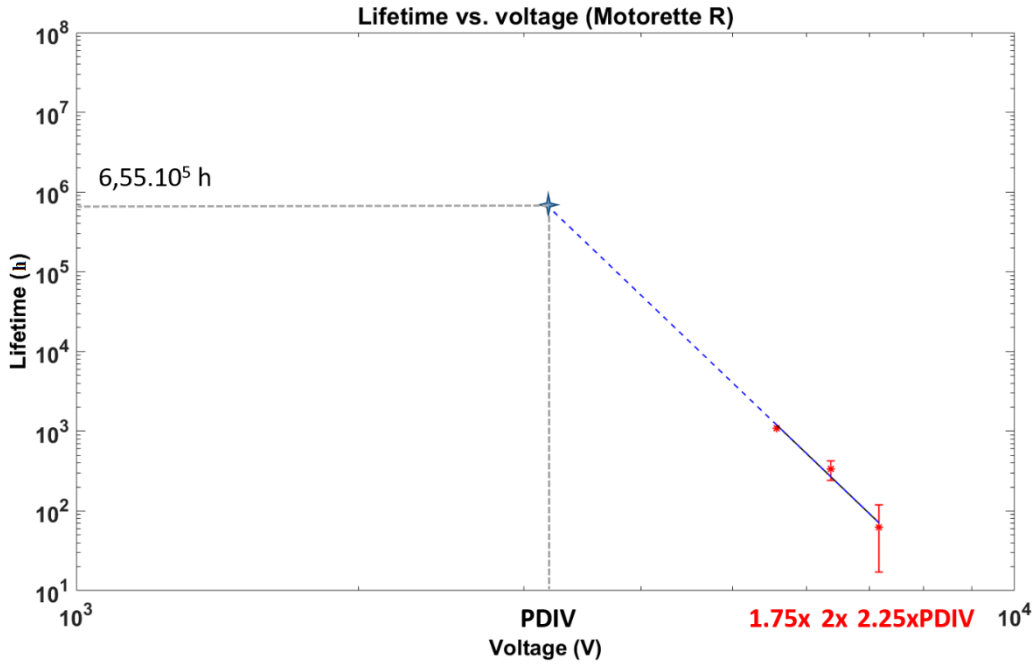

Figure IV-17: *Lifetime vs voltage plot, fitting and extrapolation for PDIV value*

$$L(U) = KU^{-n} = 10^{45.25}U^{-11.26} \quad (20)$$

The only lifetime value available (about 1081 hours, the other tests are still in progress as of this writing) for a voltage magnitude equal to 1.75xPDIV was used to plot a third point and model lifetime as a function of voltage as with the Type N motorette. Of course, more data would be necessary to perform more accurate modeling. This preliminary investigation only aims to estimate the lifetime that would be obtained at the PDIV value. Extrapolation shows that if the aging mechanisms are considered to be the same whether or not voltage is far from the PDIV, a Type R phase-to-ground insulation system subject to voltage equal to the PDIV would have an estimated lifetime of 6.55×10^5 hours, or approximately 27,279 days (74 years). Following the same reasoning as presented earlier, lifetime under sinusoidal stress for the highest frequency of machine use would be about 370 years. The difference with Type N insulation systems is considerable, and all the more so since the lowest lifetime was considered in the case of aging under a voltage stress equal to 1.75xPDIV, and the order of magnitude for lifetime is more suitable to the lifetime standards of this type of machine. However, more research work and data are needed to determine a more accurate behavioral law for Type R motorettes and to know to the extent to which results can be extrapolated to real environments.

Regarding partial discharges, PD activity could not be monitored in all cases. Indeed, as mentioned earlier, PD measurement should be performed on an isolated sample. For the lowest voltages, especially the 1.75xPDIV case, considering that the tests are still in progress, this condition could not be met. Thus, PD measurements were only used to assess the presence or absence of PD events (see Figure IV-18).

Figure IV-18: *Illustration of PDs occurring during aging on a Type R motorette*

IV.3.4.3 Remarks

Throughout the aging tests presented here, several phenomena were observed and conclusions were reached on a number of topics. The purpose of this section is to summarize these various points, which are generally relevant for studying aging of Type II phase-to-ground insulation systems.

It was observed during aging that, on a given motorette, the electrical breakdown of one of a slot's conductors could affect the adjacent conductor. It sometimes occurred that the conductor adjacent to another conductor that had previously been led to breakdown was immediately short-circuited. This contributed to reduction of the test plan, as only six conductors per motorette instead of twelve could be used for aging tests. Degradation was analyzed to attempt to understand the cause of this problem. Illustrations of the degradation are given below.

Figure IV-19: *Degradation of Type N phase-to-ground insulation systems subject to PDs*

The observation of degradation showed that, in cases where the breakdown of a conductor had an influence on the adjacent conductor, the breakdown occurred in an area located between the two conductors. In the other cases, the breakdown occurred at the interface between the conductor and one of the sides of the slot. The influence of the breakdown of one conductor on the adjacent conductor is not systematic. Moreover, when breakdown does occur, it does not occur between phases, as the insulation layer is thicker in this area, but rather between phase and ground in an area close to the interface between the conductors. It can therefore be argued that this phenomenon occurs when the most vulnerable area of the insulation is located close to this interface. Field reinforcement in this area could also aggravate the situation. Finally, considering the level of voltage that was considered, it might be possible that PDs occurred between phases, which could have helped weaken the insulation in this area without leading directly to breakdown between phases. Other factors such as insulation layer overlap could also have an impact.

As discussed earlier, a non-negligible level of dispersion was observed, both for PDIVs and lifetimes. In electrical aging, low dispersion is usually considered as a guarantee regarding the quality of results. However, in light of all the tests carried out in this study, it seems clear that this dispersion is inherent to material characteristics and nature of the PD phenomena itself, even if manufacturing can obviously have an additional impact.

Finally, an extinction of PDs for the lowest voltages was also observed. When voltage magnitude was set below the value of 1.3xPDIV, PD events tended to disappear, thus preventing aging from going the full distance. Not only is this an important point for determining stress levels for aging, but also

when looking at insulation systems in a real environment. We saw that while phase-to-ground and phase-to-phase insulation systems are the weakest point of the overall insulation system, the actual electrical constraints seen by the machine are very close to the PDIV and could only exceed this threshold for the highest DC bus voltages. Combining this with the fact that the PD events tend to disappear below a certain voltage magnitude, it would mean that Type II insulation systems are actually very similar to Type I insulation systems in the sense that they are not – or barely – subjected to PDs. This raises questions regarding the necessity of performing aging tests in the presence of PDs and regarding the extrapolation of results to a real environment. These points are addressed in the following section.

IV.4 Extrapolation to a real environment

Thorough electrical stress mapping was performed in Chapter II, enabling us to identify the maximum constraints that could be undergone by turn-to-turn, phase-to-phase, and phase-to-ground insulation systems. The influence of these constraints in terms of aging and PDs was then investigated on basic samples in Chapter III. Finally, investigations were extended to Type II machines and accelerated aging was performed on representative samples here in Chapter IV. In order to complete the picture, the question is now to know if and how the results obtained on Type II samples under sinusoidal voltage can be extrapolated to a real environment.

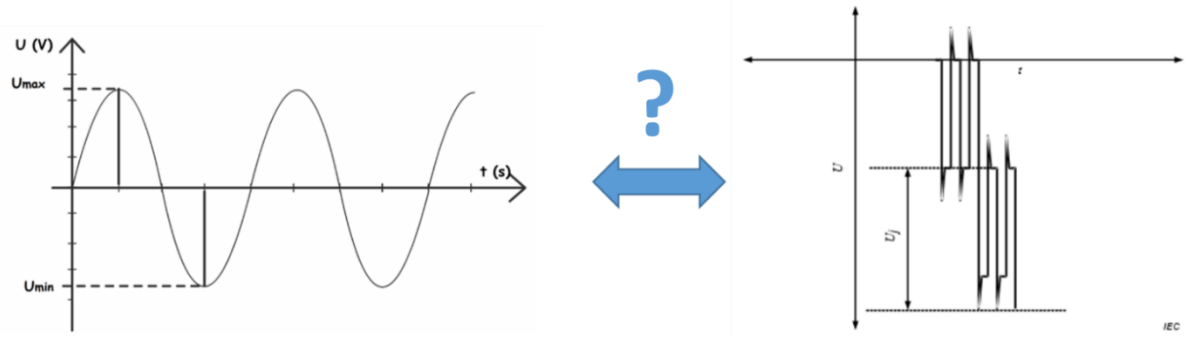

Figure IV-20: *Illustration of the problems regarding extrapolation of results to real environment*

The choice of the sinusoidal shape for aging insulation systems was justified in section IV.3.2.2. In substance, it is quite difficult to reproduce the electrical constraint induced by fast switching converters, as the process involves variable rise times and dV/dt values, overvoltages, duty cycles, and polarities. Moreover, voltage shape is different when dealing with turn-to-turn, phase-to-ground, or phase-to-phase insulation. The idea is therefore to consider the worst possible case, that is, a pure square-wave voltage with a magnitude equal to the maximum stress that could be encountered by the insulation during operation (including overvoltage), and a frequency equal to the switching frequency. The results of the study carried out in Chapter III can then be used to consider that the influence of steady-state PDs at high frequency tends to be mitigated as there are fewer of them, and thus that aging under sinusoidal or square-wave voltage gives the same results for a given voltage magnitude and frequency.

Furthermore, even if voltage magnitude is not continuously above the PDIV in reality, to consider that it is the case makes it possible to adopt a conservative approach in a configuration that is more critical than in a real environment.

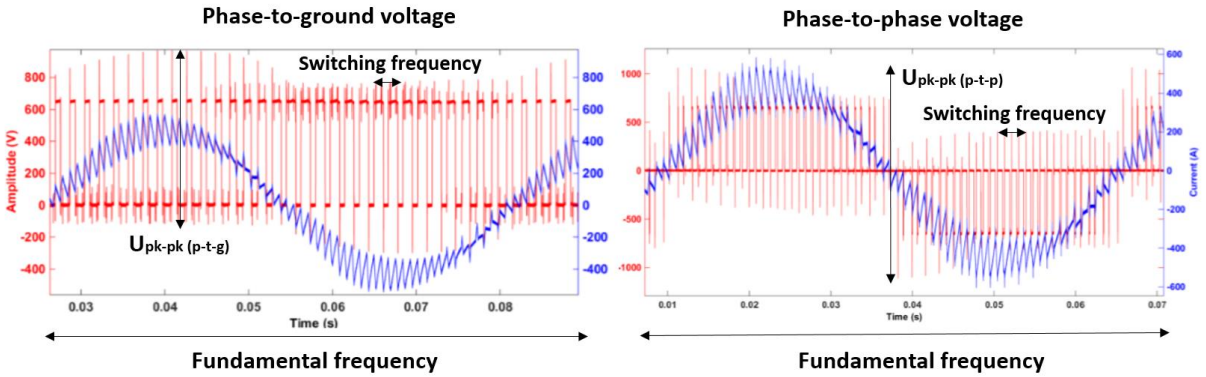

Figure IV-21: *Illustration of the different parameters that could be considered for aging*

Given the convenience of sinusoidal voltage not only for dimensioning the experimental setup, but also for interpreting and extrapolating results, it is then possible to extrapolate the results obtained at high frequency to any other frequency. The relation between lifetime and frequency is actually linear in that case. Extrapolation to square-wave voltage at low frequency is less evident. Experiments carried out throughout this study showed that, under square-wave voltage and at low frequency, additional PD phenomena come into play and help to create a difference between lifetimes under sinusoidal and impulse voltage. In particular, Table 16 shows that the ratio between lifetimes at different frequencies, unlike the sinusoidal case, is non-linear and at least varies depending on voltage magnitude and rise time. In short, the tests performed in this chapter provided insight regarding the resilience of insulation systems to PDs, and also to obtain an order of magnitude for the lifetime that would be obtained in a critical case at high frequency, regardless of voltage shape, or at low frequency under sinusoidal stress only. Additional research is required to obtain deeper insight concerning the lifetimes of such insulation systems, notably regarding aging under square-wave voltage at low frequency and to assess whether results can indeed be extrapolated further.

IV.5 Conclusion

The first tests conducted on Type II samples representative of turn-to-turn insulation systems led to a number of conclusions that are outlined in this section. First, the PDIV and breakdown measurements performed on those samples highlighted the fact that, in view of the electrical stress identification conducted in Chapter II, turn-to-turn insulation systems are very unlikely to be subject to partial discharges. The maximum turn-to-turn voltage either as an absolute figure or a percentage remains very far away from the inception voltage, even for the fastest inverters.

Notwithstanding these results, aging tests were performed in the presence of PDs throughout the entire aging process to assess the resilience of the Type II samples to PDs and to acknowledge whether or not the results of the study conducted in Chapter III were transposable to Type II. It turns out that the lifetime results confirmed established findings regarding the influence of rise time, frequency, and amplitude on aging (duty cycle was not studied). PD measurements could not be taken, which is unfortunate because they could have provided more insight into the mechanisms involved and confirmed the approach that was proposed in the previous chapter.

Tests were performed in a second part, this time on samples representative of Type II phase-to-ground and phase-to-phase insulation systems. Investigations carried out on these samples showed that the PDIV values were quite high and that even in this area, the insulation systems would not be continuously subject to PDs. The influence of mica tape was also highlighted in a comparison between Type R and Type N motorettes, and then confirmed with aging tests performed under sinusoidal voltage. To carry out these tests, a multi-channel, high voltage, high power, and high frequency experimental setup was dimensioned accordingly and the voltage shape to use for aging was chosen based on the results of Chapter III and by considering the worst case that could potentially be encountered by the insulation system. Finally, a discussion about the aging of Type II insulation systems in general and the extrapolation of results to a real environment were presented to provide overall coherence by establishing the link between the different chapters in this work.

General conclusion

The rationalization of electrical energy in many applications, including transportation, leads to an ever-growing number of questions and challenges, in particular regarding the reliability of systems and especially that of insulating materials. In the railway sector, as well as in other areas, massive evolution has been prompted to meet these new challenges. Voltage inverters based on pulse width modulation are widely used for such applications that require controlling rotation speed. Si IGBT devices are used today to create pulse width modulation. The use of IGBTs makes it possible to generate rising edges of several kV/µs, and to reach switching frequencies up to several kHz. These improvements have helped reducing switching losses and motor torque ripple but have led to the generation of more stressful constraints. Moreover, the transition from conventional silicon-based components to new wide bandgap components only exacerbated matters. De facto, there is a chance that the reliability of motors declines dramatically, though more research needs to be carried out on the topic to confirm. The causes of motor failures are due to different phenomena, but one of the main aging mechanisms is the erosion of the various insulating materials induced by partial discharges. Systems may be designed to react differently to these discharges but, in any case, the presence of PDs is an issue that affects the reliability of the entire electromechanical chain.

In this context, we addressed the issues of partial discharges and aging mechanisms for insulation systems used in rotating machines. A state of the art on degradation mechanisms and the systems on which they appear was presented. The influence of electrical stress and control strategy on aging was reviewed in detail and, finally, the aging phenomenon itself was defined and depicted.

The determination and impact of the existence of partial discharges in a railway traction system using SiC-based components was established in three steps. The first step consisted of a test campaign that sought to perform thorough electrical stress mapping depending on both geometric and electrical parameters to analyze the influence of various parameters on electrical stress, and finally to perform partial discharge measurements on a machine in real environment. We saw that the turn-to-turn voltage values in this type of motor are low. With those voltages, power electronics and thus rising edges can have little influence on the ignition of partial discharges between turns. Nevertheless, the use of fast-switching SiC-based inverters causes an increase of overvoltages for phase-to-ground and phase-to-phase voltages. These more stressful constraints eventually lead to an increase in partial discharge activity between phases or between phase and ground. These insulation systems therefore constitute the weakest point of the system in terms of reliability.

In a second step, an analysis of the impact of electrical stress on partial discharge features and aging was presented. This phenomenological study offered an opportunity to precisely study the different constituents of electrical stress in order to explain their influence on PD activity and

degradation. The study was carried out considering basic samples representative of Type I turn-to-turn insulation systems. It was shown that these parameters have a non-negligible impact on aging, at different levels. The impact of overvoltage is significant and all the more marked when it comes to steady-state voltage magnitude. A coupled impact of rise time and frequency was observed: the effect of rise time on aging tends to be mitigated at the highest frequencies. Finally, duty cycle and – indirectly – pulse duration also seem to have an impact on aging. PD measurement during aging enabled us to link these phenomena with the presence or absence of PDs during the steady part of the voltage. Those PDs, which are additional to those usually found during the edges, could possibly explain the differences induced by varying the different parameters.

Finally, the last chapter focused on reproducing the electrical constraints identified in the second chapter on more complex samples representative of Type II insulation systems. This work had the dual purpose of extending the results obtained for Type I systems to Type II systems, and studying the lifetime and degradation of real insulation systems under stress. Studies performed on Type II samples confirmed that the turn-to-turn insulation systems in Type II machines are very unlikely to be subject to PDs. Moreover, they confirmed the results obtained on Type I samples regarding the influence of electrical stress on aging. On the basis of these latter results, an experimental setup was specially dimensioned to age samples representative of phase-to-phase and phase-to-ground insulation systems, which were previously identified as higher risk areas. Despite the fact that, given the measured PDIV values, these insulation systems seem to not be subject to PDs continuously, their resilience to PDs could be assessed and it was possible to determine lifetime models and consider extrapolating these models to real environments.

To go further on the subject, future work will be devoted to extending experiments on Type I and Type II samples in efforts to understand the PD phenomena responsible for aging. Additional tests under square-wave voltage at low frequency would also be necessary to try to find complete correlation between aging under sinusoidal and square-wave voltage, and to refine the lifetime models and their extrapolation to real environments. Finally, in the context of the global increase in voltage levels, which does not only apply to the railway sector, another possible perspective could be to build on progress that has already been made and study the aging of Type II insulation systems under aeronautical conditions to anticipate the possible transition from Type I to Type II machines in other specialized fields.

References

[1] X. Roboam, “New trends and challenges of electrical networks embedded in ‘more electrical aircraft,’” in *2011 IEEE International Symposium on Industrial Electronics*, Jun. 2011, pp. 26–31, doi: 10.1109/ISIE.2011.5984130.

[2] P. Eremenko, “Building the Third Golden Age of Aerospace,” Airbus, 2017.

[3] R. Bartnikas and E. J. McMahon, *Engineering Dielectrics Volume I: Corona measurement and interpretation*. ASTM STP 669, 1979.

[4] J. P. Novak and R. Bartnikas, “Effect of dielectric surfaces on the nature of partial discharges,” *IEEE Trans. Dielectr. Electr. Insul.*, vol. 7, no. 1, pp. 146–151, Feb. 2000, doi: 10.1109/94.839353.

[5] F. Paschen, “Uber die zum Funkenübergang in Luft, Wasserstoff und Kohlensäure bei verschiedenen Drucken erforderliche Potentialdifferenz,” *Ann. Phys.*, vol. 273, no. 5, pp. 69–96, 1889, doi: 10.1002/andp.18892730505.

[6] Y. P. Raizer, *Gas discharge physics*. Berlin, Germany: Springer, 1991.

[7] R. Bartnikas and J. P. Novak, “Effect of overvoltage on the risetime and amplitude of PD pulses,” *IEEE Trans. Dielectr. Electr. Insul.*, vol. 2, no. 4, pp. 557–566, Aug. 1995, doi: 10.1109/94.407021.

[8] R. Bartnikas, “Some Observations on the Character of Corona Discharges in Short Gap Spaces,” *IEEE Trans. Electr. Insul.*, vol. EI-6, no. 2, pp. 63–75, Jun. 1971, doi: 10.1109/TEI.1971.299156.

[9] C. Abadie, “On-line non-intrusive partial discharges detection in aeronautical systems,” UT3 Paul Sabatier, Toulouse, 2017.

[10] C. Abadie, T. Billard, and T. Lebey, “Partial discharges in motor fed by inverter: from detection to winding configuration,” *IEEE Trans. Ind. Appl.*, pp. 1–1, 2018, doi: 10.1109/TIA.2018.2874875.

[11] G. C. Montanari, A. Cavallini, F. Ciani, and A. Contin, “Accelerated aging, partial discharges and breakdown of Type II turn-to-turn insulation system of rotating machines,” in *2016 IEEE Electrical Insulation Conference (EIC)*, Jun. 2016, pp. 190–193, doi: 10.1109/EIC.2016.7548692.

[12] M. Hikita, S. Okabe, H. Murase, and H. Okubo, “Cross-equipment Evaluation of Partial Discharge Measurement and Diagnosis Techniques in Electric Power Apparatus for Transmission and Distribution,” *IEEE Trans. Dielectr. Electr. Insul.*, vol. 15, no. 2, pp. 505–518, Apr. 2008, doi: 10.1109/TDEI.2008.4483471.

[13] R. Giussani, I. Cotton, and R. Sloan, “Detection of corona with RF methods and spectra analysis,” in *2012 IEEE International Symposium on Electrical Insulation*, Jun. 2012, pp. 132–136, doi: 10.1109/ELINSL.2012.6251442.

[14] “IEC 60034 - Rotating electrical machines - Part 18-41: Partial discharge free electrical insulation systems (Type I) used in rotating electrical machines fed from voltage converters - Qualification and quality control tests.”

[15] "IEC 60034 - Rotating electrical machines - Part 18-42: Partial discharge resistant electrical insulation systems (Type II) used in rotating electrical machines fed from voltage converters - Qualification tests."

[16] I. Culbert, "Experience with partial discharge testing during voltage surges as required by IEC 60034-18-41 and 60034-18-42," in *Conference Record of 2009 Annual Pulp and Paper Industry Technical Conference*, Jun. 2009, pp. 156–160, doi: 10.1109/PAPCON.2009.5185418.

[17] D. R. Johnston and M. Markovitz, "Corona-resistant insulation, electrical conductors covered therewith and dynamoelectric machines and transformers incorporating components of such insulated conductors," 4,760,296, Jul. 26, 1988.

[18] F. Guastavino, A. Ratto, and G. Coletti, "Twisted pair specimens insulated by conventional and nanocomposite enamel: Life curves and PD patterns," in *2009 9th IEEE Conference on Nanotechnology (IEEE-NANO)*, Jul. 2009, pp. 183–186.

[19] F. Guastavino, A. Ratto, E. Torello, and G. Biondi, "Aging Tests on Nanostructured Enamels for Winding Wire Insulation," *IEEE Trans. Ind. Electron.*, vol. 61, no. 10, pp. 5550–5557, Oct. 2014, doi: 10.1109/TIE.2014.2301736.

[20] D. Fabiani, G. C. Montanari, and A. Contin, "Aging acceleration of insulating materials for electrical machine windings supplied by PWM in the presence and in the absence of partial discharges," in *Proceedings of the 2001 IEEE 7th International Conference on Solid Dielectrics, 2001. ICSD '01*, 2001, pp. 283–286, doi: 10.1109/ICSD.2001.955625.

[21] F. Costa, "Les onduleurs de tension en commutation commandée." .

[22] M. R. Islam, Y. Guo, and J. G. Zhu, "Power Converter Topologies for Grid-Integrated Medium-Voltage Applications," 2014, pp. 51–107.

[23] S. K. Sahoo, A. Ramulu, S. Batta, and S. Duggal, "Performance analysis and simulation of three phase voltage source inverter using basic PWM techniques," in *IET Chennai 3rd International on Sustainable Energy and Intelligent Systems (SEISCON 2012)*, Dec. 2012, pp. 1–7, doi: 10.1049/cp.2012.2223.

[24] F. Guastavino, G. Coletti, A. Dardano, and E. Torello, "Life tests on twisted pairs subjected to PWM-like voltages," in *Proceedings of the 2004 IEEE International Conference on Solid Dielectrics, 2004. ICSD 2004.*, Jul. 2004, vol. 2, pp. 860-863 Vol.2, doi: 10.1109/ICSD.2004.1350567.

[25] F. Guastavino, D. Cordano, E. Torello, and G. Secondo, "Electrical aging tests on different kind of insulating systems adopted for induction stator motor," in *2015 IEEE Conference on Electrical Insulation and Dielectric Phenomena (CEIDP)*, Oct. 2015, pp. 808–811, doi: 10.1109/CEIDP.2015.7352068.

[26] D. Roger and S. Savin, "Fiabilité des systèmes d'isolation électrique des machines connectées à des convertisseurs SiC et GaN et des busbars laminés : Problématique, état de l'art, objectifs et investigations préliminaires." 2014.

[27] V. Mihaila, “Nouvelle conception des bobinages statoriques des machines à courant alternatif pour réduire les effets négatifs des dV/dt,” Université d’Artois, Béthune, 2011.

[28] B. Taghia, T. Billard, J. Carayon, D. Malec, H. Piquet, and A. Belinger, “Investigations on Partial Discharges Risk in Aeronautical Rotating Machine Fed by HVDC 540VDC Network,” in *2018 IEEE Electrical Insulation Conference (EIC)*, Jun. 2018, pp. 491–494, doi: 10.1109/EIC.2018.8481115.

[29] C. Zoeller, T. M. Wolbank, and M. A. Vogelsberger, “Inverter-fed drive stator insulation monitoring based on reflection phenomena stimulated by voltage step excitation,” in *2016 IEEE Energy Conversion Congress and Exposition (ECCE)*, Sep. 2016, pp. 1–8, doi: 10.1109/ECCE.2016.7855213.

[30] M. Fenger, S. R. Campbell, and G. Gao, “The impact of surge voltage rise-time on PD inception voltage in random wound motors of different designs,” in *2001 Annual Report Conference on Electrical Insulation and Dielectric Phenomena (Cat. No.01CH37225)*, 2001, pp. 352–355, doi: 10.1109/CEIDP.2001.963555.

[31] M. Fenger, G. Stone, and S. Campbell, “Partial discharges on low voltage stator windings subjected to voltage surges from adjustable speed drives,” in *2002 International Conference on Power Electronics, Machines and Drives (Conf. Publ. No. 487)*, Jun. 2002, pp. 298–302, doi: 10.1049/cp:20020132.

[32] M. Tozzi, G. C. Montanari, D. Fabiani, A. Cavallini, and G. Gao, “Off-line and on-line pd measurements on induction motors fed by power electronic impulses,” in *2009 IEEE Electrical Insulation Conference*, May 2009, pp. 420–424, doi: 10.1109/EIC.2009.5166383.

[33] G. Robles, J. M. Martinez-Tarifa, M. V. Rojas-Moreno, and J. Sanz-Feito, “Inductive Sensor for Measuring High Frequency Partial Discharges Within Electrical Insulation,” *IEEE Trans. Instrum. Meas.*, vol. 58, no. 11, pp. 3907–3913, Nov. 2009, doi: 10.1109/TIM.2009.2021239.

[34] P. Wang, A. Cavallini, and G. C. Montanari, “The influence of square voltage rise time on partial discharge spectra,” in *2012 Annual Report Conference on Electrical Insulation and Dielectric Phenomena*, Oct. 2012, pp. 129–132, doi: 10.1109/CEIDP.2012.6378738.

[35] S. Mao, T. Wu, X. Lu, J. Popovic, and J. A. Ferreira, “High frequency high voltage power conversion with silicon carbide power semiconductor devices,” in *2016 6th Electronic System-Integration Technology Conference (ESTC)*, Sep. 2016, pp. 1–5, doi: 10.1109/ESTC.2016.7764721.

[36] C. Zoeller, M. A. Vogelsberger, T. M. Wolbank, and H. Ertl, “Impact of SiC semiconductors switching transition speed on insulation health state monitoring of traction machines,” *IET Power Electron.*, vol. 9, no. 15, pp. 2769–2775, 2016, doi: 10.1049/iet-pel.2015.0988.

[37] C. Zoeller, M. A. Vogelsberger, and T. M. Wolbank, “Influence of parasitic capacitances of IGBT inverter on insulation condition monitoring of traction machines based on current signal transients analysis,” in *2016 18th European Conference on Power Electronics and Applications (EPE’16 ECCE Europe)*, Sep. 2016, pp. 1–9, doi: 10.1109/EPE.2016.7695580.

[38] F. Salameh, “Méthodes de modélisation statistique de la durée de vie des composants en génie électrique,” Institut National Polytechnique, Toulouse, 2016.

[39] G. C. Stone and J. F. Lawless, “Weibull statistical analysis of aging tests on solid electrical insulation,” in *1978 IEEE International Conference on Electrical Insulation*, Jun. 1978, pp. 13–16, doi: 10.1109/EIC.1978.7463562.

[40] C. Kaijiang, W. Guangning, Z. Liren, G. Xiaoxia, L. Kegang, and G. Bo, “Insulation life-span models for electrical and thermal aging under continuous high square impulses voltage,” in *2009 IEEE 9th International Conference on the Properties and Applications of Dielectric Materials*, Jul. 2009, pp. 285–288, doi: 10.1109/ICPADM.2009.5252428.

[41] G. Cannatà, S. De Caro, S. Panarello, T. Scimone, A. Testa, and S. Russo, “Reliability Assessment of Avalanche Mode Operating Power MOSFETs through Coffin Manson Law based Mathematical Models,” in *Automation and Motion 2014 International Symposium on Power Electronics, Electrical Drives*, Jun. 2014, pp. 139–145, doi: 10.1109/SPEEDAM.2014.6872071.

[42] M. Farahani, E. Gockenbach, H. Borsi, and M. Kaufhold, “Behavior of a Machine Insulation System during Accelerated Aging Tests,” in *Conference Record of the 2008 IEEE International Symposium on Electrical Insulation*, Jun. 2008, pp. 404–407, doi: 10.1109/ELINSL.2008.4570359.

[43] J. P. Bellomo, T. Lebey, J. M. Oraison, and F. Peltier, “Study of the aging of different dielectrics under specific electrical constraints,” in *Proceedings of 1994 4th International Conference on Properties and Applications of Dielectric Materials (ICPADM)*, Jul. 1994, vol. 2, pp. 796–799 vol.2, doi: 10.1109/ICPADM.1994.414131.

[44] M. Farahani, H. Borsi, E. Gockenbach, and M. Kaufhold, “Partial discharge and dissipation factor behavior of model insulating systems for high voltage rotating machines under different stresses,” *IEEE Electr. Insul. Mag.*, vol. 21, no. 5, pp. 5–19, Sep. 2005, doi: 10.1109/MEI.2005.1513425.

[45] A. Altmann, K. Engel, D. Peier, and K. Senske, “Partial Discharge Analysis During Accelerated Aging Tests For The Optimization Of HV Electrical Machine Insulation,” in *Proceedings of the 6th International Conference on Optimization of Electrical and Electronic Equipments*, May 1998, vol. 1, pp. 181–184, doi: 10.1109/OPTIM.1998.710468.

[46] P. Wang, G. C. Montanari, and A. Cavallini, “Partial Discharge Phenomenology and Induced Aging Behavior in Rotating Machines Controlled by Power Electronics,” *IEEE Trans. Ind. Electron.*, vol. 61, no. 12, pp. 7105–7112, Dec. 2014, doi: 10.1109/TIE.2014.2320226.

[47] K. Wu, T. Okamoto, and Y. Suzuoki, “Transition of Partial Discharge Behavior with Aging under Square-wave AC Voltage,” in *2006 IEEE 8th International Conference on Properties applications of Dielectric Materials*, Jun. 2006, pp. 36–39, doi: 10.1109/ICPADM.2006.284111.

[48] E. Sili, J. P. Cambronne, N. Naude, and R. Khazaka, “Polyimide lifetime under partial discharge aging: effects of temperature, pressure and humidity,” *IEEE Trans. Dielectr. Electr. Insul.*, vol. 20, no. 2, pp. 435–442, Apr. 2013, doi: 10.1109/TDEI.2013.6508745.

[49] L. Verardi, D. Fabiani, G. C. Montanari, and V. Plaček, “Electrical aging markers for low-voltage cable insulation wiring of nuclear power plants,” in *2012 IEEE 10th International Conference*

on the Properties and Applications of Dielectric Materials, Jul. 2012, pp. 1–4, doi: 10.1109/ICPADM.2012.6318966.

[50] C. Perrier, M.-L. Coulibaly, and M. Marugan, "Efficiency of aging markers for different transformer insulation systems," in *2016 IEEE International Conference on Dielectrics (ICD)*, Jul. 2016, vol. 2, pp. 824–827, doi: 10.1109/ICD.2016.7547743.

[51] P. Wang, N. Yang, C. Zheng, and Y. Li, "Effect of repetitive impulsive and square wave voltage frequency on partial discharge features," in *2018 12th International Conference on the Properties and Applications of Dielectric Materials (ICPADM)*, May 2018, pp. 152–155, doi: 10.1109/ICPADM.2018.8401153.

[52] S. Matsumoto, and D. Nagaba, and T. Ogiya, "Partial discharge characteristics of twisted magnet wire under high frequency AC voltage," in *Proceedings of 2014 International Symposium on Electrical Insulating Materials*, Jun. 2014, pp. 57–60, doi: 10.1109/ISEIM.2014.6870719.

[53] A. Cavallini, V. Krotov, G. C. Montanari, P. H. F. Morshuis, and L. E. Mariut, "The role of supply frequency in the evaluation of partial discharge inception voltage in XLPE-embedded cavities," in *2012 Annual Report Conference on Electrical Insulation and Dielectric Phenomena*, Oct. 2012, pp. 487–490, doi: 10.1109/CEIDP.2012.6378826.

[54] D. Fabiani, G. C. Montanari, A. Cavallini, and G. Mazzanti, "Relation between space charge accumulation and partial discharge activity in enameled wires under PWM-like voltage waveforms," *IEEE Trans. Dielectr. Electr. Insul.*, vol. 11, no. 3, pp. 393–405, Jun. 2004, doi: 10.1109/TDEI.2004.1306718.

[55] L. Lusuardi, A. Cavallini, A. Caprara, F. Bardelli, and A. Cattazzo, "The Impact of Test Voltage Waveform in Determining the Repetitive Partial Discharge Inception Voltage of Type I Turn/Turn Insulation Used in Inverter-Fed Induction Motors," in *2018 IEEE Electrical Insulation Conference (EIC)*, Jun. 2018, pp. 478–481, doi: 10.1109/EIC.2018.8481018.

[56] J. Ramirez, E. D. Silva, J. Sanz, J. Bermudez, and J. Rodriguez, "Comparison of the accelerated aging under different thermal cycles and voltages impulses in XLPE cables," in *CEIDP '05. 2005 Annual Report Conference on Electrical Insulation and Dielectric Phenomena, 2005.*, Oct. 2005, pp. 229–232, doi: 10.1109/CEIDP.2005.1560663.

[57] F. Guastavino, A. Dardano, A. Ratto, and E. Torello, "Electrical aging test on twisted pair specimens under different environmental conditions," in *2009 IEEE Conference on Electrical Insulation and Dielectric Phenomena*, Oct. 2009, pp. 81–84, doi: 10.1109/CEIDP.2009.5377744.

[58] G. Pietrini, D. Barater, F. Immovilli, A. Cavallini, and G. Franceschini, "Multi-stress lifetime model of the winding insulation of electrical machines," in *2017 IEEE Workshop on Electrical Machines Design, Control and Diagnosis (WEMDCD)*, Apr. 2017, pp. 268–274, doi: 10.1109/WEMDCD.2017.7947758.

[59] M. Szczepanski, D. Malec, P. Maussion, B. Petitgas, and P. Manfé, "Use of Design of Experiments (DoE) predictive models as a method of comparison of enameled wires used in low voltage

inverter-fed motors," in *2018 IEEE Industry Applications Society Annual Meeting (IAS)*, Sep. 2018, pp. 1–8, doi: 10.1109/IAS.2018.8544548.

[60] K. Kimura, "Multistress aging of machine insulation systems," in *Proceedings of 1995 Conference on Electrical Insulation and Dielectric Phenomena*, Oct. 1995, pp. 205–210, doi: 10.1109/CEIDP.1995.483611.

[61] T. S. Ramu, "Degradation of HV generator insulation under mechanical, electrical and thermal stresses," in *IEEE International Symposium on Electrical Insulation*, Jun. 1990, pp. 21–24, doi: 10.1109/ELINSL.1990.109699.

[62] J. P. Bellomo, T. Lebey, J. M. Oraison, and F. Peltier, "Characterisation of voltage shapes acting on the insulation of rotating machines supplied by inverters," in *Proceedings of 1994 4th International Conference on Properties and Applications of Dielectric Materials (ICPADM)*, Jul. 1994, vol. 2, pp. 792–795 vol.2, doi: 10.1109/ICPADM.1994.414130.

[63] M. Melfi, A. M. J. Sung, S. Bell, and G. L. Skibinski, "Effect of surge voltage risetime on the insulation of low-voltage machines fed by PWM converters," *IEEE Trans. Ind. Appl.*, vol. 34, no. 4, pp. 766–775, Aug. 1998, doi: 10.1109/28.703971.

[64] J. P. Bellomo, T. Lebey, J. M. Oraison, and F. Peltier, "Electrical aging of stator insulation of low voltage rotating machines supplied by inverters," in *Conference Record of the 1996 IEEE International Symposium on Electrical Insulation*, Jun. 1996, vol. 1, pp. 210–213 vol.1, doi: 10.1109/ELINSL.1996.549319.

[65] J. P. Bellomo, P. Castelan, and T. Lebey, "The effect of pulsed voltages on dielectric material properties," *IEEE Trans. Dielectr. Electr. Insul.*, vol. 6, no. 1, pp. 20–26, Feb. 1999, doi: 10.1109/94.752005.

[66] L. Gubbala, A. von Jouanne, P. Enjeti, C. Singh, and H. Toliyat, "Voltage distribution in the windings of an AC motor subjected to high dV/dt PWM voltages," in *Proceedings of PESC '95 - Power Electronics Specialist Conference*, Atlanta, GA, USA, 1995, vol. 1, pp. 579–585, doi: 10.1109/PESC.1995.474867.

[67] G. Stone, S. Campbell, and S. Tetreault, "Inverter-fed drives: which motor stators are at risk?," *IEEE Ind. Appl. Mag.*, vol. 6, no. 5, pp. 17–22, Sep. 2000, doi: 10.1109/2943.863631.

[68] H. Provencher, C. Millet, and S. Noel, "Analysis of turn insulation degradation under voltage surge stress," in *2016 IEEE Electrical Insulation Conference (EIC)*, Jun. 2016, pp. 409–413, doi: 10.1109/EIC.2016.7548625.

[69] M. Denk and M. M. Bakran, "Partial Discharge Measurement in a Motor Winding Fed by a SiC Inverter - How Critical is High dV/dt Really?," in *PCIM Europe 2018; International Exhibition and Conference for Power Electronics, Intelligent Motion, Renewable Energy and Energy Management*, Jun. 2018, pp. 1–6.

[70] T. Billard, T. Lebey, and F. Fresnet, “Partial discharge in electric motor fed by a PWM inverter: off-line and on-line detection,” *IEEE Trans. Dielectr. Electr. Insul.*, vol. 21, no. 3, pp. 1235–1242, Jun. 2014, doi: 10.1109/TDEI.2014.6832270.

[71] G. C. Stone, H. G. Sedding, and C. Chan, “Experience with on-line partial discharge measurement in high voltage inverter fed motors,” in *2016 Petroleum and Chemical Industry Technical Conference (PCIC)*, Sep. 2016, pp. 1–7, doi: 10.1109/PCICON.2016.7589241.

[72] C. Abadie, T. Billard, and T. Lebey, “Influence of pressure on partial discharge spectra,” in *2016 IEEE Electrical Insulation Conference (EIC)*, Jun. 2016, pp. 507–510, doi: 10.1109/EIC.2016.7548648.

[73] F. Guastavino, A. Dardano, and E. Torello, “Measuring partial discharges under pulsed voltage conditions,” *IEEE Trans. Dielectr. Electr. Insul.*, vol. 15, no. 6, Art. no. 6, Dec. 2008, doi: 10.1109/TDEI.2008.4712668.

[74] F. Sahlén, G. Paulsson, and E. Mårtensson, “Life-time investigation of mica-based insulation for high voltage machines subjected to converter-like voltages,” in *2016 IEEE Electrical Insulation Conference (EIC)*, Jun. 2016, pp. 460–463, doi: 10.1109/EIC.2016.7548637.

[75] J. Shao, “New thinking and methodologies on reliability engineering,” in *2009 8th International Conference on Reliability, Maintainability and Safety*, Chengdu, China, Jul. 2009, pp. 149–153, doi: 10.1109/ICRMS.2009.5270221.

[76] A. Barnard, “Ten things you should know about HALT & HASS,” in *2012 Proceedings Annual Reliability and Maintainability Symposium*, Reno, NV, USA, Jan. 2012, pp. 1–6, doi: 10.1109/RAMS.2012.6175457.

[77] “IEC 62068:2013: Electrical insulating materials and systems - General method of evaluation of electrical endurance under repetitive voltage impulses.” .

[78] “IEC 60851-5: Winding wires - Test methods - Part 5: Electrical properties.” .

[79] K. Kimura, S. Ushirone, T. Koyanagi, and M. Hikita, “PDIV characteristics of twisted-pair of magnet wires with repetitive impulse voltage,” *IEEE Trans. Dielectr. Electr. Insul.*, vol. 14, no. 3, pp. 744–750, Jun. 2007, doi: 10.1109/TDEI.2007.369539.

[80] A. Cavallini, E. Lindell, G. C. Montanari, and M. Tozzi, “Inception of partial discharges under repetitive square voltages: Effect of voltage waveform and repetition rate on PDIV and RPDIV,” in *2010 Annual Report Conference on Electrical Insulation and Dielectic Phenomena*, West Lafayette, IN, Oct. 2010, pp. 1–4, doi: 10.1109/CEIDP.2010.5724033.

[81] D. Goetz, H. Putter, F. Petzold, and S. Markalous, “PD characteristics under the aspect of different voltage wave shapes and frequencies,” in *2016 Diagnostic of Electrical Machines and Insulating Systems in Electrical Engineering (DEMISEE)*, Papradno, Slovakia, Jun. 2016, pp. 94–98, doi: 10.1109/DEMISEE.2016.7530474.

[82] P. Wang, A. Cavallini, and G. C. Montanari, “The influence of repetitive square wave voltage parameters on enameled wire endurance,” *IEEE Trans. Dielectr. Electr. Insul.*, vol. 21, no. 3, pp. 1276–1284, Jun. 2014, doi: 10.1109/TDEI.2014.6832275.

[83] F. Guastavino, G. Coletti, and E. Torello, “Twisted pairs specimens subjected to several waveform voltages in presence of partial discharges,” in *Annual Report Conference on Electrical Insulation and Dielectric Phenomena*, 2002, pp. 450–453, doi: 10.1109/CEIDP.2002.1048831.

[84] Tao Liu, Yi Xiao, Yangfei Lu, Xuwei Huang, Qingmin Li, and Zhongdong Wang, “Effect of voltage frequency on surface discharge characteristics and aging process,” in *2017 IEEE Electrical Insulation Conference (EIC)*, Baltimore, MD, USA, Jun. 2017, pp. 463–466, doi: 10.1109/EIC.2017.8004606.

[85] I. Radu, R. Bartnikas, and M. R. Wertheimer, “Frequency and voltage dependence of glow and pseudoglow discharges in helium under atmospheric pressure,” *IEEE Trans. Plasma Sci.*, vol. 31, no. 6, pp. 1363–1378, Dec. 2003, doi: 10.1109/TPS.2003.820970.

[86] R. Miller and I. A. Black, “Partial discharge measurement’s over the frequency range 0.1 Hz to 50 Hz,” in *1976 IEEE International Conference on Electrical Insulation*, Montreal, Quebec, Canada, Jun. 1976, pp. 307–310, doi: 10.1109/EIC.1976.7464225.

[87] T. Billard, T. Lebey, A. Belinger, N. Naude, and N. Gherardi, “On the nature of the discharges in samples fed by bipolar pulse like voltage and its possible impact on the detection of partial discharge in machines fed by inverter,” in *Proceedings of 2014 International Symposium on Electrical Insulating Materials*, Niigata, Jun. 2014, pp. 200–203, doi: 10.1109/ISEIM.2014.6870753.